Timing of polar protein accumulation and signaling in *Arabidopsis thaliana*

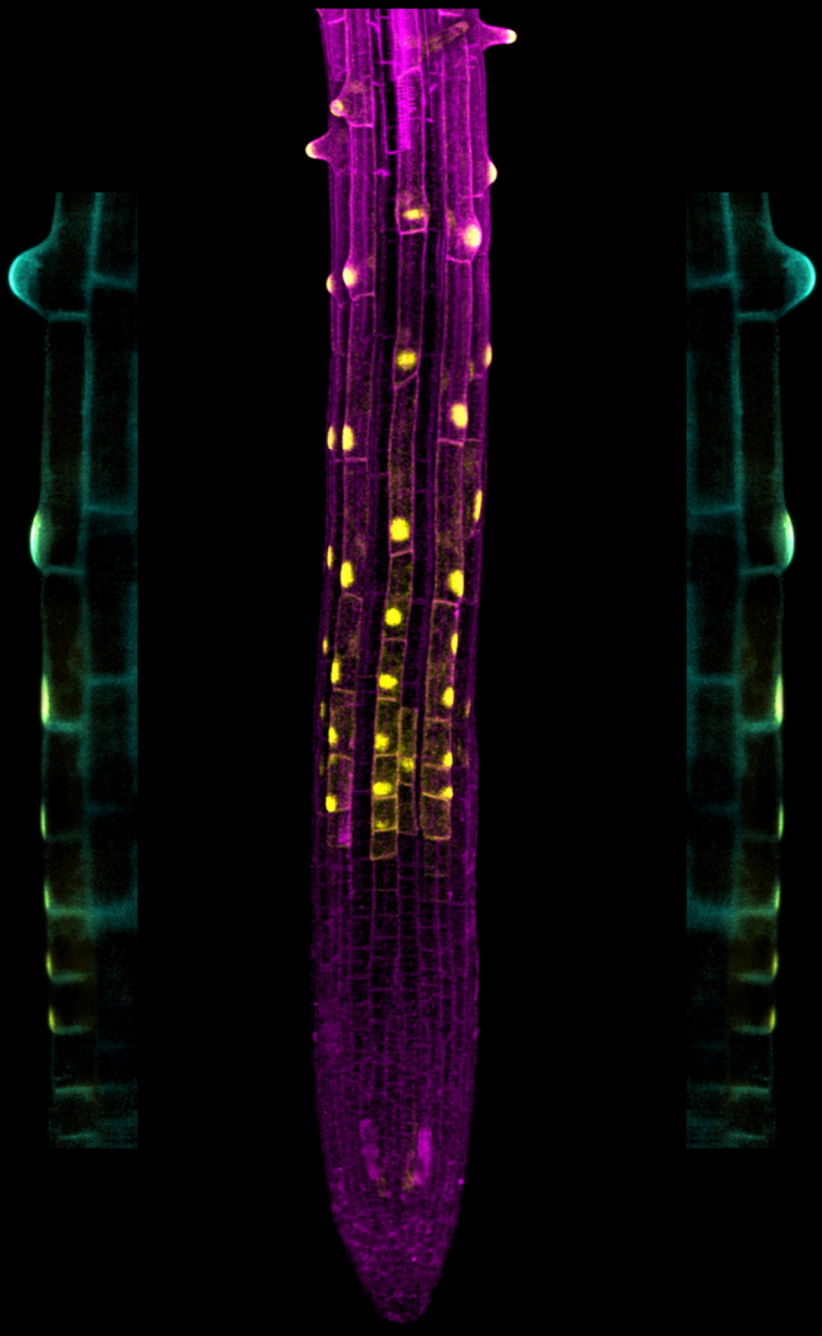

Philipp Denninger 2018

DISSERTATION

submitted to the
Combined Faculty of Natural Science and Mathematics
of the Ruperto Carola University Heidelberg, Germany
for the degree of
Doctor of Natural Science

Presented by

Philipp Denninger M.Sc.

Born in Würzburg, Germany

Oral examination: _____

Timing of polar protein accumulation and signaling in *Arabidopsis thaliana*

Referees:

Prof. Dr. Karin Schumacher

Dr. Guido Grossmann

Contents

Danksagungen (Acknowledgements)

Zuallererst möchte ich mich bei Guido bedanken! 5 Jahre lang eine tolle Zusammenarbeit, Betreuung und immer ein super Verhältnis. Ich hoffe wir werden uns auch weiterhin wissenschaftlich und privat begegnen. So einen Chef wünscht man sich! Danke Guido!

Bei meinen TAC Mitgliedern Karin Schumacher und Michael Knop möchte ich mich für die richtungsweisenden Ratschläge, gute Unterstützung, und eine tolle Atmosphäre bedanken! Ebenso großen Dank an Felix Evers, ohne dessen Einsatz für das Mikroskop alles nicht möglich gewesen wäre.

Natürlich wäre es ohne all die Kollegen aus dem COS, besonders dem alten INF329, sehr langweilig geworden. Daher danke an alle für tolle Retreats, Feste, Freitage und sonstiges weniger arbeitsrelevantes.
Besonders bedanken will ich mich bei denen die so viel Zeit mit mir verbracht habe und die dafür gesorgt haben, dass es immer Spaß gemacht, egal ob während oder nach der Arbeit. Linda, Aaron, Madeline, Vanessa und Anna (wenn auch noch nicht so lange) ihr seid Kollegen wie man sie nicht so leicht findet. Ich freue mich euch als Freunde zu haben!
Rik gets an extra section: Thanks man for being my best friend (also best man) and all your support for all this time. Thanks for endless discussions, a lot of fun and unforgettable memories.

Ganz besonderer Dank geht an meine Eltern, dafür dass sie mich immer unterstützen und ich mich immer auf sie verlassen kann. Ich werde euch für immer Dankbar sein, dass ihr mir den Weg bis hier hin ermöglicht habt.

Und zum Schluss die wichtigste Person: Andrea!
Danke für alles! Für deine Ratschläge, deine Hilfe, aber natürlich noch viel mehr für deine Unterstützung und dass du einfach immer für mich da bist.

Contributions

The work presented in this thesis has been partially published in the following publications:

Denninger, P., Bleckmann, A., Lausser, A., Vogler, F., Ott, T., Ehrhardt, D.W., Frommer, W.B., Sprunck, S., Dresselhaus, T., and Grossmann, G. (2014). Male-female communication triggers calcium signatures during fertilization in Arabidopsis. Nature Communications 5: 4645.

Xing, S., Mehlhorn, D.G., Wallmeroth, N., Asseck, L.Y., Kar, R., Voss, A., Denninger, P., Schmidt, V.A.F., Schwarzländer, M., Stierhof, Y.-D., Grossmann, G., and Grefen, C. (2017). Loss of GET pathway orthologs in Arabidopsis thaliana causes root hair growth defects and affects SNARE abundance. Proceedings of the National Academy of Sciences 114: E1544.

Denninger P., Reichelt a., Schmidt V.A.F., Mehlhorn D.G., Asseck L.Y., Stanley C.E., Keinath N.F., Evers J.F., Grefen C., and Grossmann G. (2018). ROPGEF3 acts as a landmark during the polarization of root hair cells in *Arabidopsis*. Submitted to eLIFE.

Parts of this thesis was done with contribution of co-workers:

Guido Grossmann designed the Model in Figure 1.7 and 1.17, as well as the form of data presentation in Figure 1.17

Guido Grossmann was further involved in preparation of Figure 1.22 A-E, 1.24 B-C, as well as data analysis and preparation of Figure 1.26, 2.1 and 2.2.

Anna Reichelt was involved in data collection and analysis for Figure 1.24 B-C and 1.26

Summary

Eukaryotic cells can have a plethora of different shapes. To develop these, cells have to grow polarly and therefore concentrate their resources at a defined domain at the plasma membrane. We have a great understanding how such polar growth is achieved and regulated. However, the early processes that initiate the formation of a new polar domain at the plasma membrane, especially the timing of protein recruitment, remain largely elusive.

The aim of this thesis was to understand how a polar domain is established and how the machinery for polar growth is assembled. As a model system I used *Arabidopsis thaliana* root hairs, which grow tube-like protrusions out of epidermal cells and I established a timeline of protein recruitment to the root hair initiation domain (RHID).

To enable sensitive measurements of protein localization, I quantified properties of 10 fluorescent proteins *in planta*. Using the brightest fluorophore, I was able to detect low amounts of protein and quantitatively measure accumulation at the RHID at endogenous levels. The combined analysis of timing and localization of 30 different markers showed that different proteins accumulate specifically at different phases of root hair development and led to the identification of four novel candidates that act during root hair initiation, along with the established RHID markers RhoGTPases OF PLANTS (ROPs). For ROP2 I could show that its activity, as well as the interaction domain and the C-terminus are important for membrane association and recruitment to the RHID, while posttranslational S-acylation had no effect in this process. Two of the candidates found during RHID initiation, the actin-regulating SCAR/WAVE complex and the undescribed POLLEN RECEPTOR-LIKE KINASE 7 (PRK7,) both led to the establishment of independent projects. Additionally, I identified two ROP activating GEFs, GEF3 and GEF14, that precede ROP accumulation at the RHID. I found that GEF3 is necessary for root hair initiation and sufficient to form polar domains at the plasma membrane, which recruit ROP2.

After RHID assembly, tip growth is initiated. This process is regulated by an oscillating apical $[Ca^{2+}]_{cyto}$ gradient. In a collaboration we could show that at least three CNGC Ca^{2+} channels are regulating these Ca^{2+} oscillations in root hairs.

Zusammenfassung

Eukaryotische Zellen können eine Vielzahl unterschiedlicher Formen annehmen. Um diese zu entwickeln müssen sie polar wachsen und dafür ihre Ressourcen an einer bestimmten Stelle in der Zelle konzentrieren. In den letzten Jahrzehnten wurde unser Verständnis von polarem Zellwachstum und den regulierenden Prozessen stark erweitert. Allerdings sind dabei die Initiation und besonders der zeitliche Ablauf der Proteinrekrutierung, noch immer weitestgehend unverstanden.

Ziel dieser Arbeit war es besser zu verstehen wie eine polare Domäne etabliert wird und wie sich die Wachstumsmaschinerie zusammensetzt. Als Modelsystem benutzte ich Wurzelhaarzellen von *Arabidopsis thaliana*, die schlauchartige Fortsätze aus Epidermiszellen bilden und anhand dessen etablierte ich eine Zeitreihe der Proteinanreicherung an der Wurzelhaarinitiationsdomäne (WHID).

Um sensitive Messungen zu ermöglichen, quantifizierte ich die Eigenschaften von 10 fluoreszierende Proteinen in Pflanzen. Das hellste Fluorophor ermöglichte die Erfassung kleinster Proteinmengen und deren Anreicherung and der WHID auf endogenem Niveau. Die Untersuchung des zeitlichen und räumlichen Verhaltens von 30 Proteinen zeigte, dass sich unterschiedliche Proteine spezifisch in bestimmen Phasen der Wurzelhaarentwicklung anreichern. Darüber hinaus wurden vier neue Faktoren identifiziert, die im Zusammenspiel mit bekannten RhoGTPasen (ROPs) für die Wurzelhaarinitiation wichtig sind. Für ROP2 konnte ich zeigen, dass die Aktivität, sowie die Interaktionsdomäne und der C-Terminus entscheidend für seine Membrananlagerung und die Rekrutierung zur WHID sind, wobei S-Acylierung dabei keine Rolle spielte. Zwei der identifizierten Faktoren an der WHID, der Aktin regulierende SCAR/WAVE Komplex und die unbeschriebene Rezeptorkinase PRK7, führten beide zu der Initialisierung von neuen Projekten.

Zusätzlich identifizierte ich zwei ROP aktivierende GEFs, GEF3 und GEF14, die sich vor ROP2 an der WHID anreichern. Ich konnte zeigen, dass GEF3 nötig für die Wurzelhaarbildung ist und eigenständig Domänen an der Plasmamembran bilden kann, die ROP2 dorthin rekrutiert.

Nach der Wurzelhaarinitialisierung steuert ein oszillierender $[Ca^{2+}]_{cyto}$-Gradient das Spitzenwachstum. In einer Zusammenarbeit konnten wir zeigen, dass mindestens drei CNGC Ca^{2+}-Kanäle diese $[Ca^{2+}]_{cyto}$-Oszillationen regulieren.

Chapter I

–

Protein accumulation at a polar membrane domain

–

At the right time, at the right spot

1 Introduction

1.1 Initiation of polar cell growth

Every morphological change of a cell is a complex mechanism that involves the regulation of multiple cellular processes. To grow in a polar manner, cells need to establish an interior pushing force and at the same time relax the restricting extracellular matrix to expand into this region. Additionally, it is essential that new building material is delivered to the growth region in a precise and coordinated manner, to prevent uncontrolled growth or loss of cell integrity. To control all these mechanisms, numerus factors are required and linked in multiple feedback loops. Many studies were conducted in multiple model organisms over the last decades, showing the interconnected network of cellular components. As a result, we have a profound understanding of the large regulatory networks, necessary for polar cell growth.

One of the best studied model organisms for the regulation and initiation of polar cell growth is the budding yeast *Saccharomyces cerevisiae*. Budding yeast has two forms of polar growth, budding and shmoo formation. In both processes, small GTPases of the Rat sarcoma (Ras) superfamily were found to be central players (Park and Bi, 2007; Bi and Park, 2012). These small GTPases are molecular switches that have guanosine triphosphate (GTP) bound in their active and guanosine diphosphate (GDP) bound in their inactive state. They regulate multiple downstream target proteins, controlling most aspects of polar growth (Etienne-Manneville, 2004). To control the activation of small GTPases, each molecular switch is controlled by activating GUANINE NUCLEOTIDE EXCHANGE FACTORs (GEFs), which exchange the bound nucleotide for GTP, and inactivating GTPase ACTIVATING PROTEINs (GAPs), which trigger the hydrolysis of the bound nucleotide to GDP (Etienne-Manneville et al., 2002; Schmidt and Hall, 2002). GAPs are called “activating” because they activate hydrolysis, but they inactivate GTPase function (Figure 1.1). During bud formation, the small RAS-RELATED GTPase 1 (RSR1) is controlled by the GAP BUD2 and the GEF BUD5, to define the position for polar growth initiation (Bender and Pringle, 1989; Chant et al., 1991; Park et al., 1993). Downstream of this module, RSR1 activates the GEF CELL DIVISION CYCLE 24 (CDC24), which in turn regulates the activity of the Ras homologue

(Rho)-like GTPase CELL DIVISION CYCLE 42 (CDC42) CDC42 (Hartwell et al., 1974; Adams, 1990; Johnson, 1990; Zheng et al., 1994). To further control GTPase activity GDP/GTP DISSOCIATION INHIBITORs (GDIs) inhibit GTPases by direct binding of inactive GTPases, blocking the exchange of the bound nucleotide. This binding removes small GTPases from the activation cycle by GEFs and GAPs and simultaneously removes them from the plasma membrane (Leonard et al., 1992; Dovas and Couchman, 2005) (Figure 1.1).

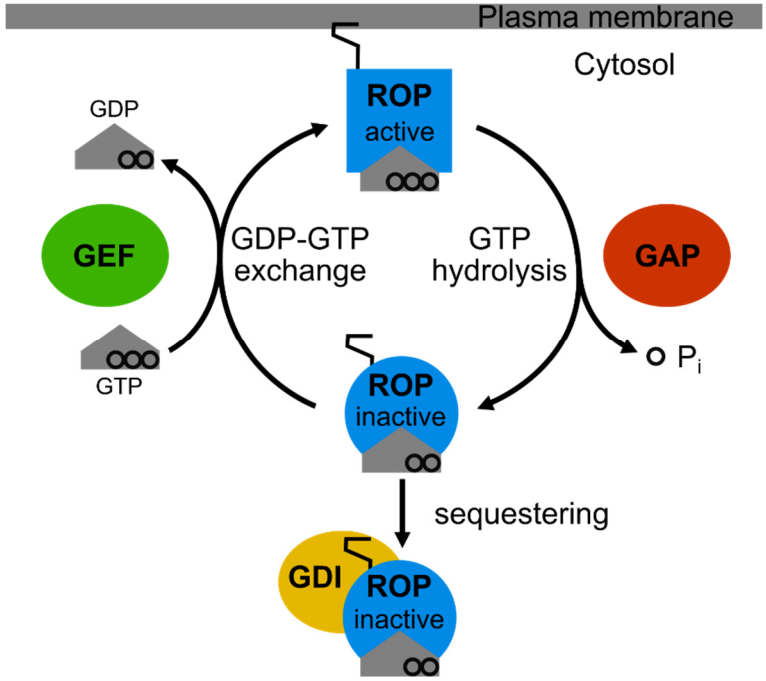

Figure 1.1 Regulation cycle of GTPase activity

Model showing the regulation of GTPase activity on the example of RHO GTPases OF PLANTS (ROP). The shown mechanisms are common for all GTPases of the Rho-family. Active ROPs are predominantly attached to the plasma membrane by a membrane anchor, inactive ROPs are predominantly in the cytosol. GAP proteins trigger GTPase activity of ROPs and thus GTP hydrolysis. GEFs mediate the exchange of the bound nucleotide from GDP to GTP in ROPs. GDI bind to inactive ROPs and sequester them in the cytosol, which also inhibits activation by GEF.

Like in other growth processes, CDC42 is the central factor regulating multiple cellular processes, such as membrane modification, modification of the extracellular matrix, or rearrangement of the cytoskeleton (Etienne-Manneville, 2004). Thus, the GEF-GTPase modules regulate multiple aspects of polar growth, like positioning of the bud and the growth process itself. Similar to *Saccharomyces cerevisiae*, also in

other model systems, like migrating animal cells, growing nerve cells, or tip growing cells of filamentous fungi, mosses and vascular plants, small GTPases were found to be major regulators of polar growth processes (Raftopoulou and Hall, 2004; Riquelme, 2013; Rounds and Bezanilla, 2013; Russell and Bashaw, 2018). This indicates that the general concept of polar growth is a very conserved mechanism, using similar components.

A difference between all these systems is the trigger, why cells get polarized and grow into a certain direction. Thus, the signaling components, including receptors and GTPase effectors, upstream of small GTPase regulation differ for each process. However, the common feature for all cells is that small GTPases need to be recruited and restricted to a certain location at the plasma membrane in order to control polar growth in a local and temporal manner (Etienne-Manneville, 2004; Park and Bi, 2007; Craddock et al., 2012). For example, in *Saccharomyces cerevisiae* the landmark proteins BUD8/BUD9 and AXIAL BUDDING 1 (AXL1)/AXL2 recruit BUD5/RSR1 and thus the CDC24/CDC42 pathway to the bud emergence site (Roemer et al., 1996; Harkins et al., 2001). Except for fungi, no special landmark proteins are known in other model systems, like in plants. As homologues to fungal Landmark proteins could not be identified in other eukaryotes, different mechanisms are required to recruit small GTPases to the plasma membrane. Despite the great knowledge we have about the growth regulation of tip growing plant cells, it is still unknown how small GTPases get initially polarized at the plasma membrane.

Additionally, to discover all components required for tip growth, its initiation and regulation, it is essential to understand the timing of action of individual components. Studies on other complex mechanisms, such as cell division or endocytosis, focused especially on the timing of the involved proteins and thereby gained a better understanding of how the cellular machineries work (Kaksonen et al., 2005; Cai et al., 2017). Proteins regulating each other do not have to be present at the point of action for the same time but can be present only when the individual function is needed. This temporal component of all parts of a cellular machinery reveals an additional regulation mechanism, which is essential to understand polar growth and especially its initiation.

1.2. The root hair as a model system for tip growth initiation

Root hairs are a very useful system to study the chronological order of the polar cell growth machinery (Frescatada-Rosa et al., 2014; Grierson et al., 2014). Root hairs are unicellular tube-like protrusions that grow perpendicular out of special epidermal cells, called trichoblasts (Figure 1.2 A-C). Trichoblasts are arranged in cell files along the root axis and thus represent a developmental timeline along this axis, as cells differentiate with increasing distance to the apical meristem at the root tip. This allows the observation of all steps of root hair development simultaneously (Figure 1.2 A-C). The first visible event is a bulging of the cell wall, transitioning into fast tip growth with 1-2 µm/min in *Arabidopsis thaliana* (*A. thaliana*), forming the root hair (Schiefelbein and Somerville, 1990; Rounds and Bezanilla, 2013; Grierson et al., 2014). Furthermore, the positioning of the root hair within the trichoblast and its size is highly uniform in *A. thaliana*, with around 10 µm wide hairs always emerging approximately 10 µm from the root ward cell pole (Figure 1.2 A-D) (Schiefelbein and Somerville, 1990; Masucci and Schiefelbein, 1994; Fischer et al., 2006; Stanislas et al., 2015). At this location, proteins accumulate and form a tip growth machinery, regulating and driving the root hair outgrowth. The region at the future site of bulge formation and subsequent root hair emergence, is hereafter called the root hair initiation domain (RHID) (Figure 1.2 D). The mechanism defining the positioning of the RHID is not known but it was shown that Rho-GTPases locate to the RHID and their localization can be controlled by the phytohormone auxin (Molendijk et al., 2001; Jones et al., 2002; Fischer et al., 2006). The morphological pattern of root hairs provides the possibility to predict the site were the root hair growth machinery is assembled and allows the observations of the first steps of polarity establishment. This is a unique advantage of the root hair as a model system for this process.

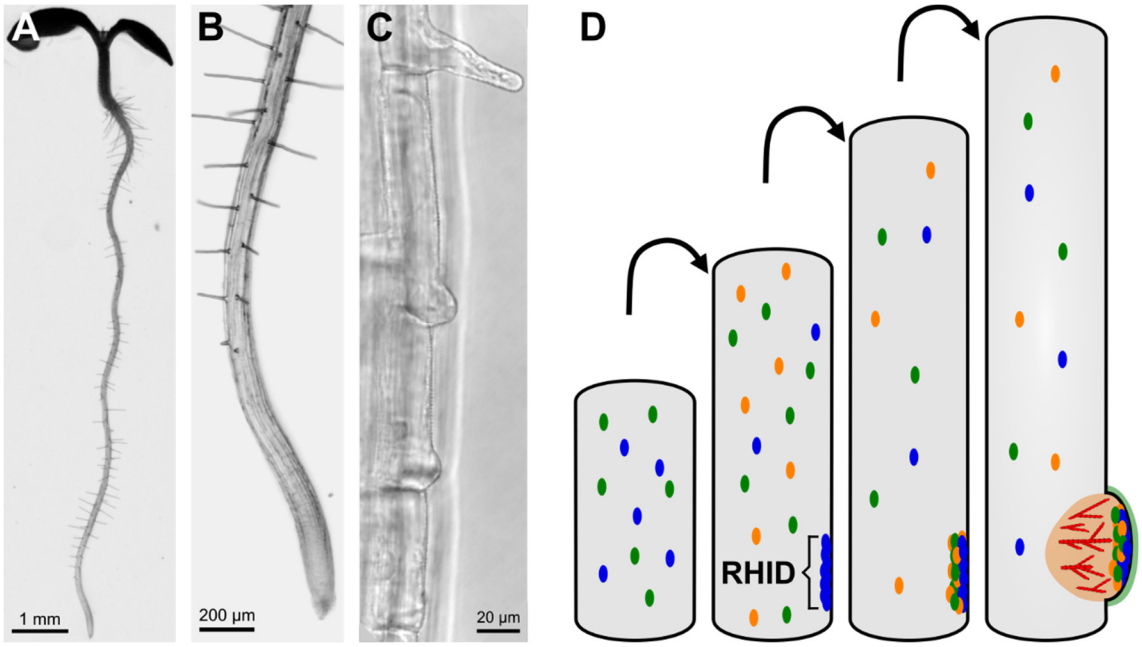

Figure 1.2 The root hair a model system for polar growth initiation

(**A**) Image of a 7-day old *Arabidopsis thaliana* seedling. (**B**) Magnified image of the primary root tip of the same seedling, with root hairs starting to emerge approximately 1 mm from the root tip. (**C**) Image of a trichoblast cell file in the elongation zone. Root hair cells can be seen in different stages of trichoblast development. From bottom to top: trichoblast just before bulging, early and late bulge, trichoblast with tip growing root hair. (**D**) Model of root hair growth initiation. From left to right: Early trichoblast without polar accumulation to the site of root hair emergence; elongating trichoblast with first proteins accumulating and defining the root hair initiation domain (RHID); recruitment of other factors important for root hair initiation to the RHID; beginning of root hair outgrowth, with the cytoskeleton pushing and a loosened cell wall, forming a bulge at a defined location.

1.3 Rho-GTPases of plants and their role in root hair development

During various growth processes, like root elongation, light and hormone sensing, stomatal closure and polar growth (Lin et al., 1996; Kost et al., 1999; Jones et al., 2002; Jeon et al., 2008; Xu et al., 2010; Hwang et al., 2011; Lin et al., 2012; Potocký et al., 2012) the plant-specific family of RHO-TYPE GTPases OF PLANTS (ROPs), were described to be key regulators. Especially in tip growing cells ROPs were shown to be crucial, with the most prominent ROPs being ROP1 in pollen tubes and ROP2 in root hairs (Lin et al., 1996; Lin and Yang, 1997; Molendijk et al., 2001; Jones et al., 2002). ROP2 was shown to localize, in a disc-like pattern, to the future

site of root hair emergence, marking the RHID already before bulging (Molendijk et al., 2001; Jones et al., 2002). However, it is so far not described how ROP2 is recruited to the RHID and how long before bulging ROP2 is present at this site.

The genome of *A. thaliana* encodes 11 ROP genes (Winge et al., 1997; Li et al., 1998) (Figure 1.3 A). They share 70-98% protein sequence identity with each other and 45-64% to other members of the Rho-family from others organisms, like CDC42 from *Saccharomyces cerevisiae* (Zheng and Yang, 2000; Berken and Wittinghofer, 2008). This high conservation of Rho-type GTPases among all eukaryotes makes it likely that results from functional studies in other organism are transferable to ROPs. Based on their hypervariable C-terminus, ROPs can be divided into two major groups, type-I ROPs (ROP1 - ROP8) and type-II ROPs (ROP9 - ROP11). The main difference is a conserved prenylation site at the C-terminus of type-I ROPs, while type-II ROPs undergo S-acylation at C- terminal cysteine residues (Zheng and Yang, 2000). According to the whole protein sequence, ROPs can be divided in a least 4 groups. Group 1 (ROP1-6) can be further divided in to two subgroups (ROP1,3,5 and ROP2,4,6). Group 2 consists of the type II ROPs (ROP9 - ROP11), while. group 3 (ROP7) and group 4 (ROP8) do not group together with any other ROP (Zheng and Yang, 2000) (Figure 1.3 A). Within group 1 and 2 ROPs are highly similar. ROP2 and ROP4 have a sequence identity of 98% and their closest homologue, ROP6, shows 91% and 92% identity, respectively (Figure 1.3 A).

The subcellular localization and especially the plasma membrane association of ROPs are important for their function. Type-I ROPs associate with the plasma membrane by a C-terminal membrane anchor, which gets prenylated with a geranyl-geranyl residue at the C-terminal “CaaX-motif”, where “a” is any aliphatic amino acid and “X” is a leucine in all type-I ROPs (Hancock et al., 1989; Lin et al., 1996; Winge et al., 1997; Li et al., 1998). This lipid moiety is added at the ER membrane, where PROTEIN GERANYLGERANLYTRANSFERASE 1 (PGGT) attaches the lipid residue to the cysteine of the “CaaX-motif” and the “aaX” gets proteolytically cleaved (Wang and Casey, 2016) (Figure 1.3 B). Additionally to prenylation, a neighboring polybasic region stabilizes this membrane association by interaction of the positively charged lysine and arginine residues with negatively charged lipid headgroups (Do Heo et al., 2006; Lavy and Yalovsky, 2006). ROP2 has seven lysins and one arginine within the 11 amino acids before the prenylated cysteine (Figure 1.3 B).

Moreover, ROP membrane attachment is regulated by reversable lipid modifications, like S-acylation at internal cysteine residues. Type-II ROPs (ROP9-11) do not have a C-terminal prenylation site, thus their membrane attachment is solely regulated by S-acylation (Lavy, 2002; Lavy and Yalovsky, 2006). Reversible S-acylation is catalyzed by transmembrane PROTEIN S-ACYLTRANSFERASEs (PATs) (Chamberlain and Shipston, 2015). During root hair growth, PAT24/ TIP GROWTH DEFECTIVE 1 is important for such lipid modifications (Hemsley et al., 2005). Besides the CaaX at the C-terminus, ROP2 has three cysteines at position 8, 20 and 157 (Figure 1.3 B), which could potentially be S-acylated. Such lipid modifications were shown to influence the association of ROP6 with different lipid environments and S-acylation could also changes the diffusion rate of ROP2 in the plasma membrane (Sorek et al., 2007; Sorek et al., 2010). However, those studies where recently corrected due to figure manipulations and republished (Sorek et al., 2017). Thus, it is not clear whether the results hold true, whether ROP2 is modified in a similar way and how this would influence ROP2 function.

Binding of GDP/GTP and the catalytic hydrolysis of GTP occur with conserved amino acids within 5 G-Boxes, spread over the protein (Berken and Wittinghofer, 2008) (Figure 1.3 B). Specific mutations in those G-Boxes prohibit GDP release, which forces the protein into its inactive form and renders the protein dominant negative (DN-*rop*). Other mutations in the G-Boxes can lock the proteins in its active, GTP bound form, rendering the protein constitutively active (CA-*rop*) (Feiguelman et al., 2017) (Figure 1.3 B).

The crystal structure of ROPs, which was resolved for ROP9 and regions of other ROPs (Sormo et al., 2006; Thomas et al., 2007), show that ROPs form a GDP/GTP binding pocket. Dependent on the bound nucleotide, reflecting the activity status, the pocket widens or closes (Feiguelman et al., 2017). This conformational change is permitted by two switch regions (Berken and Wittinghofer, 2008) (Figure 1.3 B).

To regulate ROP activity and localization, ROP effector proteins, like GEFs, GAPs and GDIs bind to the interaction domain / effector binding domain at the N-terminus (Figure 1.3 B). The switch regions are important for these protein - protein interaction, as they undergo conformational changes, and thus regulate effector binding (Berken and Wittinghofer, 2008). GEFs activate ROPs, while GAPs inactivate them (see 1.1, Figure 1.1). In other organisms, like *Saccharomyces*

cerevisiae, these proteins have additional functions in recruiting GTPases to polar plasma membrane domains (Park and Bi, 2007). It is not known if similar mechanisms exist in plants. In root hair growth, only an activating mechanism of ROP2 is described (Huang et al., 2013). Furthermore, GDIs bind to inactive ROPs, like it is described in yeast, inhibiting nucleotide exchange and membrane association by direct binding to the interaction domain and the C-terminal hypervariable region (Dovas and Couchman, 2005; Berken and Wittinghofer, 2008). Hence, membrane attachment of ROPs is dependent on their activity status.

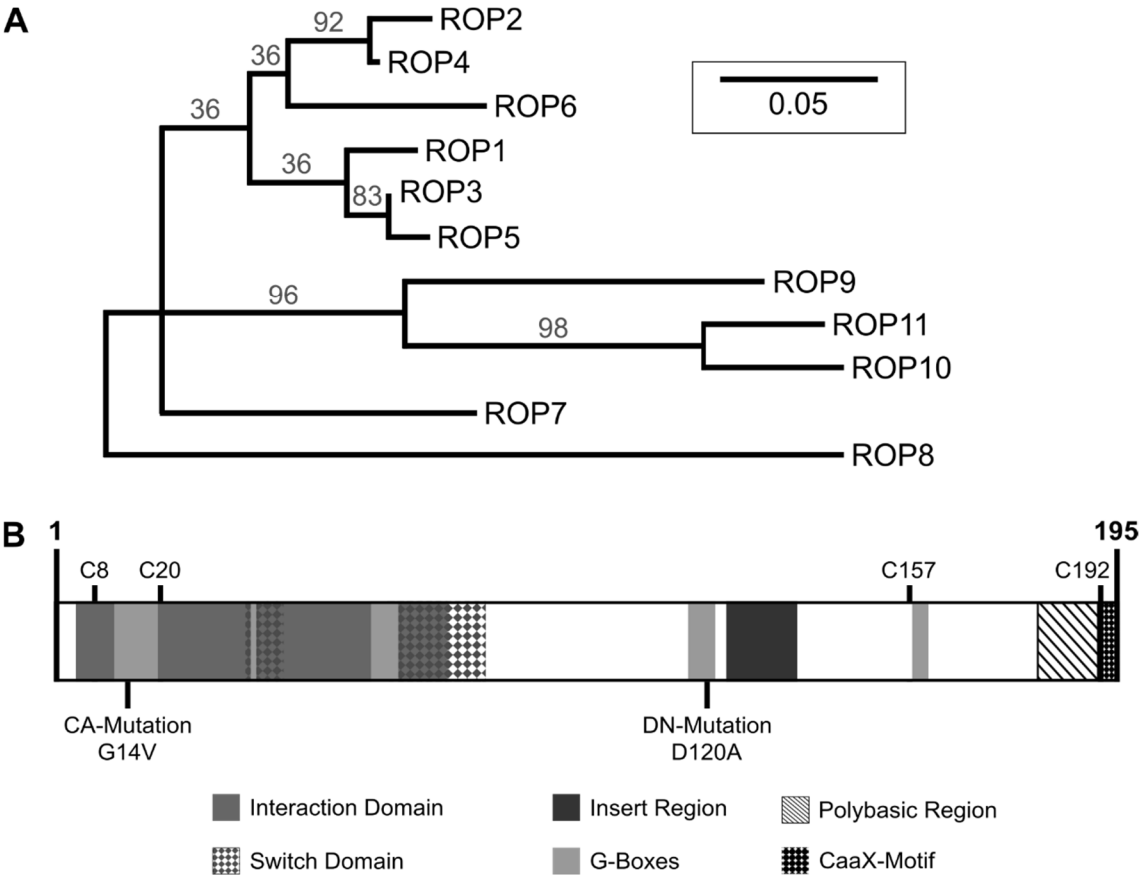

Figure 1.3 The ROP protein family and the Structure of ROP2

(A) Maximum likelihood tree of ROP proteins from A. thaliana, after a multiple sequence alignment (MUSCLE), calculated with www.Phylogeny.fr. Reliability branch support values are given in %. (B) Secondary protein structure of ROP2, from translational START (1) to STOP (195). All predicted domains and regions are indicated and specified in the legend. Position of all cysteine residues (C) is indicated, as well as position and mutation to render ROP2 constitutive active (CA-Mutation, G14V) and dominant negative (DN-Mutation, D120A).

The C-terminal half of ROPs contains a so-called insert region, a Rho-specific region that forms an exposed α-helical structure, present in all Rho-like GTPases (Sormo et al., 2006; Thomas et al., 2007; Berken and Wittinghofer, 2008) (Figure 1.3 B). The function of this domain is not fully understood, but it has been shown that the helix can undergo conformational changes and is involved in effector binding and protein activation (Sormo et al., 2006; Thomas et al., 2007; Berken and Wittinghofer, 2008; Feiguelman et al., 2017).

Many studies have analyzed how Rho-GTPases are associated with the membrane and how these proteins shuttle between membrane and cytosol. However, Rho-GTPases do not just associate with membranes, they accumulate in specific regions of the plasma membrane to form a polar growth domain. In yeast, landmark proteins like BUD8/9 are known that recruit and polarize Rho-GTPases to a plasma membrane domain (Park and Bi, 2007). But in plants it remains unclear how ROPs can be recruited to a plasma membrane domain and if ROPs possess additional intrinsic features for this polarization. It was shown that the GTPase CDC42 can spontaneously polarize in yeast cells, lacking the normal cues for its polarization (Wedlich-Soldner et al., 2003). Furthermore, modeling of ROP2 diffusion suggests that different diffusion rates of the active and inactive form of ROP2 can be sufficient for polarization at the RHID (Payne and Grierson, 2009). However, the molecular mechanisms underlying ROP polarization at the RHID and the intrinsic features of ROPs required for this process still need to be identified.

1.4 The regulatory network of tip growth in *Arabidopsis thaliana*

Multiple factors required for polar tip growth in plants were described over the last decades, using the two tip growing plant cell types – root hairs and pollen tubes – as a model system. From those studies we have a great understanding of the interplay of these factors and the current state of knowledge is reviewed in multiple articles (Qin and Yang, 2011; Guan et al., 2013; Balcerowicz et al., 2015; Mendrinna and Persson, 2015; Bascom et al., 2017) and a detailed description of the components regulating tip growth in plants is described in the following sections and summarized in Figure 1.4.

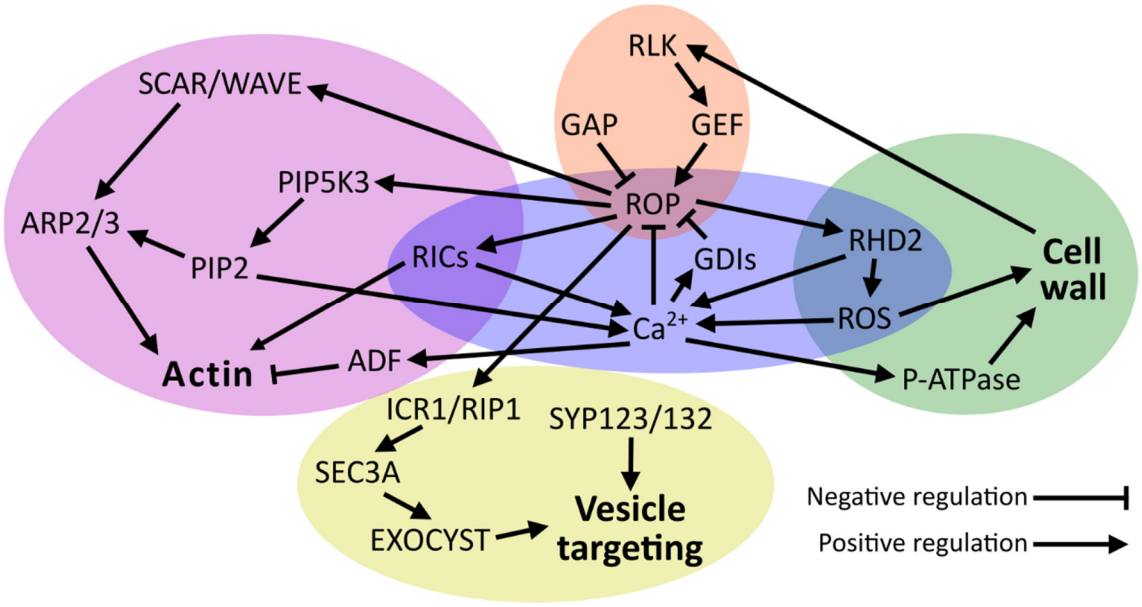

Figure 1.4 The regulatory network of tip growth

Network of factors regulating tip growth in plants. Information from different organisms and pollen tubes and root hairs is combined. Not all known factors and connections are shown, only the relevant factors for this thesis. The network is centered around ROPs and $[Ca^{2+}]_{cyto}$ according to the focus of this thesis. Different cellular processes are highlighted with different colors. Orange: signal transduction and ROP activation/Inactivation, green: Cell wall modifications, Yellow: exocytosis and vesicle trafficking, Purple: Actin cytoskeleton regulation, Blue: ROP-ROS-Ca^{2+} feedback loop.

1.4.1 Receptor-like kinases regulate polar growth

All developmental processes are triggered by internal or external cues, which are sensed by receptors. Plant extensively use transmembrane receptor-like kinases (RLKs) to transmit extracellular cues into the cell. For instance, the TRANSMEMBRANE KINASE (TMK) receptor-like kinases, a family of four genes, are broadly expressed in plants and regulate general growth (Dai et al., 2013). They positively regulate polar growth dependent on the phytohormone auxin in the leave epidermis and in the primary root (Dai et al., 2013; Xu et al., 2014). During cellular tip growth FERONIA (FER) and the members of the POLLEN RECEPTOR LIKE KINASE (PRK) family were described to be important. The receptor-like kinase FER is a regulator of various processes transmitting developmental and environmental signals and seems to be a central factor in stress signaling, connected to Ca^{2+} signaling (Escobar-Restrepo et al., 2007; Deslauriers and Larsen, 2010; Ngo et al.,

2014; Feng et al., 2018). RAPID ALKALINIZATION FACTOR (RALF) peptides were shown to be sensed by FER to convey root elongation and control immune signaling (Haruta et al., 2014; Stegmann et al., 2017), but considering the wide range of processes FER is regulating, it could be possible that FER can bind multiple ligands. In root hair development FER was shown to positively modulate root hair growth (Duan et al., 2010; Huang et al., 2013).

The PRK gene family consists of 8 members in *Arabidopsis*, of which 7 members were found to be specifically or at least highly expressed in pollen and one, PRK7, seems to be expressed in roots (Chang et al., 2012; Takeuchi and Higashiyama, 2016). It was shown that they regulate pollen tube growth (Zhang and McCormick, 2007) and are important for chemotaxis by binding LURE peptides, which are secreted from the female gametophyte (Takeuchi and Higashiyama, 2016).

In addition to these widely expressed RLKs, there are also RKLs specifically expressed in root hairs, like ROOT HAIR SPECIFIC 16 (RHS16), which is not further characterized (Won et al., 2009). Another RLK that was found to be root hair specific is RHS10/ PROLINE-RICH EXTENSIN-LIKE RECEPTOR-LIKE KINASE 13 (PERK13) (Won et al., 2009), which has been shown to negatively regulate root hair growth. It associates with the cell wall and modulates tip growth activity, as loss of function mutants show longer and overexpression lines show shorter root hairs, while bulges are still formed (Hwang et al., 2016).

1.4.2 ROP effector

One of the downstream factors of RLK signaling are GEFs, which directly bind to the intracellular part of RLKs. This binding is dependent on the activity status of the RLK and the activity of GEFs is in turn controlled by the RLK (Zhang and McCormick, 2007; Duan et al., 2010; Chang et al., 2012; Yu et al., 2017). This activation can be transmitted, amongst others, by phosphorylation of the GEF (Zhang and McCormick, 2007; Chang et al., 2012; Huang et al., 2013).

The activated GEFs then activate ROPs, by exchanging GDP to GTP. In plants, ROP activation is catalyzed by a plant-specific family of ROP-GEFs, hereafter just called GEFs, which has 14 members in *Arabidopsis* (Berken et al., 2005; Gu et al., 2006). Multiple GEFs have been shown to regulate ROP activity in tip growing cells, like GEF1 and GEF12, downstream of PRK signaling, in pollen tubes and GEF4 and

GEF10, downstream of FER signaling, during root hair elongation (Zhang and McCormick, 2007; Chang et al., 2012; Huang et al., 2013). Inactivation of ROPs happens through hydrolysis of GTP to GDP, which is catalyzed by GAPs (Etienne-Manneville et al., 2002). Even though multiple GAPs have been identified, only in pollen tubes RopGAP1 and the GAP ROP1 ENHANCER 1 (REN1) were shown to modulate ROP activity (Wu et al., 2000; Fu et al., 2001; Wu et al., 2001; Hwang et al., 2008). So far, no ROP regulating GAP was described in root hair development. Additionally to GEFs and GAPs, ROP activity is regulated by GDIs. The GDI SUPERCENTIPEDE 1 (SCN1) fulfills this function during root hair growth, where it regulates the activity of ROP2 (Carol et al., 2005).

To activate downstream targets, ROPs do not act alone. Several proteins interact with active ROPs and were shown to transmit ROP activity. The INTERACTOR OF CONSTITUTIVELY ACTIVE ROP 1 (ICR1) / ROP INTERACTIVE PARTNER 1 (RIP1) is important for vesicle trafficking, root cell elongation and pollen tube growth (Lavy et al., 2007; Li et al., 2008). Furthermore, the family of ROP-INTERACTIVE CRIB (CDC42- and RAC-interactive binding) MOTIF-CONTAINING PROTEINs (RIC) is required for activating downstream targets (Wu et al., 2001). For example, RIC7 together with ROP2 are required to regulate stoma opening and RIC1 with ROP6 and RIC4 with ROP2 regulate different aspects of the cytoskeleton during pavement cell indentation (Fu et al., 2005; Hong et al., 2015). Moreover, different RICs can bind the same ROP to transmit different actions simultaneously. RIC3 and RIC4 both bind to ROP1 during pollen tube growth to regulate Ca^{2+} signaling and actin polymerization, respectively (Gu et al., 2005).

1.4.3 A ROP-Ca^{2+}-ROS feedback loop regulates tip growth

During tip growth ROPs play an important role as they regulate multiple downstream proteins and furthermore link different cellular processes and coordinate their regulation through feedback loops. Those feedback mechanisms are important to maintain cell integrity, balancing growth and restricting mechanisms. This balance is achieved by negative feedback-loops in which one factor promotes its own inhibitor. The second messenger $[Ca^{2+}]_{cyto}$ (cytosolic calcium ion) is one key molecule in regulating those ROP dependent feedback loops during tip growth (Hwang et al., 2005). ROPs promote growth by activating actin polymerization and

in parallel initiate the increase of $[Ca^{2+}]_{cyto}$ (Kost et al., 1999; Li et al., 1999; Molendijk et al., 2001). High $[Ca^{2+}]_{cyto}$ concentrations in turn inactivate ROPs, by triggering the release of ROPs from the plasma membrane, possibly by making it -available for binding of GDIs (Hwang et al., 2010; Wu et al., 2013; Himschoot et al., 2015). This feedback system leads to an oscillation of $[Ca^{2+}]_{cyto}$ concentrations and ROP activity oscillates with slightly shifted phases in the growing region of pollen tubes (Hwang et al., 2005; Cárdenas et al., 2008). Additionally to the inhibitory effects, $[Ca^{2+}]_{cyto}$ triggers the production of reactive oxygen species (ROS) through activating NADPH oxidases, like ROOT HAIR DEVECTIVE 2 (RHD2) / RESPIRATORY BURST OXIDASE HOMOLOG C (RBOHC) (Takeda et al., 2008; Kimura et al., 2012) and acidification of the cell wall, which is executed by plasma membrane ATPases (P-ATPases). Both leads to a loosening of the cell wall (Monshausen et al., 2007; Monshausen et al., 2009; Haruta et al., 2015). This is necessary to reduce the restricting force from the extracellular matrix, while actin polymerization creates a pushing force that drives growth. This has to happen in a very controlled manner, as plant cells have a high turgor pressure and loosening the cell wall too much would result in swelling or even bursting of the cell. Therefore, it is essential that cell wall loosening is controlled and locally restricted. In a positive feedback, ROS stimulates Ca^{2+} release to further inhibit ROP function (Foreman et al., 2003). After the $[Ca^{2+}]_{cyto}$ concentration is back to a base level, ROPs can be activated and associate with the plasma membrane after they are released from GDIs and can in turn activate their downstream targets (Hwang et al., 2005; Monshausen et al., 2007). During root hair growth RHD2 and Ca^{2+} channels are among those downstream targets (Mangano et al., 2016; Schmidt and Kunkowska, 2016). This results in two intertwined feedback loops, controlling themselves and each other to fine tune cellular growth and restriction simultaneously.

1.4.4 Vesicle trafficking during tip growth

Growing cells not only need to push their boundaries forward using the cytoskeleton, it is also important to supply the growing region with new material, like proteins, membrane and cell wall components. The needed material is delivered in vesicles through exocytosis. This mechanism is regulated by the EXOCYST complex, which is an octameric protein complex and is thought to tether exocytic vesicles to the

plasma membrane, where they eventually fuse (Guo, 2015). There are components of the EXOCYST complex at the plasma membrane marking the vesicle destination, while other parts sit on the vesicle surface. When the components fuse to form the EXOCYST complex, the vesicle is tethered close to the membrane and the fusion machinery can be recruited (Guo, 2015). ROPs regulate this machinery via binding of the EXOCYST COMPLEX COMPONENT SEC3A (SEC3A) together with ICR1/RIP1 (Lavy et al., 2007). SEC3A, which is necessary for various developmental processes, localizes to the plasma membrane and is enriched in the apical region of growing root hairs (Zhang et al., 2013b).

After an exocytic vesicle reached the plasma membrane and is tethered to it by the EXOCYST complex, it fuses with the membrane by an SOLUBLE NSF (N-ETHYLMALEIMIDE-SENSITIVE-FACTOR) ATTACHMENT RECEPTOR (SNARE) complex. Similar to the EXOCYST complex, there are SNAREs on the vesicle and on the target membrane and if both parts of the complex are brought together they can change their confirmation permitting membrane fusion (Ungermann and Langosch, 2005; Han et al., 2017). The two plasma membrane localized SNAREs SYNTAXIN OF PLANTS 123 (SYP123), which is root hair specific and enriched at the root hair apex, and SYP132, which is ubiquitously expressed and evenly distributed within the cell, were both shown to be involved in root hair growth (Ichikawa et al., 2014). The enrichment of EXOCYST components and SNAREs leads to local vesicle targeting to the growing apex, which delivers new material to this region (Rounds and Bezanilla, 2013).

1.4.5 Membrane lipids regulating polar growth

The plasma membrane of pollen tube and root hair apex are characterized by enrichment of certain lipids (Helling et al., 2006; Potocký et al., 2014; Stanislas et al., 2015; Platre et al., 2018). This is partly achieved by targeted vesicle trafficking that changes the lipid composition at the target membrane (Grebnev et al., 2017). For example, sterols accumulate at the site of root hair emergence and are thought to be required for tip growth, as they are important to convey membrane curvature (Stanislas et al., 2015). Another important class of lipids for polar growth are phosphatidylinositols (PtdIns), as they are an important common aspect of Ca^{2+} and ROP signaling pathways. The special feature of PtdIns is that the inositol headgroup

can be phosphorylated at 3 hydroxy groups. Those different phosphorylated forms can be recognized by proteins due to the individual structure and the negative charge of the phosphate groups (Cole and Fowler, 2006; Munnik and Nielsen, 2011). Moreover, it was shown that individual PtdIns predominantly appear in specific membrane compartments of the secretory pathway (Simon et al., 2014; Platre et al., 2018). The two most prominent PtdIns in root hair tip growth are phosphatidylinositol-4-phosphate (PI4P) and phosphatidylinositol 4,5-bisphosphate (PI4,5P2 or PIP_2), which are both most abundant in the plasma membrane. PI4P localizes to the subapical regions of the root hair, while PIP_2 accumulates at the root hair apex (Kost et al., 1999; Vincent et al., 2005; van Leeuwen et al., 2007; Thole et al., 2008; Vermeer et al., 2009). PIP_2 localization is controlled by the PHOSPHATIDYLINOSITOL-4-PHOSPHATE 5-KINASE 3 (PIP5K3), which phosphorylates PI4P to generate PIP_2 (Kusano et al., 2008). Another factor maintaining PIP_2 localization in root hairs is CAN OF WORMS1 (COW1) that localizes to the root hair apex by direct binding of PIP_2 and stimulation of PI4P production, which is the precursor of PIP_2 (Böhme et al., 2004). Both proteins are important for normal root hair growth, as mutants of PIP5K3 and COW1 have short hairs or hairs with aberrant morphology (Böhme et al., 2004; Kusano et al., 2008). PIP_2 is an important signaling molecule, which can be cleaved into inositol1,4,5-trisphosphate (IP3) and diacylglycerol (DAG). Both are second messenger molecules regulating multiple cellular processes, like Ca^{2+} release from internal sources, or actin polymerization (Munnik and Nielsen, 2011; Heilmann, 2016). Additionally, PIP_2 acts as a binding platform for proteins at the plasma membrane. Proteins with positively charged domains, like the polybasic region of ROPs, can specifically bind the negatively charged PIP_2 and thereby be localized to certain regions within the membrane (Cho and Stahelin, 2005; Do Heo et al., 2006; Skwarek and Boulianne, 2009). Those properties of PIP_2 link different pathways, like ROP and Ca^{2+} signaling, and allow signaling events in a locally restricted area. To restrain PIP_2 to the root hair apex and to avoid uncontrolled growth it is important to balance PIP_2 levels (Munnik and Nielsen, 2011; Heilmann, 2016). Necessary for this regulation are for example ROOT HAIR DEVECTIVE 4 (RHD4), a phosphatidylinositol-4-phosphate phosphatase; MUTANT ROOT HAIR 3 (MRH3) (Jones et al., 2005), a phosphatidylinositol-5-phosphate phosphatase; and the

ADP RIBOSYLATION FACTOR-GAP (ARF-GAP) ARF-GAP DOMAIN 1 (AGD1), which regulate secretion and thus delivery of lipids. Those factors localize to intracellular vesicles of the Golgi or the *trans*-Golgi network and regulate PI4P production and delivery to the growing tip to balance and fine-tune PIP_2 levels (Jones et al., 2005; Thole et al., 2008; Yoo et al., 2011).

1.4.6 The actin cytoskeleton drives tip growth

A central downstream effector of ROP signaling is actin polymerization, which is a major driving force for tip growth. ROPs trigger actin polymerization by modulating actin polymerization together with RICs, like RIC4 (Gu et al., 2005). Therefore, ROPs bind and regulate the SCAR/WAVE complex, with its core component SUPRESSOR OF cAMP RECEPTOR (SCAR), or Wiskott–Aldrich syndrome protein family Verprolin-homologous protein (WAVE), which activates actin nucleation and polymerization factors (Basu et al., 2004; Szymanski, 2005). In *Arabidopsis* five putative SCAR proteins are present. Additionally to the SCAR/WAVE protein, the complex consists of the essential components NCK-ASSOCIATED PROTEIN 1 (NAP1), SPECIFICALLY RAC1-ASSOCIATED PROTEIN 1 (SRA1), ABL INTERACTOR 1 (ABI1) and the regulatory component BRICK1 (BRK1), which are all single copy genes in *A. thaliana* (Szymanski, 2005). The primary function of this complex, which associates with membranes and was shown to physically interact with ROP2, is to regulate the ACTIN REALATED PROTEIN (ARP) 2/3 complex (Szymanski, 2005; Yanagisawa et al., 2013). The ARP2/3 complex is a multi-subunit complex, which nucleates actin filament polymerization from existing filaments in a defined angle. Thus, the ARP2/3 complex leads to formation of branched actin networks, which are important to push the growing tip forward (Mathur, 2005; Yanagisawa et al., 2013). To control actin polymerization, $[Ca^{2+}]_{cyto}$ regulated ACTIN DEPOLYMERIZATION FACTORS (ADF) or actin severing proteins like PLASMA MEMBRANE ASSOCIATED CALCIUM BINDING PROTEIN 2 (PCAP2) / MICROTUBLE-ASSOCIATED PROTEIN 18 (MAP18) arrest the polymerization of new filaments in a special and temporal controlled manner (Smertenko et al., 1998; Dong, 2001; Augustine et al., 2008; Kato et al., 2010; Zhu et al., 2013). Thus, multiple pathways, which are all linked by feedback loops control

actin polymerization, which creates a pushing force that drives tip growth through a fine actin network.

1.5 The aim of Chapter I

The described factors form a signaling and regulatory network with multiple feedback loops to control root hair growth. Tip growth is a fine balance between cell growth and cell integrity and requires fine-tuning of all involved cellular processes. Even though this tip growth machinery is well described in plants and other model organisms, its initial assembly and how the factors are recruited to a specific location at the plasma membrane is not well understood. Only in yeast cells, landmark proteins are described, that define the location to which the Rho-GTPase dependent growth machinery gets recruited. In plants, no such proteins are known, and it is still unclear how the proteins are recruited to the RHID and how the tip growth machinery is assembled.

The goal of this chapter of this thesis was to understand the initial steps of polarity establishment and to investigate how the location of a polar domain, like the RHID, is defined. Therefore, I analyzed the temporal recruitment of known and unknown factors involved in tip growth or ROP2 signaling and created a spatiotemporal map of RHID establishment. This allowed conclusions about the functional order of the involved factors function and lead to the identification of novel players required for RHID establishment and root hair initiation.

As ROP2 was described as the first RHID marker, an additional goal was to identify structural features of ROP2, important for its recruitment to the RHID and its function in root hair development. For this several ROP2 mutant derivatives were investigated for localization und functionality.

2 Results

2.1 ROP2 as a marker for timing of root hair development

2.1.1 ROP2 localization during root hair development

ROPs are crucial factors for tip growth as many factors modulate ROP pathways or are in turn regulated by ROPs. For instance, ROP2 was described to be important for root hair initiation (Jones et al., 2002) and further studies suggest that also other ROPs, like ROP4 and ROP6 are involved in this process, as they accumulate at the RHID (Molendijk et al., 2001; Stanislas et al., 2015). As all ROPs are very similar, it is likely that multiple ROPs can have redundant functions during root hair development (Figure 1.3). To investigate if other ROPs are present in trichoblasts and regulate root hair initiation, the expression profile of all 11 ROPs was analyzed *in silico* using GENVESTIGATOR. Utilizing expression data from three different studies (Birnbaum et al., 2003; Brady et al., 2007; Wang et al., 2008), ROP expression in trichoblasts was compared to atrichoblasts, neighboring cells in the epidermis that do not grow hairs, and pollen, which is an other cell type in plants that shows tip-growth (Figure 1.5).

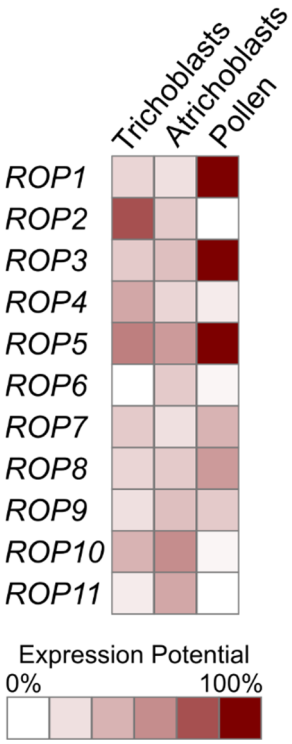

Figure 1.5 Expression of ROPs in tip growing cells

(**A**) Expression profile of all 11 ROP genes of *A. thaliana* in trichoblasts, atrichoblasts and pollen, analyzed with GENEVESTOGATOR with data from {Brady:2007fr, Birnbaum:2003ba, Wang:2008ea}. These cell types were chosen to compare ROP expression between two tip growing cell types (Trichoblasts vs. Pollen), or root epidermal cells with or without root hair (Trichoblast vs. Atrichoblast).

Comparing expression profiles of individual ROPs, it is striking that a group of ROP genes (*ROP1*, *ROP3* & *ROP5*) is expressed predominately in pollen, another group (*ROP7*, *ROP8* & *ROP9*) does not show any clear specificity for a cell type, while others (*ROP6* & *ROP11*) seem to be excluded specifically from these tip growing cell types (Figure 1.5). Additionally, there are 3 ROP genes (*ROP2*, *ROP4* and *ROP10*) that are not expressed in pollen but in the primary root. *ROP10* is preferably expressed in atrichoblasts, while *ROP2* & *ROP4* are higher expressed in trichoblasts (Figure 1.5). Thus, *ROP2* and *ROP4* represent promising targets to investigate their role in root hair development further.

ROP2 was already described to localize to the RHID before any morphological change is visible in trichoblasts (Molendijk et al., 2001; Jones et al., 2002). I therfore chose ROP2 as a developmental reference marker and analyzed described and undecribed factors of root hair development based on their expression, localization and timing in respect to each other.

For this approach a functional fluorescent labeled ROP2 marker line was essential. For this purpose, I expressed *ROP2* under the endogenous promoter fused to different fluorophores (mTurquoise2 (mTrq2), mCitrine (mCit) and mRuby2) in Col-0 plants to be able to combine the ROP2 lines with other markers. Furthermore, ROP2::mCit-ROP2 was transformed into the *rop2-1* T-DNA insertion line (Table 4.1) (Jeon et al., 2008) to test the functionality of the derivative. Additionally, an estradiol inducible mCit-ROP2 construct (mCit-ROP2_ind) was created and transformed into Col-0 to overcome expression level limitations of the native promoter and to analyse overexpression phenotyps in a controlled manner. For each construct and genetic background, a line with moderate expression and no obvious phenotypes was selected. For the inducible construct a line with reliable, homogeneous expression was chosen. All fusion constructs under native and inducible promoter showed similar behavior regarding localization and accumulation at the RHID (Figure 1.6 A – E') and resemble published data (Jones et al., 2002). ROP2 is expressed throughout the root, but its localization varied in individual cell types (Figure 1.6 A, F - J). In the root tip ROP2::mCit-ROP2 was evenly distributed (Figure 1.6 A, F), but in more differentiated cells, beginning in the transition zone between meristem and elongation zone, showed a higher protein abundance at the cell sides perpendicular to the root axis, even though it could not be distinguished between root or shootward

side of the cell (Figure 1.6 A, G). Only in trichoblasts ROP2 additionally accumulated at the cell periphery on the outer side of the cell, the RHID (Figure 1.6 A, H, I). Consistent with earlier reports (Jones et al., 2002), this accumulation started multiple cells before bulging and could be observed throughout root hair development (Figure 1.6 A – E'). In all lines, ROP2 appeared to be both cytosolic and associated with the cell periphery, which became apparent as a discrete line along the cell outline (Figure 1.6 F - J). The localization to the cytoplasm was homogeneous and no association with any cell compartment could be observed, but ROP2 was excluded from the nucleus (Figure 1.6 F, H, I). Previous studies showed, that active ROP is mostly membrane associated (Li et al., 1999; Gu et al., 2003), therefore the observed localization of ROP2 at the cell periphery should indicate its active state. In inducible mCit-ROP2 lines, localization and behavior was similar 3-7 hours after induction (haind) (Figure 1.6 E-E'). Only after long-term overexpression for more than 8 h phenotypes of shifted hairs to the rootward side of the cell and initiation of second hairs within one cell appeared (for effects of inducible overexpression see 2.4.2), which is similar to phenotypes observed in lines constitutively overexpressing ROP2 (Jones et al., 2002).

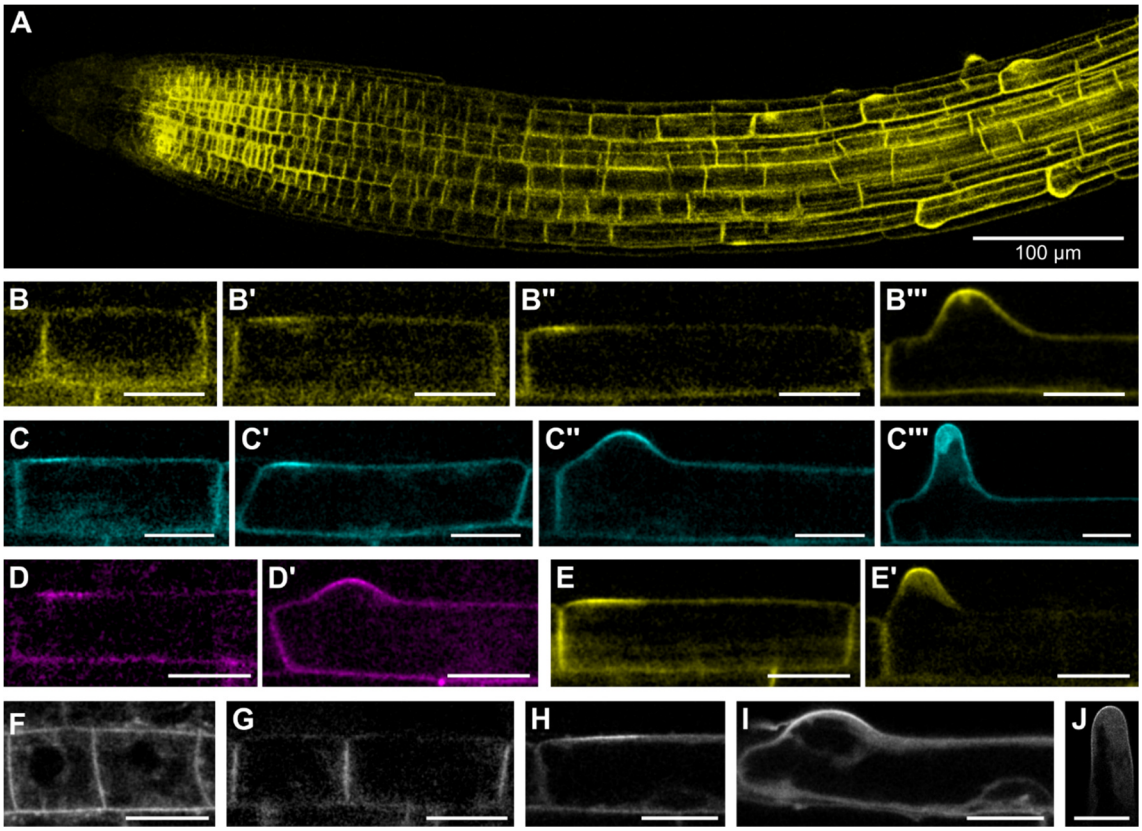

Figure 1.6 Expression and localization of different ROP2 expression constructs in roots

Expression and localization ROP2::mCit-ROP2 primary root tip (**A**) and trichoblast cells in different stages of root hair development (**B-B'''**)in *rop2-1* mutants. Trichoblast in the early elongation zone, without accumulation of mCit-ROP2 at the RHID (**B**); the first cell with mCit-ROP2 accumulation at the RHID (**B'**); cell before root hair bulging (**B''**); trichoblast after bulging (**B'''**). (**C-C'''**) Trichoblast cells in different stages of root hair development expressing ROP2::mTrq2-ROP2. Trichoblast in the early elongation zone, without accumulation of mTrq2-ROP2 at the RHID (**C**); cell before root hair bulging (**C'**); trichoblast after bulging (**C''**); trichoblast with tip growing root hair (**C'''**). (**D-D'**) Expression of ROP2::mRuby2-ROP2 in trichoblast before (**D**) and after (**D'**) bulging. (**E-E'**) Trichoblasts expressing estradiol inducible UBI10::XVE-olexTATA::mCit-ROP2 (mCit-ROP2_ind) before (**E**) and after (**E'**) bulging, 4 hours after induction (haind). (**F-J**) high resolution images of cells in different stages of root hair development expressing ROP2::mTrq2-ROP2. Meristematic cells (**F**), trichoblasts without bulge, before (**G**) and after (**H**) mTrq2-ROP2 accumulation, trichoblast after bulging (**I**) and a growing root hair (**J**) show mTrq2-ROP2 in the cytosol (excluded from the nucleus) and associated with the plasma membrane, visible as a thin line at the cell periphery. Scale bars 20 µm, if not mentioned otherwise.

2.1.2 Quantitative timing analysis of protein accumulation at the RHID

To be able to analyze the timed association of all factors with the RHID, it is important to define reference points for the individual developmental steps. One distinct marker for root hair development is the onset of bulging. This point, where first the morphological outgrowth on the trichoblast surface is visible, can be used to divide the developmental process into an initiation phase and a growth phase. For quantification of protein accumulation, I defined the cell that just starts growing a bulge at the RHID as "cell +1" and the one before that "cell -1" (Figure 1.7 A). To sort proteins of interest into this developmental timeline, their association with the RHID in different developmental steps was analyzed by measuring the signal intensities of corresponding fusion proteins at the RHID normalized to the signal intensity outside the RHID (Int_{in}/Int_{out}, Figure 1.7 B-B'). This ratio, named the polarity index (Pol-Idx), was calculated for each cell along a trichoblast cell file and the average Pol-Idx of multiple cell files (n > 10) was then used to define the timepoint of protein accumulation. Therefore, the plasma membrane marker GFP-LTI6B (Cutler et al., 2000) was used as a reference for nonpolar localization

(Figure 1.7 C-C'). The Pol-Idx values of GFP-LTI6B were close to 1 (SD < 0.172) in all cells and stages (Figure 1.7 E) confirming its property as nonpolar membrane marker. A protein was thereafter defined as polar if its Pol-Idx was significantly higher (p-value < 0.05) than the Pol-Idx of GFP-LTI6B in the same developmental stage. To test the method and to characterize accumulation of ROP2, a functional ROP2::mCit-ROP2 fusion construct in the *rop2-1* mutant background was analyzed (Figure 1.7 D, E). mCit-ROP2 was nonpolar in early developmental steps (cell -7 to -5), but showed a significantly increased Pol-Idx in cell -4 compared to GFP-LTI6B. The Pol-Idx of mCit-ROP2 further increased until the signal at the RHID was approximately two times brighter than outside the RHID (Pol-Idx ~ 2) in cell +1 and stayed at this level (Figure 1.7 E). To further confirm the quantification method and also ROP2 as a stable marker for protein accumulation at the RHID, other ROP2 fusion constructs (ROP2::mTrq2-ROP2; mCit-ROP2_ind) as well as estradiol inducible lines of mCit-ROP4_ind and mCit-ROP6_ind, the two closest homologous of ROP2, were analyzed and compared to GFP-LTI6B (Figure 1.7 F). Both ROP2 constructs, as well as mCit-ROP4_ind, showed a similar behavior compared to ROP2::mCit-ROP2. At cell -4 the first significant protein accumulation could be observed and a maximum Pol-Idx of ~2 was reached at cell +1. mCit-ROP6_ind accumulated one cell later (cell -3) at the RHID in a similar way (Figure 1.7 F). The inducible lines showed a slower increase of the Pol-Idx, which is likely due to stronger expression and higher cytosolic pool affecting the Pol-Idx (Figure 1.6 E and 1.7 F). Those results show that ROP2 consistently accumulates at cell -4, which is not ROP2 specific but seems to be a general feature of ROPs demonstrated by mCit-ROP4_ind and mCit-ROP6_ind, the two closest homologues of ROP2. Taken together, the beginning of root hair bulging, as a morphological marker, GFP-Lti6B as a nonpolar reference and ROP2 as a reliable early polar molecular marker for the RHID, provide a strong system to characterize the timing of protein accumulation at the RHID.

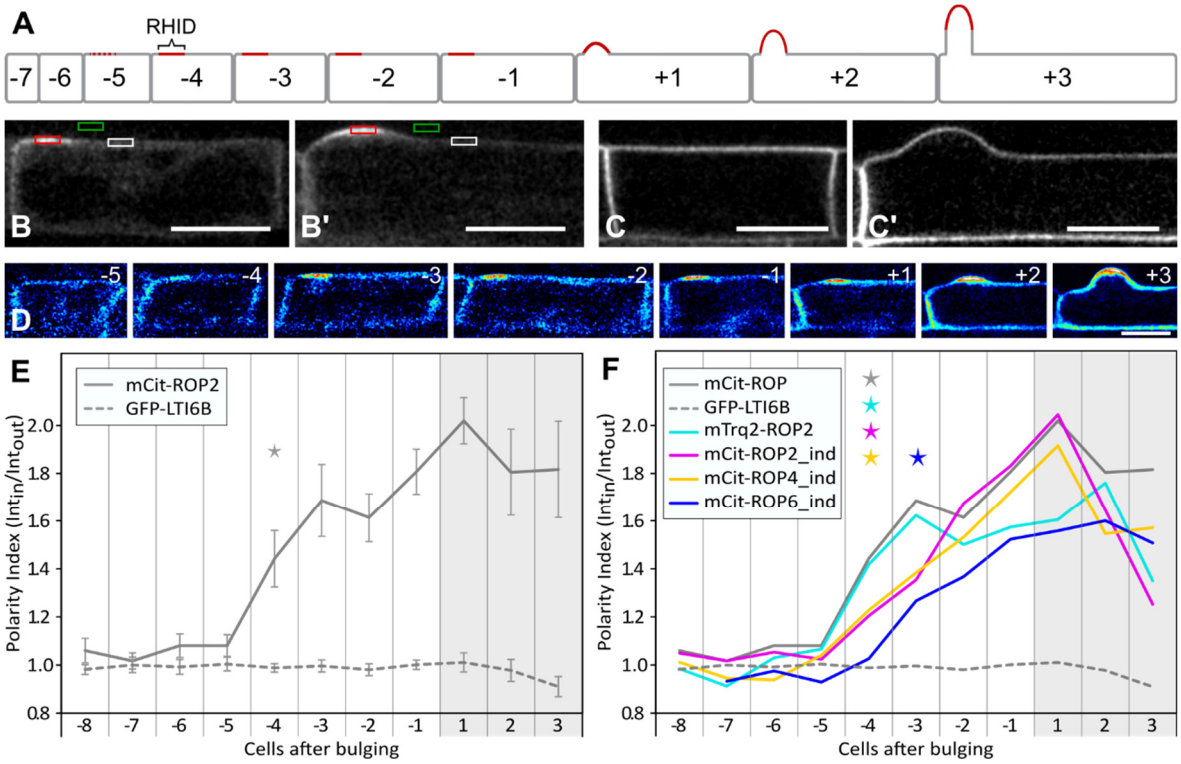

Figure 1.7 ROP2 as early marker for protein accumulation during RHID establishment

(**A**) Model of root hair development and RHID establishment. The first cell with a visible morphological change (root hair bulging) is defined as cell +1. The neighboring cells are numbered accordingly. The RHID is initiated several cells before bulging, with ROP2 being the earliest known marker, accumulating at cell -4, and builds a functional tip growth machinery until cell -1. After bulging, tip growth is usually initiated in cell +3 or cell +4. (**B-C'**) Example images of mCit-ROP2_ind, a marker accumulating at the RHID (**B-B'**) and the equally distributed plasma membrane marker 35S::GFP-LTI6B (**C-C'**). Cells just before (**B, C**) and after bulging (**B', C'**) are shown. Boxes in **B-B'** show regions used to calculate the polarity index (Pol-Idx). Therefor the signal intensity at the RHID (red) was divided by the signal intensity outside the RHID (white). Before this calculation the background value (green) was subtracted from both values. (**D**) Root hair file from cell -5 to +3 expressing ROP2::mCit-ROP2 in *rop2-1* shown in pseudo-color ("Royal" look up table (LUT)). mCit-ROP starts accumulating in cell -4. (**E**) Pol-Idx of root hair files expressing ROP2::mCit-ROP2 (n = 11) or 35S::GFP-LTI6B (n = 14) calculated for cell -8 to cell +3. Grey background indicates cells after bulging, error bars show standard error of mean (SEM), star indicates first Pol-Idx significantly different from GFP-LTI6B. (**F**) Pol-Idx of root hair cell files expressing different ROP fusion proteins, the Pol-Idx of mCit-ROP2 and GFP-LTI6B from (**E**) are shown again as reference. Stars in the according color indicate first Pol-Idx significantly different from GFP-LTI6B. n of measured cell files: mTrq2-ROP2 = 10; mCit-ROP2_ind = 13; mCit-ROP4_ind = 17; mCit-ROP6_ind = 11. Scale bars 20 µm.

2.2 Timing and localization of different proteins at the RHID

In trichoblasts, a subset of proteins specifically localizes to the RHID, at the outer side of the cell and form a functional growth domain permitting polar cell outgrowth. To get a better insight into the chronological order of protein recruitment at the RHID, 28 different proteins from various cellular processes were investigated (a list of the investigated markers is given Table 1.1. Furthermore, markers for the signaling molecules $[Ca^{2+}]_{cyto}$ and PIP_2 were included. All chosen candidates were described to be involved in root hair development, reported to be highly expressed in root hair cells, or shown to interact directly or indirectly with ROP2. For all candidates the Pol-Idx values were determined for all stages of early root hair development and sorted into a timeline for protein accumulation at the RHID.

Table 1.1 Genes investigated during RHID establishment

Name	Gene-ID	Function	Construct	Plant source
ArpC2	AT1G13180	ARP2/3 component	ArpC2::GFP-ARPC2	(Havelková et al., 2015)
BRK1	AT2G22640	SCAR/WAVE component	Brk1_BRK1-YFP	(Djakovic et al., 2006)
Fer	AT3G51550	RLK	Fer::FER-GFP	Keinath, unpublished
GEF10	AT5G19560	RopGEF	Gef10::mCit-GEF10	This work
GEF11	AT1G52240	RopGEF	Gef11::mCit-GEF11	This work
GEF12	AT1G79860	RopGEF	Gef12::mCit-GEF12	This work
GEF14	AT1G31650	RopGEF	Gef14::mCit-GEF14	This work
GEF3	At4G00460	RopGEF	Gef3::mCit-GEF3	This work
GEF4	AT2G45890	RopGEF	Gef4::mCit-GEF4	This work
Lti6b	AT3G05890	membrane protein	35S::GFP-LTI6B	(Cutler et al., 2000)
MRH3	AT5G65090	PtdIns-5-P Phosphatase	MRK3-mCit_ind	This work
NAP1	AT2G35110	SCAR/WAVE component	Nap1::GFP-NAP1	(Wang et al., 2016)
PCAP1	AT4G20260	cytoskeleton organization	PCAP1-mCit_ind	This work
PCAP2	AT5G44610	cytoskeleton organization	PCAP2-mCit_ind	This work
Perk13	AT1G70460	RLK	Perk13::PERK13-GFP	Mendrinna unpublished
PIP5K3	AT2G26420	PtdIns-4-P 5-Kinase	Pip5k3::PIP5K3-mCit	This work
PRK7	AT4G31250	RLK	PRK7-mCit_ind	This work
RHD2	AT5G51060	NADPH oxidase	mCit-RHD2_ind	This work
RHS16	AT4G29180	RLK	RHS16-mCit_ind	This work
ROP2	AT1G20090	small GTPase	Rop2::mCit-ROP2	This work
ROP4	AT1G75840	small GTPase	mCit-ROP4_ind	This work
ROP6	AT4G35020	small GTPase	mCit-ROP6_ind	This work
SCN1	AT3G07880	RopGDI	SCN1-mCit_ind	This work
Sec3a	AT1G47550	EXOCYST component	Sec3a::SEC3A-GFP	(Zhang et al., 2013b)
SYP123	AT4G03330	SNARE	Syp123::GFP-SYP123	(Ichikawa et al., 2014)
SYP132	AT5G08080	SNARE	Syp132::GFP-SYP132	(Ichikawa et al., 2014)
TMK1	AT1G66150	RLK	TMK1-mCit_ind	This work
TMK3	AT2G01820	RLK	TMK3-mCit_ind	This work

2.2.1 The actin polymerization machinery at the RHID

The actin cytoskeleton was shown to be essential for tip growth and its polymerization is, amongst others, regulated by the SCAR/WAVE complex. NAP1 is one of the core proteins of the SCAR/WAVE complex and conveys membrane association, while SRA1 was reported to directly interact with ROP2 influencing the activity status of the SCAR/WAVE complex (Basu et al., 2004; Szymanski, 2005; Zhang et al., 2013a). To dissect the timing of actin polymerization at the RHID, the localization of the regulatory SCAR/WAVE complex component BRK1 (Djakovic et al., 2006) and NAP1 (Wang et al., 2016) were investigated in this study. In young trichoblasts, as in most other cells of the root tip, BRK1-YFP and GFP-NAP1 appeared in small puncta at cell edges (Figure 1.8 A, B, D, F) as reported in previous studies (Djakovic et al., 2006; Wang et al., 2016). Later in trichoblast development BRK1-YFP re-localized from the cell edges to the RHID (Figure 1.8 A). This transition happened within cell -4 to -2 and is accompanied by a reduction of fluorescence signal intensity in BRK1::BRK1-YFP lines. After cell -4 the BRK1-YFP was found at the RHID throughout root hair development similar to ROP2 (Figure 1.8 A, J). However, ROPs show a homogeneous distribution at the RHID, whereas BRK1 appears in small, approximately 0.5 - 1 µm, puncta at the cell periphery of the RHID (Figure 1.8 E). It remains unclear what those structures are and if this is functionally relevant. However, this could be an indication that there are hotspots of actin polymerization within the RHID. GFP-NAP1 showed a very similar behavior like BRK1-YFP, but was generally more cytoplasmic. It also localized into puncta at the cell corners and relocalized to the RHID at cell -3 (Figure 1.8 B, F).

The primary function of the SCAR/WAVE complex is to regulate the actin polymerization complex ARP2/3, which leads to actin polymerization at the bound actin filaments creating actin branch sides (Goley and Welch, 2006). To label the ARP2/3 complex I used a marker line expressing a functional GFP-ARPC2 under control of its endogenous promoter (Havelková et al., 2015). GFP-ARPC2 showed homogeneous distribution before bulging and accumulated at the RHID just after bulging, with a significant increase of the Pol-Idx in cell +1 (Figure 1.8 C, J). Compared to the specific localization of GFP-NAP1 and BRK1-YFP of the SCAR/WAVE complex, GFP-ARPC2 of the ARP2/3 complex is more equally distributed throughout the cell and mainly localizing to the cytoplasm (Figure 1.8 C,

G). Only in some cases, GFP-ARPC2 was found to associate with the cell periphery at the RHID, forming a fine line at the tip of RH bulges (Figure 1.8 H, I).

These results show that the actin polymerization machinery accumulates in different phases, with the regulators SCAR/WAVE complex associating clearly before the actin polymerizing ARP2/3 complex.

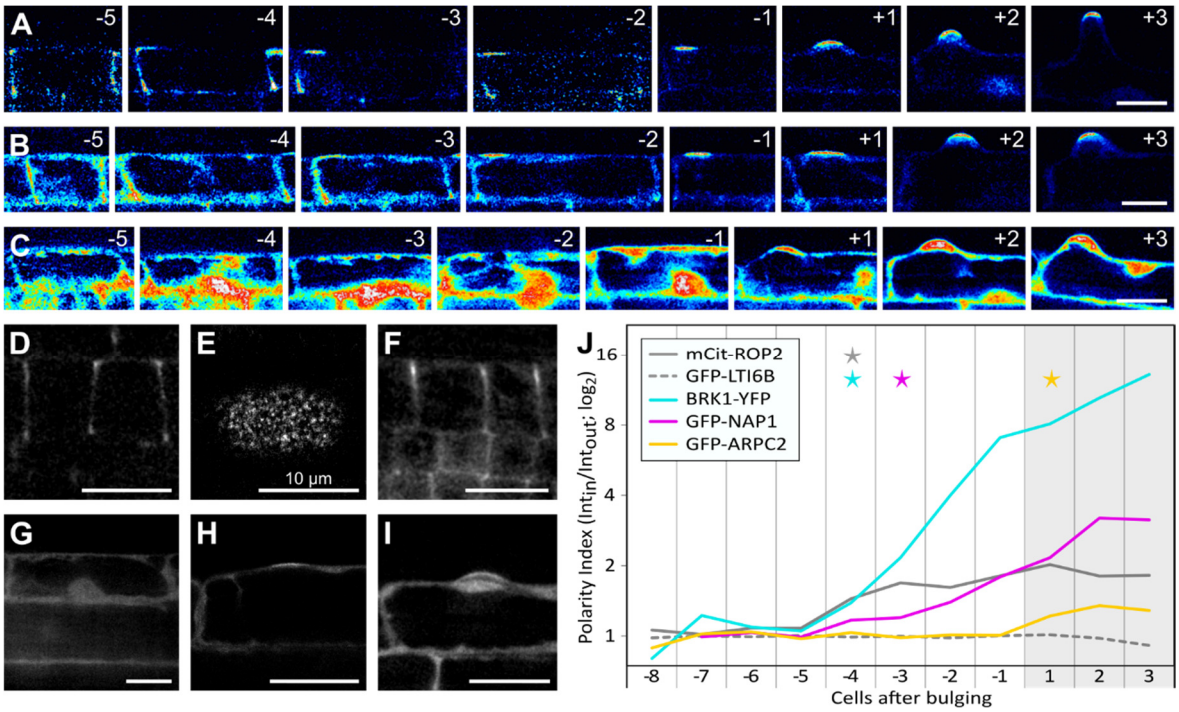

Figure 1.8 Markers for actin polymerization at the RHID

(**A-C**) Root hair files expressing BRK1::BRK1-YFP (**A**), NAP1::GFP-NAP1 (**B**) and ARPC2::GFP-ARPC2 Developmental stage of trichoblasts is indicated by -5 to +3. (**D-E**) high resolution images the markers shown in (**A-C**). BRK1-YFP localizes to cell edges in meristematic cells (**D**) and accumulates in puncta at the RHID (top-view of the RHID) (**E**). (**F**) GFP-NAP1 localizes to cell edges in meristematic cells. GFP-ARPC2 mainly localizes to the cytosol (**G**). After bulging GFP-ARPC2 occasionally localizes to a fine line at the cell periphery of the RHID (**H-I**). (**J**) Pol-Idx of markers shown in (**A-C**) with Pol-Idx values in $\log_2$ scale to account for great value differences. Pol-Idx of mCit-ROP2 and GFP-LTI6B from (Figure 1.6) are shown as reference. Stars in the according color indicate first Pol-Idx significantly different from GFP-LTI6B. n of measured cell files: BRK1-YFP = 12; GFP-NAP1 = 11; GFP-ARPC2 = 12. Scale bars 20 µm, if not mentioned otherwise.

2.2.2 Markers for vesicle trafficking at the RHID

Vesicle trafficking is an important aspect of tip growth as new material needs to be delivered to the growing region and other material needs to be removed to control the fast growth process. I used SEC3A-GFP as a marker for the EXOCYST complex, which was shown to be necessary for root hair growth (Zhang et al., 2013b). During root hair development SEC3A-GFP localized to the plasma membrane and some vesicular structures in the cytosol. SEC3A-GFP was homogeneously distributed in the plasmamembrane before bulging. Polar protein accumulation started in cell +1 ($p = 0.0523$) but a significant Pol-Idx could be measured in cell +2 (Figure 1.9 A, D). As reported before, SEC3A-GFP accumulation was very subtle (Zhang et al., 2013b), which I could confirm as its Pol-Idx reached only 1.5. Nevertheless, the SEC3A-GFP marker indicates that exocytosis is initiated at the RHID during bulging and does not seem to be particularly required before this time point. To confirm those results I also investigated two SNAREs, SYP123 and SYP132, known to be involved in root hair growth (Ichikawa et al., 2014). GFP-SYP123 was shown to be root hair specific and to accumulate at the root hair apex (Ichikawa et al., 2014). I could confirm the root hair specific expression and could detect the first signal in cell -2. GFP-SYP123 localized to the cell periphery with some cytosolic background and significantly accumulated at the RHID (Pol-Idx 1.422) in cell+1 (Figure 1.9 B, D). In contrast to GFP-SYP123, GFP-SYP132 was described to be ubiquitously expressed without obvious accumulations (Ichikawa et al., 2014). I could confirm this expression pattern with similar signal levels in all cells of the primary root and a localization exclusively to the plasma membrane (Figure 1.9 C). GFP-SYP132 showed no obvious polarization to the RHID, but a mild exclusion from the RHID after cell +1 resulting in a Pol-Idx reduction. (Figure 1.9 C, D). GFP-SYP132 did also not polarize in any other region of the cell, instead it homogeneously labeled the cell outlines. Those results show that secretory vesicle trafficking is directed to the RHID at bulging (cell +1). Additionally, special SNAREs, which are required for tip growth, are recruited to the RHID, while others stay homogeneously distributed.

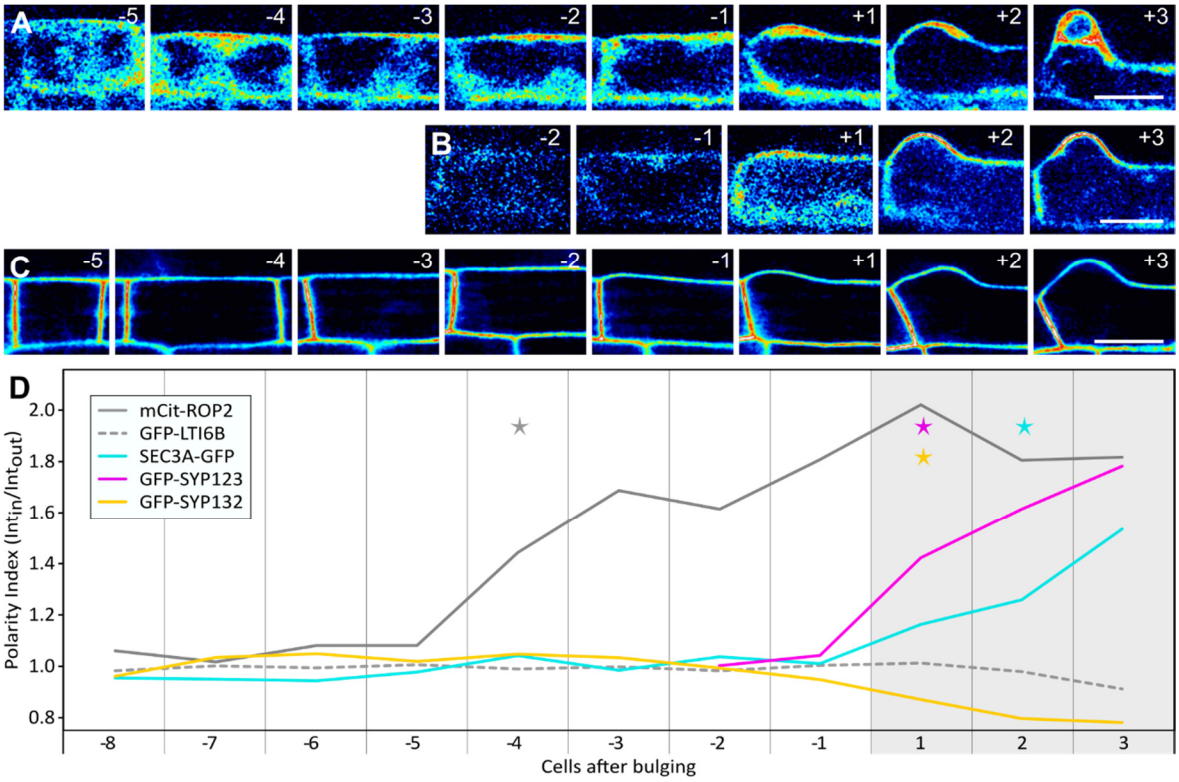

Figure 1.9 Markers for exocytosis at the RHID

(**A-C**) Root hair files expressing SEC3A::SEC3A-GFP (**A**), SYP123::GFP-SYP123 (**B**) and SYP132::GFP-SYP132 (**C**). Developmental stage of trichoblasts is indicated by -5 to +3. For GFP-SYP123 no images before cell -2 are shown as no signal can be detected in these cells. (**D**) Pol-Idx of markers lines shown in (**A-C**). Pol-Idx of mCit-ROP2 and GFP-LTI6B from (Figure 1.6) are shown as reference. Stars in the according color indicate first Pol-Idx significantly different from GFP-LTI6B. n of measured cell files: SEC3A-GFP = 10; GFP-SYP123 = 5; GFP-SYP132 = 10. Scale bars 20 µm.

The work on the SNARES GFP-SYP123 and GFP-SYP132 led to a collaboration with the group of Christopher Grefen (ZMBP, University of Tübingen). SNARES are tail-anchored membrane proteins, which get inserted into membranes by a noncanonical pathway, called the GUIDED ENTRY OF TAIL-ANCHORD PROTEINS (GET) pathway. The group of Christopher Grefen could show that the GET pathway exists in *Arabidopsis* and is required for proper root hair growth (Xing et al., 2017). It was shown that *Arabidopsis* GET proteins insert tail-anchored proteins into membranes, as GFP-SYP123 abundance in the plasma membrane is reduced in *get1* and *get3a* mutants. The fact that GFP-SYP123 still reached the plasma membrane in those mutants, even though significantly reduced, suggests

that there must be an additional mechanism for SNARE membrane insertion, which could also explain the mild phenotype in mutants without a functional GET pathway (Xing et al., 2017). Furthermore, I could show that loss of GET function does not affect SYP123 polarity, as GFP-SYP123 is still accumulating in root hair bulges and growing hairs in *get1* and *get3a* mutants (Figure 1.10), which showed that SNARE trafficking in the plasma membrane is GET independent. The described results, to which I contributed measurements of the GFP-SYP123 polarity in root hair bulges of wild type (WT) and mutant lines, were published in PNAS (Xing et al., 2017).

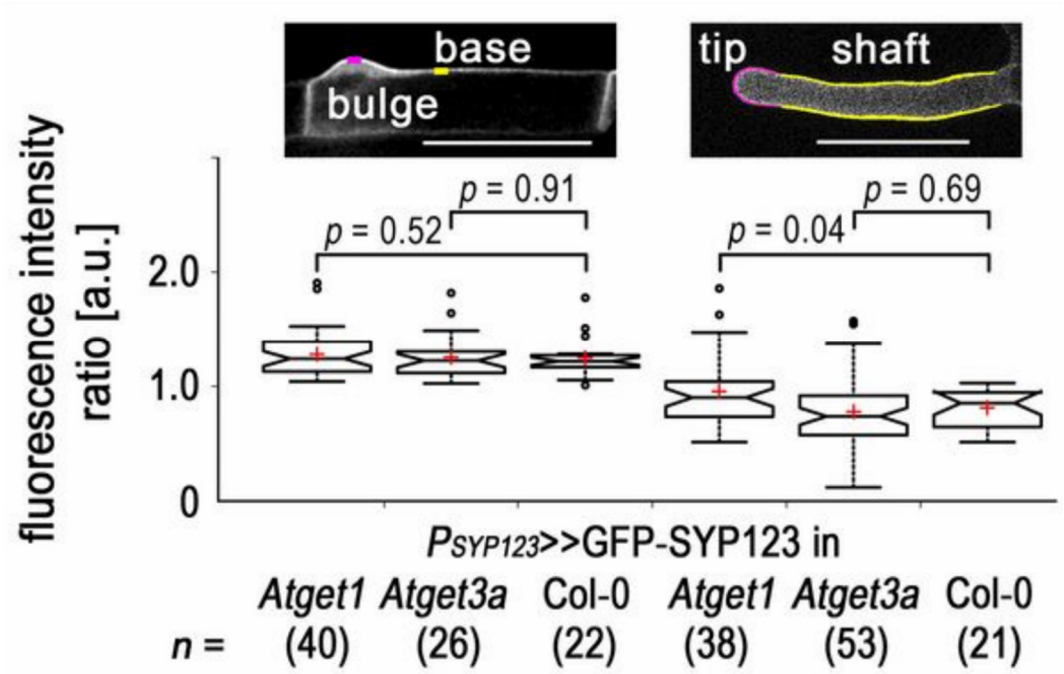

Figure 1.10 SYP123 polarity in root hairs is independent of GET function

(**A**) Fluorescence intensity ratio calculated for bulges (left) and hairs (right) of SYP123::GFP-SYP123 lines in *get1* and *get3a* mutants compared to Col-0. The fluorescence intensity ratio was calculated from values measured in regions indicated in the example images (Mean[pink] / Mean[yellow]). Number of measured cells are indicated (n), Scalebars 50 µm. This figure is part of Figure S7 in Xing et al., 2017.

2.2.3 Ca^{2+} and ROS signaling during root hair development

For proper tip growth a feedback system between ROPs, $[Ca^{2+}]_{cyto}$ and ROS signaling is essential. $[Ca^{2+}]_{cyto}$ was shown to from a tip localized gradient, which oscillates over time in tip growing cells to negatively regulate ROP activity (Hwang et al., 2005; Yan et al., 2009). However, it has not been described at which stage of root hair development this oscillating $[Ca^{2+}]_{cyto}$ gradient is initiated. To visualize $[Ca^{2+}]_{cyto}$ at the RHID during early root hair development I used the cytosolic intensiometric Ca^{2+} indicator R-GECO1 expressed under control of the ubiquitous UBIQUITIN10 (UBI10) promoter (Zhao et al., 2011; Keinath et al., 2015). Intensity measurements of R-GECO1 showed no obvious changes in the $[Ca^{2+}]_{cyto}$ level before cell +1, but an increasing $[Ca^{2+}]_{cyto}$ concentration during root hair bulging (Figure 1.11 A, C). The $[Ca^{2+}]_{cyto}$ concentration first increases at the RHID and then slowly and unsteadily starts to oscillate (Figure 1.11 D - F). This fluctuation of the $[Ca^{2+}]_{cyto}$ concentration transforms into a more regular oscillation upon transition from bulging to fast tip growth (Figure 1.11 D, E, G). This indicates that the controlling feedback loops that cause the regular oscillations known from pollen and root hair growth are established with irregular fluctuations in the beginning.

As a marker for ROS signaling I inducibly expressed the NADPH oxidase RHD2 as an mCit fusion protein. RHD2 is known to be important for ROS production during root hair growth (Monshausen et al., 2007). Before the increase of $[Ca^{2+}]_{cyto}$ concentration in cell +1, mCit-RHD2_ind accumulated at the RHID in cell -1, with a slight but not significant increase starting already in cell -2 (Figure 1.11 B, C). These results show that $[Ca^{2+}]_{cyto}$ and ROS signaling relevant for root hair growth starts after ROP accumulation and indicates that ROS signaling might precede Ca^{2+} signaling.

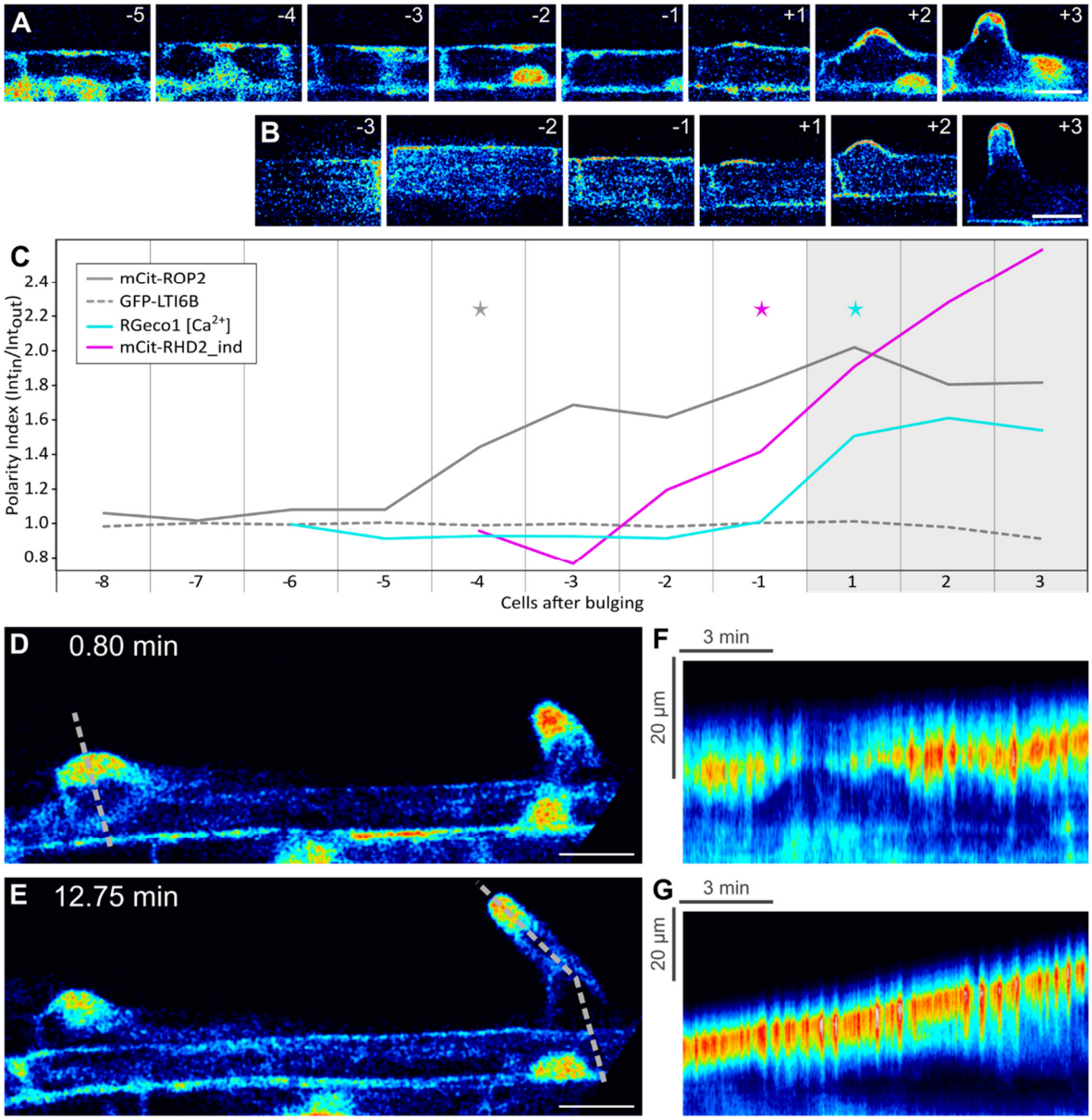

Figure 1.11 Markers for $[Ca^{2+}]_{cyto}$ and ROS at the RHID

(**A-C**) Root hair files expressing the $[Ca^{2+}]_{cyto}$ indicator UBI10::R-GECO1 (**A**), mCit-RHD2_ind (**B**) . Developmental stage of trichoblasts is indicated by -5 to +3. For mCit-RHD2_ind no images before cell -2 are shown as no signal can be detected in these cells. (**C**) Pol-Idx of markers shown in (**A-B**). The Pol-Idx of mCit-ROP2 and GFP-LTI6B from (Figure 1.6) are shown as reference. Stars in the according color indicate first Pol-Idx significantly different from GFP-LTI6B. n of measured cell files: R-GECO1 = 11; mCit-RHD2_ind = 7. (**D-G**) $[Ca^{2+}]_{cyto}$ oscillations in root hair bulge and a tip growing root hair. (**D, E**) Images of a time laps experiment at the indicated time points. (**F, G**) Kymograph of R-GECO1 signal at the RHID during bulging (**F**), along the line indicated in (**D**) and in a tip growing root hair, along the line indicated in (E). Shift of the signal towards the top indicates growth of the bulge / root hair. Scale bars 20 µm.

2.2.4 PIP_2, its regulator and binding proteins at the RHID

PIP_2 is a major lipid involved in signaling at the apex of tip growing cells. To investigate PIP_2 localization during root hair development, I used a fluorescent reporter binding the headgroup of PIP_2. This reporter is called P15Y and consists of mCitrine fused to the C-terminal domain of TUBBY, which specifically binds to PIP_2 (Simon et al., 2014). According to (Simon et al., 2014), P15Y predominantly labels the plasma membrane with signal in the nucleus and the cytoplasm in root tip cells. I could confirm this localization in cells of the root meristem and atrichoblasts. However, in trichoblasts of the elongation zone I found that P15Y was mostly cytosolic (Figure 1.12 A). This could be an indication that there is low abundance of PIP_2 at the plasma membrane so that the P15Y reporter cannot sufficiently bind to the membrane. In later stages of root hair development P15Y accumulated very specifically at the RHID in cell +1 (Figure 1.12 A, E). Already in cell -1 P15Y started to accumulate, however, its Pol-Idx (~ 1.5) was not significantly different to normal distributed GFP-LTI6B, as the Pol-Idx values in this stage were very inconsistent between different cell files. In cell +1 all cells showed P15Y accumulation, suggesting a fast accumulation of PIP_2 at the RHID simultaneously with growth initiation (Figure 1.12 E). In line with this, the PI4P-5 kinase PIP5K3-mCit accumulated at the RHID starting in cell -3 with a significant Pol-Idx increase in cell -2 and gradually increased its polarity further until tip growth was initiated (Figure 1.12 B, E). PIP5K3 accumulation increased slowly from cell -3 to +3 with a maximum Pol-Idx of 2.96, while PIP_2 accumulated very fast with a Pol-Idx of 1.09 in cell -2 and a Pol-Idx of 4.09 two cells later (Figure 1.12 E). This suggests that PIP5K3 produces little PIP_2 in the beginning, but with higher concentration at the RHID between cell -1 and +1 a threshold is reached and PIP5K3 reaches full activity.

In root hairs, PCAP2/MAP18, which has an N-terminal PIP binding domain, was reported to regulate microtubules and ROP2 in a Ca^{2+} dependent manner. PCAP2 can directly bind ROP2 and competes with the GDI SCN1 for ROP2 binding (Wang et al., 2007; Kato et al., 2010; Kato et al., 2013; Kang et al., 2017). In line with its published localization, upon inducible expression, PCAP2-mCit_ind localized to the cytosol and the cell periphery. In young trichoblasts the signal is stronger in the cytoplasm, similar to P15Y, and becomes more membrane associated in more differentiated cells (Figure 1.12 C). PCAP2-mCit_ind did not show membrane

association in the bulge or the root hair tip (Figure 1.12 C, cell +3), which is in in line with the localization reported by (Zhang et al., 2015), They showed PCAP2 mainly at the flanks of growing hairs and only cytosolic signal in the apex, but contradicts a recent report that shows PCAP2 accumulation at the root hair apex (Kang et al., 2017). During root hair development my PCAP2-Cit_ind showed a mostly nonpolar distribution. However, PCAP2-mCit_ind slightly accumulated at the RHID in cell -4 & -2, but afterwards the Pol-Idx decreased and PCAP2-mCit_ind even seemed excluded from the RHID after bulging (Figure 1.12 E). This restriced window of polar association with the RHID was unique amongst the studied candidates, as most proteins stayed at the RHID once accumulated. This behavior is specific for PCAP2, as PCAP1-mCit_ind, a protein with a very similar N-terminal PIP binding domain, showed no polar association with the RHID and also no clear exclusion (Figure 1.12 D, E). However, the exact function of PCAP2 and especially how it is regulated by $[Ca^{2+}]_{cyto}$, PIP2 and ROP signaling feedback loop remains to be elucidated.

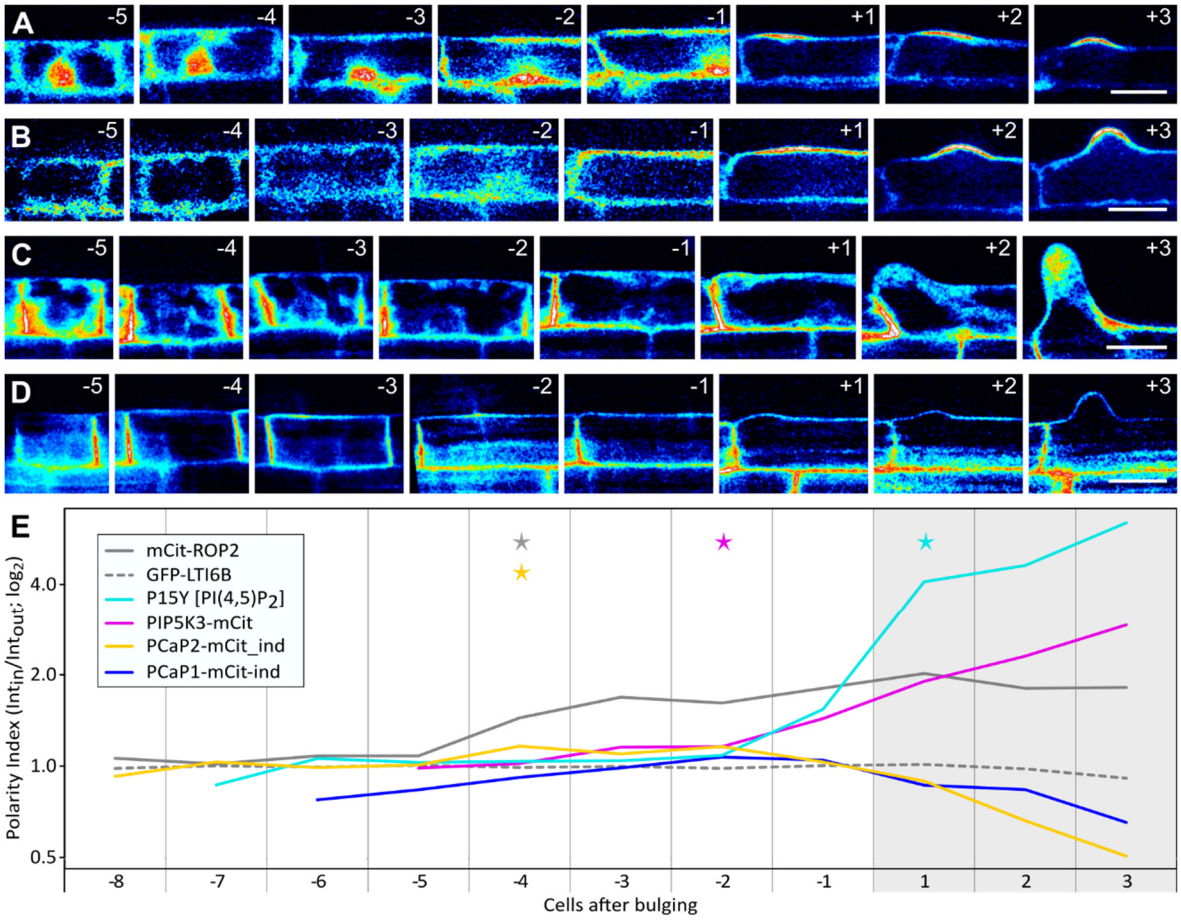

Figure 1.12 Markers for PIP_2 and PIP binding proteins at the RHID

(**A-D**) Root hair files expressing the PIP_2 marker UBI10::mCit-TUBBY^C (P15Y) (**A**), PIP5K3::PIP5K3-mCit in *pip5k3-3* (**B**), PCAP2-mCit_ind (**C**) and PCAP1-mCit_ind (**D**) . Developmental stage of trichoblasts is indicated by -5 to +3. (**E**) Pol-Idx of markers shown in (**A-D**) with Pol-Idx values in log_2 scale to account for great value differences. Pol-Idx of mCit-ROP2 and GFP-LTI6B from (Figure 1.6) are shown as reference. Stars in the according color indicate first Pol-Idx significantly different from GFP-LTI6B, PCAP1-mCit_ind does not significantly differ from GFP-LTI6B. n of measured cell files: P15Y = 11; PIP5K3-mCit = 10; PCAP2-mCit_ind = 11; PCAP1-mCit_ind = 11. Scale bars 20 µm.

2.2.5 Receptor like kinases during root hair development

The PM localised receptor like kinase FERONIA (FER) was shown to positively modulate ROP activity via GEF4 & GEF10 during root hair development (Huang et al., 2013). Previous reports showed that *FER* is broadly expressed in most tissues, which could be confirmed in a line expressing a functional FER::FER-GFP construct, generated by Nana Keinath (Schumacher Lab, unpublished). FER-GFP localized to the plasma membrane, as well as cytoplasmic vesicles and accumulated late at the RHID (cell +2, Figure 1.13 A, F).

Even though, the TRANSMEMBRANE KINASEs (TMKs) were so far not linked to root hair development, they were shown to regulate ROP activity in other developmental processes (Xu et al., 2014). Thus, I investigated if TMKs also have a role in regulating ROPs during root hair development. TMK1 and TMK3 were chosen as their mutants showed the strongest reduction of root elongation (Dai et al., 2013). Unfortunately, expression levels of both TMK fusion constructs under their endogenous promoter was not sufficient for imaging. Thus, only the subcellular localization of TMK1 & TMK3 was analyzed using an estradiol inducible promoter. Both, TMK1-mCit_ind and TMK3-mCit_ind localized mainly to the plasma membrane with some vesicular structures in the cytoplasm (Figure 1.13 B, C). TMK3-mCit_ind was mainly nonpolar in trichoblast cells and even seemed to be excluded from the RHID after bulging, however, low signal intensity made the analysis difficult (Figure 1.13 C, F). In contrast, TMK1-mCit_ind already accumulated slightly at the RHID in cell -2 and -1, but this accumulation was only significant in cell -2. Starting in cell -1 TMK1-mCit_ind significantly accumulated at

the RHID.(Figure 1.13 B, F). This showed that both TMKs behave differently during root hair development and that TMK1-mCit_ind accumulates earlier than FER-GFP, even before bulging. Despite its accumulation at the RHID, TMK1-mCit_ind additionally showed subcellular accumulatios at other locations in various cell types of the primary root, such as meristematic cells, cortical cells and atrichoblasts (Figure 1.13 G - J). This was especially the case when TMK1-mCit_ind was overexpressed (8-10 haind). In those roots TMK1-mCit_ind was found to accumulate in the outer, shootward corners of cells in the early elongation zone (Figure 1.13 G). This localization was not specific for any cell type and rarely occurred in older cells. Interestingly, TMK1-mCit_ind was also found to form polar domains on the flanks of various cells, like cortical cells (Figure 1.13 H) and atrichoblasts (Figure 1.13 I, J), which looked similar to the RHID, but varied in size and position. As native TMK1 expression is very low in young root cells, it is unclear whether those observed localizations of TMK1-mCit_ind are functionally relevant or artefacts of the ectopic overexpression. However, no root hair phenotypes of this overexpressio could be observed.

The only member of the POLLEN RECEPTOR LIKE KINASE (PRK) family, which is not expressed in pollen is *PRK7* (Takeuchi and Higashiyama, 2016). Instead, according to transcriptome databases (Brady et al., 2007), *PRK7* is expressed in the root. So far, the localization or function of this receptor is not characterized and thus I cloned PRK7-mCit under its endogenous and an estradiol inducible promoter. PRK7::PRK7-mCit lines showed expression in the whole primary root and were further analyzed by Jagriti Shrivastava. In estradiol-inducible lines, PRK7-mCit_ind localized to the plasma membrane and to cytoplasmic vesicles (Figure 1.13 C, K). In trichoblasts PRK7-mCit_ind accumulated at the RHID in cell +1 (Figure 1.13 C, F). In cells -3 to -1 the Pol-Idx of PRK7-mCit was slightly elevated, but not significantly different to GFP-LTI6B (Figure 1.13 F). Interestingly, root hairs that showed strong expression of PRK7-mCit_ind were found to be wider and swollen (Figure 1.13 K). This phenotype and the accumulation of PRK7-mCit at the RHID hints to a possible role of PRK7 in root hair development and will be further investigated by Jagriti Shrivastava.

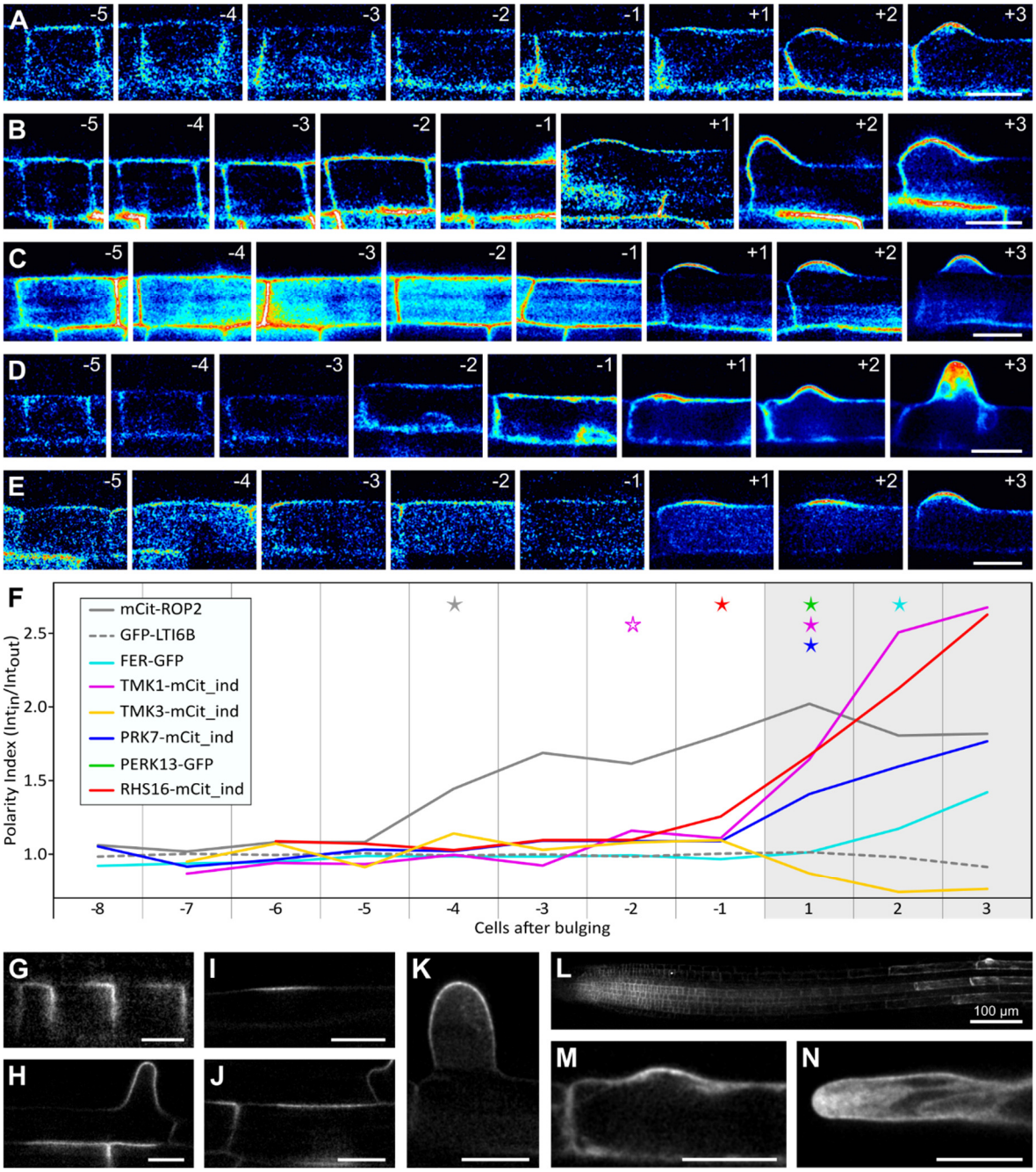

Figure 1.13 Accumulation of RLKs at the RHID

(**A-E**) Root hair files expressing FER::FER-mCit (**A**), TMK1-mCit_ind (**B**), PRK7-mCit_ind (**C**), PERK13::PERK13-GFP (**D**) and RHS16-mCit_ind (**E**). Developmental stage of trichoblasts is indicated by -5 to +3. (**E**) Pol-Idx of markers shown in (**A-E**) and of TMK3-mCit_ind. Pol-Idx of mCit-ROP2 and GFP-LTI6B from (Figure 1.6) are shown as reference. Filled stars in the according color indicate first Pol-Idx significantly different from GFP-LTI6B. For TMK1-mCit_ind, unfilled star indicates single significantly different value, before overall Pol-Idx increase. TMK3-mCit_ind does not significantly differ from GFP-LTI6B. n of measured cell files: FER-GFP = 10; TMK1-mCit_ind = 9; TMK3-mCit_ind = 6; PRK7-mCit_ind = 12; PERK13-GFP = 7; RHS16-

mCit_ind = 7.(**G-J**) Polar accumulation of TMK1-mCit_ind at the plasma membrane of meristematic cells (**G**), a cortical cell (below the root hair cell) (**H**), and patch-like accumulations at the plasma membrane of an atrichoblast (**I**) and a cortical cell (**J**). (**K**) PRK7-mCit_ind localizes to the plasma membrane and cytosolic vesicles. A slightly swollen root hair, which was observed occasionally after strong induction, is shown. This phenotype did not alter the localization of PRK7-mCit_ind. (**L**) PERK13::PERK13-GFP expression in the root tip, with signal in the meristematic region and trichoblast specific signal in the late elongation zone. PERK13-GFP localizes to the plasma membrane and cytosolic background in bulging cells (**M**) and growing root hairs (**N**). Scale bars 20 µm, if not mentioned otherwise.

In addition to the more broadly expressed FER, TMKs and PRK7, I also investigated root hair specific receptors. Previous expression studies reported that *PROLINE-RICH EXTENSIN-LIKE RECEPTOR KINASE 13* (*PERK13*) is specifically expressed in root hairs (Won et al., 2009). Contrary, the newly generated reporter line PERK13::PERK13-GFP (Amelie Mendrinna, Persson Lab, unpublished) was highly expressed throughout the root tip, without any obvious cell type specificity. The signal was strongly reduced in the early elongation zone, but increased again in the late elongation zone in a trichoblast specific pattern (Figure 1.13 L). Before bulging, PERK13-GFP is equally distributed in the plasma membrane with cytosolic some signal visible in the cytoplasm (Figure 1.13 D, M, N) and just after bulging accumulation at the RHID could be measured (Figure 1.13 F).

The receptor-like kinase *ROOT HAIR SPECIFIC 16* (*RHS16*) was shown to be expressed specifically in root hairs, but despite that the gene has not been further characterized (Won et al., 2009). Inducible RHS16-mCit_ind localized, like most other investigate RLKs, to the plasma membrane and to cytoplasmic vesicles. During root hair development it accumulated at the RHID one cell before bulging (cell -1) and showed a slight elevated signal at the RHID already in cell -3 and -2, which was not yet significantly different to GFP-LTI6b (Figure 1.13 E, F). Thus, RHS16-mCit_ind was, together with TMK1-mCit_ind, the earliest RLK accumulating at the RHID, followed by PRK7-mCit_ind.

2.2.6 GEFs, mediators of ROP-signaling, at the RHID

Previous studies showed that GEF4 and GEF10 are important for proper root hair growth, but even loss-of-function double mutants were still able to initiate hairs normally (Huang et al., 2013). Thus, there might be other GEFs important for ROP activation during early root hair development. To investigate whether other GEFs are involved in root hair development it is important to know which genes are expressed in the tissue. The expression profile of all 14 GEFs was first analyzed *in silico* using GENVESTIGATOR as described for ROPs in 2.1.1, using the same expression data sets (Birnbaum et al., 2003; Brady et al., 2007; Wang et al., 2008). Comparing the expression of GEFs, there is a group (*GEF2*, *GEF8*, *GEF9* and *GEF13*) of predominantly pollen expressed genes. *GEF5* & *GEF6* do not show any cell type specific expression pattern, while *GEF1* & *GEF7* seem to be excluded from tip growing cells (Figure 1.14). Some of the GEF genes that are enriched in root hair cells are expressed in both tip growing cell types (*GEF10*, *GEF11*, *GEF12*), while *GEF3*, *GEF4* and *GEF14* are predominately expressed in trichoblasts (Figure 1.14). These 6 GEF genes, which show higher expression in trichoblasts than in atrichoblasts were further investigated.

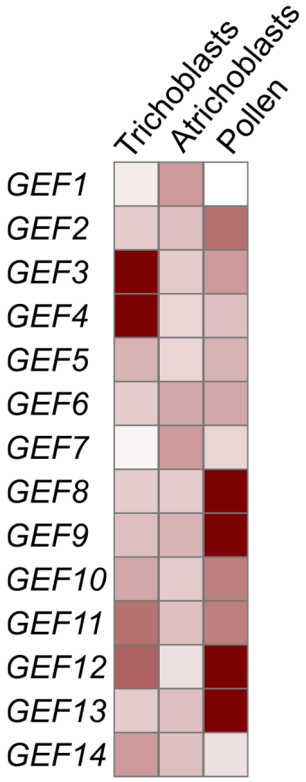

Figure 1.14 Expression of GEFs in tip growing cells

(**A**) Expression profile of all 14 GEFs of *A. thaliana* in trichoblasts, atrichoblasts and pollen, analyzed with GENEVESTOGATOR with data from {Brady:2007fr, Birnbaum:2003ba, Wang:2008ea}. These cell types were chosen to compare GEF expression between two tip growing cell types (Trichoblasts vs. Pollen), or root epidermal cells with or without root hair (Trichoblast vs. Atrichoblast).

To verify the transcriptome-based expression pattern *in vivo*, *GEF3, 4, 10, 11, 12* and *14* were cloned under their respective endogenous promoter, fused to mCit and transgenic lines were generated. As already described in 2.1.1, ROP2::mCit-ROP2 was expressed ubiquitously throughout the primary root. It accumulated at the RHID, beginning in the elongation zone, but signal in the cytosol always remained (Figure 1.6 and 1.7). Compared to mCit-ROP2, GEF3::mCit-GEF3 was expressed specific in root hairs cells, with the first signal detectable in the beginning of the elongation zone (Figure 1.15 A). After the first signal could be detected, mCit-GEF3 first localized to the rootward cell pole with some cytosolic signal. Afterwards, mCit-GEF3 started accumulating specifically at the RHID, while the signal at the cell poles vanished. Finally, mCit-GEF3 localized specifically to the RHID with hardly any cytosolic background and stayed at the RHID and the tip of the root hair throughout hair development (Figure 1.15 A). In those cases, where the cells were observed from a top-view, the disc-like structure of the RHID could be observed (Figure 1.15 A). A similar expression pattern was found for GEF4::mCit-GEF4, which is also expressed specifically in trichoblasts, but the expression started in the elongation zone, later than mCit-GEF3, just before bulging (Figure 1.15 B). mCit-GEF4 was equally distributed throughout the cell in cell- -2 to -1, but later clearly accumulated in bulges and root hair tips. mCit-GEF4 localized mostly to the cytoplasm and the accumulation at the RHID was due to a stronger cytoplasmic signal at this location (Figure 1.15 B).

In roots expressing GEF10::mCit-GEF10, very low signal was observed and the expression started only in the differentiation zone approximately in cell +2. The localization of mCit-GEF10 could not be defined, due to the low signal intensity, but no obvious accumulations could be observed (Figure 1.15 C).

GEF11::mCit-GEF11 was the most ubiquitous GEF analyzed, with expression in all cell types in the root tip and a cytosolic localization without any obvious accumulations (Figure 1.15 D).

In contrast, GEF12::mCit-GEF12 was very similar to mCit-GEF4, with a trichoblast specific expression and the first signal detectable shortly before bulging. The localization of mCit-GEF12, was cytosolic and an accumulation was detectable in cell +1 (Figure 1.15 E).

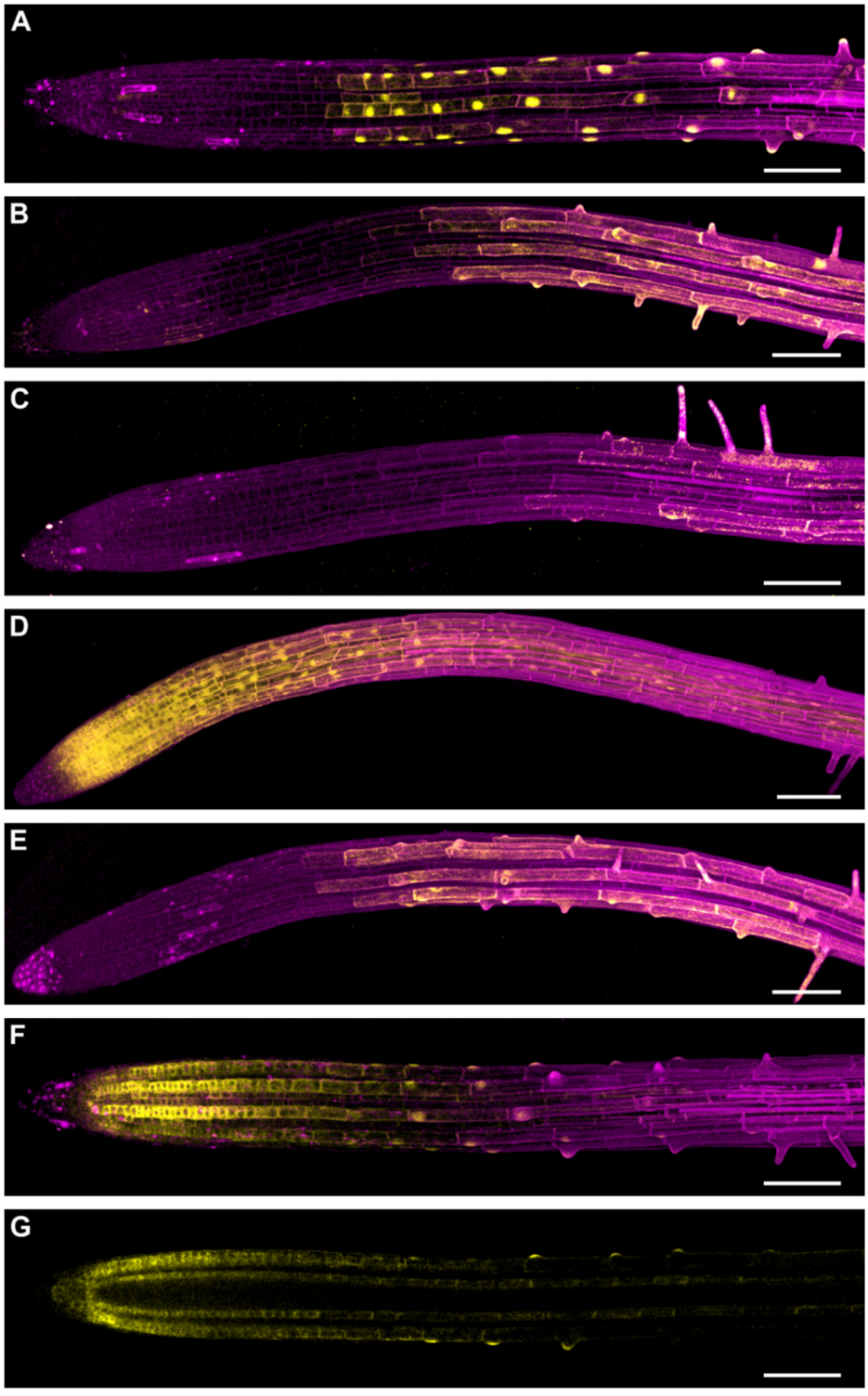

Figure 1.15 Expression and localization of GEFs in the primary root

(**A-F**) Maximum intensity projection of primary root tips expressing different mCit-GEF fusion proteins. Roots are stained with propidium iodide (PI) to indicate the cell outline. (**A**) GEF3::mCit-GEF3, (**B**) GEF4::mCit-GEF4, (**C**) GEF10::mCit-GEF10, (**D**) GEF11::mCit-GEF11, (**E**) GEF12::mCit-GEF12, (**F**) GEF14::mCit-GEF14. (**G**) single confocal image of the root shown in (**F**) to highlight main signal of GEF14::mCit-GEF14 in epidermal and endodermal tissue. Scale bars 100 µm.

GEF14::mCit-GEF14 was expressed in the whole root tip, with signal in multiple cell types, but strongest in the epidermis and the endodermis (Figure 1.15 F, G). Already in the meristematic zone, the signal was significantly higher in those cell files that later became trichoblasts compared to atrichoblast precursors. Entering the elongation zone, overall signal intensity was reduced and mCit-GEF14 was only detectable in trichoblasts and the endodermis, as the signal in most cell types vanished below the detection limit. The localization of mCit-GEF14 was cytosolic in the meristem but entering the elongation zone it became polarized and accumulated at the cell periphery of the RHID (Figure 1.15 F, G). Even though mCit-GEF14 accumulated strongly at the cell periphery of the RHID, there was cytosolic signal visible and the accumulation was not as specific as for mCit-GEF3 (Figure 1.15 A, F).

Taken together, GEF3, GEF4, GEF12 and GEF14 show expression in trichoblasts, accumulate clearly at the RHID and are therefore candidates to regulate ROP accumulation activity to control root hair initiation.

To further characterize the association of the investigated GEFs with the RHID, I quantified their Pol-Idx during root hair development. As mCit-GEF10 was only expressed late in root hair development (first signal detectable ~ cell +2) and lines carrying an inducible construct did not show any fluorescence, GEF10 was not included in the temporal analysis. GEF11::mCit-GEF11 showed ubiquitous expression in the whole root tip and localized to the cytoplasm. In trichoblasts it did not show any accumulation at the RHID before cell +3, where its Pol-Idx was just slightly elevated (Figure 1.16 E, H). Signal of the trichoblast specific GEF4::mCit-GEF4 and GEF12::mCit-GEF12 were detectable shortly before bulging, starting in cell -3 and -2, respectively. Both fusion proteins were nonpolar in the first cells they were expressed, but started to accumulate at the RHID in cell +1 and stayed polarly localized in later stages (Figure 1.16 C, F, H). The polarization could be confirmed using an inducible mCit-GEF4_ind construct, which accumulated strongly in cell +1. Due to the high variability in the Pol-Idx, which was > 1 in all measured cells of this stage, rendered the result not significantly different from GFP-LTI6B (Figure 1.16 D, H). mCit-GEF4, as well as mCit-GEF12 localized mainly to the cytoplasm, but especially mCit-GEF4 showed some association with the cell periphery at the RHID after bulging. (Figure 1.16 C, cell +2 and +3).

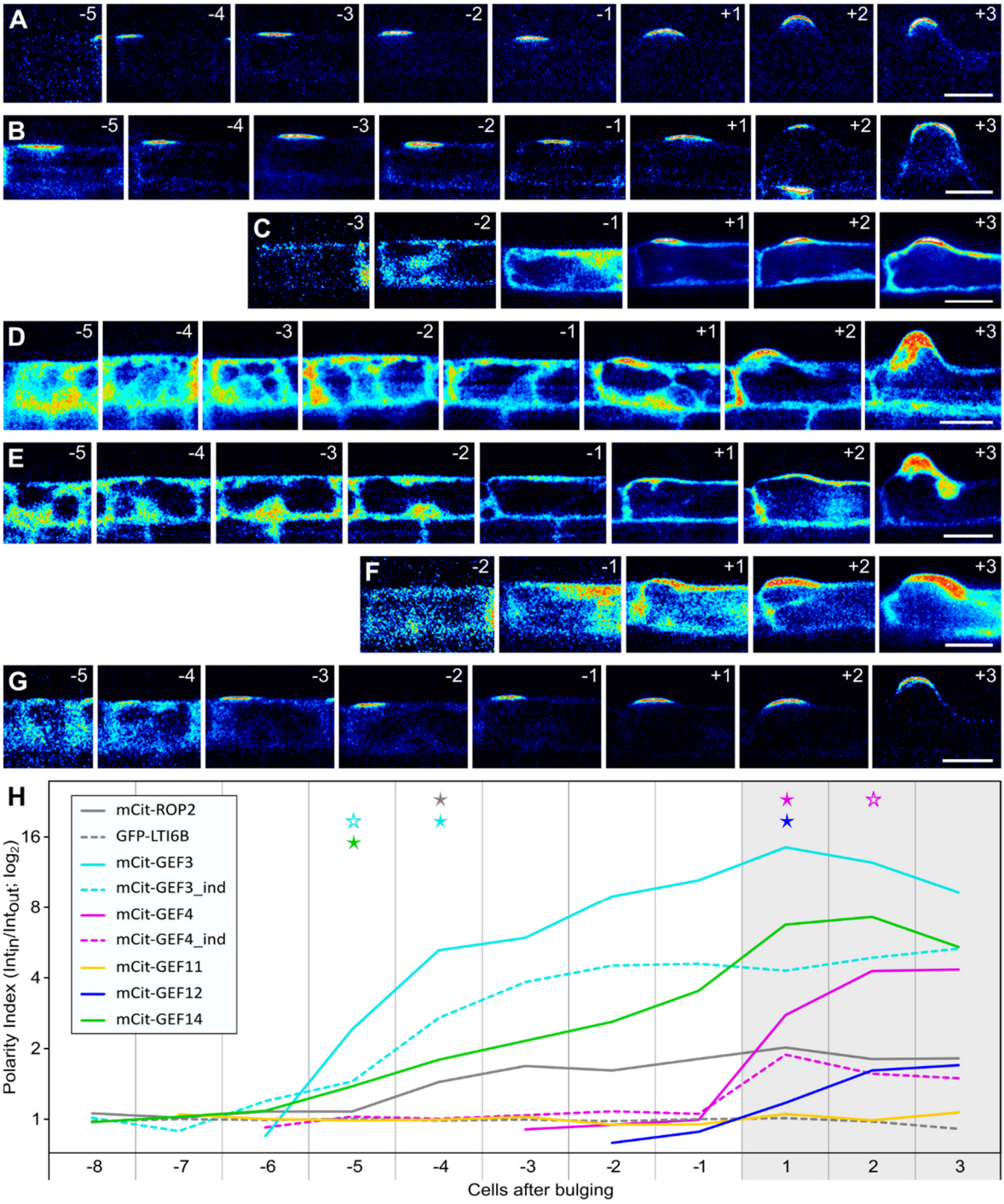

Figure 1.16 Accumulation of GEFs at the RHID

(**A-E**) Root hair files expressing GEF3::mCit-GEF3 (**A**), mCit-GEF3_ind (**B**), GEF4::mCit-GEF4 (**C**), mCit-GEF4_ind (**D**), GEF11::mCit-GEF11 (**E**), GEF12::mCit-GEF12 (**F**) and GEF14::mCit-GEF14 (**G**). Developmental stage of trichoblasts is indicated by -5 to +3. For mCit-GEF4 (**C**) and mCit-GEF12 (**F**) no images of early stages (cell -5 to -3) are shown as no signal can be detected in these cells. (**H**) Pol-Idx of markers shown in (**A-G**), with Pol-Idx values in $\log_2$ scale to account for great value differences. Pol-Idx of mCit-ROP2 and GFP-LTI6B from (Figure 1.6) are shown as reference. Filled stars in the according color indicate first Pol-Idx significantly different from GFP-LTI6B.

Unfilled stars indicate the same for inducible lines in the according color. mCit-GEF11 does not significantly differ from GFP-LTI6B. n of measured cell files: mCit-GEF3 = 11; mCit-GEF3_ind = 10; mCit-GEF4 = 12; mCit-GEF4_ind = 6; mCit-GEF11 = 8; mCit-GEF12 = 13; mCit-GEF14 = 11. Scalebars 20 µm.

GEF14::mCit-GEF14 was expressed throughout the root tip and localized to the cytoplasm. In trichoblast cell -5 it starts to associate with the cell periphery specifically at the RHID (Figure 1.16 G, H). Even though mCit-GEF14 showed a clear association with the cell periphery at the RHID, signal remained in the cytosol throughout root hair development. In contrast to the more widely expressed GEF14, the trichoblast specific GEF3::mCit-GEF3 was first detectable in cell -7 to -5, depending on the individual cell files.In these cells mCit-GEF3 localized to the cell periphery, especially to the rootward cell pole (Figure 1.16 A). In cell -4, mCit-GEF3 localized specifically to the cell periphery at the RHID and stayed there throughout root hair development (Figure 1.16 A, H). In the first cells expressing mCit-GEF3 it did not accumulate at the RHID. As GEF3::mCit-GEF3 started to be expressed in cell -7 to -5, the Pol-Idx of cell -5 was highly variable and thus not significantly different to GFP-LTI6B. However, the absolute Pol-Idx value (2.418) showed that mCit-GEF3 was able to accumulate at the RHID already at cell -5 (Figure 1.16 H).
Those fluorescence-based measurements are dependent on expression levels of the transgenic line and sensitivity of the detection system. To analyze whether mCit-GEF3, if expressed earlier, could also associate with the RHID at an earlier time point, an inducible mCit-GEF3_ind construct was analyzed. In this ubiquitously expressing construct, GEF3 showed a clear polarization in cell -5, with an elevated Pol-Idx already in cell -6, which was not yet significant (Figure 1.16 B, H).
In summary, analyzing different GEFs during root hair development showed that all GEFs have different localization and different timing to accumulate at the RHID. Additionally, my investigations showed that GEF3 and GEF14 accumulate at the RHID before ROP2 and thus represent the earliest RHID markers.

2.3 Comparing the timing of protein accumulation at the RHID

2.3.1 A comparative timeline analysis for protein accumulation at the RHID

A plethora of factors are known to regulate root hair growth and I could show that many of these factors accumulate at the RHID at different time points during root hair development. To get a more integrated and comparative view of all analyzed factors - in total 28 genes and markers for PIP_2 and $[Ca^{2+}]_{cyto}$ (Table 1.1). I sorted all markers into a timeline based on their Pol-Idx during root hair development, using cell +1 (first detectable bulge) as common reference point (Figure 1.17).

During all steps of root hair development markers for different cellular processes accumulated successively at the RHID. mCit-ROP2, under both its own and an inducible promoter, was among the first ones to define the RHID, accumulating at cell -4. From the tested candidates, this was only preceded by mCit-GEF3 and mCit-GEF14, accumulating at cell -5, which are thus the first proteins that mark the RHID. For mCit-GEF3_ind, which is expressed throughout the root tip, the time point of accumulation was not significantly altered, indicating that GEF3 accumulation is independent of its promoter activity. Similar to ROP2, the two closest homologues ROP4 and ROP6 accumulated in cell -4 and -3, respectively.

Simultaneously with ROP2, the SCAR/WAVE complex associated with the RHID represented by BRK1-YFP and GFP-NAP1. The SCAR/WAVE complex regulates actin polymerization and thus those proteins might be the first downstream factors of ROP signaling at the RHID. Shortly before the onset of bulging (cell -2 and -1) PIP5K3-mCit, mCit-RHD2_ind, TMK1-mCit_ind, and RHS16-mCit_ind started to accumulate at the RHID. PIP5K3 and RHD2 represent two proteins involved in a feedback system to control ROP activity. TMK1 and RHS16 are two RLKs and could be among the first upstream regulators of GEFs and ROPs activating root hair growth. Just at bulging (cell +1) many factors started to accumulate at the RHID bringing most crucial factors for tip growth to the RHID. These genes accumulating in cell +1 at the RHID are the two RLKs PERK13-GFP and PRK7-mCit_ind, GFP-SYP123 a marker for exocytosis, the ARP2/3 complex (represented by GFP-ARPC2), $[Ca^{2+}]_{cyto}$ (measured by R-GECO1), PIP_2 (represented by P15Y), as well as mCit-GEF4 and mCit-GEF12. The time point of accumulation of GEF4 was also not significantly altered when it was inducibly expressed in the whole root, which hints to a specific function of GEF4 during bulging, but not for RHID establishment.

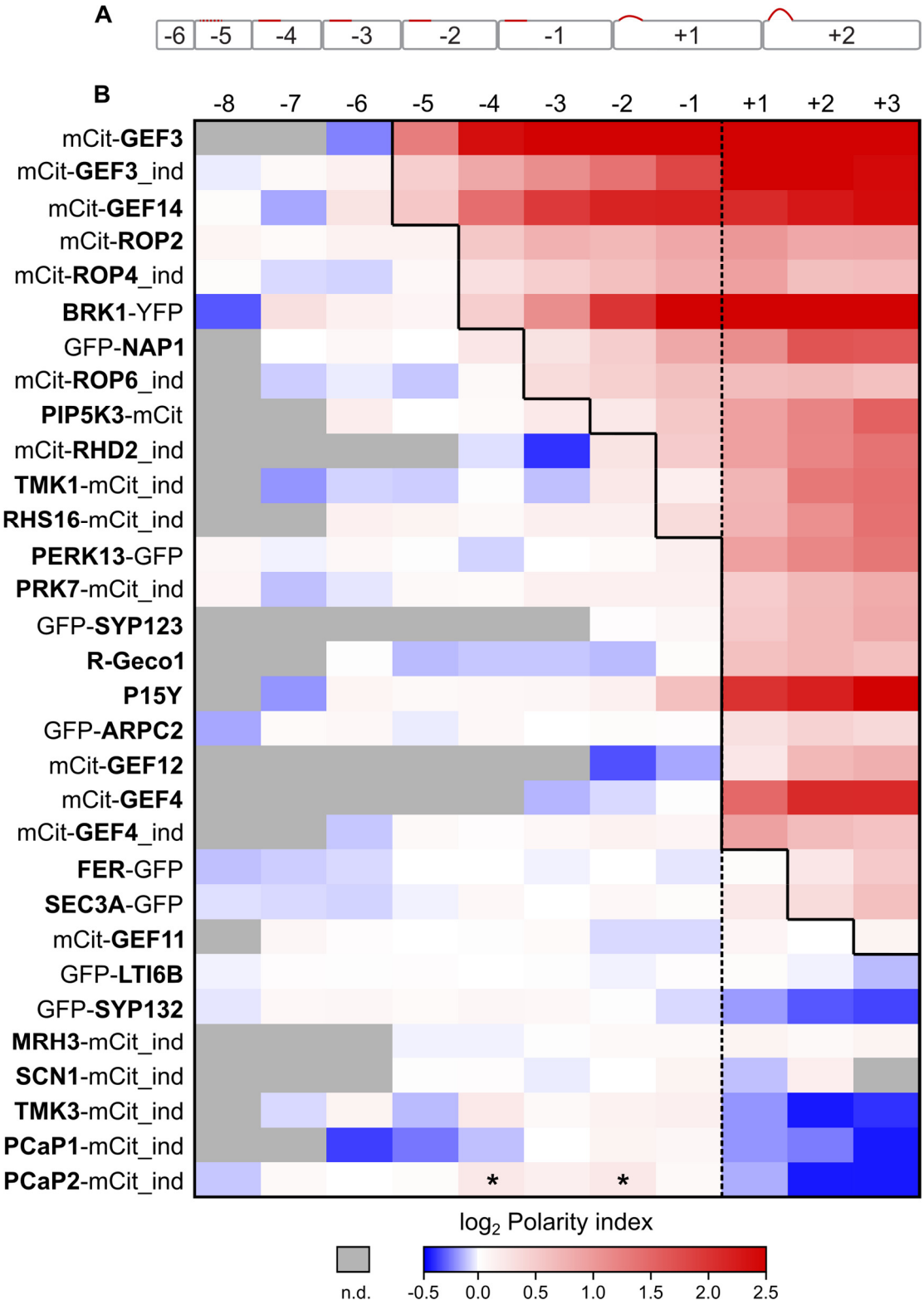

Figure 1.17 Timeline of protein accumulation at the RHID

(**A**) Model of root hair development and RHID establishment like shown in Figure 1.6 to highlight cell labeling according to their developmental stage. (**B**) Protein accumulation at the RHID throughout the early development of root hairs for all 30 different markers analyzed in this thesis (Figure excludes GEF10 as no signal could be detected before cell +2). Genes are sorted by the timing of accumulation. The values

shown in Figure 1.5 to 1.15 were used to combine them in this summarizing representation. For each stage average Pol-Idx values from multiple cells are shown. Color coding represents the log2 Pol-Idx values (Intensity in/out of RHID) for each developmental step. Red: protein accumulation at the RHID; white: equally distributed proteins; blue: protein exclusion from the RHID; gray: no available data. Dotted line indicates transition of cell before and after bulging. Stages -8 to -1 represent cells in the initiation phase before bulging, +1 to +3 cells after bulging. GFP-LTI6B is used as reference for protein accumulation, as described in Figure 1.6. Black line highlights the first cell with significant difference of the Pol-Idx to GFP-LTI6B. Asterisks indicate single transient polar accumulation.

Rather late in the assembly of the growth machinery (cell +2), SEC3A, a marker for exocytosis, as well as the RLK FER enriched at the RHID. Some other candidates did not show any accumulation and stayed nonpolar throughout root hair development. Those proteins were MRH3-mCit, GFP-SYP132, mCit-GEF11, TMK3-mCit_ind, SCN1-mCit_ind, PCAP1-mCit_ind and the nonpolar control GFP-LTI6B. The proteins GFP-SYP132, MK3-mCit_ind, and PCAP1-mCit_ind were even slightly excluded from the RHID after bulging. The only protein that initially showed polarity but did not stay polar throughout the developmental process was PCAP2, which accumulated before bulging (cell -4 & -2) and was excluded from the RHID after bulging (Figure 1.17).

2.3.2 Colocalization of proteins during RHID establishment

The analysis shown in 2.2 and 2.3.1 was based on plant lines expressing a single marker to quantify their accumulation at the RHID. To confirm that proteins associate with the RHID at different time points, some of the candidates were combined with ROP2 marker lines (Figure 1.6 and 1.18). This allowed a direct comparison of the timing of accumulation at the RHID relative to ROP2. Markers accumulating at the RHID in different stages of root hair development were chosen, according to the results shown in 2.3.1. Using single marker lines, ROP2 accumulated at the RHID in cell -4, while mCit-GEF4 and FER-GFP accumulated at the RHID in cell +1 and +2, respectively. This could be confirmed in lines co-expressing mTrq2-ROP2 and mCit-GEF4_ind as well as mRuby2-ROP2 and FER-GFP, as both markers clearly accumulated 2 to 4 cells later than ROP2 (Figure 1.18 A, B).

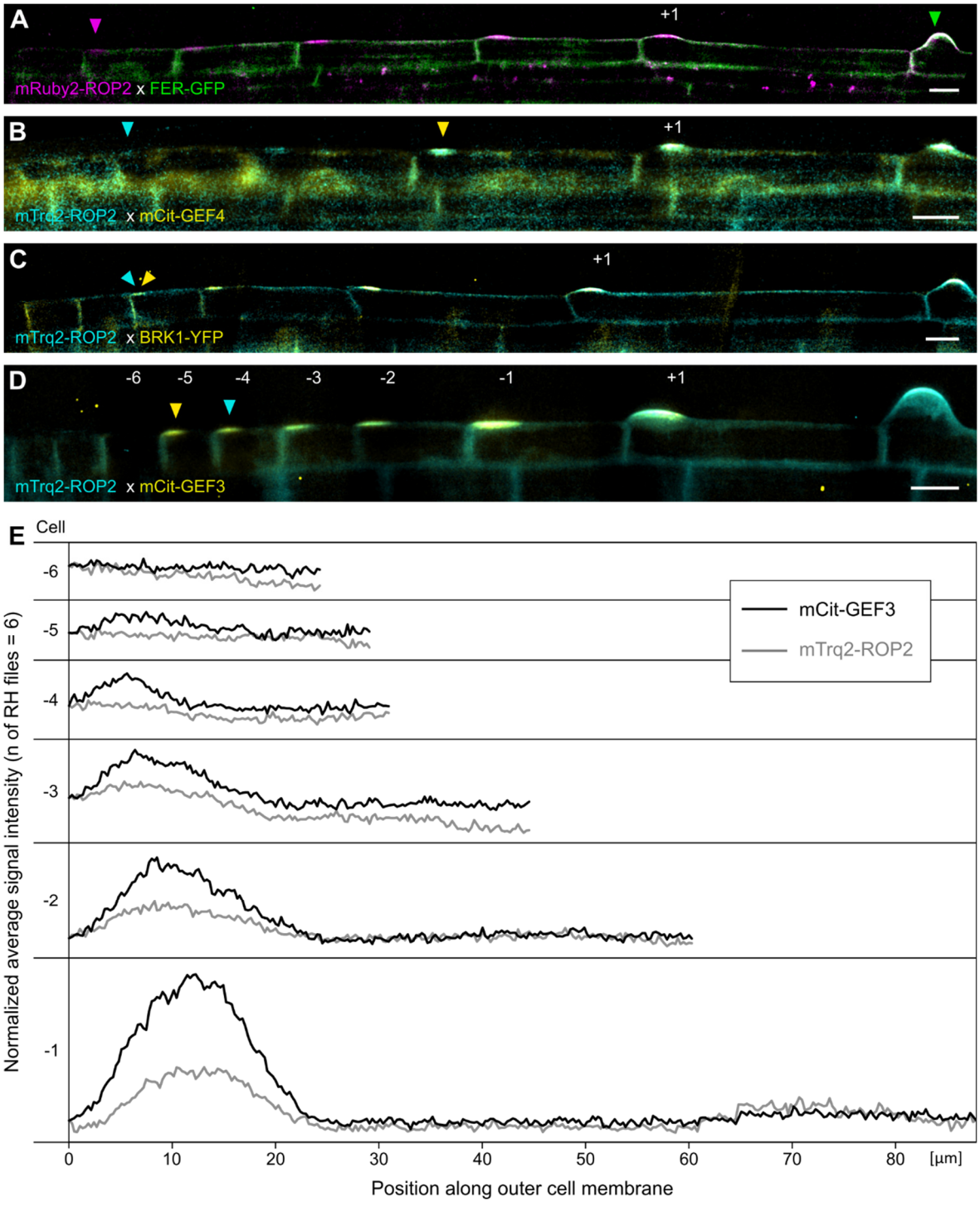

Figure 1.18 Colocalization of ROP2 with proteins accumulating at different stages during root hair development

(**A**) Root hair file expressing ROP2::mRuby2-ROP2 (magenta) and FER::FER-GFP (green). (**B-D**) Root hair files expressing ROP2::mTrq2-ROP2 (cyan) and GEF4-mCit_ind (**B**, yellow), or BRK1::BRK1-YFP (**C**, yellow), or GEF3::mCit-GEF3 (**D**, yellow). (**A-D**) Arrowheads highlight first visible accumulation of the according marker. First cell with bulge is indicated with +1. Scale bars 20 µm. (**D**) Cells from -6 to -1 are additionally labeled to show the stages analyzed in (**E**). (**E**) Normalized

average intensity profiles of mTrq2-ROP2 (grey) and mCit-GEF3 (black) along the outer cell periphery of 6 root hair cell files. Cells are sorted from youngest (-6) to oldest (-1) like in (**D**). mCit-GEF3 starts accumulating in cell -5, while mTrq2-ROP2 starts accumulating in cell -4. Afterwards both proteins colocalize and show the same accumulation pattern.

The SCAR/WAVE marker BRK1-YFP accumulated at the same time as mCit-ROP2 and also mTrq2-ROP2, according to the timeline analysis in 2.3.1. This could be confirmed in plant lines co-expressing BRK1-YFP and mTrq2-ROP2 (Figure 1.18 C). mCit-GEF3 accumulation preceded mCit-ROP2 and mTrq-ROP2 accumulation at the RHID in the timeline analysis of 2.3.1 by just one cell. This small difference in the timing of both proteins was also visible in double marker lines, in which GEF3 accumulation started shortly before ROP2 (Figure 1.18 D). The behavior of both proteins in the double marker line was additionally quantified by comparing the intensity profiles of both markers in each developmental step (Figure 1.18 E). In cell -5, mCit-GEF3 levels slightly increased in an 10-15 µm wide domain approximately 5 µm away from the cell border (Figure 1.18 E, cell -5). mCit-GEF3 polarity became more pronounced in cell -4 and at the same time mTrq2-ROP2 signal intensity started to elevate in the same region. Both markers enriched further in the same region until cell -1, where mTrq2-ROP2 and mCit-GEF3 colocalized in an approximately 20 µm wide area, with its center in approximately 12 µm distance from the rootward cell border (Figure 1.18 E, cell -1).
These experiments confirmed the results of the temporal analysis using individual marker lines (Fugure 1.17). Furthermore, simultaneous expression of GEF3 and ROP2 verified that GEF3 accumulates earlier than ROP2 at the RHID.

2.4 How are ROPs regulated by GEFs during root hair development?

2.4.1 GEF3 is necessary for ROP dependent root hair initiation

The timing analysis of protein accumulation at the RHID (2.2 and 2.3) showed that different GEFs have different subcellular localizations and accumulate at distinct time points during root hair development, suggesting specific roles of the individual

GEFs in this process. To investigate GEF function and their impact on root hair initiation and development, corresponding mutants were analyzed for root hair phenotypes and compared to mutants of ROP2 and ROP4. In focus was mainly the effect on early developmental steps, meaning the initiation of root hair bulging. Thus, the root hair density, representing the general ability to initiate root hair growth was analyzed. Additionally, the distance of the first bulge to the root apical meristem was measured as an indicator of the timing of bulge initiation. Delayed initiation would indicate effects on the early setup of the growth machinery.

Despite the known localization of ROP2 and many studies on ROP function in root hairs, the only described phenotype of a ROP mutant in root hairs were shorter hairs in *rop2-1* T-DNA insertion lines, which were described to be knockout mutants (Kang et al., 2017). This minor phenotype could be due to gene redundancy, as the sequence of all 11 ROP proteins is highly similar (Winge et al., 1997; Li et al., 1998). The two ROPs with the most specific expression in root hairs and a known function in root hair development are ROP2 and ROP4. They are also the closest homologues with a protein sequence identity of 98%. A T-DNA mutant of ROP4 (*rop4-1*, Table 4.1) was previously described to be a knockout mutant (Fu et al., 2005), but not analyzed for root hair phenotypes. *rop2-1* and *rop4-1* were tested individually for their effects on root hair development especially during the initiation process. Compared to Col-0, *rop2-1* has no significant effect on either root hair density or the distance of the first bulge to the root tip. In contrast, *rop4-1* showed slight effects on both analyzed characteristics (Figure 1.19 A, B). However, this effect of *rop4-1* had a high variability and could not be confirmed in further experiments performed by Anna Reichelt (Denninger et al., submitted). As ROP2 and ROP4 are highly similar, double mutants were created and investigated for root hair phenotypes in order to test if they have redundant function in root hair development. In terms of root hair density and distance to the tip, *rop2-1*/*rop4-1* double mutants showed significant effects, with on average 62% less hairs and a 2.25 times higher distance between the root tip and the first bulge (Figure 1.19 A, B). Nevertheless, in both categories the variability was very high. The root hair density was clearly reduced, but in some areas hairs could still be frequently observed. Likewise, the distance of the first bulge to the tip was increased in almost all cases, but especially here the distance variability was very high. To confirm that

the observed effects are due to loss of ROP function, I made complementing lines expressing ROP2::mCit-ROP2 in the *rop2-1*/*rop4-1* double mutant. The complementing line was analyzed by Anna Reichelt and showed that the complementation construct clearly rescued the *rop2-1/rop4-1* phenotype (Denninger et al., submitted). Together with the published phenotype, these results showed that ROP2 and ROP4 are both important in root hair initiation and development and that they have redundant functions in this process.

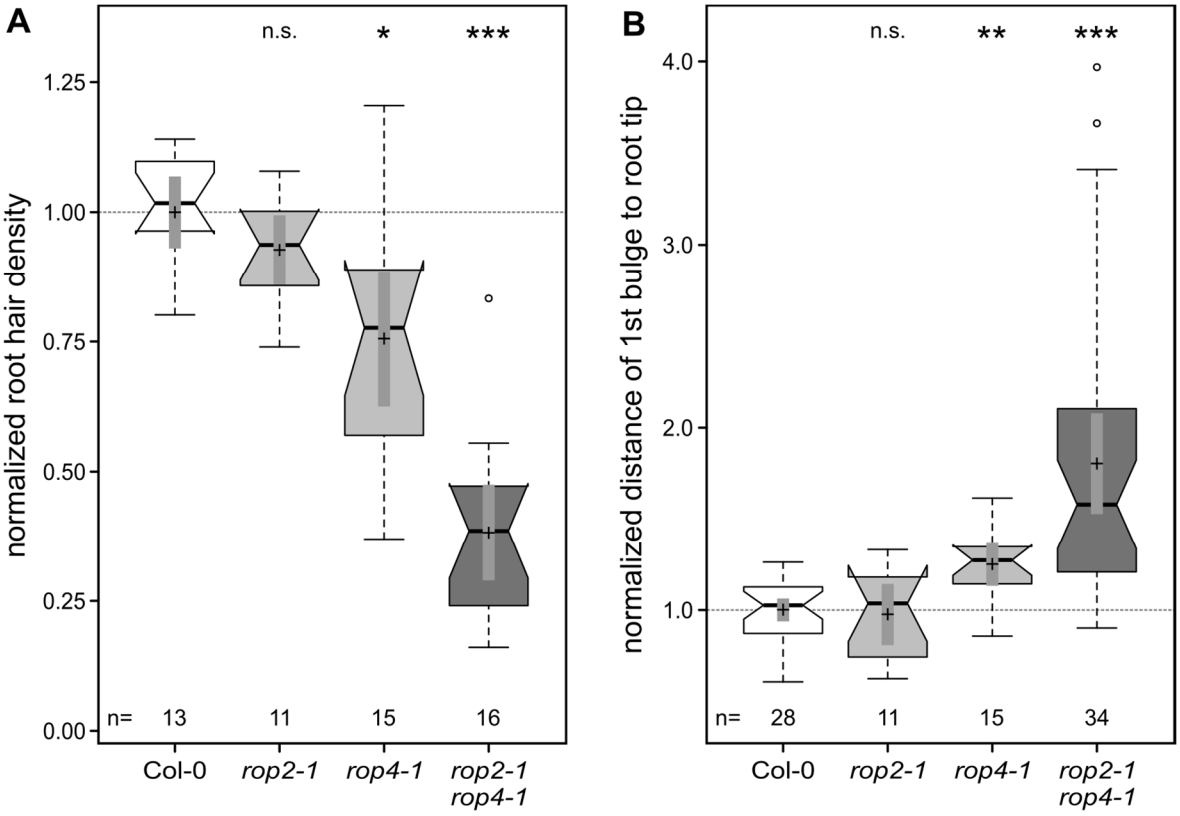

Figure 1.19 ROP2 and ROP4 are necessary for root hair initiation

(**A**) Root hair density of *rop2-1*, *rop4-1* and *rop2-1/rop4-1* double mutant lines, normalized to Col-O (absolute value was 17 hairs per mm in Col-0). (**B**) Normalized distance of first bulge to root tip in *rop2-1*, *rop4-1* and *rop2-1/rop4-1* double mutant lines, compared to Col-0 (absolute value was 1100 µm in Col-0). (**A-B**) n = number of measured roots; + = sample mean; dotted line indicates mean value of Col-0; Center line = sample median. Statistical differences were calculated in comparison to Col-0. n.s. = $p \geq 0.01$; * = $p < 0.01$; ** = $p < 0.001$; *** = $p < 0.0001$. Detailed description of box plots and statistical tests in Chapter IV, 4.2.1.

As ROP activity is crucial for root hair initiation and GEFs are activators of ROPs, GEF function is expected to be crucial as well. Therefore, T-DNA insertion lines of GEFs expressed in root hairs (GEF3, 4, 10, 11, and 14, see Table 4.1 for mutant details) were analyzed for their function in root hair initiation. Of these lines, only gef4-2 and gef10-1, which were described as knockout mutants, were previously investigated for a root hair phenotype, both showing reduced root hair growth and a redundant function in root hair elongation (Huang et al., 2013). In my phenotypic quantification, measuring root hair density and distance of the first bulge to the root tip, only the T-DNA insertion line *gef3-1* (Figure 1.20 A) showed significant effects, with a 40% reduction in root hair density and a 1.48 times higher distance of the first bulge to the root tip (Figure 1.20 A, B). These effects were not as strong as in the *rop2-1/rop4-1* double mutant and indicate that there might be residual ROP activity left in *gef3-1*. This could be due to functional redundancy with other GEFs. Of the other investigated lines, only *gef4-2* had a slightly increased distance of the first bulge to the root tip (1.16 times more than WT, $p = 0.103$, Figure 1.20 B) and *gef14-2* had a slightly reduced hair density (7% less than WT, $p = 0.126$, Figure 1.20 A). This hints to possible functions of GEF4 and GEF14 for root hair initiation in addition to GEF3. *gef10-1* and *gef11-1* did not show any effects (Figure 1.20 A, B) and for *gef12-1* no homozygous mutants could be obtained as this mutant has an embryo lethal effect (Chang et al., 2012). Interestingly, the function of GEF3 is specific for the root hair initiation process and not for general hair growth, as root hair length was not significantly reduced in *gef3-1*, but in *gef4-2* (data by Anna Reichelt, Denninger et al., submitted), which was already known from previous studies (Huang et al., 2013).

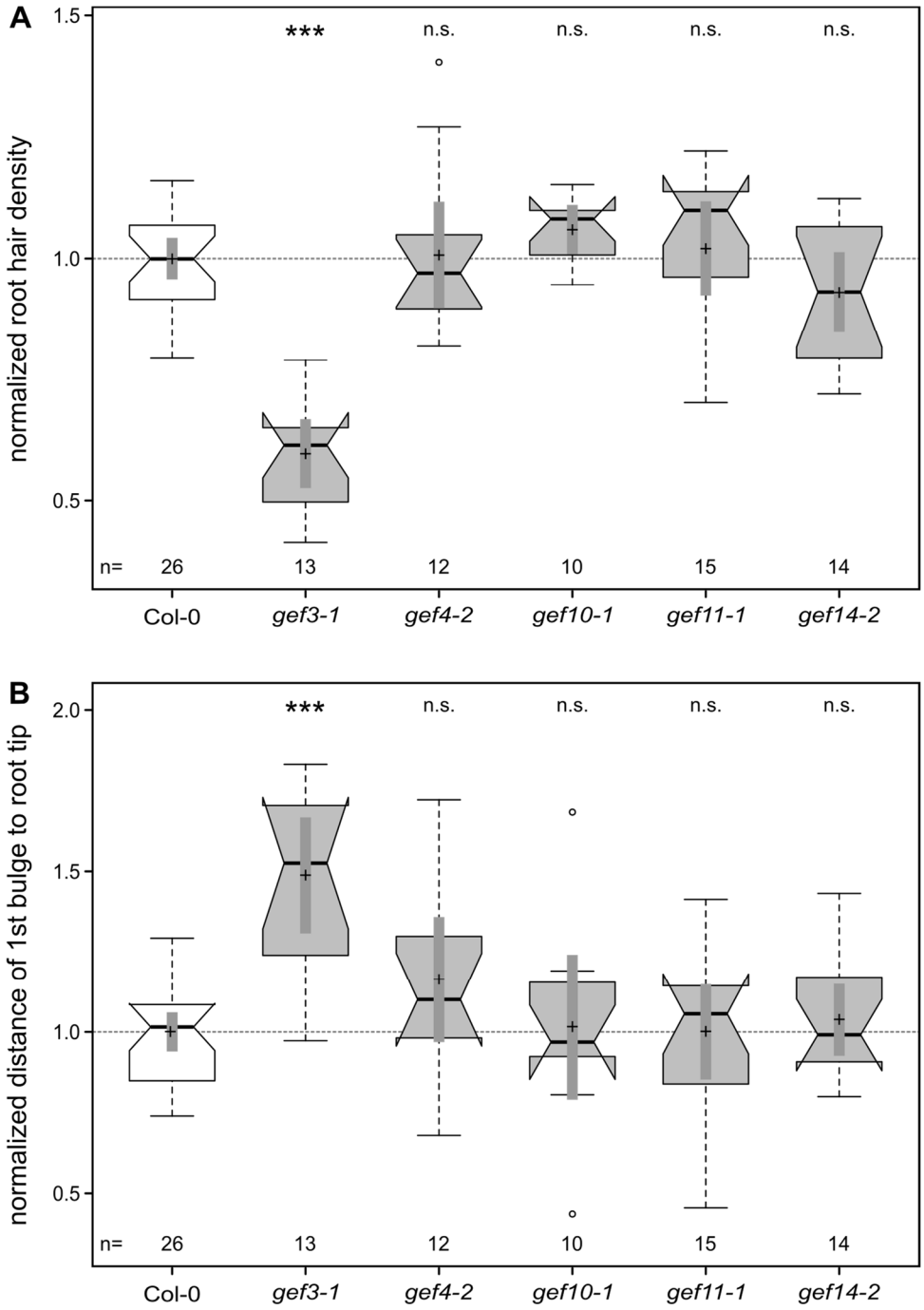

Figure 1.20 GEF3 shows root hair initiation defects

(**A**) Normalized root hair density of different *gef* mutant lines, compared to Col-0. (**B**) Normalized distance of first bulge to root tip in the same lines as in (**A**). (**A-B**) n = number of measured roots; + = sample mean; dotted line indicates mean value of Col-0; center line = sample median. Statistical differences were calculated in comparison to Col-0. n.s. = $p \geq 0.01$; *** = $p < 0.0001$. Detailed description of box plots and statistical tests in Chapter IV, 4.2.1.

To confirm that phenotypes observed in *gef3-1* are due to loss of GEF3 and not caused by any other effects, additional control experiments were performed. First, the absence of GEF3 mRNA in *gef3-1* was tested by reverse transcription (RT)-PCR from primary root RNA of *gef3-1* and Col-0. This complementary DNA (cDNA) was used for subsequent PCRs in front, over, and after the T-DNA insertion site (Figure 1.21 A) to compare mRNA abundance in *gef3-1* and Col-0 (Figure 1.21 B). cDNA quality was tested by GEF4 amplification which shows a similar expression pattern and thus is a suitable control for the presence of trichoblast expressed genes. To control PCR functionality and genomic DNA (gDNA) contamination in the cDNA, gDNA was used as template. Compared to Col-0 hardly any PCR product could be detected before and over the T-DNA insertion site. Only a faint band could be amplify using *gef3-1* cDNA, showing that the amount of full length mRNA is strongly reduced. Behind the T-DNA insertion site, 2 PCR products were present in *gef3-1* cDNA, with the same sizes as Col-0 cDNA and the gDNA control, respectively (Figure 1.21 B). This shows that the 3' region of *GEF3* is still expressed in *gef3-1*, but apparently correct splicing is affected. Taken together these results show that GEF3 function is important for root hair initiation, while GEF4 function seems to control ROP activity specifically during tip growth. However, it is possible that GEF4 and GEF14 have redundant functions to GEF3, which could be tested in double or triple mutants.

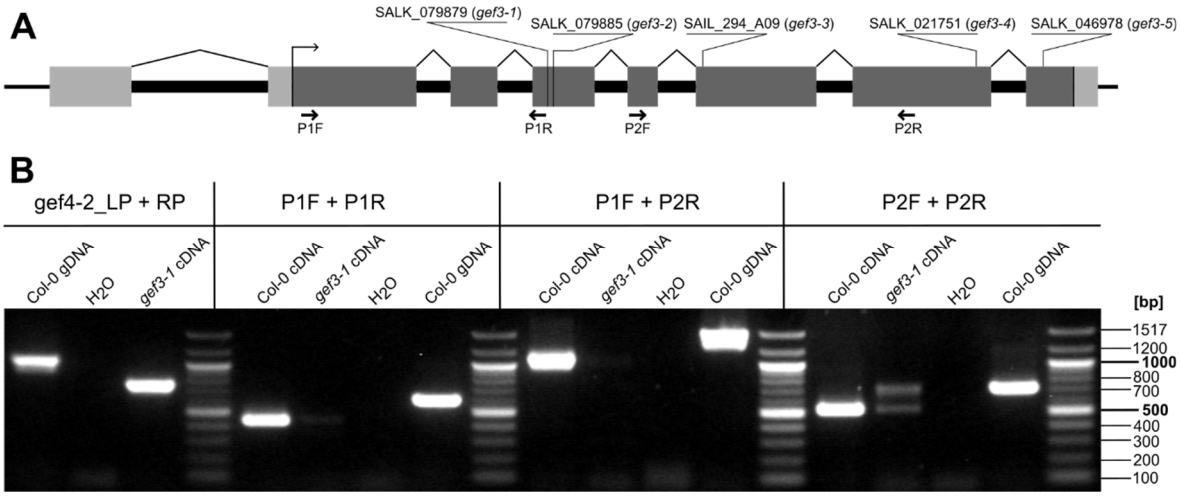

Figure 1.21 *GEF3* mRNA levels are strongly reduced in *gef3-1* mutants

(**A**) Gen structure of *GEF3* (AT4G00460.2) according to The Arabidopsis Information Resource (TAIR). Black boxes show introns, grey boxes show exons (light grey: 5' and 3' UTR, dark grey translated regions). Arrow indicates translational Start. Position and

ID of used T-DNA insertion lines are indicated. *gef3-2, gef3-3 gef3-4* and *gef3-5* were not further investigated in this thesis. Primers used for expression analysis of *GEF3* in *gef3-1* are indicated by black arrows under the gen structure. (**B**) expression analysis of *GEF3* in Col-0 and *gef3-1*. cDNA from seedling roots (10 dag) was used. As a quality control of the *gef3-1* cDNA, *GEF4* was amplified, as it has a similar expression pattern compared to *GEF3*. gDNA served as a control for the PCR and indicator of the product size. H_2O control did not contain any PCR template. Band sizes of ladder are indicated on the right. Three primer sets for *GEF3* were used which amplified fragments in front (P1F+P1R), over (P1F+P2R) and behind (P2F+P2R) the T-DNA insertion site.

2.4.2 GEF3 and GEF4 trigger different growth steps in root hairs

The analyzed mutants showed that ROP2, GEF3 and GEF4 have crucial and specific functions during root hair development. To further understand the functions of these proteins, overexpression lines were investigated. For this, estradiol inducible lines were used and analyzed 24 haind. Overexpression of mCit-ROP2_ind led to multiple hairs, mostly 2, within one cell in 28.3% of all measured cells, while only 0.9% of all hairs were branched (Figure 1.22 B, E). The additional hairs were always right next to each other like they emerged from one bulge. The hair at the rootward cell pole, the regular position, was usually longer.

Overexpression of mCit-GEF4_ind led to bulge formation at the regular position forming multiple tips that did not elongate to full hairs. 30.5% of alle cells showed these branched tips and the short emerging hair tips were wavy and additionally branched (Figure 1.22 C, E). In mCit-GEF4_ind only 1.3% of the measured cells had multiple bulges. The overexpression effects of ROP2 and GEF4 matched already published data by (Jones et al., 2002; Huang et al., 2013).

Lines overexpressing mCit-GEF3_ind rarely showed long hairs, but bulges with multiple branched tips in 20.6% of the observed cells, similar to mCit-GEF4_ind lines. Additionally, in mCit-GEF3_ind lines multiple bulges appeared within one cell in 5.5% of the cells, similar to mCit-ROP2_ind lines (Figure 1.22 D, E). Moreover, in mCit-GEF3_ind overexpression lines 21.4% of the cells had multiple bulges, which were additionally branched (Figure 1.22 D, E).In those cases multiple bulges occurred in one cell, bulges were mostly next to each other and the most rootward bulge was the largest, like in mCit-ROP2_ind. But in contrast to mCit-ROP2_ind, in mCit-GEF3_ind lines frequently more than 2 bulges occurred within one cell and rarely appeared in further distance from the original bulge position (Figure 1.22 D).

Thus, overexpression of ROPs or GEFs leads to different and specific effects, which hints to distinct functions of these proteins in different stages of root hair development. It is to note that in all overexpression lines, bulges were only observed in trichoblasts and never in atrichoblasts. Additionally, none of the overexpression lines showed a changed timing in bulging, as the distance of the first bulge to the root tip was not significantly different from WT (Figure 1.22 F).

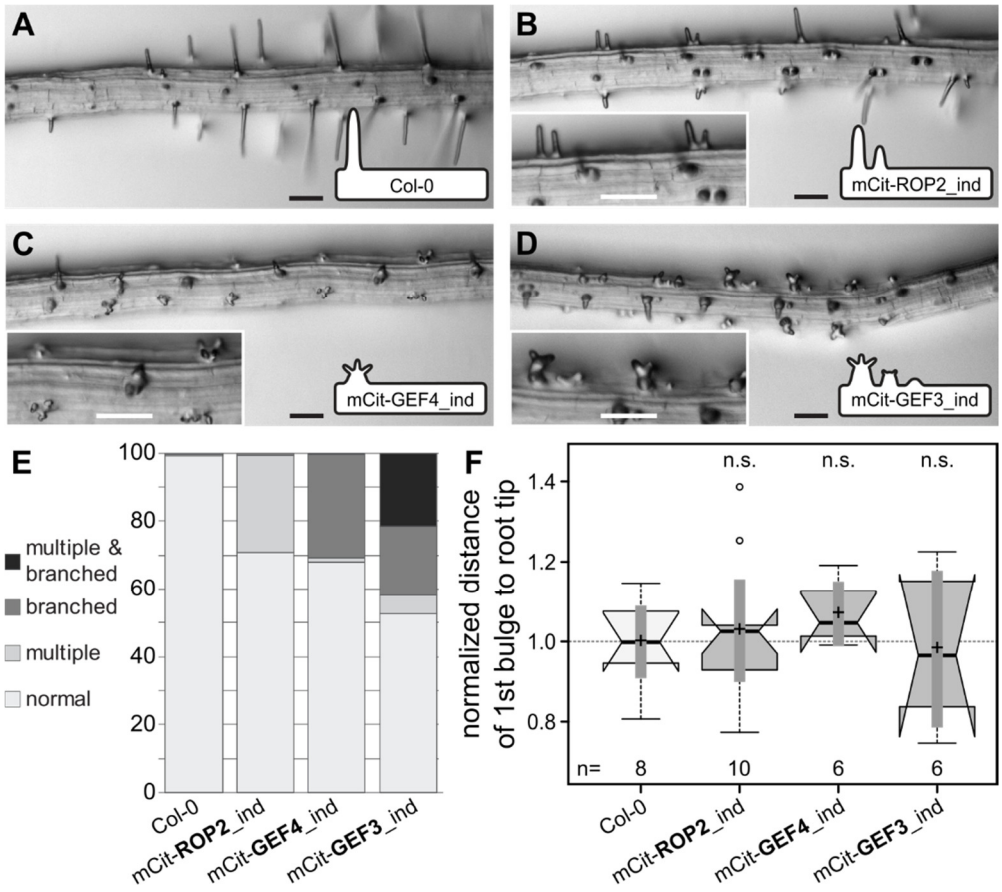

Figure 1.22 GEF3 and GEF4 have distinct functions in root hair development.

(**A-D**) Representative images of Col-0 root (**A**) and roots overexpressing mCit-ROP2_ind (**B**), mCit-GEF4_ind (**C**) and mCit-GEF3_ind (**D**) (24h after estradiol induction). Inserts show root hair phenotypes in detail and an idealized sketch of the predominant shape. Scale bars 100 µm. (**E**) Frequency of phenotypes in % of total observed hairs (n= Col-0: 337; mCit-ROP2_ind: 421; mCit-GEF3_ind: 238; mCit-GEF4_ind: 233). (**F**) Normalized distance of first bulge to root tip in the same lines as in (**A-D**). n = number of measured roots; + = sample mean; dotted line indicates mean value of Col-0; center line = sample median. n.s. = $p \geq 0.01$. Detailed description of box plots and statistical tests in Chapter IV, 4.2.1.

2.4.3 GEF3 is necessary for ROP2 accumulation at the RHID

Loss of GEF3 function led to fewer root hairs and a delay in root hair emergence, furthermore ROP2 accumulation and activation is necessary for root hair initiation and growth. If there is a direct connection between GEF3 function and ROP2 accumulation, the recruitment of ROP2 should be affected in GEF3 loss of function lines. I used *gef3-1* mutant lines expressing mCit-ROP2. Compared to mCit-ROP2 in Col-0 (Figure 1.23 A, B, B'), no accumulations of mCit-ROP2 at the RHID was found in gef3-1 (Figure 1.23 F, G, G'). Quantification of the Pol-Idx of mCit-ROP2 in *gef3-1* and in *rop2-1* mutants confirmed that mCit-ROP2 polarity was completely lost in *gef3-1* cells before and after bulging (Figure 1.23 H).

To verifiy if effects on ROP localization are specific for GEF3, mutants of FER and RHD2, which are known to regulate ROP dependent root hair growth (Foreman et al., 2003; Takeda et al., 2008; Duan et al., 2010), were tested. Published loss of function T-DNA insertion lines *fer-5*, *rhd2-1* (Masucci and Schiefelbein, 1994; Foreman et al., 2003; Duan et al., 2010) were used (Table 4.1). Both mutants had no effects on ROP2 polarity, as mCit-ROP2 accumulated at the RHID in *fer-5* and *rhd2-1* (Figure 1.23 C-D'), like in Col-0 (Figure 1.23 B).

Additionally, I investigated ROOT HAIR DEFECTIVE 6 (RHD6), a transcription factor required for trichoblast differentiation and trichoblast specific expression of several genes important for tip growth (Masucci and Schiefelbein, 1994), to investigate if root hair cell identity is required for ROP accumulation at the RHID. In the published *rhd6-1* mutant (Table 4.1), which does not make root hairs (Masucci and Schiefelbein, 1994), mCit-ROP2 polarity was completely abolished, while the signal intensity was not significantly reduced (Figure 1.23 E).

As ROP2 polarity is lost in *rhd6-1*, ROP2 association with the RHID seems to be dependent on a root hair specific gene. Furthermore, ROP2 polarity is lost in *gef3-1* mutants, which confirms that GEF3 is necessary for root hair initiation through ROP2 polarization.

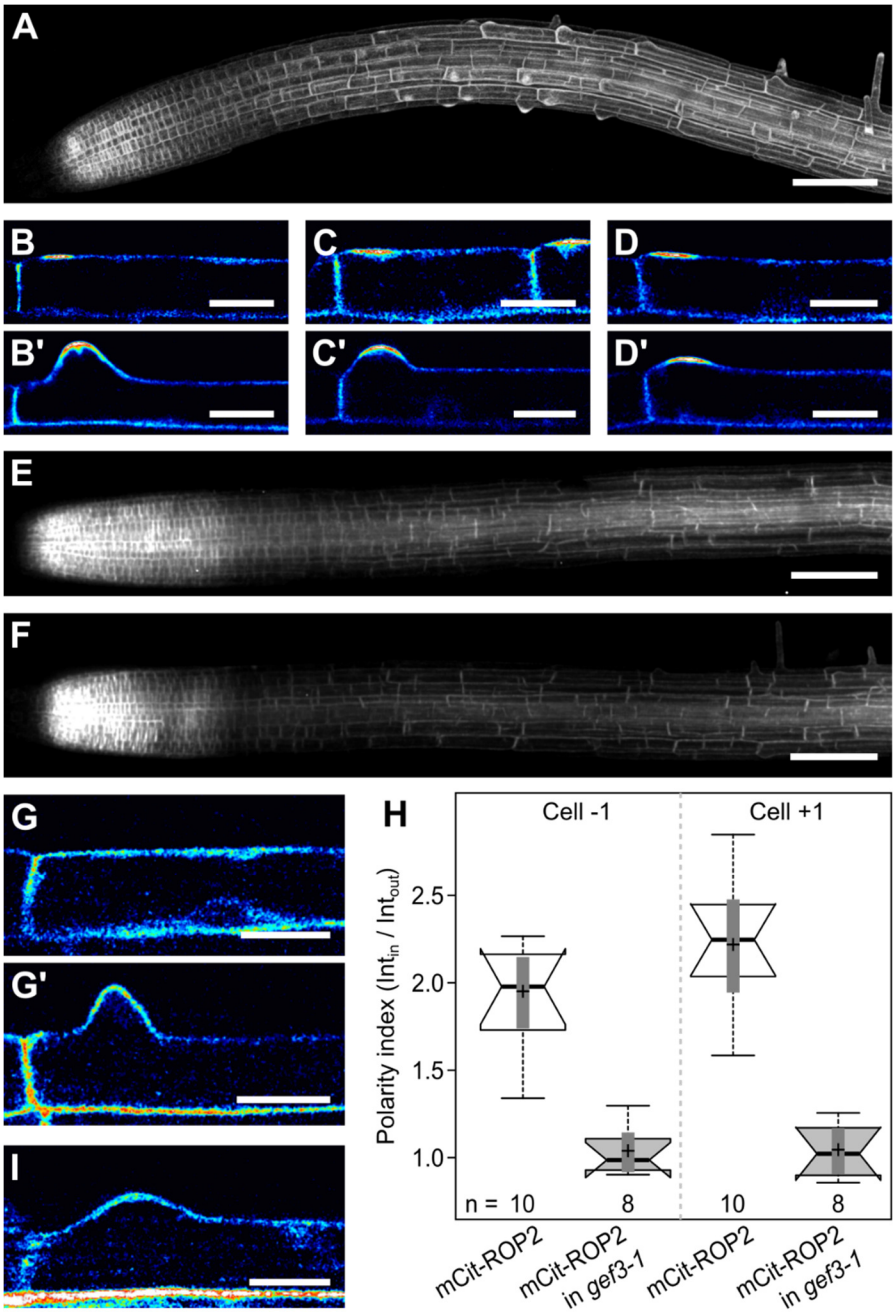

Figure 1.23 ROP2 association with the RHID depends on root hair identity and GEF3

(**A**) Primary root expressing ROP2::mCit-ROP2 in *rop2-1* (same root as in Figure 1.5). Association of mCit-ROP2 with the RHID before (**B**) and after bulging (**B'**). Localization of mCit-ROP2 in *fer-5* (**C, C'**) and *rhd2-1* (**D, D'**) mutant lines. (E-F) ROP2::mCit-ROP2 expressed in primary roots of *rhd6-1* (**E**) and *gef3-1* (**F**) mutant lines. Localization of mCit-ROP2 in *gef3-1* mutant lines, before (**G**) and after bulging (**G'**). (**H**) Quantification of the Pol-Ind of mCit-ROP2 in *gef3-1*, before (cell -1) and after bulging (cell +1). (**I**) Localization of mCit-*rop2*ΔN79_ind (lacking the N-terminal inderction domain) in trichoblasts after bulging. Scale bars 100 µm (**A, E, F**), 20 µm (**B-D', G, G' , I**)

To test, if GEF3 dependent polarization of ROP2 to the RHID is dependent on direct physical interaction, protein-protein interaction studies were performed in collaboration with the group of Christopher Grefen (ZMBP, U. Tübingen). Using both, a “mating-based cytosolic split-ubiquitin” (mbCytoSU) and a “ratiometric bimolecular fluorescence complementation” (rBiFC) assay, the Grefen group found that GEF3 specifically interacted with the active and inactive form of ROP2. The results of those experiments will be published in Denninger et al., (submitted). The interaction assays also showed that ROP2 variants lacking the interaction domain (rop2ΔN79, see Chapter III for a more detailed description) did not interact with GEF3. In line with this result, mCit-rop2ΔN79 did not accumulate at the RHID (Figure 1.23 I), which confirms that the direct physical interaction to GEF3 is necessary for ROP2 recruitment.

2.4.4 Development and dimensions of the GEF3 domain

In this study GEF3 was shown to be the earliest known factor accumulating at the RHID and is necessary to recruit ROP2 to this location. Thus, GEF3 seems to be important to establish the RHID. To better understand the role of GEF3 during RHID establishment, I further characterized the GEF3 localization domain by defining size and position during early RHID development. Just before bulging, in cell -1, the GEF3 domain in GEF3::mCit-GEF3 lines was approximately 20 µm wide, with a full width at half maximum (FWHM) of 9.6 µm (± 2.5 µm) and the maximum of signal intensity 9.0 µm (± 2.1 µm) way from the rootward cell pole (Figure 1.24 A). Time lapse experiments of the same lines showed that the domain formed gradually, with the highest signal close to the rootward cell pole in very early RHID development. This maximum shifted and the domain size increased to its final form and position within 40 min (Figure 1.24 B, C). This was confirmed by the stepwise analysis of individual cells from cell -5 to cell -1 before bulging (Figure 1.24 D - F). In cell -5 the maximum signal was just 3.2 µm (± 1.7 µm) from the rootward cell pole and the FWHM was 6.8 µm (± 0.4 µm). Both values increased gradually from cell to cell until the signal maximum reached a distance of 10.3 µm (± 3.4 µm) to the cell pole, with a FWHM of 10.6 µm (± 2.0 µm) (Figure 1.24 D - F). In lines overexpressing mCit-GEF3_ind the position and size of the GEF3 domain also changed over time, but the final size (12.2 µm ± 4.6 µm) and position (12.2 µm ± 3.1 µm) was reached

already in cell -4 and cell -3, respectively (Figure 1.24 D - F). This shows that the GEF3 domain forms over time and that position and size seem to be predetermined to a certain degree, but can be modulated dependent on the protein level.

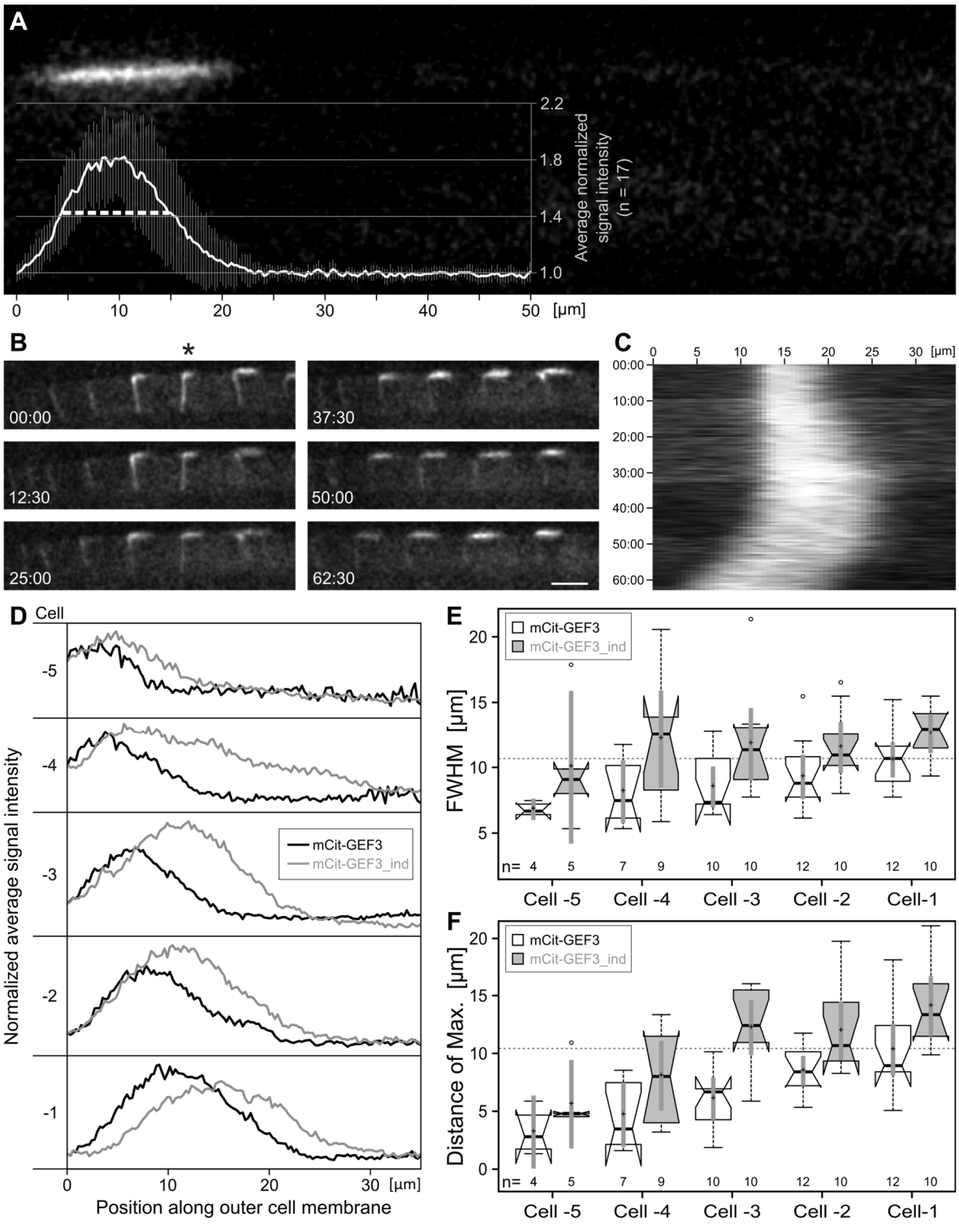

Figure 1.24 GEF3 forms a polar domain of defined size that develops gradually at the RHID

(**A**) Background shows mCit-GEF3 in an exemplary trichoblast (cell -1). Graph shows normalized average signal intensity profiles of mCit-GEF3 along the outer cell periphery of 17 root hair cells (cell -1). Distance from the rootward cell border is indicated below; Error bars indicate SD; dotted line indicates FWHM. (**B**) Time course of a trichoblast cell file before bulging, expressing GEF3::mCit-GEF3. Time points of shown images are indicated (min:sec). Scale bar 20 µm. (**C**) Kymograph of mCit-GEF3 accumulation at the RHID of cell shown in (**B**, used cell marked by asterisk). Kymograph was made along a line at the outer cell periphery (x-axis: position along line) over time (y-axis). (**D**) Normalized average intensity profiles of mCit-GEF3 (black) and mCit-GEF3_ind (gray) along the outer cell periphery of root hair cell files. Cells are sorted from youngest (-5) to oldest (-1), number of measured cells is given in (**E**). (**E**) Quantification of the FWHM of cells shown in (**D**). (**F**) Quantification of the distance of the maximum to the rootward cell border of cells shown in (**D**). (**E-F**) n = number of measured roots; + = sample mean; dotted line indicates mean value of mCit-GEF3 in cell -1; center line = sample median. Detailed description of box plots in Chapter IV, 4.2.1.

2.4.5 GEF3 forms microdomains of low mobility at the RHID

GEF3 is the first protein to localize to the RHID, forming a polar domain without any visible restrictions. The question how GEF3 is immobilized and contained in this region is still open. To address this, I visualized the structure of the mCit-GEF3 domain in high resolution and compared it to the structure of mCit-ROP2 localization. Furthermore, I measured the mobility of both proteins using fluorescence recovery after photobleaching (FRAP). Looking from the top, the RHID has a disk like shape that can be seen in mCit-GEF3 lines (Figure 1.25 A). Taking high resolution images from the RHID, mCit-GEF3 is not equally distributed within the disc, but forms small puncta and short strings (Figure 1.25 A). Thus, the RHID separates into areas low and high GEF3 abundance. Those microdomains are very similar to those observed for BRK1-YFP (Figure 1.8 E). Compared to GEF3, mCit-ROP2 is more equally distributed at the RHID and does not form clear structures (Figure 1.25 B).

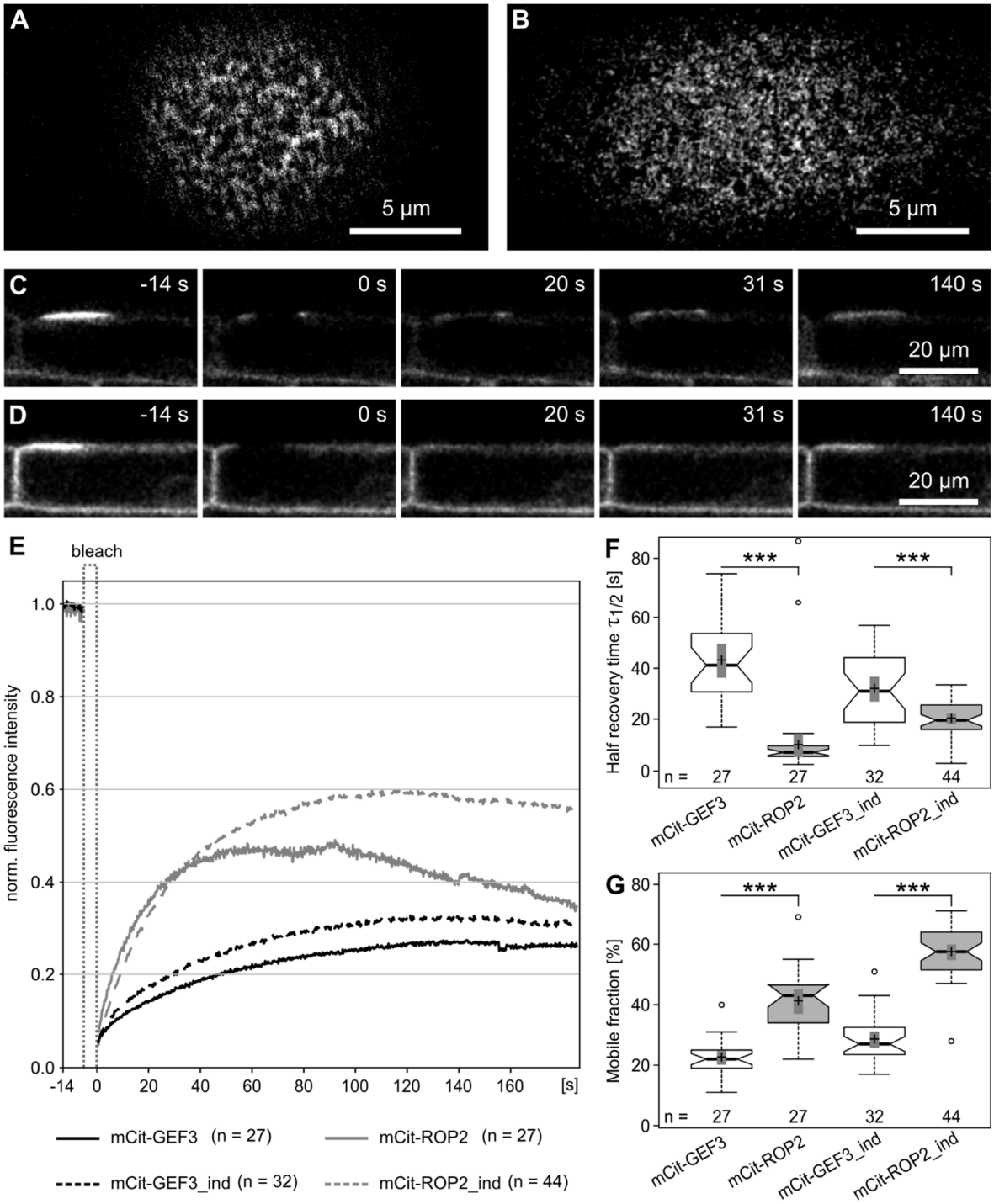

Figure 1.25 GEF3 appears in microdomains and is less mobile than ROP2 at the RHID

(**A-B**) High resolution top-view of the RHID in cell -1 of GEF3::mCit-GEF3 (**A**) and ROP2::mCit-ROP2 (**B**) lines. (**C-D**) Representative time course of FRAP experiments. mCit-GEF3_ind (**C**) and mCit-ROP2_ind (**D**) lines are shown. Bleaching for FRAP experiments was done in a 10 x 2.5 µm region at the RHID. Images show fluorescent signal shortly before bleaching (-14 s), after bleaching (0 s), at the half recovery time ($\tau_{1/2}$) of mCit-ROP2 (20 s), the $\tau_{1/2}$ of mCit-GEF3 (31 s), and after both markers are fully recovered (140 s). (**E**) Average recovery curve of FRAP experiments performed in

GEF3::mCit-GEF3 (black), ROP2::mCit-ROP2 (grey), mCit-GEF3_ind (black dotted) and mCit-ROP2_ind (grey dotted) lines. Number of recorded cells are indicated (n). cells in stage -2 to +2 were used. (**F**) Quantification of the $\tau_{1/2}$ of recordings shown in (**E**). (**G**) Quantification of the mobile fraction of recordings shown in (**E**). (**F-G**) n = number of measured roots; + = sample mean; dotted line indicates mean value of mCit-GEF3 in cell -1; center line = sample median. *** = $p < 0.0001$. Detailed description of box plots and statistical tests in Chapter IV, 4.2.1.

GEF3 recruits ROP2 and concentrates it at the RHID. To do so, one would expect that GEF3 serves like an anchor, immobilizing ROP2 at this location. As GEF3 directly interacts with ROP2, GEF3 should be less mobile than ROP2 in order to act like a binding platform. To measure the mobility of both proteins at the RHID, FRAP experiments with lines expressing mCit-GEF3 and mCit-ROP2 under native and inducible promoters were performed (Figure 1.25 C - G). mCit-GEF3 did recover significantly slower than ROP2, with half recovery times ($\tau_{1/2}$) of 41.3 s (± 15.8 s) and 9.6 s (± 3.0 s) respectively (Figure 1.25 E, F). The mobile fraction (MF) was lower in mCit-GEF3 compared to mCit-ROP2, with 22,4% (± 5.6%) and 41.0% (± 10.2%) respectively (Figure 1.25 E, G). Also in the inducible lines, GEF3 had a smaller mobile fraction and recovered slower ($\tau_{1/2}$: 30.6 s ± 12.7 s; MF: 28.4% (± 7.4%) compared to ROP2 ($\tau_{1/2}$: 19.5 s ± 6.3 s; MF: 57% ± 8.4%). In both cases the mobile fractions were higher in the inducible lines, which hence influenced the recovery times of both proteins (Figure 1.25 E - G). Those results suggest that mCit-GEF3 localizes to membrane microdomains and is significantly slower than mCit-ROP2 at the RHID, which is another strong indication for GEF3 being a recruitment factor for ROP2.

2.4.6 GEF3 is sufficient to recruit ROP2 to membrane domains

The results so far showed that GEF3 recruits ROP2 to the RHID through direct physical interaction and concentrates it at its location as GEF3 is less mobile than ROP2. But it remains unclear if GEF3 is able to independently form such ROP2 recruiting, polar domains at the plasma membrane, or if additional trichoblast specific factors are required. To investigate this, I utilized double marker lines, expressing ROP2::mTrq2-ROP2 and inducibly overexpressing mCit-GEF3_ind. In these lines mCit-GEF3_ind was expressed ubiquitously in all cell types. In

trichoblast cells, the mCit-GEF3_ind lead to the formation of multiple RHID-like mCit-GEF3 accumulations (Figure 1.26 A - D), which explains the overexpression phenotype of mCit-GEF3_ind.

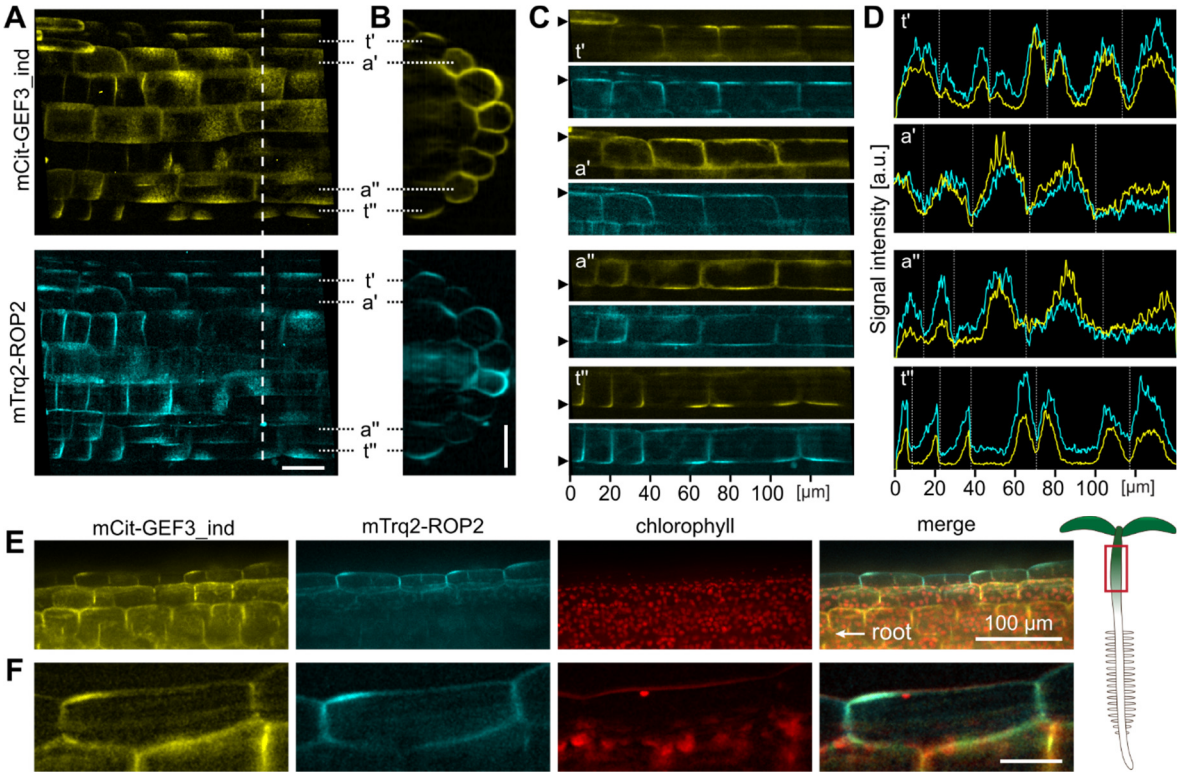

Figure 1.26 GEF3 forms ectopic RHID-like domains and recruits ROP2.

(**A, B**) Localization of ROP2::mTrq2-ROP2 (cyan) in roots overexpressing mCit-GEF3_ind (yellow) in trichoblasts (t' and t'') and atrichoblasts (a' and a''). (**A**) Maximum intensity projection of the early root elongation zone. (**B**) Cross-section along the dashed line in (**A**) shows the cell identity, as trichoblasts are in contact with two, atrichoblasts with one underlying cortical cells. (**C**) Single confocal slice of the cells files indicated in (**A, B**) show ectopic accumulations of both markers in trichoblasts and atrichoblasts. (**D**) Intensity profiles along cell periphery, starting at position indicated with arrowhead in (**C**), dotted lines indicate cell borders. (**E-F**) Subcellular localization of ROP2::mTrq2-ROP2 (cyan) in hypocotyl cells ectopically expressing mCit-GEF3_ind (yellow). Chlorophyll autofluorescence is shown in red. (**E**) Upper row shows maximum intensity projection of the hypocotyl tissue. (**F**) Lower row shows single confocal slice of a hypocotyl epidermal cell. Scale bars 20 µm, if not mentioned otherwise.

In atrichoblasts similar mCit-GEF3_ind domains were present (Figure 1.26 A - D). Compared to the domains in trichoblasts, in atrichoblasts mCit-GEF3_ind domains were not as concise in size and their distribution appeared more random within the cell. At all those polar mCit-GEF3_ind domains, in trichoblasts and atrichoblasts, mTrq2-ROP2 was also accumulated and both markers colocalized (Figure 1.26 D). This indicates that both proteins always appear at the same location if they are expressed in the same cell. The same effect was observed in lines expressing ROP2::mCit-ROP2 and overexpressing mTrq2-GEF3_ind.

In the inducible mCit-GEF3_ind lines, fluorescent signal could also be observed in aerial tissues. In epidermal cells of the hypocotyl mCit-GEF3_ind accumulated in RHID-like domains (Figure 1.26 E, F). This confirms that GEF3 can form polar domains at the plasma membrane and strikingly, mTrq2-ROP2 was also found to accumulate in those mCit-GEF3_ind domains.

The accumulation of ROP2 in atrichoblasts en epidermal hypocotyl cells is dependent on the ectopic expression of GEF3, as neither mCit-ROP2 nor mTrq2-ROP2 alone showed RHID-like accumulations in these cell types. Furthermore, the observation that ROP2 accumulates at ectopic GEF3 domains showed that GEF3 directly recruits ROPs to a polar membrane domain.

2.5 Structural features of ROP2 important for RHID association

I could show that ROP2 is recruited to the RHID by GEF3., which requires direct interaction via the interaction domain of ROP2. However, other studies suggest that also intrinsic features of Rho-GTPases can lead to their polarization (Wedlich-Soldner et al., 2003; Payne and Grierson, 2009). Thus, I investigated, which features of ROP2 have an effect on its membrane association, recruitment to the RHID and restriction to this location.

2.5.1 Activity status regulates ROP2 plasma membrane association

As a molecular switch, the activity status of ROP is important for their function and regulation. To investigate the influence of ROP2 function on localization and its recruitment to the RHID, constitutively active mCit-CA-*rop2*_ind and dominant negative mCit-DN-*rop2*_ind variants (Figure 1.2 B) were analyzed in root hair cells.

As constitutive expression of those mutant variants induces pleiotropic phenotypes, such as swelling of root hairs and the whole root, mCit fusions of CA-*rop2* and DN-*rop2* were inducible expressed and compared to the localization of mCit-ROP2_ind (Figure 1.27 A). mCit-DN-*rop2*_ind mainly localized to the cytoplasm, the association to the cell periphery is strongly reduced (Figure 1.27 B). Additionally, hardly any accumulation of mCit-DN-*rop2*_ind could be seen at the RHID, before and after bulging. However, the morphology of the observed bulges was not altered (Figure 1.27 B), which indicates that expression of DN-*rop2* arrests root hair growth, or that the induction time was not sufficient to induce a phenotype. Also, mCit-CA-*rop2*_ind showed localization changes compared to mCit-ROP2_ind. The cytoplasmic pool was almost completely lost as mCit-CA-*rop2*_ind associated mainly with the cell periphery (Figure 1.27 C). Besides this strong association with the plasma membrane, mCit-CA-rop2_ind did not exhibit any accumulation at the RHID before and after bulging, but showed an equal distribution at the plasma membrane (Figure 1.27 C). The expression of mCit-CA-*rop2*_ind lead to strong phenotypes already 4 haind, which was most obvious in bulging cells, as mCit-CA-*rop2*_ind induced wider bulges (Figure 1.27 D, F), sometimes almost as wide as the cell (Figure 1.27 E). This shows that the activity status strongly influences ROP2 localization and the shape of the outgrowing root hair.

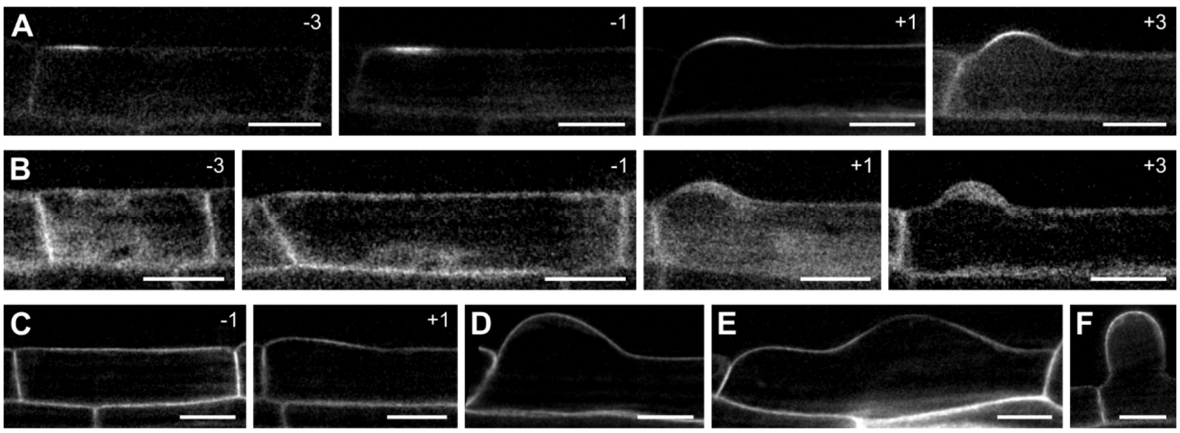

Figure 1.27 ROP2 activity status influences its localization

Localization of mCit-ROP2_ind (**A**), mCit-DN-*rop2*_ind (**B**) and mCit-CA-*rop2*_ind (**C**) in trichoblast cells of the indicated stage. (**D-E**) Exemplary phenotypes caused by expression of mCit-CA-*rop2*_ind, with enlarged bulges (**D**), swollen cells (**E**), or swollen root hairs (**F**). Scale bars 20 µm.

2.5.2 Multiple functional domains influence ROP2 localization

To identify protein regions essential for ROP2 localization and accumulation at the RHID, truncated mCit-ROP2 derivatives were inducible expressed in root hair cells (Figure 1.28 A). Transgenic plants were obtained for all these deletion constructs, but only three could be investigated during the course of this thesis.

In the root tip mCit-*rop2*ΔN79_ind, lacking the N-terminal interaction domain, localized like mCit-ROP2_ind partly to the plasma membrane with signal accumulation at the rootward / shootward cell poles. But the accumulation at the RHID, normally starting in cell -4, was completely lost in mCit-*rop2*ΔN79_ind (Figure 1.28 B).

The additional deletion of the undescribed region in front of the polybasic tail in mCit-*rop2*ΔN160_ind localizes almost exclusively to the cell periphery without any polar accumulations at the RHID (Figure 1.28 C). This is not surprising, as only the membrane anchor of ROP2 remains and it was previously reported that the C-terminus of ROPs can convey membrane attachment to fluorescent proteins (Escobar-Restrepo et al., 2007). In line with that, a construct lacking this C-terminal domain (mCit-*rop2*ΔC161_ind) completely lost its ability to associate with the plasma membrane and localized to the cytosol, without any polar accumulation at the RHID (Figure 1.28 D).

This shows that the C-terminal domain, including the polybasic tail and the CaaX motif are important for ROP2 membrane association. The N-terminal interaction domain, on the other hand, is important for the polar accumulation of ROP2 at the RHID. Finally, the shuffling of ROP2s from the plasma membrane to the cytosol seems to be conveyed by the region between position 80 and 160, as ROP2 variants containing this domain still localize to the cytoplasm, while without this part ROP2 variants are mostly membrane attached.

These results are still preliminary and were not quantitatively analyzed but provide a good based to understand which protein domains regulate ROP localization. Vanessa Schmidt will investigate the described and additional constructs in more detail to characterize the functional domains of ROP2.

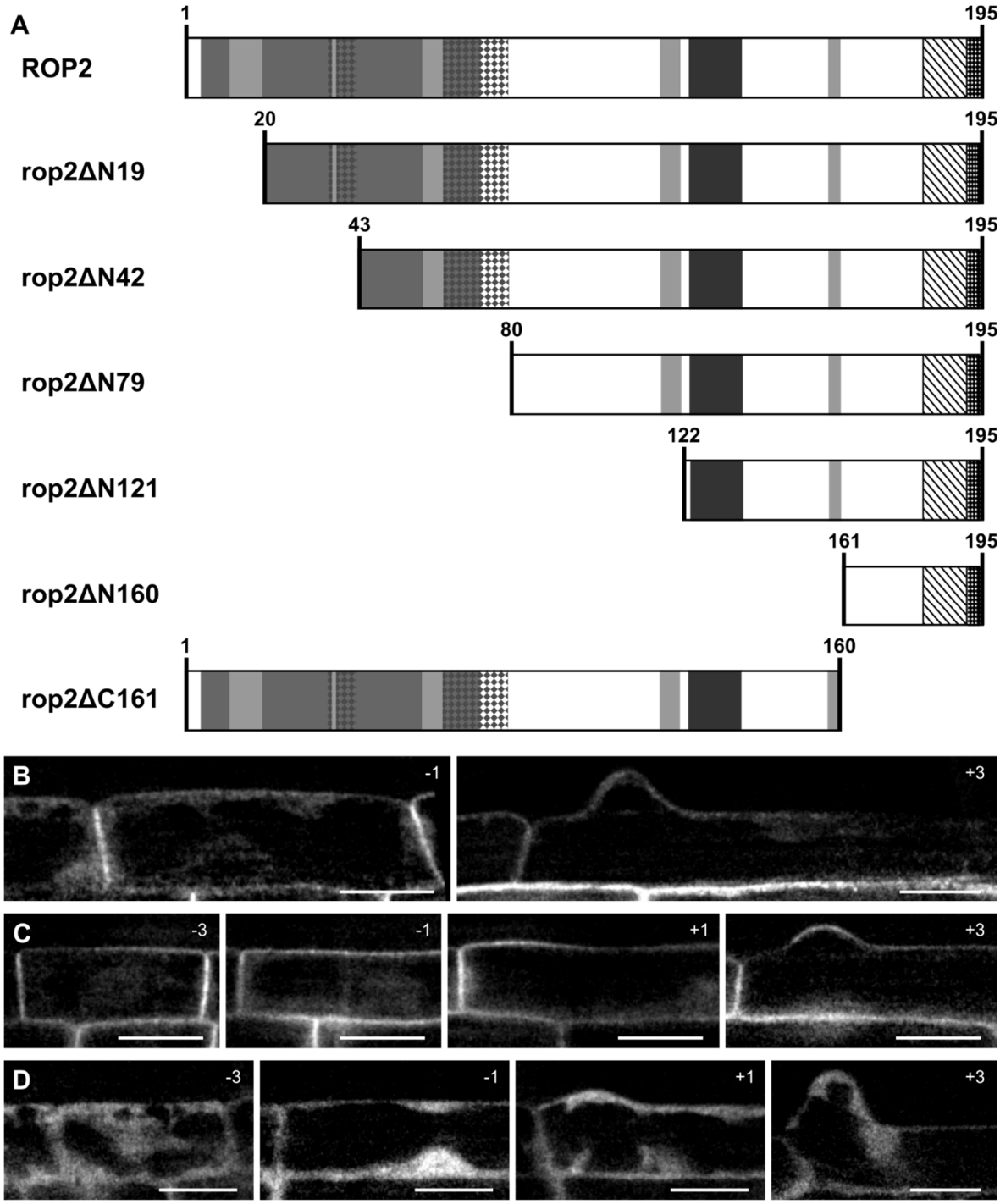

Figure 1.28 ROP2 localization is conveyed by multiple domains

(**A**) Model of ROP2 secondary protein structure (for details see Figure 1.2) and the deletion derivatives made during this thesis. (**B-D**) Localization of mCit-*rop2*ΔN79_ind (**B**), mCit-*rop2*ΔN160_ind (**C**) and mCit-*rop2*ΔC161_ind (**C**) in trichoblast cells of the indicated stage. The other deletion derivatives shown in (**A**) were not investigated during this thesis but will be analyzed by Vanessa Schmidt. Scale bars 20 µm.

2.5.3 Mutations to disturb ROP2 membrane attachment

The truncated derivatives and the mutations influencing the activity of ROP2 already showed that multiple features of ROP2 are important for its localization. Especially the C-terminal domain, containing the CaaX-motif and the polybasic tail, is crucial for its plasma membrane attachment. To investigate which of the two known elements is essential, or if both are necessary for proper membrane attachment, ROP2 derivatives were expressed that had either region mutated (Figure 1.29 A). Transgenic plants expressing these constructs were obtained and will be analyzed by Vanessa Schmidt.

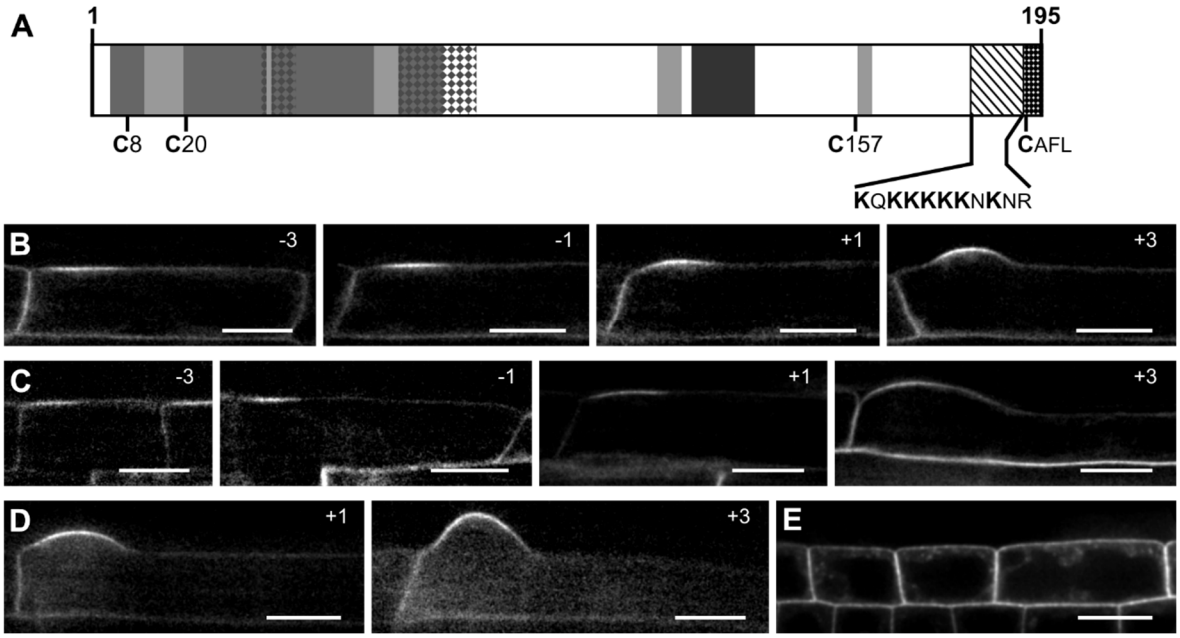

Figure 1.29 Internal cysteines don't contribute to ROP2 association with the RHID

(**A**) Model of ROP2 secondary protein structure highlighting all cysteine residues (C) and the lysine residues (K) of the polybasic region (for details see Figure 1.2). (**B-D**) Localization of mCit-*rop2*C8A_ind (**B**), mCit-*rop2*C20A_ind (**C**) and mCit-*rop2*C8,20,157A_ind (**C**) in trichoblast cells of the indicated stage. (**E**) Localization of mCit-*rop2*C8,20,157A_ind in the meristematic zone. Scale bars 20 µm.

In addition to the C-terminal membrane anchor, ROPs contain three internal conserved cysteines, which are supposed to be acylated and involved in shuffling of ROPs from the cytoplasm to the plasma membrane (Figure 1.29 A). Transgenic lines expressing mCit-ROP2_ind versions that have all combinations of these cysteines exchanged to alanine were obtained, but only 3 mutation constructs were

investigated in this thesis. The localization of mCit-*rop2*C8A_ind and mCit-*rop2*C20A_ind was undistinguishable from mCit-ROP2_ind, with a clear association to the RHID before and after bulging (Figure 1.29 B, C). Removal of all three internal cysteines (mCit-*rop2*C8,20,157A_ind) did not affected the localization, as this fusion protein still associated with the RHID like mCit-ROP2_ind (Figure 1.29 D). However, in cells of the root meristem and in the early elongations zone mCit-*rop2*C8,20,157A_ind formed small clusters in the cytosol, which could not be observed in older cells (Figure 1.29 E).

2.5.4 Altering the proton gradient reduces ROP polarization

The membrane association of ROP2 is important for its function in root hair development, as it must act in a very concise location restricted to the RHID. For the attachment of ROPs to specific domains in the plasma membrane, binding of the positively charged polybasic region to negatively charged lipids, like PIP_2, is required (Do Heo et al., 2006; Lavy and Yalovsky, 2006). This mechanism is influenced by the surrounding pH, and changes in the intracellular pH can therefore influence ROP2 membrane association. The cytoplasm of plant cells has a neutral pH, while the extracellular space is acidified by plasma membrane ATPases (Palmgren, 2001). How this chemical potential, established by the proton gradient, influences ROP2 localization and function was investigated by uncoupling the proton gradient with the protonophore Carbonyl cyanide m-chlorophenyl hydrazine (CCCP). CCCP destroys the proton gradient of cellular membranes and thus may leads to local temporary excess of protons at the cytosolic side of the plasma membrane, which could influence ROP2 localization. ROP2::mTrq2-ROP2 expressing roots were perfused with 5 µM CCCP for 10 min in a RootChip perfusion chamber. mTrq2-ROP2, lost its membrane association shortly after perfusion starts and distributed more equally within the cell. The overall gradient of ROP2 was not completely lost, as mTrq2-ROP2 signal remained stronger in the root hair tip, but the membrane attachment was gradually reduced within approximately 5 min. This loss of ROP2 polarity was accompanied by a stop of root hair growth (Figure 1.30 A, B). After washout of CCCP, mTrq2-ROP2 became repolarized in 23 of 27 observed hair cells, but the repolarization was slower (within approx. 30 min) than the loss of polarity and the polarity was not reestablished to the same degree (Figure

1.30 A, B). Additionally, the growth of the observed root hairs did only restart in 3 of those cells within 30 min after washout. The observed effects were specific to CCCP, as in mock controls no loss of mTrq2-ROP2 polarity could be observed (Figure 1.30 C, D). Those experiments showed that CCCP can abolish ROP2 polarity at the RHID and arrest root hair growth, but if this effect is due to changes in cellular pH, changes in the membrane potential, or other possible side effects of CCCP is unclear. This preliminary finding has to be further tested, for example by investigating ROP localization in mutants affecting the proton gradient, or using other more specific chemicals that influence the cellular pH.

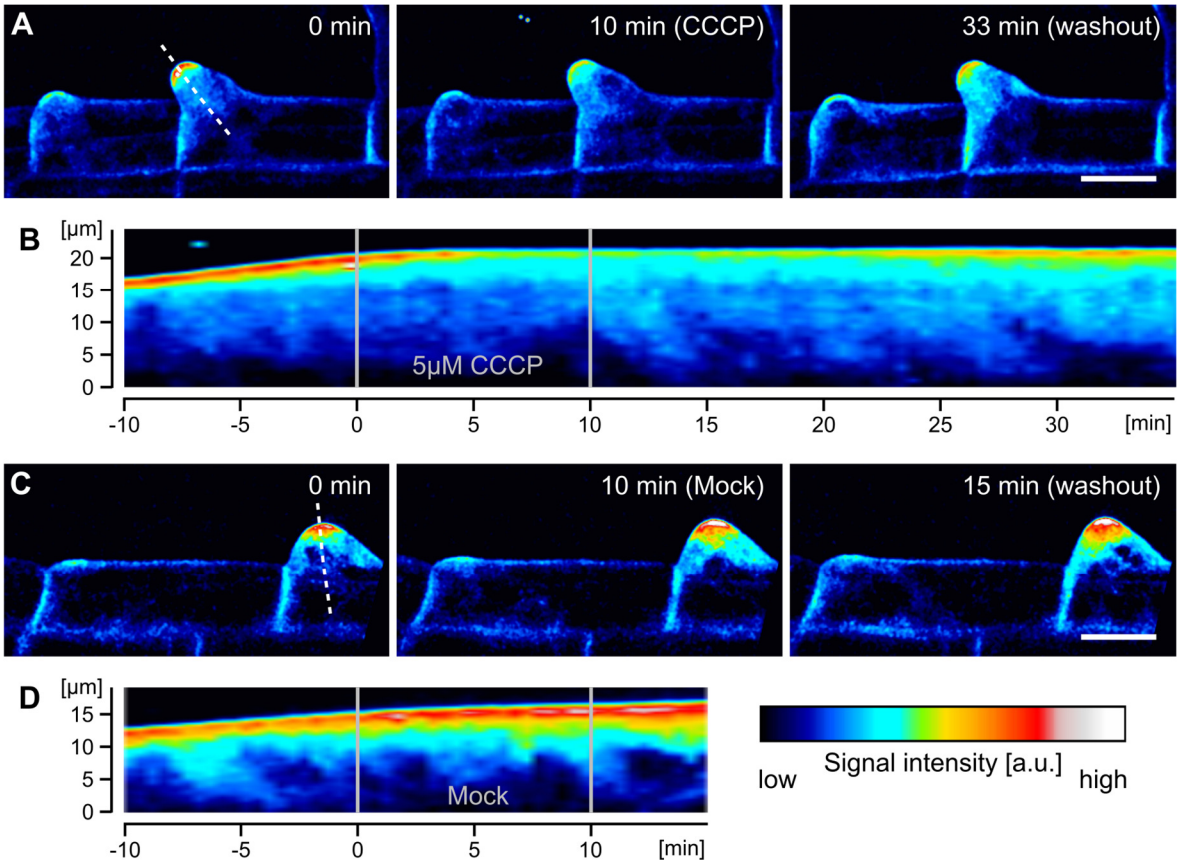

Figure 1.30 ROP2 localization is dependent on membrane potential

(**A, C**) Time course of root hairs expressing ROP2::mTrq2-ROP2, treated with 5 µM CCCP, or the according mock (0.01% DMSO in medium). Images before (0 min), after (10 min) CCCP/ mock treatment and during washout (33 min, 15 min) are shown. (**B, D**) Kymograph of CCCP/ mock treatment along the dotted line in (**A, C**). Grey lines indicate beginning and end of CCCP/ mock treatment. Scale bar 20 µm.

3 Discussion

Root hairs are a common model for tip growth and together with pollen tubes they have been used to provide a thorough understanding of how tip growth is regulated and how the individual components of the machinery work together. However, in plants only few studies investigated the early steps of tip growth initiation. Especially the mechanisms that recruit the involved factors of the tip growth machinery to the initiation domain are not understood. Using root hairs as a model system I investigated the chronical order in which the root hair machinery is assembled. The obtained results led to the identification of a ROPGEF, which is required for root hair initiation, can form domains at the plasma membrane and recruits ROPs to the RHID.

3.1 The timeline of root hair initiation

Previous studies that described proteins involved in root hair formation showed that these factors accumulated at some point in root hair development or mentioned that they were present before or during bulging (Jones et al., 2002; Kusano et al., 2008; Takeda et al., 2008; Huang et al., 2013; Stanislas et al., 2015). In this thesis I combined the previously described factors in a timeline of protein accumulation at the RHID. For the first time this allows direct comparison of a large set of proteins for their chronological order in which they accumulate at the RHID clarifying their point of action during tip growth. Including proteins with potential role in root hair development or known connections to other described factors in the same timeline analysis, it was possible to make assumptions at which point in time they function during root hair development. For the timeline analysis I chose two reference points - bulging as a morphological marker and the accumulation of ROP2, which has been the earliest described protein at the RHID (Jones et al., 2002). Different transgenic lines lines, ROP2 consistently associated with the RHID starting in cell -4 (Figure 1.7), providing a stable reference point in root hair development. ROPs were among the first proteins to accumulate at the RHID, while other factors accumulated specifically during the following steps of root hair development and two GEFs even before this point (Figure 1.17).

3.1.1 ROP2 precedes known upstream ROP regulators

Several factors are known to control ROP activity during root hair development. FER was shown to regulate ROP2 via GEF4 and GEF10 (Duan et al., 2010; Huang et al., 2013). Interestingly, FER and both GEFs accumulate at the RHID significantly later than ROP2 (Figure 1.17). Especially GEF4 and GEF10 seem not to be present at the time of ROP2 accumulation, as they are expressed later in root hair development (Figure 1.15). FER is present at the time of ROP2 accumulation but does not accumulate at the RHID. Thus it remains unclear if FER already activates ROP2 at these early stages via different GEFs, or if it is not required for those initial steps of root hair development. However, in *fer* and *gef4/10* mutant lines root hair growth is affected, but the number of initiated root hairs is not reduced (Duan et al., 2010; Huang et al., 2013), pointing towards a role of FER and GEF4/10 for normal root hair growth, but not for root hair initiation.

PRKs have been described to act upstream of ROPs in pollen tube growth (Chang et al., 2012; Xu et al., 2014; Takeuchi and Higashiyama, 2016). Yet, none of these proteins was investigated for a function in root hair development. PRK7 is the only PRK family member that is not expressed predominantly in pollen (Takeuchi and Higashiyama, 2016) and preliminary results from Jagriti Shrivastava (unpublished) show that PRK7 is expressed in root hair cells. Furthermore, she could show that loss- and gain-of-function mutants of PRK7 have an effect on root hair growth (unpublished). I could show that PRK7 slightly associates with the RHID already before bulging and significantly accumulates at the RHID in cell +1 (Figure 1.13). Taken together, this suggest a role of PRK7 in root hair development and the preliminary results provide a basis for further investigations on PRK7 function.

The TMK family has been described to regulate ROP activity in pavement cells and additionally regulate root growth (Dai et al., 2013; Xu et al., 2014). So far, no TMKs have been investigated in root hair development and it remains elusive if they also regulate ROP activity in this process. In this thesis I attempted to observe TMK1 and TMK3 under their respective native promoters, but no fluorescent signal could be observed in either line, probably due to low expression levels, or missing promoter elements in my expression constructs. However, overexpression of TMK1-mCit led to the accumulation of the fusion protein in polar domains in the plasma membrane (Figure 1.13). This was not root hair specific, but there are until now no

other proteins described to form such domains. This is interesting as especially the initial formation of a polar domain is not understood. Hence TMK1 might provide a model how proteins can cluster in large domains in the plasma membrane. Additionally positioning of ROP accumulation was shown to be dependent on an auxin gradient (Fischer et al., 2006) and TMKs regulate ROP activity in an auxin dependent manner in pavement cells (Dai et al., 2013; Xu et al., 2014). Therefore, it might be possible that TMKs are involved in conveying this positional information, even though their expression level is very low. To test a role of TMK1 in RHID establishment, markerlines of GEF3 or ROP2 could be observed in *TMK1* mutant background. However, no root hair phenotype is described in *TMK1* mutants or lines with multiple *TMK*s mutated.

3.1.2 The feedback system to control ROP activity is established at bulging

As shown in Figure 1.3 a feedback system controls tip growth. Those feedback loops involve ROPs with their binding partners (RICs) and inhibitors (GDIs), $[Ca^{2+}]_{cyto}$, ROS and PIP_2 production and are necessary to control cell growth and ROP activity (Hwang et al., 2005; Takeda et al., 2008). Compared to the investigated ROPs all other components of this feedback system accumulate significantly later, showing that they are in involvel in root hair development but have no function in the initiation prozess. PIP5K3 and RHD2, enzymes producing PIP_2 and ROS during root hair growth, accumulate in cell -2 and -1, respectively, followed by accumulation of $[Ca^{2+}]_{cyto}$ and PIP_2 in cell +1 (Figure 1.17). This shows that the known feedback system to control ROP activity is just in place during and after bulging and is probably required to control tip growth, but not for the establishment of the RHID. A remaining question is how ROP2 activity is controlled in the early stages of RHID establishment, when ROPs already accumulated, but all other factors are not yet present. The GDI SCN1 was shown to inhibit ROPs during root hair development (Carol et al., 2005; Takeda et al., 2008). However, analyzing SCN1 localization did not reveal any striking accumulations or exclusions from the RHID, instead it was homogeneously distributed in the cytosol throughout root hair development (Figure 1.17). Thus, other ROP inhibiting proteins, like GAPs in pollen tubes (Wu et al., 2000; Hwang et al., 2008; Hwang et al., 2010), might be required. So far, there is no GAP with a known role in root hair development. A different

possibility is that ROPs accumulating at the RHID are not activated befor bulging and thus do not need inhibition during this time. This is unlikly, as ROP proteins were described to bind the plasma membrane preferably in its active state (Gu et al., 2005). Furthermore, I found two ROP-activating proteins accumulating at the RHID even before ROPs (Figure 1.16). Nevertheless, the activity status of ROPs at the RHID cannot be determined with certainty without investigating ROP activity sensors, like RIC4$^{\Delta C}$ or FRET sensors for Rho-activity, which have been employed in other systems (Hwang et al., 2005; Nakamura et al., 2006; Donnelly et al., 2014).

3.1.3 Actin regulators are present early in root hair development

The SCAR/WAVE complex was found to be one of the earliest factors appearing at the RHID. It accumulated starting in cell -4 together with ROP2 and both factors co-localized throughout root hair development. Thus, it is possible that the SCAR/WAVE complex is involved in ROP recruitment to the RHID. ROP2 can directly interact with members of the SCAR/WAVE complex (Basu et al., 2004) and studies in stomatal cell division suggest that the SCAR/WAVE complex is the recruiting factor of ROP to define the cell division plane (Park et al., 2015). In this study the authors showed that the SCAR/WAVE complex precedes ROP accumulation and that loss-of-function lines of the SCAR/WAVE complex are defective in ROP recruitment. In root hair development this seems to be different, as ROP2 appears at the same time as BRK1 and even before NAP1 (Figure 1.8, 1.18). Furthermore, loss-of-function mutants of the SCAR/WAVE complex only seem to affect trichomes, but not root hair development (Basu et al., 2004; Brembu et al., 2004; Szymanski, 2005).

Compared to the SCAR/WAVE complex the downstream ARP2/3 complex is mostly cytosolic and hardly associates with the plasma membrane. In addition to the different subcellular localization it also accumulates later at the RHID (Figure 1.8). The clear accumulation and specific association with the cell periphery at the RHID is a strong indication that the ARP2/3 complex is involved in root hair development (Figure 1.8). However, also loss-of-function mutants of the ARP2/3 mainly affect trichome and pavement cell development and show only slightly wavy growing root hairs (Mathur et al., 2003).

The specific accumulation of the SCAR/WAVE complex and the downstream actin polymerizing ARP2/3 complex as well as the previously described role of fine actin in tip growth (Fu et al., 2001; Gu et al., 2005) speak for a function of the investigated complexes in root hair development. The lack of a mutant phenotype could be explained by redundancy amongst the SCAR or ARP proteins (Szymanski, 2005), or by alternative actin polymerizing proteins, like formins (Carol et al., 2005; Yi et al., 2005; Rosero et al., 2016), which could compensate ARP2/3 function. However, it remains unclear if ROPs regulate the SCAR/WAVE complex, or vice versa. Furthermore, it remains elusive at which point actin polymerization is important for root hair development, as only the accumulation of the regulatory complexes, but not their activity could be observed. With this thesis I provided a based to investigate these topics and to elucidate the connection between ROP signaling and the actin network.

3.2 Different GEFs fulfill specific functions in root hair development

3.2.1 GEFs accumulate at specific times during root hair initiation

GEF3 and GEF14 were the earliest proteins to accumulate at the RHID (Figure 1.16). Both preceded ROP accumulation by one cell. Interestingly, the promoter activity or rather the protein concentration did not seem to influence the timing of accumulation. GEF14 was expressed already in the root tip and throughout trichoblast development. GEF3, expressed under the control of its endogenous promoter, was just detectable shortly before its polarization and overexpression did not change the timing of protein accumulation. Thus there must be an additional clue that is responsible for GEF accumulation at a specific point in time. This trigger is specific for GEF3 and GEF14, as other GEFs do not accumulate as early in root hair development. GEF4 and GEF12 only accumulate in cell +1, GEF10 and GEF11 hardly show any polarization and accumulated only after bulging even when ubiquitously expressed (Figure 1.15, 1.16). Still it is unclear what this trigger could be. It is possible that specific genes, which become expressed at a defined time during trichoblast differentiation (Wachsman et al., 2015), or auxin signaling, which

was shown to be able to influence root hair positioning (Fischer et al., 2006), are determining. The overall auxin gradient in the root reaches a local minimum in the transition zone between meristem and differentiation zone (Di Mambro et al., 2017). In this region the first cells show GEF3 and GEF14 accumulation at the RHID. Another possibility for a developmental trigger would be an extracellular signal such as a peptide, which may be sensed by an RLK. Examples for this mechanism include FER signaling (Haruta et al., 2014) or pollen tube guidance by PRK-sensed LURE peptides (Takeuchi and Higashiyama, 2016). As the developmental program is auxin regulated and possible signals could be expressed dependent on the stage of differentiation, it is also possible, that a combination of these mechanisms is required for proper root hair initiation and positioning. Whatever the inducing signal is, the different behavior of the investigated GEFs shows that each GEF has its own function in root hair development and that there are mechanisms that influence the subcellular localization of specific GEFs.

3.2.2 GEF3 is the most crucial GEF for ROP dependent root hair initiation.

In loss-of-function and overexpression analysis of ROPs, I could show that ROP2 and ROP4 are important for root hair initiation and growth (Figure 1.19, 1.22). However, occasionally root hairs still initiated in *rop2-1*/*rop4-1* double mutants. It could be that there is still functional ROP2 or ROP4 protein made in these lines, possibly by splicing of the T-DNA insertion from the transcript. However, previous reports showed absence of full-length transcripts in both mutant lines (Fu et al., 2005; Jeon et al., 2008). Alternatively, it is possible that other ROPs are redundant in this process. Expression data from transcriptome analysis indicates that other closely related ROPs, like ROP3 and ROP5, are expressed in trichoblasts (Figure 1.5) and could compensate loss of ROP2 and ROP4. Also for ROP6, the clostest homologe of ROP2 and ROP4, it was shown that it is expressed in trichoblasts and that it accumulates at the RHID (Stanislas et al., 2015). I was able to confirm that ROP6 can accumulate at the RHID using an inducible construct (Figure 1.7). However, a different study showed that ROP6 is expressed specifically in lateral roots and not in trichoblasts (Poraty-Gavra et al., 2013), questioning a function of ROP6 in root hair initiation. This would be in line with the transcriptome data showing low expression of ROP6 in trichoblasts (Figure 1.5). Nevertheless, to confirm that

ROP function is absolutely essential for root hair growth, higher order mutants would be required.

GEFs are the activating factors of ROPs. Loss-of-function mutants of the investigated GEFs showed that GEF3 is important for root hair initiation (Figure 1.20). To control that this effect is due to loss of GEF3, I showed the almost complete absence of full-length mRNA (Figure 1.21). Furthermore, together with Anna Reichelt, by investigating multiple *gef3* mutant alleles (Figure 1.21) and complementation experiments, which are both shown in Denninger et al. (submitted), we could confirm that the phenotype is caused by loss of GEF3 function. Other GEFs did not show significant effects on root hair initiation, only in *gef4-2* and *gef14-2* mutants small effects on root hair initiation could be observed (Figure 1.20). In *gef3-1* root hair initiation is only reduced and not completely lost. This indicates remaining ability to recruit and activate ROPs, which is sufficient to start root hair initiation. Possible redundancy of GEF function could explain the observed phenotypes. To test this, combinatory mutants of GEFs have to be investigated. Yet, loss of GEF3 had the strongest effect on root hair initiation among the tested GEFs.

Similar conclusions can be drawn from overexpression experiments. Inducible GEF3 overexpression led to the formation of multiple hairs within one cell, which were additionally branched (Figure 1.22). Inducible GEF4 overexpression led to hair branching, which had already been shown in previous studies (Huang et al., 2013), but not to the induction of additional hairs (Figure 1.22).

In addition to ROP activation and resulting root hair initiation, GEF3 is also required for ROP2 recruitment to the plasma membrane. As ROP2 accumulation closely follows GEF3 accumulation, it gets recruited to ectopic GEF3 domains and does not get polarized in *gef3-1* mutants (Figure 1.18, 1.23, 1.26). The formation of ectopic domains and ROP2 recruitment to these domains was only observed for GEF3 and no other overexpressed GEF, which points towards a unique function of GEF3 for RHID establishment.

Taken together, this shows that GEF3 is necessary for RHID establishment, root hair initiation and possibly to control root hair growth, while GEF4 seems to be only involved in root hair growth, together with other GEFs, like GEF10 (Huang et al., 2013).

3.2.3 Controlling GEF activity before root hair initiation.

GEF3 and GEF14 are present together with ROP2 and ROP4 at the RHID long before root hair initiation. As described in 3.1.2 it is unclear if ROPs are already active this early before bulging or if they are accumulating and get activated just for bulging. Either way, GEF and thus ROP activity needs to be regulated to prevent premature root hair outgrowth or too strong growth induction, as this will lead to deformed hairs (Jones et al., 2002; Huang et al., 2013). The GDI SCN1 is required to prevent too much growth induction, as in SCN1 mutants multiple bulges emerge from one cell, right next to each other (Carol et al., 2005). This phenotye is similar to the overexpression phenotype of mCit-GEF3_ind (Figure 1.22), but it is unclear if SCN1 controls ROP activity already during RHID establishment, or just during bulging. Additionally, there might be other ROP inactivating proteins that are important to balance ROP activity, like it was shown for ROP-GAP3 and GEF4 in cell wall patterning (Oda and Fukuda, 2012). As alternative to a balance of ROP activators and deactivators, GEF activity could also be regulated directly by posttranslational modifications. GEF12 activity is regulated by phosphorylation of its upstream RLK during pollen tube growth (Zhang and McCormick, 2007). It is possible that GEFs accumulate at the RHID and recruit ROPs, but do not activate them. Only after a RLK receives an additional trigger, GEFs get activated and subsequently activate ROPs to promote root hair outgrowth. Thus, GEF3 would have two distinct functions in RHID establishment. First, recruit ROP2 and the subsequent growth machinery and second, activating ROPs upon a trigger signal to start growth.

It needs to be determined whether RLKs are required for either step of ROP polarization and growth initiation. However, growth initiation is controlled by external cues, like nutrient availability (Stanley et al., 2017), and it is likely that there are proteins directly controlling GEF3 in this process. If additional factors, like RLKs are also required for the initial GEF3 domain formation remains unclear. GEF3 seems to be able to form polar domains at the plasma membrane, even if it is expressed outside its normal trichoblast context (Figure 1.26). Nevertheless, the ectopic domains were not as concise as the RHID and varied in size and position. Therefor

other proteins might regulate the exact timing, position and domain size of GEF3 at the RHID.

3.3 The mechanism for protein polarization

3.3.1 Spontaneous protein domain formation

In plants only few examples of proteins forming stable polar domains in the plasma membrane are known. For example PIN-FORMED (PIN) auxin transporters form stable domains on one side of the cell (Müller et al., 1998; Iweiler et al., 1998), the microtubule regulating protein MICROTUBULE DEPLETION DOMAIN 1 (MIDD1) forms domains during cell wall formation in xylem cells (Oda and Fukuda, 2012). But in both cases, the cellular context and other proteins are required for the formation of these domains (Petrášek et al., 2006; Oda and Fukuda, 2012). Another example of a protein that forms stable domains in plants is BASL, which formes a very defined domain in developing stomata to control the cell division plane. Additionally, BASL is able to from ectopic domains in hypocotyl and root cells (Dong et al., 2009). In this thesis I found two other proteins that spontaneously form such domains, TMK1 and GEF3 (Figure 1.13, 1.26). In all three cases - BASL, TMK1 and GEF3 - this domain formation seems to be independent from other factors, or that the cofactors required for domain formation are also present in the observed cells types, as polar domains could be observed in also in ectopic cells. If the mechanism regulating this domain formation is similar for these proteins, if it depends on additional factors, or on intrinsic protein properties is an still open question.

When discussing domains at the plasma membrane, it is important to differentiate between large “macrodomains”, like the RHID which is 17.4 µm (± 2.6 µm) in diameter (Figure 1.24) and clusters of few proteins in the plasma membrane, called micro- or nanodomains, which are just up to 1 µm in size (Ott, 2017). Multiple proteins like FLOTILLINS, REMORINS, or RLKs have been shown to form such microdomains (Jarsch et al., 2014; Liang et al., 2018). Interestingly GEF3 seems to form microdomains within the macrodomain (Figure 1.25). These microdomains are also seen for BRK1 (Figure 1.8), but it is unclear if both proteins locate to the same microdomains or if they are distinct. ROP2 is more evenly spread in the RHID than GEF3 and BRK1, but some clusters are detectable (Figure 1.25).It could be that ROP2 is recruited into GEF3 microdomains and enriched there, as GEF3 shows a significantly reduced diffusion rate as compared to ROP2 (Figure 1.25).

How proteins cluster together in a polar fashion to form a macrodomain like the RHID is not yet understood. In yeast it was proposed that CDC42 can spontaneously form polar domains in the absence of other polarity clues (Wedlich-Soldner et al., 2003). This polarization is thought to be based on Turing's reaction diffusion model, in which diffusion rates of the accumulating factor are influenced by an activator and an inhibitor, connected by a positive feedback system, leading to an accumulation of protein at a specific site (Turing, 1952; MEINHARDT and GIERER, 1974). For ROP2 such a mechanism was proposed by (Payne and Grierson, 2009). This model presumed that the influence of auxin and ethylene, which were shown to to control ROP and root hair positioning (Fischer et al., 2006), leads to a spontaneous local ROP activation and a inhibition of ROP GDI binding. A positive feedback then activates more ROP at this location, leading to the formation of the RHID. Therefor it is essential that active and inactive ROP have different diffusion rates (Turing, 1952; Payne and Grierson, 2009). I could show that active and inactive ROP2 have a different subcellular localization, with mCit-CA-*rop2* being predominantly membrane associated and mCit-DN-*rop2* being mainly cytosolic (Figure 1.27). However, both ROP2 mutants show a reduced RHID association and the diffusion rate of both still needs to be determined. S-acylation of ROPs depends on their activity state, like it was shown for ROP6 (Sorek et al., 2010; Sorek et al., 2011). This lipid modification could be responsible for such differences in the diffusion rate, but the corresponding studies were both retracted and it is not clear if these findings hold true (See also 1.3). However, using a ROP2 version with mutantions in all cysteine positions, which are the potential sites for S-acylation, I could show that ROP2 still accumulates at the RHID (Figure 1.29). This proves, that S-acylation is not necessary for normal ROP2 polarization. Furthermore, interaction studies of GEF3 and ROP2, which were performed in collaboration with the group of Christopher Grefen (Denninger et al., submitted), and the investigation of ROP2 derivatives lacking the interaction domain (Figure 1.3, 1.28) supporte the notion that the interaction to GEF3 is the main driving force to polarize ROP2 at the RHID. Still, it is possible that a mechanism proposed by (Payne and Grierson, 2009) exists, able to polarize ROP2 in the absence of other cues, as mCit-CA-rop2 seems to associate with the plasma membrane independent of GEF3. Nevertheless, the results of this thesis show that ROP2 polarization is achieved by GEF3. Nevertheless, it is still

unclear how GEF3 itself gets polarized at the RHID and if any other factors are required for this.

3.3.2 Cell identity regulating protein polarity

I found that ROP2 accumulation at the RHID was abolished in *gef3-1* and *rhd6-1* lines (Figure 1.23). The loss of ROP2 polarity in *gef3-1* can be explained by lack of the recruitment factor. Why ROP2 is not polarized in rhd6-1 still remains elusive. RHD6 is a transcription factor required for trichoblast development and in mutant lines no root hairs are produced (Masucci and Schiefelbein, 1994). RHD6 is responsible for the expression of multiple root hair specific genes (Won et al., 2009) and thereby controls root hair outgrowth. Trichoblast identity itself is conferred by transcription factors upstream of RHD6 (Grierson et al., 2014), thus epidermal cells in *rhd6-1* should have regular trichoblast identity, but lack the expression of downstream trichoblast specific genes. Examples of RHD6 downstream factors are the root hair specific (RHS) genes, like *RHS16*, *RHS10/PERK13* and *RHS11/GEF4* (Won et al., 2009). GEF3 was not identified as a a downstream target of RHD6, but one explanation for the lack of ROP2 polarity in *rhd6-1* mutants could be loss of GEF3 expression. This could be tested by RT-PCR of *rhd6-1* roots or crossing of a GEF3 reporter line into the *rhd6-1* background. Another possibility for lacking ROP2 polarity in *rhd6-1* lines is that an additional factor required to polarize GEF3 is missing in these lines and thus the GEF3 dependent ROP2 recruitment is affected. Either way, the loss of ROP2 polarity in *rhd6-1* provides a good starting point to get a better inside into the mechanisms that polarize GEF3 and subsequent ROP2 recruitment.

3.3.3 Domain stabilizing mechanisms

After GEF3 polarization it recruits ROP2 and possibly subsequent factors. To stabilize the domain in size and at its location, Turing-based models use a positive feedback loop in which the polarized factor positively regulates its activator (Turing, 1952). In yeast this is done by the scaffold protein BUD EMERGENCE1 (BEM1) which links CDC42 and the GEF BUD5 at the bud emergence site (Chant et al., 1991; Peterson, 1994; Wedlich-Soldner et al., 2004). In plants, no scaffolding proteins are known in root hair development, but ROP binding proteins like ICR1 and ARMADILLO REPEAT ONLY 1 (ARO1) have been proposed to act as

scaffolding proteins in ROP signaling during pollen germination (Lavy et al., 2007; Li et al., 2008; Hazak et al., 2010; Vogler et al., 2015). If these scaffolding proteins are required, or if plant GEFs function as scaffolds themselves remains unclear.
In addition to scaffold proteins, protein recruitment and complex formation can depend on landmark proteins. In budding yeast, transmembrane proteins heve been described to act as landmark proteins during bud or shmoo formation, recruiting CDC42 (Roemer et al., 1996; Harkins et al., 2001). So far, no protein with such landmark function has been described, but the ability of GEF3 to form spontanious domains and its ability to recruit ROP2 suggest that GEF3 itself acts as a landmark protein during cell polarization in trichoblasts. It is also possible that an yet unknown factor, like an upstream RLK, fulfills this function. Such a protein, or a closely related protein, would need to be expressed also in other cell types than trichoblasts, as GEF polarization also occurs in atrichoblasts, cortex cells and hypocotyl cells (Figure 1.26). However, this would contradict the observation that the polarizing factor is expressed in a trichoblast specific manner and lost in *rhd6-1* (see 3.3.2, Figure 1.23). This argues for GEF3 acting independently as a landmark protein in RHID formation.

3.3.4 The general function of GEFs as recruitment factors.

The results of this thesis suggest that GEF3 represents the polarization factor at the RHID and acts as a landmark protein for ROP recruitment. The mechanism that GEFs can be involved in GTPase recruitment is already known from yeast. During bud formation the GEF BUD5 is polarized by landmark proteins and recruits the GTPase RSR1 (Chant et al., 1991; Roemer et al., 1996; Harkins et al., 2001). This leads to recruitment of the GEF CDC24, which then polarizes CDC42 (Bender and Pringle, 1989; Zheng et al., 1994; Chiou et al., 2017). Thus there are two GEF-GTPase pairs acting during bud formation and are polarized by landmark proteins. More recent work in *Drosophila melanogaster* showed that during embryo cellularization the two GEFs DIZZY and ELMO-SPONGE are required for polarization of the GTPase RAP1 and subsequent recruitment of further downstream factors (Bonello et al., 2018; Schmidt et al., 2018). Also during wound closing GEFs are essential to polarize GTPases. In this case RhoGEF2 was shown to recruit Rho1 and two more downstream GEF-GTPase modules (Nakamura et al.,

2017). In case of wound closing RhoGEF2 becomes polarized by binding to ANNEXIN (Nakamura et al., 2017), but during cellularization no upstream factors are known for GEF polarization (Schmidt et al., 2018).

These examples together with the results of this thesis suggest a common principle, in which GEFs act as landmark proteins for targeted accumulation of the growth machinery. This might include additional organism-specific factors like upstream positional cues or scaffold proteins, but the general process of GEFs recruiting the control switch seems to be a common theme in eukaryotic cells. This could be necessary to prevent spontaneous polarization of GTPases and to guide growth in a directed and controlled manner.

Chapter II

–

Intracellular polar Ca^{2+} signaling

–

Not just up and down, it’s also about how and where

1 Introduction

1.1 $[Ca^{2+}]_{cyto}$ - a ubiquitous messenger

Ca^{2+} is one of the most important ions for the cell, involved in a plethora of cellular processes, like regulation of protein activity, fusion of membranes, or signal transduction (Clapham, 2007; Dodd et al., 2010). In the 1990s, the first investigations of $[Ca^{2+}]_{cyto}$ in plant cells showed changing cellular $[Ca^{2+}]_{cyto}$ concentrations in response to hormones, external biotic or abiotic stresses, during gamete fusion and tip growth (McAinsh et al., 1990; Knight et al., 1991; Schiefelbein et al., 1992; Ehrhardt et al., 1996; Digonnet et al., 1997). Since then, numerous studies have linked Ca^{2+} signals to various cellular processes in plants. For example, $[Ca^{2+}]_{cyto}$ was shown to be an important long-range messenger for environmental stresses, like salt or cold stress, or in response to mechanical stimuli, like bending or touching (Knight et al., 1991; Choi et al., 2014; Choi et al., 2016; Wilkins et al., 2016). Additionally, Ca^{2+} signaling is an important response to the interaction with symbionts, or infectious microbes (Ehrhardt et al., 1996; Blume et al., 2000; Keinath et al., 2015). Like in responses to other organisms, plant cells also respond with $[Ca^{2+}]_{cyto}$ signals to cell-cell contacts during the fertilization process (Iwano et al., 2004; Iwano et al., 2012; Dresselhaus and Franklin-Tong, 2013; Denninger et al., 2014; Hamamura et al., 2014; Kaya et al., 2014).

Even though the described processes in hormone signaling, stress response, microbe interaction and fertilization involve $[Ca^{2+}]_{cyto}$, the nature of these $[Ca^{2+}]_{cyto}$ fluctuation is different for all processes and leads to different and specific responses. For example, abiotic stresses cause a strong $[Ca^{2+}]_{cyto}$ signal within individual cells, which propagates in a wave-like pattern from cell to cell through the whole organism (Choi et al., 2014). In contrast, responses to biotic signals are usually more restricted (Keinath et al., 2015). During the fertilization process, $[Ca^{2+}]_{cyto}$ fluctuations appear in various forms, like oscillations in different frequencies in pollen tubes, or synergid cells, or in longer lasting transients during the gamete fusion process (Iwano et al., 2012; Denninger et al., 2014; Hamamura et al., 2014; Ngo et al., 2014). Additionally, differences in amplitude and frequency of the $[Ca^{2+}]_{cyto}$ transient leads to different gene expression profiles and thus to different cellular responses (Whalley and Knight, 2012).

Furthermore, the intracellular location of $[Ca^{2+}]_{cyto}$ maxima affects the cellular response and cell polarity, as contact to NODULATION (Nod)-factor, a molecule secreted from symbiotic bacteria to communicate with their host plant, leads to nuclear Ca^{2+} transients initiated in the nucleus, while contact with bacterial flg22, an 22 amino acid peptide of bacterial flagellin, triggers cytosolic Ca^{2+} peaks (Ehrhardt et al., 1996; Blume et al., 2000). To understand how $[Ca^{2+}]_{cyto}$ transients translate into specific cellular responses, it is essential to investigate the exact nature of the $[Ca^{2+}]_{cyto}$ transient and to know the location, spreading, frequency, and amplitude.

1.2 Ca^{2+} channels and transporters in tip growth

Subcellular distribution of $[Ca^{2+}]_{cyto}$ and its resulting function was extensively studied in tip growing cells, where it integrates internal cellular processes, mechanical stress from the fast growth process and external cues from chemo-attractants (Steinhorst and Kudla, 2012; Higashiyama and Takeuchi, 2015). In two tip growing cells type in plants, root hairs and pollen tubes, it seems that the role of $[Ca^{2+}]_{cyto}$ in controlling tip growth is very similar and findings are mostly interchangeable between the two cell types (Mendrinna and Persson, 2015). As described in Chapter I, $[Ca^{2+}]_{cyto}$ is an important part of a feedback system with ROPs and ROS signaling to regulate cell wall integrity and actin polymerization during tip growth (Mangano et al., 2016; Gilroy and Swanson, 2017). $[Ca^{2+}]_{cyto}$ and ROPs were shown to oscillate in shifted phases, regulating each other to balance growth and cell restriction, thus, preserving cellular integrity in this fast-growing system (Hwang et al., 2005).

For coordinated and quick changes in the $[Ca^{2+}]_{cyto}$ levels like seen in pollen tubes and root hairs, it is essential that coordinated $[Ca^{2+}]_{cyto}$ import and export systems are present in the cell. GLUTAMATE-LIKE RECEPTORS (GLRs), which are amino acid-gated cation channels, were shown to be important for directional guidance of pollen tubes and general tip growth (Qi et al., 2006; Michard et al., 2011). The investigated GLRs were shown to localize to endomembrane systems, but the observed $[Ca^{2+}]_{cyto}$ fluxes suggest the presents of GLRs also in the plasma membrane (Wudick et al., 2018).

Additionally, CYCLIC NUCLEOTIDE-GATED CHANNELS (CNGCs) were shown to be important for tip growth. CNGCs are activated by cyclic nucleotides, cAMP or

cGMP, and mediate influx of Ca^{2+} into the cytosol. In plants CNGCs have been shown to mainly localize to the plasma membrane, but also to intracellular compartments (Frietsch et al., 2007; Shih et al., 2015; Zhang et al., 2017). In Arabidopsis, GLRs and CNCGs protein families have multiple members (Mäser et al., 2001; Qi et al., 2006), which are expressed in different tissues and localize to different membranes (Frietsch et al., 2007; Zhang et al., 2017; Wudick et al., 2018). Furthermore, there are other Ca^{2+} channels and transporters, which I do not further introduce, as they are not relevant for this thesis. The multiple Ca^{2+} channels and transporters, as well as their diverse localizations lead to a complex network of proteins regulating Ca^{2+} fluxes.

1.3 $[Ca^{2+}]_{cyto}$ signals during double fertilization

During the fertilization process, pollen grains germinate on the stigma of the pistil, forming a tip growing pollen tube. Growing through the floral tissue, pollen tubes approach the female gametophyte, carrying two sperm cells. The female gametophyte contains three different cells types that are important for fertilization. Synergid cells, required for pollen tube reception and to trigger sperm cell release, as well as two female gametes the central cell and the egg cell, which both get fertilized and form the endosperm and the embryo, respectively. As two male sperm cells fertilize two female gametes, this process is referred to as double fertilization (Bleckmann et al., 2014; Higashiyama and Takeuchi, 2015). Once the pollen tube reaches the female gametophyte, it comes in contact with two synergid cells and grows along the synergid cell surface. Contact between the two cells triggers pollen tube growth arrests, synergid degeneration due to programmed cell death and pollen tube rupture. The rupture of the pollen tube propels the two sperm cells towards the fusion site between the egg and the central cell (Hamamura et al., 2011; Leshem et al., 2013; Bleckmann et al., 2014). After sperm cell release, one cell fuses with the central cell, while the other cell fuses with the egg cell, completing double fertilization (Hamamura et al., 2011; Dresselhaus and Franklin-Tong, 2013; Leshem et al., 2013; Bleckmann et al., 2014).

$[Ca^{2+}]_{cyto}$ signals were shown to be involved in many of the aforementioned processes. Pollen germination on the stigma, as well as pollen tube growth within

the floral tissue is regulated by Ca^{2+} signaling (Iwano et al., 2004; Iwano et al., 2014). Furthermore, pollen tube contact with the synergid cells triggers $[Ca^{2+}]_{cyto}$ oscillations in synergid cells, which is important for synergid cell death and sperm cell release (Iwano et al., 2012; Ngo et al., 2014).

During my master thesis in the lab of Thomas Dresselhaus (Regensburg University), in a collaboration with the labs of Wolf Frommer and David Ehrhardt (Carnegie Institution, Department of Plant Biology, Stanford), together with Guido Grossmann, I could show that synergid cells exhibit $[Ca^{2+}]_{cyto}$ oscillations, confirming these results. In addition to these observations, I could demonstrate already in my master thesis that the $[Ca^{2+}]_{cyto}$ level did not oscillate equally within the synergid, when they are in close contact to a pollen tube, with a maximum $[Ca^{2+}]_{cyto}$ elevation at the contact site of both cells (Denninger et al., 2014). Moreover, I could show during my Master thesis that two $[Ca^{2+}]_{cyto}$ peaks occur in the egg cell after sperm cell release. The first $[Ca^{2+}]_{cyto}$ elevation correlates with sperm cell release from the pollen tube and the other occurred shortly later, but the exact timing of the second elevation could not be correlated to any event of fertilization during my master thesis (Denninger et al., 2014).

Additionally, in a cooperation, Andrea Bleckmann (Regensburg University) showed that similar events happen in the central cell. The central cell showed only one $[Ca^{2+}]_{cyto}$ elevation which correlates with sperm cell release (Denninger et al., 2014). These results were part of the publication (Denninger et al., 2014) and were in parallel published by another group (Hamamura et al., 2014).

These results showed that the different cells respond with different $[Ca^{2+}]_{cyto}$ signals during fertilization and that the localization of these signals within one cell might be important for proper fertilization. However, at the beginning of this thesis, still open questions were if the $[Ca^{2+}]_{cyto}$ signals in the egg cell are equally or polar distributed within the cell and which events of fertilization the observed signals correlate to.

1.4 The aim of Chapter II

To get a better understanding of the cellular processes leading to $[Ca^{2+}]_{cyto}$ oscillations in tip growing cells, the role of CNGCs during root hair growth were investigated. Our collaborator Petra Dietrich (Erlangen University) had identified three CNGCs (CNGC6, CNGC9 and CNGC14), which are expressed in trichoblasts and are required for root hair growth. The aim of this part of the thesis was to investigate the effect of these three CNGCs on the establishment of the tip-focused $[Ca^{2+}]_{cyto}$ gradient and $[Ca^{2+}]_{cyto}$ oscillations during root hair growth in cooperation together with the lab of Petra Dietrich.

An additionally goal of this thesis was to further investigate the diverse $[Ca^{2+}]_{cyto}$ signals of the female gametophyte during the fertilization process. The main focus was to define the subcellular localization of the $[Ca^{2+}]_{cyto}$ elevations in synergid cells and the egg cell and to correlate those signals to the events of double fertilization.

2 Results

2.1 Ca^{2+} signaling during root hair growth

To unveil the role of CNGCs for root hair growth, CNGC6, CNGC9 and CNGC14 were investigated. These CNGCs were chosen by the group of Petra Dietrich (University Erlangen-Nürnberg), as these showed an expression maximum in root hairs and T-DNA mutant lines of these genes exhibited root hair growth defects. To observe the effects of these CNGCs on the $[Ca^{2+}]_{cyto}$ level in root hairs, the cytosolic intensiometric Ca^{2+} indicator RED FLUORESCENT GENETICALLY ENCODED CALCIUM INDICATORS FOR OPTICAL IMAGING 1 (R-GECO1) (Zhao et al., 2011) was crossed into a mutant line of CNGC9 and a double mutant line of CNGC6 and CNGC14, by the group of Petra Dietrich (Table 4.1). I monitored the $[Ca^{2+}]_{cyto}$ oscillations in growing root hairs of these lines using the RootChip (Grossmann et al., 2011), a microfluidic device that allows observation of roots without perturbation due to plant handling.

On the morphological level, no difference between root hairs of WT, *cngc9-1* mutants, or *cngc6/cngc14* double mutants could be observed. All three lines still showed a tip-focused $[Ca^{2+}]_{cyto}$ gradient and fluctuations of this gradient (Figure 2.1 A-E). Kymograph analysis of the $[Ca^{2+}]_{cyto}$ levels showed that in Col-0 and *cngc9* the $[Ca^{2+}]_{cyto}$ levels oscillate regularly, while in *cngc6/cngc14* double mutants no regular fluctuations of the $[Ca^{2+}]_{cyto}$ level could be observed (Figure 2.1 A-C). Additionally, *cngc6/cngc14* root hairs burst frequently, which rarely happened in WT under constant conditions (Figure 2.1 F). Furthermore, *cngc6/cngc14* root hairs grew slower compared to WT and *cngc9* (1 µm/s vs. 1.2 µm/s and 1.2 µm/s, Figure 2.1 G). In bursting *cngc6/cngc14* root hairs the $[Ca^{2+}]_{cyto}$ levels dramatically increased in the whole root hair tip shortly before the burst (Figure 2.1 D), similar to bursting pollen tubes described in other studies (Iwano et al., 2012; Ngo et al., 2014).

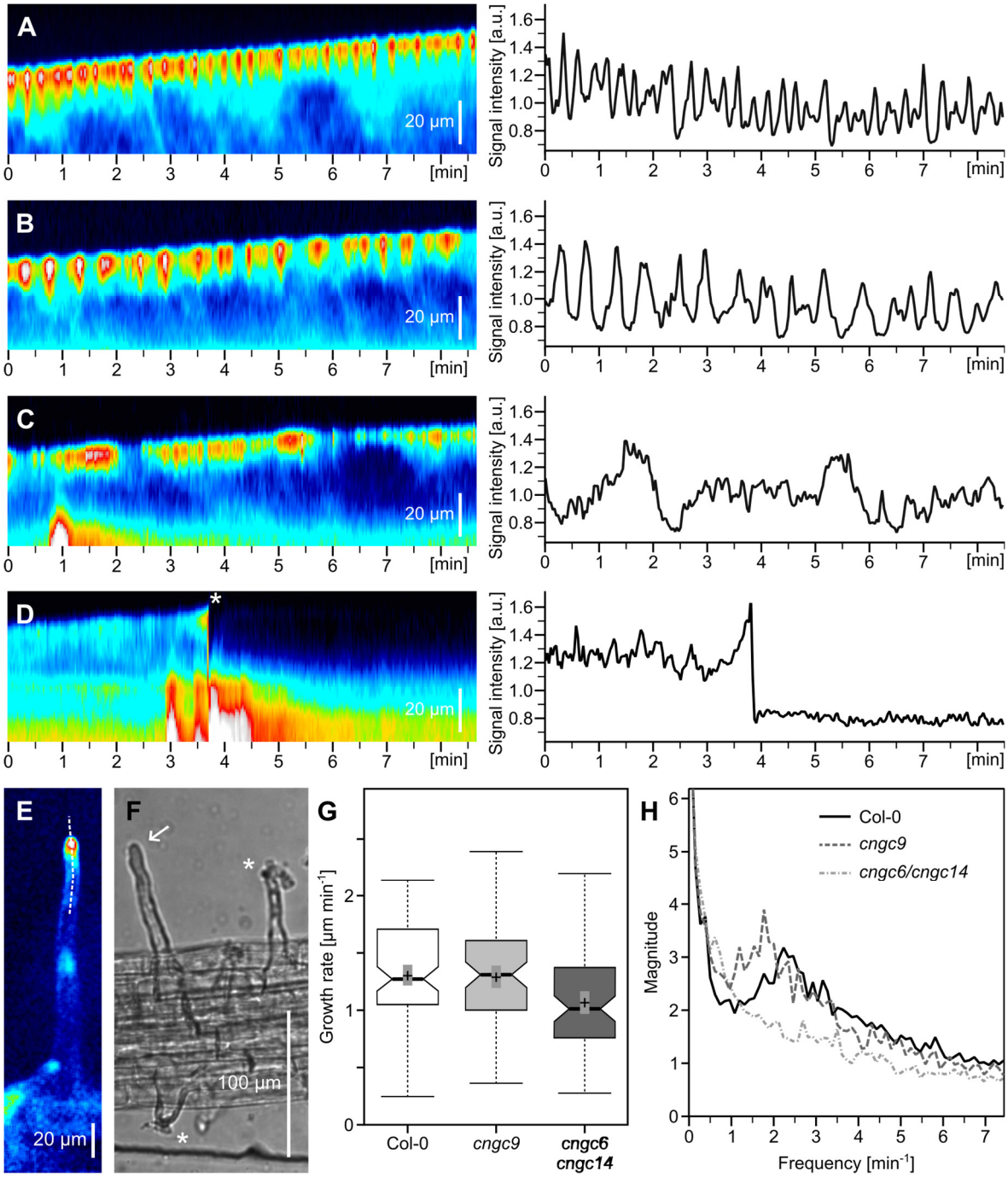

Figure 2.1 CNGC9, CNGC6 and CNGC14 contribute to $[Ca^{2+}]_{cyto}$ oscillations in root hairs

(**A-D**) $[Ca2+]_{cyto}$ oscillations in growing root hairs expressing R-GECO1 in Col-O (**A**), cngc9 (**B**) and *cngc4/cngc14* double mutants (**C-D**). (**C**) normally growing root hair, (**D**) bursting root hair (time of rupture marked by asterisk) of *cngc4/cngc14* double mutants. Left panels show exemplary kymographs along a line like indicated in (**E**). Right penal shows intensity profile along the growing edge of the root hair in the kymograph on the left. (**E**) Representative root hair expressing R-GECO1. (**F**) Transmitted light image of *cngc4/cngc14* double mutant root hairs, with normally growing (arrow) and burst hairs (asterisks). (**G**) Quantification of the growth rate in

the three used genotypes. + = sample mean; dotted line indicates mean value of mCit-GEF3 in cell -1; Center line = sample median. Detailed description of box plots in Chapter IV, 4.2.1. (**H**) Fourier transformation of the $[Ca2+]_{cyto}$ oscillation frequencies of the three used genotypes. X-axis shows the Ca^{2+} oscillation frequency and Y-axis the abundance of the frequency.

To characterize the oscillatory behavior in those lines, Fourier transformations of the intensity plots of each individual growing root hair were performed by Guido Grossmann using IgorPRO software. WT root hairs showed a wide spectrum of oscillation frequencies, but a predominant oscillation frequency could be detected at a frequency of 2.31 min^{-1} (Figure 2.1 H). *cngc9* mutants also showed a similar degree in variability, however, the predominant frequency lied at 1.85 min^{-1} (Figure 2.1 H). In contrast, *cngc6/14* double mutants did not show any obvious regular frequency (Figure 2.1 H). The observed change in $[Ca^{2+}]_{cyto}$ oscillations showed that all analyzed CNGCs are involved in establishing $[Ca^{2+}]_{cyto}$ oscillations in root hairs. However, in the *cngc9* mutant and the *cngc6*/*cngc14* double mutant lines root hairs were still able to grow and exhibited a tip-focused $[Ca^{2+}]_{cyto}$ gradient.
The disturbed frequency of $[Ca^{2+}]_{cyto}$ oscillations and the bursting root hair in *cngc6*/*cngc14* double mutant shows that the $[Ca^{2+}]_{cyto}$ fluctuations are required for cell survival. The bursting indicates a loss of cell integrity, probably due to a lack of growth inhibition.

2.2 Ca^{2+} signaling during fertilization

The process of double fertilization involves cell-cell communication between different male and female cells. Ca^{2+} signaling can be observed in all steps of this process (Bleckmann et al., 2014). To observe the growing pollen tube during double fertilization, a marker line, expressing HTR10::HTR10-mRFP, labeling the sperm cell nuclei, and LAT52::tagRFP-T-MtSYMREM1, labeling the pollen tube membrane, was used (Denninger et al., 2014). To monitor the $[Ca^{2+}]_{cyto}$ levels in the gametophytic cells, the FRET based Ca^{2+} indicator CerTN-L15 (Heim et al., 2007) was expressed under cell type specific promoters (MYB98 for synergid cells, EC1.1 for egg cell, and DD65 for central cell) (Denninger et al., 2014).

During the beginning of my PhD thesis, I performed additional experiments observing the $[Ca^{2+}]_{cyto}$ levels in synergid cells and egg cells during fertilization, confirming the previous results of my master thesis and increasing the number of biological replicates to allow further statistical analysis. Moreover, I performed more detailed analysis of the oscillations in synergid cells and could show that the $[Ca^{2+}]_{cyto}$ elevation is always maximal at the point of contact with the pollen tube tip. This is also the case when the pollen tube grows around the synergid cells (Denninger et al., 2014).

Furthermore, more detailed analysis of the $[Ca^{2+}]_{cyto}$ elevations in egg cells were performed. During fertilization, two $[Ca^{2+}]_{cyto}$ signals could be observed. The first $[Ca^{2+}]_{cyto}$ elevation clearly correlated with the pollen tube burst and could be due to mechanical stress or sensing of pollen tube content (Figure 2.2 A, C). It remained unclear to which event of fertilization the second $[Ca^{2+}]_{cyto}$ elevation in the egg cell corresponded. To get a more detailed insight into the timing of events, the movement of the sperm cells was tracked at the fusion site (Figure 2.2 A, B). First, the sperm cells, which were just released from the pollen tube, moved fast to a location between egg and central cell (Phase I). Shortly afterwards, the sperm cell that later fused with the egg cell (SP_{EC}), underwent a small, fast shift of approximately 1 µm towards the egg cell and away from the other sperm cell (Phase II). During that shift, the other sperm cell, which later fused with the central cell (SP_{CC}), hardly changed position and did not move as the SP_{EC} continuously moved into the egg cell (Phase III). Finally, the SP_{CC} underwent a fast, small shift towards the central cell and shortly afterwards moved continuously into the central cell (Phase IV) (Figure 2.2 A, B).

When comparing the observed shift of the SP_{EC} with the $[Ca^{2+}]_{cyto}$ levels in the egg cell, the shift perfectly correlated with the onset of the second $[Ca^{2+}]_{cyto}$ elevation of the egg cell (Figure 2.2 C, D). Additionally, when observing the morphology of the egg cell, just after the shift of the SP_{EC} the Citrine signal of the egg cells protruded beyond the egg cell boundaries into the direction of the sperm cell, indicating cell fusion (Figure 2.2 E). At the same time the $[Ca^{2+}]_{cyto}$ elevation was detectable in the egg ell, with its maximum close to the position of the SP_{EC}. This movement of fluorescent signal to the sperm cell position, after the sperm cell shifted towards the egg cell shows that this event represents the fusion of both cells, as only then

cytosolic material can be exchanged. Thus, the second $[Ca^{2+}]_{cyto}$ elevation in the egg cell might occurs as a result of cell fusion.

The results obtained during my master thesis, together with the new results obtained during my PhD was published in Nature Communications (Denninger et al., 2014) and the according figure is shown in Figure 2.2.

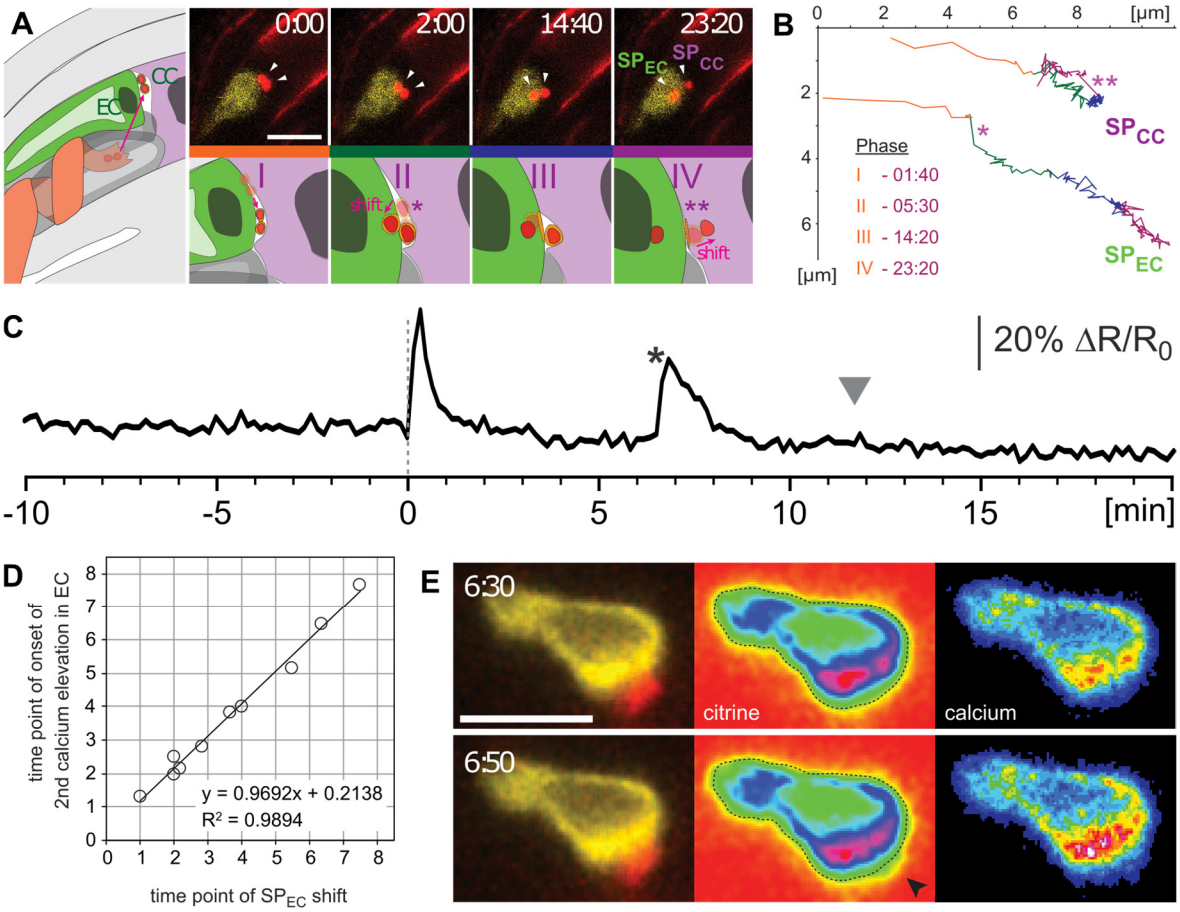

Figure 2.2 Successful fertilization is accompanied by a $[Ca^{2+}]_{cyto}$ transient in egg cells

(**A**) Left: scheme depicting sperm cell (SP, red) release from a pollen tube growing around receptive synergid (grey). After burst SP are located at the fusion site between egg (green) and central cell (violet). Upper panel: time series of SP (red, arrowheads) fertilizing an egg cell expressing the CerTN-L15 sensor (yellow). SP_{EC}: SP fusing with egg cell, SP_{CC}: SP fusing with central cell. Lower panel: scheme of different phases of SP movement before and during fusion. Phase I: parallel movement of SPs along fusion site. Phase II: shift of SP_{EC} (single asterisk) towards egg cell. Phase III: arrest of SP_{CC} and movement of SP_{EC} nucleus towards egg cell nucleus. Phase IV: shift of SP_{CC} (double asterisk) and subsequent fast sperm nuclei separation. (**B**) Tracking of SPs at fusion site of experiment shown in (**A**). Different colors of the tracks indicate the four phases and numbers indicate end of each phase after sperm delivery in minutes. Shift

of SP_{EC} occurs at 1:40 min (single asterisk) and shift of SP_{CC} at 14:20 min (double asterisk). (**C**) $[Ca^{2+}]_{cyto}$ signal in the egg cell during successful fertilization. Graphs are normalized, dotted line indicates time of PT rupture (0.0 min). Asterisk marks shift of SP_{EC}, arrowhead marks fast separation of sperm nuclei indicating successful fertilization of both female gametes. Two $[Ca^{2+}]_{cyto}$ transients occur: a short transient during pollen tube rupture and a longer transient after SP_{EC} shift (Phase II). (**D**) Correlation of SP_{EC} shift towards EC and beginning of second $[Ca^{2+}]_{cyto}$ transient in egg cells (n = 10). Formula of linear regression and calculated coefficient of determination (R^2) are given. (**E**) Diffusion of sensor molecules into sperm cells upon gamete fusion. Time points before (top) and after SP_{EC} shift (bottom). Left: fluorescent micrographs of egg cell (yellow) and sperm cell nuclei (red). Middle: false color representation of egg cell (citrine signal of CerTN-L15). The dotted line displays the egg cell outline before the SP_{EC} shift. Arrowhead indicates spreading of citrine signal towards the position of sperm cells. Right: Ratiometric image of CerTN-L15 FRET sensor to show $[Ca^{2+}]_{cyto}$ elevation after SP_{EC} shift. Scale bar 20 µm. This figure and its description is adapted from Figure 4 in Denninger et al., 2014.

3 Discussion

During root hair growth a tip localized $[Ca^{2+}]_{cyto}$ gradient controls ROP activity (see Chapter I, Figure 1.4). Thereby the $[Ca^{2+}]_{cyto}$ level oscillates in the root hair tip, which leads to oscillating ROP activity (Hwang et al., 2005). In plants, different $[Ca^{2+}]_{cyto}$ transporters and channels are known and especially GLRs and CNGCs are also described to be important for root hair growth. However, it is not yet understood how they work in concert to establish the $[Ca^{2+}]_{cyto}$ gradient and the $[Ca^{2+}]_{cyto}$ oscillations. Investigating the $[Ca^{2+}]_{cyto}$ levels in growing root hairs of *cngc9* mutant and *cngc6/cngc14* double mutant lines, I could show that $[Ca^{2+}]_{cyto}$ oscillations are affected in both mutant background, but the tip focuses $[Ca^{2+}]_{cyto}$ is still present (Figure 2.1). While in *cngc9* only a slight reduction of the oscillation frequency could be observed, oscillations were almost abolished or very infrequent in *cngc6/cngc14* mutants (Figure 2.1). Additionally, in *cngc6/cngc14* lines bursting root hairs were frequently observed, which was not the case in WT or *cngc9* roots. From these results it is not clear, if CNGC9 is less important for $[Ca^{2+}]_{cyto}$ oscillations in root hairs and proper tip growth than CNGC6 or CNGC14, because no individual mutant lines of CNGC6 or CNGC14 could be investigated in this thesis. For CNGC14 it was recently shown that the single mutant has mild effects on $[Ca^{2+}]_{cyto}$ oscillations (Zhang et al., 2017). Thus, it is possible that all three channels have redundant functions in this process. To better understand possible individual functions of each channels, or to what extend they are required for proper tip growth, $[Ca^{2+}]_{cyto}$ oscillations need to be observed in all single and combinatory mutants. These mutant lines are currently being generated by the lab of Petra Dietrich. Furthermore, there might be additional Ca^{2+} channels involved in root hair growth, as the $[Ca^{2+}]_{cyto}$ gradient does not seem to be affected in the investigated *cngc* mutants. Possibly yet unknown GLRs are important for regulating the $[Ca^{2+}]_{cyto}$ levels in root hairs, similar to their role in pollen tubes. An open question is why multiple channels are required to control $[Ca^{2+}]_{cyto}$ oscillations. One possibility is that channels with different kinetics are required to form stable oscillations, as it was proposed that channels with high sensitivity to the activating factor allow an initial $[Ca^{2+}]_{cyto}$ influx, which triggers the activation of additional channels, leading to a strong controlled $[Ca^{2+}]_{cyto}$ release (Putney, 1986; Parekh and Putney, 2005; Dupont et al., 2011).

Multiple Ca^{2+} channels at different cellular membrane would be required for this mechanism, like it was described for GLRs (Wudick et al., 2018). If CNGCs in root hairs are located to different membranes or have different polar localization within the plasma membrane still has to be determined.

Also during fertilization, I could show that localized $[Ca^{2+}]_{cyto}$ oscillation in synergid cells or $[Ca^{2+}]_{cyto}$ elevations in the egg cell seem to be important (Figure 2.2) (Denninger et al., 2014). Roles for the $[Ca^{2+}]_{cyto}$ signals were proposed to be important for blocking additional sperm cells, cell fusion, or egg activation (Dresselhaus and Franklin-Tong, 2013; Bleckmann et al., 2014). So far, only the RLK FER, together with adjacent membrane proteins, was described to be required for proper Ca^{2+} signaling in synergid cells (Ngo et al., 2014). However, no receptors linking sperm cell arrival with Ca^{2+} signaling are known in the egg or central cell. Additionally, no Ca^{2+} channels, or other factors of intracellular Ca^{2+} signaling are described in either cell of the female gametophyte. Especially, it is not understood if the polar nature of the observed $[Ca^{2+}]_{cyto}$ signals is established and how this is required for the fertilization process. Thus, further investigations are needed to identify how Ca^{2+} signaling regulates cell recognition, fusion and further development after successful fertilization.

Chapter III

–

Comparing fluorescent proteins in planta

–

Choose the right tools for your experiment

1 Introduction

1.1 The discovery and structure of fluorescent proteins

Since the discovery and optimization of the green fluorescent protein (GFP) from the jellyfish *Aequorea victoria* (Shimomura et al., 1962; Prasher et al., 1992; Heim et al., 1994; Heim et al., 1995; Cormack et al., 1996) and its first use as a fluorescent reporter (Chalfie et al., 1994; Wang and Hazelrigg, 1994), multiple variants of fluorescent proteins (FPs) and various methods to use them in cell biology have been described in a plethora of studies (Shaner et al., 2005; Day and Davidson, 2009).

Wild type GFP (wtGFP) of *Aequorea victoria* is a dimeric protein that has two excitation peaks, a major peak at 395 nm and a minor peak at 475 nm GFP. *Aequorea victoria* produces blue light with the Ca^{2+} dependent luminescent protein Aequorin. The produced energy is transferred to GFP via a Fluorescence/Förster resonance energy transfer (FRET), which results in emission of green light. In wtGFP the amino acids Ser65–Tyr66–Gly67 form, by spontaneous cyclization, the chromophore 4-(p-hydroxybenzylidene) imidazolidin-5-one (HBI) which is only fluorescent within a supportive barrel like structure (Tsien, 1998; Day and Davidson, 2009).

All GFP derivatives and FPs from other organisms, have a barrel like structure made of 11 β-strands and one α-helix running through the barrel, containing the chromophore. Amino acid side chains of the β-strands, facing the inside of the barrel, help catalyzing the chromophore maturation and influencing the conjugated pi system. Alterations in those side chains, or the amino acids of the chromophore itself change the properties of the chromophore (Tsien, 1998; Day and Davidson, 2009). The first improvement made to GFP was the S65T mutation, which showed increased brightness, stability and shifted the major excitation peak to 488 nm, but did not alter the emission peak (509 nm) (Heim et al., 1995). This mutation did not only erase the inconvenient dual-excitation properties of wtGFP, but also allowed the usage of common excitation light sources and filter sets in fluorescent microscopy. The second important alteration was the F64L mutation, which has an increased folding efficiency at 37°C (Cormack et al., 1996). The combined mutations resulted in an enhanced GFP (eGFP), which is a bright and stable FP that was

usable in most model organisms. eGFP is still the most commonly used FP derivative from *Aequorea victoria* (Day and Davidson, 2009). A very common mutation for all FPs based on GFP is the A206K mutation, which prevents the dimerizing nature of GFP variants (Zacharias et al., 2002). The monomeric property of FPs is important, as possible dimerization or oligomerization can alter the localization and function of fusion constructs. Thus, it is desirable that FPs have monomeric properties and fluorophores that were optimized for monomeric behavior are denoted with 'm' in front of the FP acronym. However, depending on the application, weak dimerization properties can remain for all FPs.

Despite the described common mutations, further alterations in the barrel or chromophore structure lead to GFP variants with differences in maturation time, color, stability and intensity. Until today, those modifications lead to the creation of a set of different FPs in a wide spectrum of color and brightness (Shaner et al., 2005; Day and Davidson, 2009). An overview over the most recent FP variants and their properties is given on http://www.fpvis.org/FP.html.

1.2 Properties of fluorescent proteins and their applications

FP are widely used as expression reporter, in which FPs are fused to a promoter of interest to investigate the temporal or tissue specific activity of gene transcription. Additionally, FPs are transcriptionally and translationally fused to a gene of interest to study subcellular protein localization in living cells. It is also possible to fuse binding domains for specific molecules to FPs to create sensors for this molecule by which it is possible to investigate the location and the abundance of the molecule *in vitro* and *in vivo* (Shaner et al., 2005; Day and Davidson, 2009). For all FPs applications three major properties are crucial, maturation efficiency, stability of the chromophore, as well as brightness (Tsien, 1998). Maturation efficiency directly influence the brightness of a FP population, as light can only be emitted by properly matured chromophores (Balleza et al., 2017). The maturation is influenced by the chromophore environment and the temperature, which differ for every organism (Griesbeck et al., 2001; Balleza et al., 2017). Thus, FP brightness due to chromophore maturation varies between organisms and has to be taken into account for the used model organism. FP brightness itself is a product of the

extinction coefficient (ε), the ability to absorb energy, and the ability to emit the absorbed energy in form of light, referred to as quantum yield (QY) (Tsien, 1998). It is important that FPs efficiently mature, are stable and bright, as this means that only a small number of molecules and low light energy is needed for visualization in living cells. This reduces the phototoxicity by the emission light and possible negative side effects of the ectopic protein expression (Icha et al., 2017). Thus, it is desirable to use fluorophores with advantageous properties for each spectral class of FPs. The mainly used spectra for live cell imaging, are FPs in the visible spectrum. Each class has advantages and disadvantages, and dependent on the purpose it is necessary to choose the according FP.

The need of bright and stable FPs lead to the development of a plethora of different FPs in the whole light spectrum. In the recent years, the better understanding of the structure of FPs accelerated this even more, creating a huge assortment of FPs with different properties and for different purposes. A selection of these FPs, which are commonly used for live cell imaging, or were shown to have best properties among all FPs at the beginning of this thesis, are described I the following section.

1.3 Origin and properties of the used fluorescent proteins

Cyan FPs (CFPs) are good FRET donors for yellow FPs (YFPs), as they have a wide stoke shift, and the emission spectrum has a spectral overlap with the excitation spectrum of YFPs (Piston and Kremers, 2007). The first published CFP was optimized multiple times to improve CFP properties and one of these approaches resulted in the generation of the super CFP3A (SCFP3A) (Kremers et al., 2006). This FP has moderate brightness, but further optimization led to mTurquoise and its most recent version mTurquoise2 (mTrq2), which should have the best combination of high brightness, stability and spectral properties, based on the *in vitro* measured characteristics, among all available CFPs (Goedhart et al., 2010; Goedhart et al., 2012). mTrq2 is superior to other CFPs and thus, mTrq2 was used in this study and no alternatives were tested.

In the green spectrum of FPs, eGFP is still the most prominent. Besides optimization in folding no improvements in brightness could be made for eGFP, without changing its spectral properties. Recently, alteration in eGFP lead to Clover and its latest

variant mClover3 (mClv3), a green FP similarly stable and brighter compared to eGFP (Lam et al., 2012; Bajar et al., 2016). However, mClv3 was so far not described in plants and it is unclear if the *in vitro* properties also apply *in planta*. Additionally, the excitation and emission spectra of mClover3 are shifted towards longer wave lengths, which does not fit to the commonly used microscope equipment. Similar characteristics were found for a FP originating from *Branchiostoma lanceolatum* YFP (LanYFP), called mNeonGreen (mNG) (Shaner et al., 2013). This green FP has similar spectral properties like mClover3, but exceeds its brightness and is thus the brightest known monomeric FP *in vitro*. Also for mNG, little is known about its properties *in planta*, and it was especially not compared to eGFP in any plant model organism.

Due to their brightness, YFPs are widely used for live cell imaging. Besides the recently published mClover3 and mNeonGreen, YFPs are the brightest FPs. However, the brightness is accompanied by a significant reduction in stability and a high environmental sensitivity of the chromophore, e.g. to low pH (Shaner et al., 2005). Still, YFPs are widely used, as their spectral shift compared to green FPs, allows spectral separation of CFPs and YFPs, which is not easily possible for GFPs. Thus, YFPs depict good partners for FRET experiments and multicolor imaging (Shaner et al., 2005). Especially the YFP variants mCitrine, Venus and mYPet, which have greater brightness and less environment sensitivity compared to the original YFP, are useful tools (Griesbeck et al., 2001; Nagai et al., 2001; Nguyen and Daugherty, 2005; Shaner et al., 2005).

Red FPs (RFPs) have the advantage of low phototoxicity, as light of longer wavelength carries less energy and allow deeper penetration depth into the tissue. Thus, RFPs are particularly useful for imaging of dense thick tissue, or very sensitive processes that would be altered by high energy light exposure (Shaner et al., 2005). Even though, no RFP variant could be successfully made from wtGFP, a great variety of FPs from mainly two organisms exists. The first RFP was isolated from *Discosoma sp.* (DsRed) and further improved to mRFP1 and later mCherry, which is the most commonly used RFP in all organisms (Matz et al., 1999; Shaner et al., 2004). Besides RFPs based on DsRed, most other RFPs are based on two FPs of *Entacmaea quadricolor*, eqFP578 and eqFP611.

Modifications of eqFP578 lead to the bright TagRFP and its more stable version TagRFP-T (Merzlyak et al., 2007; Shaner et al., 2008). eqFP611 lead to Ruby variants, which were created as efficient FRET acceptors for Clover (Kredel et al., 2009; Lam et al., 2012). The latest version, mRuby3, shows the highest brightness among all red FPs *in vitro* (Bajar et al., 2016), but recent reports indicate, that the brightness of mRuby2 and mRuby3 is not necessarily achieved *in vivo* due to incomplete chromophore maturation (Bindels et al., 2016).

1.4 The aim of Chapter III

All described FPs have different properties, advantages, or disadvantages for specific methods or in different organisms. Due to this large selection of FPs, many of them are not tested in all model organisms and the properties of FPs are often only investigated *in vitro*, or in cell culture. But, as mentioned before, the use of FPs strongly depends on folding efficiency and the environment of the FP within a cell. Thus, the published properties might not apply *in planta*, or to other model systems and it is important to characterize the used FPs to find the ideal protein for the desired usage. The published properties of the investigated FPs are shown in Table 3.1. The goal of this thesis was to observe fusion proteins *in planta* under noninvasive conditions. For live cell imaging, FPs with a good folding efficiency and a good balance of brightness and stability *in vivo* were required. Additionally, FPs with different spectral properties were needed, to observe multiple proteins simultaneously. The aim of this part of my thesis was to find FPs fitting the requirements for this work. I chose FPs that were described to have the best properties at the beginning of my thesis. CFP, GFP, YFP and RFP variants were chosen, as their spectral properties fit most microscope setups and allow multi-color imaging. To investigated brightness and stability of the FPs *in planta* and especially to compare their properties to each other, all FPs were cloned in the same way and expressed under comparable conditions.

2 Results

2.1 Brightness

To characterize the properties of FPs *in planta*, they were expressed in *Nicotiana benthamiana* (*N. benthamiana*) leaf cells and their brightness and stability was analyzed. To compare the different FPs, they were analyzed in 2 groups, green-yellow emitting FPs and red emitting FPs. Example images, of *N. benthamiana* leaf cells expressing the respective FP, used for the brightness analysis are shown in Figure 3.1 A-D. To allow the comparison of green and yellow proteins, even though they are excited at different wavelength, the laser output was measured, and the same laser intensity was used (5 mW laser input resulted in 0.1 mW Laser output at the objective). The results were normalized to mCit, as this protein was used in all experiments. All green fluorophores showed less brightness compared to mCit (Figure 3.1 E). With 74.3 % relative brightness of mCit, eGFP was the least bright FP among the green fluorescent proteins tested, followed by mNG (76.2 %). Slightly brighter was mClv3 with 89.1 % relative brightness (Figure 3.1 E). Among the yellow fluorescent proteins, Venus was similar bright to mCit (96.6 %), but mYPet exhibited only 46.7% relative brightness (Figure 3.1 E). These results showed that among the green-yellow fluorophores, mCit and Venus are the brightest and eGFP, mNG and mClv3 are dimmer than these yellow fluorophores.

Comparing the brightness of the red fluorophores was done with higher laser intensity (20mW Laser input, resulted in 0.32 mW laser output at the objective) as these fluorophores were generally dimmer than the green-yellow FPs. As reference protein mRuby2 was used and all values were normalized to it (Figure 3.1 F). The successor of mRuby2, mRuby3, showed 128.4 % brightness, while tagRFP-T, with 91.0 %, was slightly dimmer than mRuby2 (Figure 3.1 F). mCherry exhibited 125.0 % relative brightness, similar bright like mRuby3. High variability in the expression levels between the individual replicates lead to p-values which were > 0.01, but a clear tendency of FP brightness could be observed, which shows that mCherry and mRuby3 are similarly bright and superior to mRuby2 and tagRFP-T.

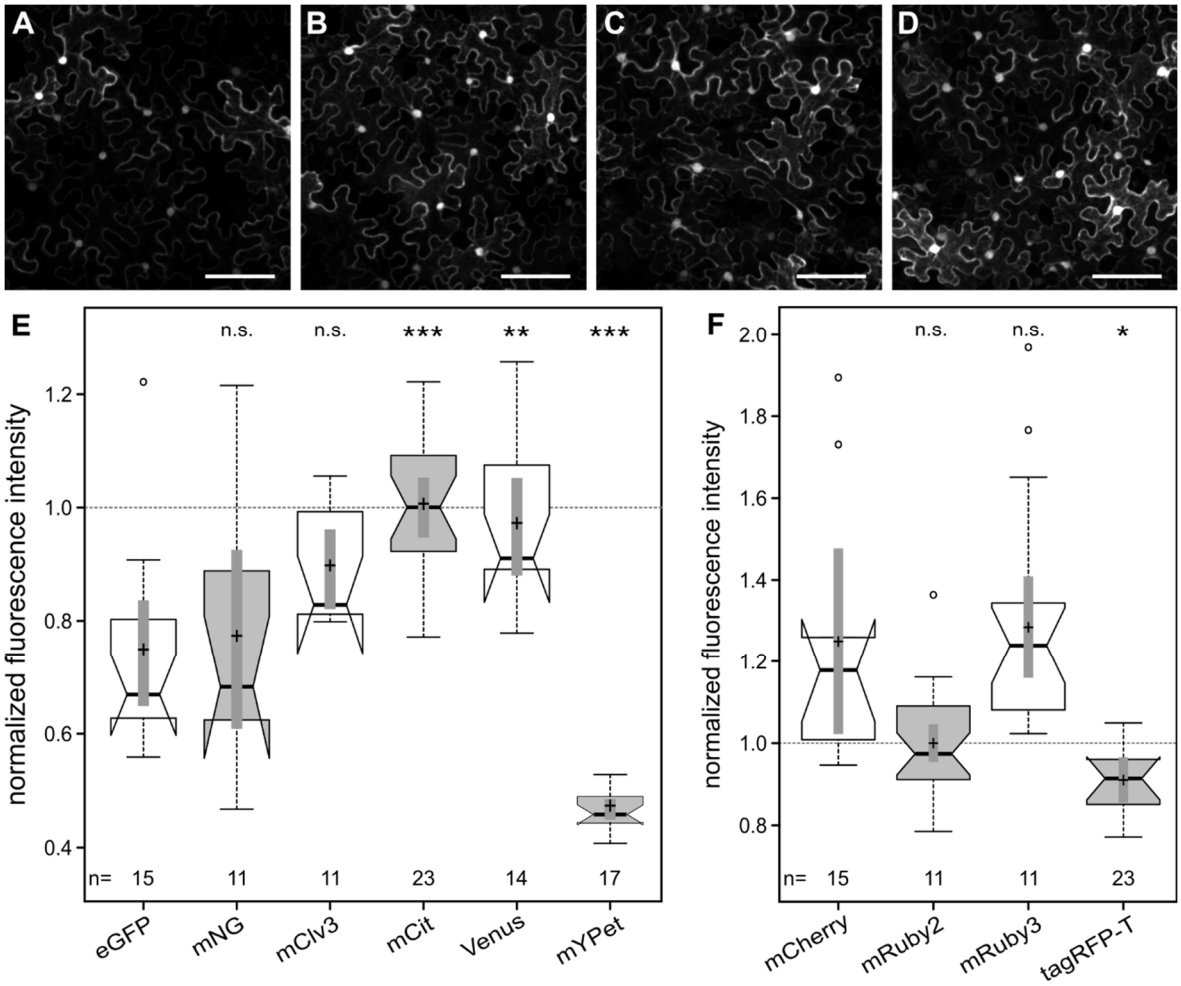

Figure 3.1 Brightness of different fluorescent proteins in planta

(**A-D**) Representative image of field of views for brightness measurements of UBI10::FP constructs transiently infiltrated in *N. benthamiana*, two day after infiltration (dainf). Whole field of view was measured. (**A**) UBI10::eGFP; (**B**) UBI10::mCit; (**C**) UBI10::mCherry; (**D**) UBI10::mRuby3. Scale bars 100 µm. (**E-F**) Brightness of analyzed fluorophores in *N. benthamiana* leaves. Fluorescence intensity normalized to mCit (**E**) and mRuby2 (**F**). n = number of measured field of views; + = sample mean; dotted line indicates mean value of normalization FP; Center line = sample median. Statistical differences were calculated in comparison to eGFP (**E**) and mCherry (**F**). n.s. = $p \geq 0.01$; * = $p < 0.01$; ** = $p < 0.001$; *** = $p < 0.0001$. Detailed description of box plots and statistical tests in Chapter IV, 4.2.1.

2.2 Stability

For a fluorescent protein brightness is a central factor, but also its stability against photobleaching is of importance. This is especially a factor for time-laps imaging with short time intervals. To quantify the fluorophore stability against photobleaching, cells were imaged under high laser intensities (Laser output at the objective 0.75 mW for green and yellow proteins, 1.0 mW for red proteins) and constantly imaged for 6 min.

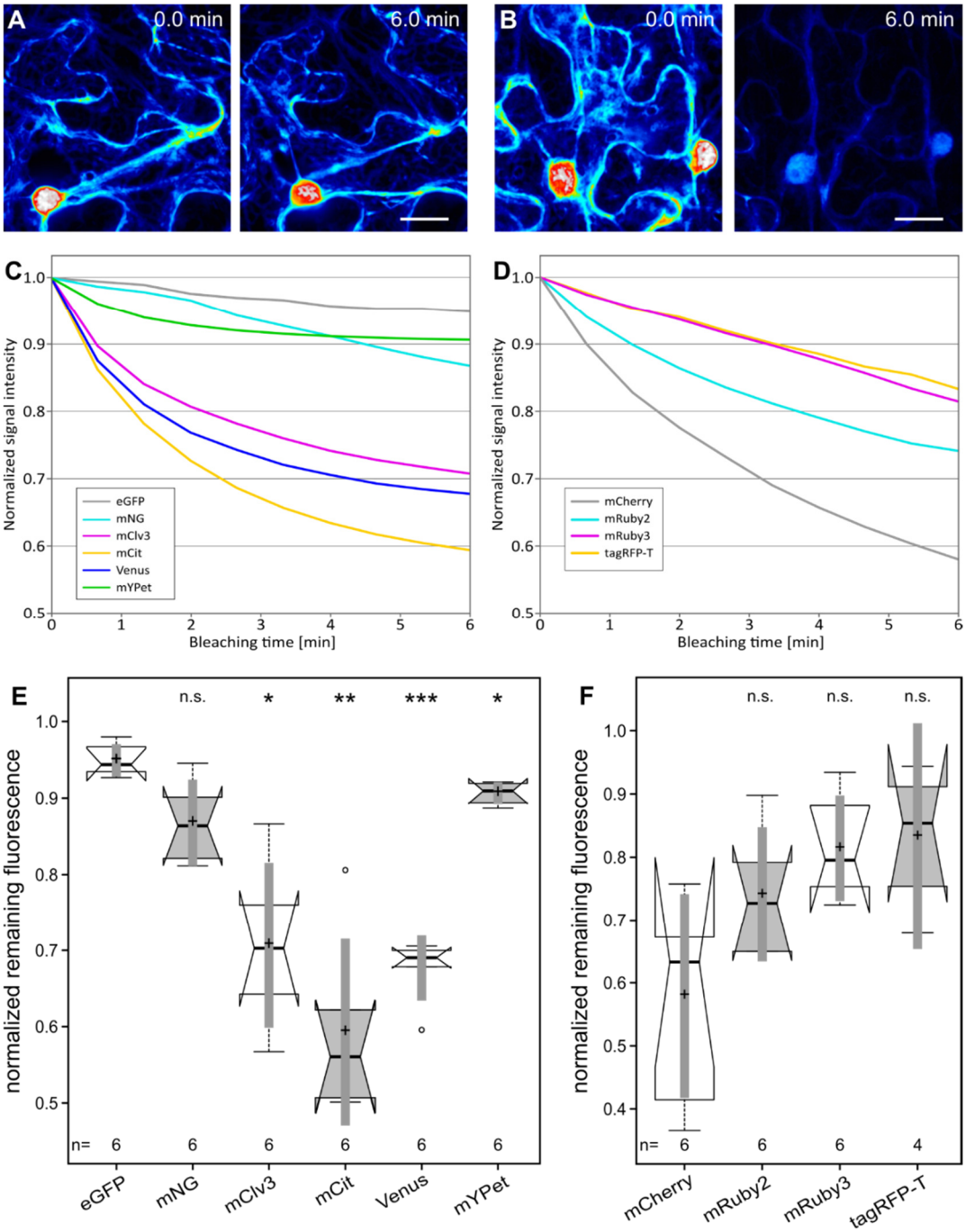

Figure 3.2 Stability of different fluorescent proteins in planta

(**A**-**B**) Bleaching experiments of UBI10::eGFP (**A**) and UBI10::mCit (**B**), transiently expressed in *N. benthamiana*, 2 dainf. Before (0.0 min) and after (6.0 min) bleaching is shown. Whole field of view was measured. (**C**-**D**) Average fluorescence decay during the bleaching experiment. Values are normalized to starting value for each FP. Number of measurements is same as in (**E**-**F**). (**E**-**F**) Quantification of the fluorescence decay. Normalized remaining fluorescence ($Intensity_{END}/Intensity_{START}$) of analyzed fluorophores in *N. benthamiana* leaves is shown. n = number of measured field of views; + = sample mean; dotted line indicates mean value of normalization FP; Center line = sample median. Statistical differences were calculated in comparison to eGFP (**E**) and mCherry (**F**)n.s. = $p \geq 0.01$; * = $p < 0.01$; ** = $p < 0.001$; *** = $p < 0.0001$. Detailed description of box plots and statistical tests in Chapter IV, 4.2.1.

The loss of fluorescence strongly varied between the tested FPs (Figure 3.2 A, B). Differences between the FPs were not just observed for overall loss of fluorescence, but also how this reduction took place over the time course of the experiment (Figure 3.2 C, D). For some FPs the intensity decreased linearly, like for eGFP, mNG, mRuby3 and tagRFP-T, while fluorescence intensity of the other FPs decreased faster in the beginning of the experiment and later stabilized. For quantification, the stability was defined as the remaining fluorescence compared to the starting value. For the green and yellow proteins eGFP was most stable, with 94.9 % of its fluorescence left. Similar stable was mYPet and mNeonGreen, with 90.7 % and 86.8 % remaining fluorescence. Compared to this, mClover3, Venus and mCitrine were not as stable as eGFP with only 70.7 %, 67.7 % and 59.3 % remaining fluorescence (Figure 3.2 E). This showed for the green-yellow proteins, that the stability of fluorescent proteins behaves invers to protein brightness. eGFP, was found to be the most stable protein, but also exhibits poor brightness, while mCitrine and Venus were the brightest fluorophores, but had the least stability. For the red fluorescent proteins TagRFP-T was found to be the most stable protein with 83.3 % fluorescence remaining, similar to mRuby3 with 81.1 %. mRuby2 was slightly less stable with 74.1 % remaining fluorescence, while mCherry was found to be the least stable with only 57.9 % remaining fluorescence (Figure 3.2 F). Additionally, a large variety in mCherry stability was found, with values ranging from 36.6 % to 75.8 % remaining fluorescence. These results showed that mRuby3 is a bright and stable red fluorescent protein in *N. benthamiana*, while mCherry is less stable despite its brightness.

3 Discussion

I showed that mCit is the brightest and eGFP the most stable FP among the green-yellow FPs investigating *in planta* (Figure 3.1, 3.2 and Table 3.1). For the investigated red FPs mRuby3 is the brightest and tagRFP-T the most stable FP (Figure 3.1, 3.2 and Table 3.1). According to published data, eGFP is the most stable FP and the differences to the other investigated FPs fits my results. The only exception is Venus, which is published to be less stable than mCit, but I found it to be more stable. Thus, eGFP and mNG are the most stable FPs and significantly more stable than the investigated YFPs.

Table 3.1: Investigated fluorescent Proteins

Name	Published Brightness	Measured brightness [relative to mCit or mRuby2]	Published Stability [sec for 50% reduction]	Measured Stability [% of starting value]	Reference
mTurquoise2	27.9	-	90	-	Goedhart et al., 2012
eGFP	33.6	74,3	174	94.9	Yang et al., 1996
mNeonGreen	92.8	76.7	158	86.8	Shaner et al., 2013
mClover3	85	89.1	80	70.7	Bajar et al., 2016
mCitrine	58.5	100	49	59.3	Griesbeck et al., 2001
Venus	52.5	96.6	15	67.7	Nagai et al., 2001
mYPet	80.1	46.7	-	90.7	Nguyen and Daugherty, 2005
mCherry	15.8	125.0	96	57.9	Shaner et al., 2004
mRuby2	43	100	123	74.1	Lam et al., 2012
mRuby3	57.6	128.4	349	81.4	Bajar et al., 2016
TagRFP-T	33.2	91.0	337	83.3	Shaner et al., 2008

However, mCit and Venus show significantly more brightness than eGFP and mNG, while mClv3 is between these two pairs in brightness and stability. This is surprising, as mNeonGreen and mClover3 are both published with significantly greater brightness compared to eGFP, as well as mCitrine (Table 3.1). Also, mYPet is published to be brighter than mCitrine (Table 3.1), but I found it to be the least bright FP among the investigates green-yellow FPs. The differences in in brightness can have multiple reasons, like maturation of the chromophore and chemical properties of the organism (Tsien, 1998). The maturation time of the FP is influenced by the temperature of the model system (Balleza et al., 2017) and most FPs were

optimized for efficient maturation time at 37°C (Shaner et al., 2005). Therefore, FPs might behave very differently at temperatures of plant growth conditions. Additionally, chemical environments can influence FP brightness. Especially the mutations leading YFPs seemed to render YFPs sensitive to ion concentrations, with chloride being the most relevant (Griesbeck et al., 2001). A higher chloride concentration could explain the low brightness of mYPet, as this was not optimized for chloride sensitivity like mCit (Griesbeck et al., 2001).

Of the investigated red FPs mRuby3 is superior with great brightness and stability. However, it was shown that mRuby3 exhibits great photochromic behavior, a reversible change in spectral properties dependent on excitation light, which is undesirable for quantitative imaging methods, like FRET measurements (Bindels et al., 2016). Most recently the new RFP variant mScarlet was created based on the structure of mCherry. mScarlet has similar brightness like mRuby3 but less drawbacks, like higher maturation rate and negligible photochromic behavior. Furthermore, mScarlet has the highest QY of all RFPs, which makes it a great FRET acceptor and along with its faster maturing variant mScarlet-I they seem to superior to all other RFPs (Bindels et al., 2016). However, properties of mScarlet were described in mammalian cell culture cells and are so far not tested *in planta*.

From my investigations no superior FP can be defined, as higher brightness seems to be linked with a loss in stability. Furthermore, there are additional properties, like maturation and photochromic behavior, which can influence the used FP. My *in planta* studies showed that it is not sufficient to relay on the published *in vitro* properties, similar to observations in other *in vivo* comparisons of FPs (Bindels et al., 2016). It seems to be necessary that the properties of FPs are always tested in the used model system to know the best fitting FP. Furthermore, it is important to choose the FP according to the planed experiments and the required properties as so far, no FP is available that combines all advantages.

Chapter IV

–

Material and Methods

1 Molecular Biology

If not mentioned otherwise, chemicals and reagents were used in “pro analysis” quality and all kits and enzymatic reactions were used according to the manufacturers protocol.

1.1 Molecular cloning

All plasmids created in this thesis were constructed using “GoldenGate” cloning, utilizing the entry and destination vector sets of the “GreenGate” cloning system as it is described in (Lampropoulos et al., 2013). As restriction enzyme BsaI-HF from NEB®, as Ligase T4 DNA Ligase from NEB® or ThermoFisher Scientific™ was used. A list of all vectors cloned in this thesis is given in Section 5.1 and 5.3 of this Chapter. Additionally, example maps of the used vectors are given in Appendix.

1.1.1 PCR and PCR fragment purification for molecular cloning

PCRs for cloning were performed using Q5® high-fidelity DNA polymerase (NEB®), with the according reaction buffer, using following protocol:

PCR volume	1.0	µl	Template (2 ng Plasmid, gDNA 50 $^{ng}/_{µl}$)				
(25 µl)	5.0	µl	Buffer (5X)	2’	@	98°C	
	1.0	µl	Primer 1 (10 µM)	20’’	@	98°C	
	1.0	µl	Primer 2 (10 µM)	20’’	@	T_m	30 cycles
	0.25	µl	dNTPs (10 mM)	30 $^{sec}/_{kb}$	@	72°C	
	0.25	µl	Q5® DNA polymerase	2’	@	72°C	
	16.5	µl	H_2O	∞	@	8°C	

All cloning-primers were designed for a T_m of ~ 60 °C and all PCRs were performed at this annealing temperature. In case a fragment was larger than 3 kb, the PCR volume was increased to 50 µl to increase PCR-fragment yield.
20 µl of the PCR reaction were purified using the PeqGold Gel extraction Kit from PeqLab / VWR and finally eluted with 20 µl H_2O.
In case multiple fragments were used for one Ligations step, the individual PCR products were pooled prior to purification.

1.1.2 General entry vector production

Purified PCR product was used (~17 µl) and mixed with 1 µl (100 ng) entry vector, 2 µl CutSmart buffer, 0.25 µl BsaI-HF (if more than 3 PCR fragments were combined 0.5 µl enzyme were used) and incubated 30 – 60 min at 37°C. Afterwards, the mix was purified using the PeqGold extraction kit and eluted again in 20 µl. The purified fragments were mixed with 2 µl 10X T4-Ligase buffer, 0.5 µl T4-Ligase from NEB (1 µl Ligase was used for combining 3 or more fragments) and incubated for more than 1 h at room temperature. Finally, the whole reaction mix was transformed into the Escherichia coli (*E. coli)* strain DH5α.

1.1.3 Removal of undesirable internal BsaI-sites

In case the desired DNA fragment had internal BsaI recognition sites, the PCR fragment was split at that site, by performing two separate PCR reactions in front and behind the BsaI-site. One primer of one of the PCRs covered the site and introduced a single base exchange to mutate the restriction enzyme recognition site. To fuse both PCR fragments, BsaI-sites were attached at the 5’ end of the primers in a way that the recognition site is cut off and leaves complementary ends.

1.1.4 Creation of a A-D entry vector module

For constructs that contained genes under control of their native promoter and were C-terminally fused to a tag, a new entry vector module was created, which allowed cloning of promoter and coding sequence in one piece in a GreenGate compatible way. Therefor the GreenGate entry vector module A was mutated to contain overhangs A and D. For this, the GreenGate cassette of pGGA000 was PCR amplified, thereby mutated to the according overhangs and cloned into pGGA000 using the restriction enzymes HindIII and EcoRI (see Primers oPD0001-fwd and oPD0001D-rev). The Product was termed pGGAD000 (pPD0002) and allows GreenGate compatible C-terminal tagging of genes without an artificial cloning decoy between promoter and coding sequence.

1.1.5 Assembly of an estradiol-inducible entry-vector module

The Estradiol inducible system was adapted from the system first published by Zuo et al., 2000. To create a single GreenGate compatible entry-vector module (promoter module A) for estradiol inducible gene expression, the chimeric transcription activator composed of the DNA-binding domain of the bacterial repressor LexA (X), the acidic transactivating domain of VP16 (V) and the regulatory region of the human estrogen receptor (E) (XVE) gene was ligated to the promoter (635 bp) and terminator of UBIQUITIN10 (*UBI10,* AT4G05320). This expression cassette was than ligated in reverse orientation upstream to eight copies of the LexA operator upstream of the -46 35S minimal promoter (oLexA) and cloned into pGGA000. Furthermore, both elements were separated by a 560 bp spacer.

1.1.6 Destination-Vector assembly

All expression constructs were cloned into the GreenGate destination vector pGGZ003, which is based on pGreenII (Hellens et al., 2000). The assembly reaction was performed using the following protocol:

Final volume	1.5 µl	each entry vector (Module A-F 100 $^{ng}/_{µl}$)	2’ @ 37°C	
(15.5 µl)	1.5 µl	Destination Vector (100$^{ng}/_{µl}$)	5’ @ 37°C	50
	1.5 µl	10x CutSmart Buffer	5’ @ 16°C	cycles
	1.5 µl	ATP (10 mM)	10’ @ 50°C	
	1.0 µl	BsaI-HF	10’ @ 80°C	
	1.0 µl	T4 Ligase HC (30 U/µl)	∞ @ 12°C	

The 5 min restriction and ligation step can be reduced to 2 min and cycle number could be reduced to 30 for good working Ligations, but for most reactions, the mentioned protocol was used.
Finally, the whole reaction mix was transformed into *E. coli* (DH5α).

1.2 Plasmid selection & quality control

For all standard cloning procedures, the *E. coli* strain DH5α was used. For retransformation and alteration of source vectors, which contain the CcdB gen, the *E. coli* strain DB3.1 was used, as it is tolerant to CcdB. The protocol for preparation of competent cells and transformation was used for both strains.

1.2.1 Preparation of chemically competent *E. coli*

4 ml LB-Medium were inoculated with a single colony and incubated over night at 37°C. 500ml LB-Medium were inoculated with 1 ml overnight culture and incubated at 16°C to an OD_{600} of 0.4 to 0.5. Culture was chilled on ice for 10 min and kept as cold as possible for all following steps. Cells were harvested (10 min, 4000 g, 4°C) and supernatant was removed. The cell pellet was carefully resuspended with 100 ml sterile prechilled TB-buffer and chilled on ice for 10 min. Cells were harvested as before and resuspended in 50 ml sterile prechilled TB-Buffer. Slowly, 3.5 ml DMSO were added, while stirring the cells on ice. After incubating the cells for 10 min on ice, they were aliquoted in 100 µl into prechilled 1.5 ml reaction tubes and immediately frozen in liquid nitrogen.

TB-Buffer: prepare fresh from sterile Stocks

10 mM	PIPES (pH 6.4, adjusted with NaOH)
55 mM	$MnCl_2$
15 mM	$CaCl_2$
250 mM	KCl
10 % (v/v)	Glycerol (alternatively, helps cells to thaw)
	sterile ddH_2O

1.2.2 Transformation and selection of *E. coli*

Cells were defrosted on ice. Afterwards DNA was added and incubated on ice for 20-30 min. Cells were heat-shocked for 40-50 sec and immediately afterwards chilled on ice for 2 min. ~ 900 µl LB-Medium were added and cells were incubated up to 1 hour at 37°C, depending on the used antibiotics for selection. Cells were harvested (30 s at > 12000 g), plated on selection medium and incubated overnight at 37°C. The following antibiotics concentrations were used for *E. coli* selection: Ampicillin 100 µg/ml, Chloramphenicol 25 µg/ml, Kanamycin 50 µg/ml, Spectinomycin or Streptomycin 50 µg/ml, Tetracycline 10 µg/ml.

1.2.3 Colony PCR

After each transformation colonies were tested by colony-PCR for the presents of the desired plasmid and insert(s), using Taq DNA Polymerase (NEB®). Colonies were first picked and dipped into the PCR reaction, afterwards directly transferred on a LB-Medium selection plate to have a backup of the tested colony.

PCR volume	1		Colony as template				
(25 µl)	2.5	µl	Buffer (10X)	2'	@	95°C	
	0.25	µl	Primer 1 (10 µM)	20''	@	95°C	⎫
	0.25	µl	Primer 2 (10 µM)	20''	@	T_m	⎬ 30 cycles
	0.2	µl	dNTPs (10 mM)	60 $^{sec}/_{kb}$	@	68°C	⎭
	0.1	µl	Taq DNA polymerase	∞	@	8°C	
	21.7	µl	H_2O				

1.2.4 Plasmid isolation from *E. coli*

Plasmids were isolated from 4 ml overnight culture, using the GenElute™ Plasmid Miniprep Kit from Sigma-Aldrich® / MERCK.

1.2.5 Sequencing

The insert of all entry vector clones was completely sequenced, by the company Eurofins, using Sanger sequencing. All prepared expression vectors, using GreenGate assembly, were sequenced, with at least 3 primers, for the presents and correct assembly of all fragments.

1.3 Agrobacterium transformation

For all experiments the *Agrobacterium tumefaciens* (*A. tumefaciens*) strains C58C1 or GV3101-pMP90RK (based on C58C1, with Gent^r, transformed with pMP90RK (Rif^r & Kan^r)) (Koncz and Schell, 1986) were used. C58C1 was co-transformed with the helper-plasmid pSoup (Hellens et al., 2000) for transformations using the pGreenII based pGGZ003 expression vector. GV3101-pMP90 was pre-transformed with pSoup and afterwards cells were made competent for further transformations.

1.3.1 Preparation of chemically competent *A. tumefaciens*

A single colony was used to inoculate 10 ml LB-Medium (with antibiotics in case of GV3101-pMK90RK) and incubated overnight at 28 °C. Afterwards 500 ml LB-Medium was inoculated with this overnight culture and incubated at 28 °C to an OD_{600} of 0.5. The cells were harvested (15 min at > 3700g), the supernatant removed and resuspended in 100 ml 0.15 M NaCl. Cells were harvested again (15 min at > 3700g), supernatant removed and resuspended on ice in 20 ml prechilled 20 mM $CaCl_2$, containing 10 % (v/v) Glycerol. 200 µl aliquots were made into 1.5 ml reaction tubes and immediately frozen in liquid nitrogen.

1.3.2 Transformation of *A. tumefaciens*

Cells were thawed on ice, 100 to 500 mg plasmid DNA was added and incubated on ice for 5 min. Mixture was frozen in liquid nitrogen for ~ 5 min and immediately heat shocked for 5 min at 37 °C. Afterward 1 ml LB-Medium was added and cells were inoculated for 1-4 hours at 28 °C, before plating on selection medium. The following antibiotics concentrations were used for Agrobacterium tumefaciens selection: Gentamycin 50 µg/ml, Kanamycin 50 µg/ml, Rifampicin 10 µg/ml, Spectinomycin 100 µg/ml or Spectinomycin / Streptomycin 50 / 50 µg/ml, Tetracycline 10 µg/ml.

1.4 Nucleic acid isolation and testing methods

1.4.1 DNA isolation from *A. thaliana*

1 large or 2 small rosette leaves were frozen in liquid nitrogen. 1.5 ml tubes were used for grinding with a precooled pistil, or 2 ml tubes for grinding with grad beads in a tissue-lyser (Qiagen). After thoroughly grinding leave tissue, 750 µl extraction buffer was added, mixed and incubated for 10 min at 65°C, afterward 200 µl 5 M potassium acetate was added, mixed and incubated 20 min on ice. Then the mixture was centrifuged (10 min, > 16.000 g), supernatant was transferred into a 2 ml tube and mixed with 1 ml (> 1 volume of supernatant) Isopropanol. Precipitating DNA was pelleted for 2 min with > 16.000g, the supernatant was removed, and pellet was

washed with 500 µl 70 % (v/v) Ethanol. After removal of the supernatant, the pellet was completely dried and resuspended in 100 µl H_2O.

Extraction Buffer:

200 mM	Tris
100 mM	NaCl
10 mM	EDTA
1% w/v	SDS
10 mM	β-Mercaptoethanol

set pH to 8.0 with HCl

1.4.2 Genotyping PCR

Genotyping PCRs were performed with Taq DNA Polymerase (NEB®). In case T-DNA insertion mutant lines were analyzed, 3 primer PRCs were performed, with two gene specific primers, flanking the T-DNA and one T-DNA specific primer. The presence of a reporter construct was tested with two primers and ddH_2O was added to replace the missing volume.

PCR volume (25 µl)	1 µl	gDNA (~50 - 100 ng)	
	2.5 µl	Buffer (10X)	2’ @ 95°C
	1 µl	Primer 1 (10 µM)	20’’ @ 95°C
	1 µl	Primer 2 (10 µM)	20’’ @ T_m
	1 µl	Primer 3 (10 mM)	60 $^{sec}/_{kb}$ @ 68°C
	0.2 µl	dNTPs (10 mM)	∞ @ 8°C
	0.1 µl	Taq DNA polymerase	
	18.2 µl	H_2O	

40 cycles

1.4.3 RNA isolation from *A. thaliana*

Total RNA of Arabidopsis roots was extracted using the RNeasy Plant Mini Kit (Qiagen). Seedlings were grown on a mesh placed on a ¼ Murashige-Skoog-Medium (MS) plate and root tissue was harvested 10 days after germination (dag). Immediately after harvesting, tissue was frozen in liquid nitrogen and ground in a tissue-lyser (Qiagen), using metal beads.

1.4.4 cDNA synthesis and following PCR

Before cDNA synthesis, genomic DNA was degraded by DNaseI (ThermoFisher Scientific™). After heat inactivation of the DNaseI 500 ng RNA was used for cDNA synthesis with oligo(dT) primers, using the RevertAid First Strand cDNA Synthesis Kit (ThermoFisher Scientific™). To test the presents of a specific mRNA, 2 µl of this cDNA was used for PCR amplification (40 cycles).

2 Plant handling

2.1 Growth conditions

2.1.1 Standard plant growth conditions

A. thaliana was grown under long day conditions (16 h light / 8h dark) at 21 °C on soil in a growth chamber, or on sterile ¼ MS-Medium plates (MS-Salts from Serva, 0.1 % MES, pH 5.7 adjusted with KOH, 0.8% plant agar (Duchefa).
Nicotiana benthamiana was grown under long day conditions (16 h light / 8 h dark) at 26 °C in a growth chamber.

2.1.2 Root chip experiments

RootChip experiments using the RootChip16 ($[Ca^{2+}]_{cyto}$ measurements in WT compared to CNGC mutants) were performed as described in (Grossmann et al., 2011). Time lapse imaging of mCit-GEF3 was done in a RootChip-S8 as described in Denninger et al. (submitted)

2.2 Plant transfection and transformation

2.2.1 Transfection of *N. benthamiana* leaves

A single colony of an *A. tumefaciens* transformation was used to inoculate 4 ml selective LB-Medium and incubated over night at 28°C. 1 ml of this overnight culture was used to inoculate 4 ml fresh, selective LB-Medium and incubated 4-5 hours at 28°C. The cells were harvested (10 min @ > 3700 g, at 4°C), the supernatant removed, and the pellet resuspended in 2 ml prechilled AS-Medium. After determining the OD_{600}, the suspension was diluted with cold AS-Medium to an OD_{600} of 0.2 (in case two constructs were co-transfected, each suspension was diluted to an OD_{600} of 0.1 and suspensions were mixed before injection) and incubated on ice for 1 h. The cell suspension was infiltrated into the lower side of the leave, using a 1 ml syringe. The transfected tissue was analyzed 2-3 days after infiltration.

AS medium:

5 %	Sucrose (w/v)	0.01%	Glucose (w/v)
0.01 %	Silwet L77 (v/v)	450 µM	Acetosyringon
0.01 %	MgSO4 (w/v)		

2.2.2 Transformation of *A. thaliana*

Stable transformation of *A. thaliana* was done using the “floral dipping” method, modified from (Clough and Bent, 1998). A single colony of an *A. tumefaciens* transformation was used to inoculate 4 ml selective LB-Medium and incubated over night at 28 °C. The whole overnight culture was used to inoculate 100 ml LB-Medium and incubated at 28 °C to an OD_{600} of 0.6 – 0.8. Cells were harvested (10 min, 4000 g), the supernatant removed, and the pellet resuspended in 200 – 250 ml Transformation Medium (5 % Sucrose and 0.05 % Silwet L77). Inflorescences were dipped into cell suspension solution for ~ 5 min. Afterwards, plants were covered with plastic bags to keep a high humidity for 12 – 24 hours.

2.2.3 Isolation and testing of transgenic *A. thaliana* lines

As a general principle, constructs containing fluorescent proteins had the same resistance for the same color range: CFP – Kanamycin-Resistance; GFP/YFP – Glufosinate-Resistance; RFP – Hygromycin-Resistance. This color code allowed easy selection of lines containing combination of different markers. T1 seeds were selected in different ways depending the resistance mediated by the T-DNA. Glufosinate selection was done on soil, spraying 1 – 2 week old seedlings with Basta®-Solution (Bayer, 200 µg/ml Glufosinate-ammonium and additional 0.05 % Tween20). To ensure selection, seedlings were sprayed 3 times in 4-5 day intervals. Later generations were partly selected on ¼ MS-Medium containing 7.5 µg/ml Glufosinate-ammonium. Kanamycin selection was done on ¼ MS-Medium containing 50 µg/ml Kanamycin. Plated seeds were kept dark for 2 – 3 days before transfer to light, as Kanamycin effect is more obvious on mildly etiolated seedlings. Hygromycin selection was done on ¼ MS-Medium containing 20 µg/ml Hygromycin. Plates were kept vertically, as Hygromycin selection effects root elongation.
At least five independent lines were obtained for each transformed construct and checked for fluorescence and expression pattern.
To confirm the presents of the desired construct, each used plant line was genotyped with construct specific primers.

2.3 Estradiol inducible gene expression

Arabidopsis seedlings containing an estradiol inducible constructed were induced with ¼ MS-Medium containing 20 µM Estradiol (20 mM Stock in Ethanol) and 0.01% Silwet L77. If single seedlings were induced, to observe protein localization, the seedlings were covered with cellulose tissue, drenched in induction medium, for 30-60 min. Microscopy of the induced seedlings differed between the individual constructs, but usually ranged from 3 – 12 hours. For overexpression experiments, seedlings were sprayed twice with induction medium within 12 hours and observed 24 - 26 hours after the first induction. For the analysis of the overexpression phenotype of mCit-ROP2, mCit-GEF3 and mCit-GEF4, a region approximately 2-4 mm from the root tip was used.

2.4 Phenotyping of T-DNA insertion mutant lines

All T-DNA mutant lines were tested for the presents of the T-DNA by genotyping PCR before usage.

Table 4.1 T-DNA insertion mutant lines used in this thesis

Genotype	gene ID	T-DNA ID	Ecotype	Left primer	Right primer	Internal primer
cngc14-2	AT2G24610	WiscDsLox437E09	Col-0	genotyped by collaborator		
cngc6-1	AT2G23980	SALK_042207	Col-0	genotyped by collaborator		
cngc9-3	AT4G30560	GK-802D06	Col-0	oPD0192-LP	oPD0192-RP	o8409-GABI
fer-5	AT3G51550	SALK_029056C	Col-0	oPD0196-LP	oPD0196-RP	LB1.3x_Salk
gef3-1	At4G00460	SALK_079879C	Col-0	oPD0197-LP	oPD0197-RP	LB1.3x_Salk
gef4-2	AT2G45890	SALK_107520	Col-0	oPD0181-LP	oPD0181-RP	LB1.3x_Salk
gef10-1	AT5G19560	SALK_009456	Col-0	oPD0110-LP	oPD0110-RP	LB1.3x_Salk
gef11-1	AT1G52240	SALK_126725C	Col-0	oPD0168-LP	oPD0168-RP	LB1.3x_Salk
gef12-1	AT1G79860	SALK_103614	Col-0	oPD0175-LP	oPD0175-RP	LB1.3x_Salk
gef14-2	AT1G31650	SALK_046067	Col-0	oPD0176-LP	oPD0176-RP	LB1.3x_Salk
pip5k3-3	AT2G26420	SALK_000024C	Col-0	oPD0107-LP	oPD0107-RP	LB1.3x_Salk
rhd2-1	AT5G51060	SALK_018814	Col-0	oPD0169-LP	oPD0169-RP	LB1.3x_Salk
rhd6-1	AT1G66470	T-DNA Insertion	Ws-2	Phenotyped / Genotyped by Kan-resistance		
rop2-1	AT1G20090	SALK_055328C	Col-0	oPD0104-LP	oPD0104-RP	LB1.3x_Salk
rop4-1	AT1G75840	(Fu et al., 2005)	Ws-2	oPD0009-fwd	oPD0009-rev	JL-202_LB

Primary roots (7 dag) were used for all phenotyping experiments. For phenotyping of knockout mutant lines, the distance of the first bulge to the root tip was defined. The first visible swelling of the cell outline was defined as first bulge. The root hair density was analyzed 2 mm following the first bulge. The root hair length was analyzed measuring root hairs growing perpendicular to the root in a region 3-6 mm away from the root tip.

3 Imaging

3.1 Transmitted light imaging for phenotyping

Root hair phenotyping of mutant and overexpression phenotypes was performed by transmitted light microscopy on a Nikon SMZ18 stereo microscope, equipped with SHR Plan Apo 0.5x (N.A. 0.075) and 2x (N.A. 0.3) objectives (Nikon) and an Orca Flash 4.0 sCMOS camera (Hamamatsu, Japan).

3.2 Confocal spinning-disk and fluorescence microscopy

Live-cell fluorescence imaging was performed on a custom-built spinning-disk confocal microscope, consisting of a Nikon Ti-E stand, equipped with 20x multi-immersion (N.A. 0.75) and 60x water immersion (N.A. 1.2) objectives (Nikon), a motorized stage (Applied Scientific Instrumentation, USA), a spinning disk with customized hole pattern (CREST Optics, Italy), a motorized filter wheel (Cairn Research, UK), a laser launch (Omicron, Germany), two dichroic mirrors (Chroma triple band 440/514/561 and Chroma quad band 405/488/561/640) and an EMCCD camera (Photometrics, USA). Image acquisition was operated through Nikon NIS Elements software or Micro-Manager (Edelstein et al., 2010).

Table 4.2 Excitation source and emission filters used for fluorescence microscopy

Fluorophore	Excitation Wavelength	Emission Filter
mTurquoise2	445 nm	Bandpass 480nm/40 (Semrock)
eGFP, mNeonGreen, mClover3	488 nm	Bandpass 525nm/45 (Semrock)
mCitrine, Venus, mYPet	515 nm	Bandpass 542nm/20 (Semrock)
tagRFP-T, mRuby2, mRuby3, mCherry, Chlorophyll	561 nm	Bandpass 605nm/70 (Semrock)
		Longpass 630nm/92 (Semrock)

The excitation laser intensity and the EM-Gain of the camera were adjusted according to the sample for each experiment and signal intensities are thus not comparable. Only for the FP brightness and stability experiments, laser output and gain were kept constant to allow quantification of the signal output. If not mentioned otherwise, images were acquired with 70 µm pinholes on the spinning disk. Only for $[Ca^{2+}]_{cyto}$ measurements of the CNGC mutant analysis and mTrq2-ROP2 time laps imaging for CCCP treatments the spinning disk was removed to allow non-confocal fluorescence microscopy. For all imaging of red FP in roots or chlorophyll autofluorescence the longpass filter was used, for imaging of red FPs in *N. benthamiana* leaves the bandpass filter was used to avoid chlorophyll autofluorescence.

3.3 Confocal point scanning microscopy

A Leica SP5 point scanning confocal microscope was used, equipped with a 20x multi-immersion (N.A 0.7) and a 60x water immersion (N.A. 1.2) objective (Leica), two Hybrid-Detectors (set to Gain 200 %), an argon laser and a 561 diode. Image acquisition was operated through the Leica Application Suite software and the used settings are listed below.

Table 4.3 Excitation and emission filters used for confocal point scanning microscopy

Fluorophore	Excitation Wavelength	Emission Filter
mTurquoise2	458 nm (Argon)	465 – 505 nm
mCitrine	514 nm (Argon	520 – 550 nm
propidium iodide	561 nm (Diode)	570 – 650 nm

3.4 FRAP

All FRAP experiments were performed with the FRAP-Wizard implemented in the Leica Application Suite software, using the “Zoom-in Modus” for bleaching. For all experiments the general microscope settings were kept constant, only excitation intensities were adjusted if necessary (3-5% Laser output). The following settings were used for FRAP experiments: 60x water immersion (N.A. 1.2), 3x Zoom, Pinhole 3 AU, 256x256 pixel scanning field, 1000 Hz scanning speed (bidirectional), 2x line average, 0.265 s time interval. The bleaching was performed with full 60 % Laser output in a 10x2.5 µm region at the RHID, for 20 frames. 30 pre-bleach and 700 post-bleach images were recorded.

3.5 Propidium iodide staining

Primary roots (7dag) were stained for 5 min in 10 µg/ml propidium iodide (diluted in ¼ MS, from 1mg/ml Stock), washed in medium and imaged directly on a Leica SP5 as described above, with 20x water immersion objective (N.A 0.7), 1x Zoom, Pinhole 1AU, 1024x1024 pixel scanning field, 400 Hz scanning speed, 2x line average and 2 µm Z-Steps as settings. Both channels were imaged in sequential scans to avoid crosstalk between mCit and propidium iodide.

3.6 $[Ca^{2+}]_{cyto}$ measurements in root hairs and during fertilization

$[Ca^{2+}]_{cyto}$ measurements in root hairs of CNGC mutant lines using R-GECO1 were performed on an epifluorescence microscope (Nikon, see 3.2) using a 20x multi-immersion objective (N.A 0.75Nikon). All measurements were done with a 2 sec time interval for 256 frames.

$[Ca^{2+}]_{cyto}$ measurements during fertilization using CerTN-L15 were done on a Leica SP8. The exact experimental procedure and the microscope settings are described in (Denninger et al., 2014).

4 Image and data analysis

4.1 Image analysis and processing

4.1.1. General image processing

Image processing, analysis and measurements was done using FIJI (ImageJ) (Schindelin et al., 2012). A gaussian filter (radius 0.6 - 0.8) and a rolling ball (radius 50 – 100) background subtraction was applied to all shown images. The “Royal” lookup table was used for images shown in intensity pseudo color. Images of propidium iodide staining for visualization of the root outlines, the gamma settings were adjusted to 0.75 to reduce the contrast between weakly and strongly stained regions of the root. The adjustment was only done in the PI channel. The signal of the mCitrine-fusions was not altered.

4.1.2 Fiji plugins

Kymographs were generated using the multi-kymograph plugin in FIJI. Movement in time-laps experiments ($[Ca^{2+}]_{cyto}$ measurements or FRAP experiments) were corrected using the MultiStackReg plugin in Fiji.

4.2 Data analysis

4.2.1 General Data analysis

All data analysis was done in Microsoft Excel, if not mentioned otherwise. As statistical test, t-tests (two-tailed, unequal variances) were performed in Excel.
Box plots were created using the web-tool BoxPlotR (http://shiny.chemgrid.org/boxplotr/) provided by the Tyers (Montreal) and Rappsilber (Edinburgh) labs. For all plots number of measurements (n) is given. Center lines show the medians; Notches indicate 95 % confidence interval of the medians; box limits indicate the 25th and 75th percentiles as determined by R software; whiskers extend 1.5 times the interquartile range from the 25th and 75th percentiles, outliers are represented by dots; crosses represent sample means; bars indicate 95 % confidence intervals of the means.

4.2.2 Polarity index (Pol-Idx) analysis

Polarity indices were analyzed on the original unprocessed images by measuring in 3x15 pixel regions at the RHID, outside the RHID and outside the root, as a background value. This background value was subtracted from both regions and the value outside the RHID was divided by the RHID value. This polarity index was calculated for each cell within a root hair file, all files were aligned to the first cell with a visible bulge and the average polarity index for each developmental step was calculated. A signal was defined as polar, if its value differed (p-value <0.05, according to two-tailed t-test with unequal variances) to the polarity index of the membrane marker GFP-Lti6b.

4.2.3 FWHM analysis and RHID size description

For defining the FWHM of the mCit-GEF3 patch and to compare the size of the mCit-GEF3 and the mTrq2-ROP2 signal accumulation at the RHID. The signal intensity was measured along a 3 pixel wide line along the outer cell periphery, starting at the rootward cell pole. For comparison of mCit-GEF3 and mTrq2-ROP2 multiple cells were measured, aligned to their starting point and the values were normalized to the first value. Shown are the average intensity profiles of all measured cells. For the FWHM analysis, each measurement was analyzed individually. The basal intensity of the cell periphery (defined 25-35 µm away from the cell pole) was subtracted from all values, the maximum and half-maximal points were defined by excel and the FWHM and the distance of the maximum to the cell pole was read out manually.

4.2.4 FRAP analysis

For FRAP experiments signal intensities were measured at the bleached region and intensities values were further analyzed in Microsoft Excel. For calculation of the half-recovery time and the mobile/immobile fraction the standalone MatLab package EasyFRAP (http://ccl.med.upatras.gr/index.php?id=easyfrap) was used as described in (Rapsomaniki et al., 2012). The output values are further processed in Microsoft Excel.

5. Appending Lists

5.1 Cloned entry vector constructs

Table 4.4 Entry vectors cloned in this thesis

Insert	Plasmid	Backbone	Description
pGGAD000	pPD0002	pUC19	GreenGate entry vector with AD overhangs
GEF3 Promoter	pPD0329	pGGA	GEF3-Promoter (-1742)
GEF4 Promoter	pPD0063	pGGA	GEF4 Promoter (-1500)
GEF10 Promoter	pPD0065	pGGA	GEF10 Promoter (-1534 bp)
GEF11 Promoter	pPD0075	pGGA	GEF-Promoter (-1458 bp)
GEF12 Promoter	pPD0178	pGGA	GEF12 Promoter (-701 bp)
GEF14 Promoter	pPD0180	pGGA	GEF14 Promoter (-2000 bp
ROP2 Promoter	pPD0010	pGGA	ROP2-Promoter (-1503 bp)
Ubi-XVE_OlexTATA35S	pPD0161	pGGA	Estradiol inducable Promoter (E-ind)
PI5K3	pPD0056	pGGAD	PIP5K3 genomic Promoter+ORF
PRK7	pPD0068	pGGAD	PRK7 genomic Promoter+ORF
TMK1	pPD0124	pGGAD	TMK1 genomic Prom+ORF
eGFP	pPD0007	pGGB	eGFP as N-Tag with GAGAGA-Linker
mCherry	pPD0289	pGGB	mCherry as N-Tag with GAGAGA-Linker
mCitrine	pPD0160	pGGB	mCitrine as N-Tag with GAGAGA-Linker
mClover3	pPD0356	pGGB	mClover3 as N-Tag with GAGAGA-Linker
mNeonGreen	pPD0354	pGGB	mNeonGreen as N-Tag with GAGAGA-Linker
mRuby2	pPD0020	pGGB	mRuby2 for as N-Tag with GAGAGA-Linker
mRuby3	pPD0358	pGGB	mRuby3 as N-Tag with GAGAGA-Linker
mTurquoise2	pPD0022	pGGB	mTurquoise2 as N-Tag with GAGAGA-Linker
mYPet	pPD0264	pGGB	mYPet as N-Tag with GAGAGA-Linker
tagRFP-T	pPD0260	pGGB	tagRFP-T as N-Tag with GAGAGA-Linker
Venus	pPD0287	pGGB	Venus as N-Tag with GAGAGA-Linker
C-Decoy	pPD0037	pGGC	Cecoy for constructs with Stop after B-Module
GEF4 ORF	pPD0064	pGGC	GEF4 genomic ORF
GEF3 CDS	pPD0331	pGGC	GEF3 CDS
GEF3 ORF	pPD0330	pGGC	GEF3 genomic ORF
GEF4 CDS	pPD0293	pGGC	GEF4 CDS
GEF10 ORF	pPD0066	pGGC	GEF10 genomic ORF
GEF10 CDS	pPD0294	pGGC	GEF10 CDS
GEF11 ORF	pPD0076	pGGC	GEF11 genomic ORF
GEF11 CDS	pPD0295	pGGC	GEF11 CDS
GEF12 ORF	pPD0179	pGGC	GEF12 genomic ORF
GEF12 CDS	pPD0296	pGGC	GEF12 CDS
GEF14 ORF	pPD0181	pGGC	GEF14 genomic ORF
GEF14 CDS	pPD0297	pGGC	GEF14 CDS
MRH3 ORF	pPD0171	pGGC	MRH3 genomic ORF
PCaP1 ORF	pPD0167	pGGC	PCaP1 genomic ORF
PCaP2 ORF	pPD0168	pGGC	PCaP2 genomic ORF
PRK7 ORF	pPD0173	pGGC	PRK7 genomic ORF
PRK7 CDS	pPD0298	pGGC	PRK7 CDS
RHD2 ORF	pPD0123	pGGC	RHD2 genomic ORF
RHS16 ORF	pPD0177	pGGC	RHS16 genomic ORF
ROP2 ORF	pPD0011	pGGC	ROP2 genomic ORF
ROP2 CDS	pPD0095	pGGC	ROP2 CDS
ROP2-CA	pPD0128	pGGC	constitutivly active ROP2 CDS (G14V)
ROP2-DN	pPD0129	pGGC	dominant negative ROP2 CDS (D120A)
ROP2ΔN-19	pPD0130	pGGC	ROP2 CDS_20-195

ROP2ΔN-42	pPD0131	pGGC	ROP2 CDS_43-195
ROP2ΔN-79	pPD0132	pGGC	ROP2 CDS_80-195
ROP2ΔN-121	pPD0133	pGGC	ROP2 CDS_122-195
ROP2ΔN-161	pPD0134	pGGC	ROP2 CDS_161-195
ROP2ΔC-161	pPD0135	pGGC	ROP2 CDS_1-160
ROP2-C8A	pPD0078	pGGC	ROP2 CDS_C8A
ROP2-C20A	pPD0079	pGGC	ROP2 CDS_C20A
ROP2-C157A	pPD0080	pGGC	ROP2 CDS_C157A
ROP2-C8,20A	pPD0081	pGGC	ROP2 CDS_C8,20A
ROP2-C8,157A	pPD0290	pGGC	ROP2 CDS_C8,157A
ROP2-C20,C157A	pPD0291	pGGC	ROP2 CDS_C20,20A
ROP2-C8,20,157A	pPD0082	pGGC	ROP2 CDS_C8,20,157A
ROP2-C192A	pPD0183	pGGC	ROP2 CDS_C192A
ROP2-K-A	pPD0249	pGGC	ROP2 CDS_with Mutation K181,183-187,189A
ROP4 ORF	pPD0014	pGGC	ROP4 genomic ORF
ROP6 ORF	pPD0016	pGGC	ROP6 genomic ORF
SCN1 ORF	pPD0169	pGGC	SCN1 genomic ORF
TMK1 ORF	pPD0175	pGGC	TMK1 genomic ORF
TMK3 ORF	pPD0176	pGGC	TMK3 genomic ORF
eGFP	pPD0003	pGGD	eGFP as C-Tag with GAGAGA-Linker
mCitrine	pPD0159	pGGD	mCitrine as C-Tag with GAGAGA-Linker
mClover3	pPD0355	pGGD	mClover2 as C-Tag with GAGAGA-Linker
mNeonGreen	pPD0353	pGGD	mNeonGreen as C-Tag with GAGAGA-Linker
mRuby2	pPD0019	pGGD	mRuby2 as C-Tag with GAGAGA-Linker
mRuby3	pPD0357	pGGD	mRuby3 as C-Tag with GAGAGA-Linker
mTurquoise2	pPD0021	pGGD	mTurquoise2 as C-Tag with GAGAGA-Linker
mCherry	pPD0288	pGGD	mCherry as C-Tag with GAGAGA-Linker
mYPet	pPD0263	pGGD	mYPet as C-Tag with GAGAGA-Linker
Venus	pPD0286	pGGD	Venus as C-Tag with GAGAGA-Linker
HSP18.2-Terminator	pPD0059	pGGE	Terminator with enhanced Gene expression

5.2 Cloned destination vector constructs

Plant lines were made for all cloned destination constructs

Table 4.5: Entry vectors cloned in this thesis

Insert	Plasmid	Backbone	Description
GEF3-mCit	pPD0332	pGGZ003	Gef3::mCit-GEF3::HSP18.2T::Basta
GEF3-mCit_ind	pPD0333	pGGZ003	E-ind::mCit-GEF3::HSP18.2T::Basta
GEF3-mTrq2_ind	pPD0334	pGGZ003	E-ind::mTrq2-GEF3::HSP18.2T::Kan
GEF4-mCit	pPD0301	pGGZ003	Gef4::mCit-GEF4::HSP18.2T::Basta
GEF4-mCit_ind	pPD0202	pGGZ003	E-ind::mCit-GEF4::HSP18.2T::Basta
GEF10-mCit	pPD0302	pGGZ003	Gef10::mCit-GEF10::HSP18.2T::Basta
GEF10-mCit_ind	pPD0203	pGGZ003	E-ind::mCit-GEF10::HSP18.2T::Basta
GEF11-mCit	pPD0303	pGGZ003	Gef11::mCit-GEF11::HSP18.2T::Basta
GEF11-mCit_ind	pPD0204	pGGZ003	E-ind::mCit-GEF11::HSP18.2T::Basta
GEF12-mCit	pPD0304	pGGZ003	Gef12::mCit-GEF12::HSP18.2T::Basta
GEF12-mCit_ind	pPD0205	pGGZ003	E-ind::mCit-GEF12::HSP18.2T::Basta
GEF14-mCit	pPD0305	pGGZ003	Gef14::mCit-GEF14::HSP18.2T::Basta
GEF14-mCit_ind	pPD0206	pGGZ003	E-ind::mCit-GEF14::HSP18.2T::Basta

MRH3-mCit_ind	pPD0218	pGGZ003	E-ind::MRH3-mCit::HSP18.2T::Basta
PCaP1-mCit_ind	pPD0214	pGGZ003	E-ind::PCaP1-mCit::HSP18.2T::Basta
PCaP2-mCit_ind	pPD0215	pGGZ003	E-ind::PCaP2-mCit::HSP18.2T::Basta
PIP5K3-mCit	pPD0241	pGGZ003	PIP5K3::PIP5K3-mCit::HSP18.2T::Basta
PRK7-mCit	pPD0283	pGGZ003	PRK7::PRK7-mCit::HSP18.2T::Basta
PRK7-mCit_ind	pPD0220	pGGZ003	E-ind::PRK7-mCit::HSP18.2T::Basta
RHD2-mCit_ind	pPD0209	pGGZ003	E-ind::mCit-RHD2::HSP18.2T::Basta
RHS16-mCit_ind	pPD0224	pGGZ003	E-ind::RHS16-mCit::HSP18.2T::Basta
ROP2-mCit	pPD0240	pGGZ003	Rop2::mCit-ROP2::HSP18.2T::Basta
ROP2-mRuby2	pPD0084	pGGZ003	Rop2::mRuby-ROP2::RbcsT::Hyg
ROP2-mTurqouise2	pPD0042	pGGZ003	Rop2::mTrq2-ROP2::RbcsT::Kan
ROP2_ORF-mCit_ind	pPD0199	pGGZ003	E-ind::mCit-ROP2::HSP18.2T::Basta
ROP2_CDS-mCit_ind	pPD0184	pGGZ003	E-ind::mCit-ROP2::HSP18.2T::Basta
ROP2-CA-mCit_ind	pPD0191	pGGZ003	E-ind::mCit-CA-ROP2(G14V)::HSP18.2T::Basta
ROP2-DN-mCit_ind	pPD0192	pGGZ003	E-ind::mCit-DN-ROP2(D120A)::HSP18.2T::Basta
ROP2ΔN-19-mCit_ind	pPD0193	pGGZ003	E-ind::mCit-ROP2ΔN-19::HSP18.2T::Basta
ROP2ΔN-42-mCit_ind	pPD0194	pGGZ003	E-ind::mCit-ROP2ΔN-42::HSP18.2T::Basta
ROP2ΔN-79-mCit_ind	pPD0195	pGGZ003	E-ind::mCit-ROP2ΔN-79::HSP18.2T::Basta
ROP2ΔN-121-mCit_ind	pPD0196	pGGZ003	E-ind::mCit-ROP2ΔN-121::HSP18.2T::Basta
ROP2ΔN-160-mCit_ind	pPD0197	pGGZ003	E-ind::mCit-ROP2ΔN-160::HSP18.2T::Basta
ROP2ΔC-161-mCit_ind	pPD0198	pGGZ003	E-ind::mCit-ROP2ΔC-161::HSP18.2T::Basta
ROP2C8A-mCit_ind	pPD0186	pGGZ003	E-ind::mCit-ROP2-C8A::HSP18.2T::Basta
ROP2C20A-mCit_ind	pPD0187	pGGZ003	E-ind::mCit-ROP2-C20A::HSP18.2T::Basta
ROP2C157A-mCit_ind	pPD0188	pGGZ003	E-ind::mCit-ROP2-C157A::HSP18.2T::Basta
ROP2C8,20A-mCit_ind	pPD0189	pGGZ003	E-ind::mCit-ROP2-C8,20A::HSP18.2T::Basta
ROP2C8,157A-mCit_ind	pPD0316	pGGZ003	E-ind::mCit-ROP2-C8,157A::HSP18.2T::Basta
ROP2C20,157A-mCit_ind	pPD0317	pGGZ003	E-ind::mCit-ROP2-C20,157A::HSP18.2T::Basta
ROP2C8,20,157A-mCit_ind	pPD0190	pGGZ003	E-ind::mCit-ROP2-C8,20,157A::HSP18.2T::Basta
ROP2C192A-mCit_ind	pPD0185	pGGZ003	E-ind::mCit-ROP2M(C192A)::HSP18.2T::Basta
ROP2-K-A_CDS-mCit_ind	pPD0251	pGGZ003	E-ind::mCit-ROP2_K181,183-187,189A::HSP18.2T::Basta
ROP4-mCit_ind	pPD0200	pGGZ003	E-ind::mCit-ROP4::HSP18.2T::Basta
ROP6-mCit_ind	pPD0201	pGGZ003	E-ind::mCit-ROP6::HSP18.2T::Basta
SCN1-mCit_ind	pPD0216	pGGZ003	E-ind::SCN1-mCit::HSP18.2T::Basta
TMK1-mCit_ind	pPD0222	pGGZ003	E-ind::TMK1-mCit::HSP18.2T::Basta
TMK1-mCit	pPD0284	pGGZ003	Tmk1::TMK1-mCit::HSP18.2T::Basta
TMK3-mCit_ind	pPD0223	pGGZ003	E-ind::TMK3-mCit::HSP18.2T::Basta
mTrq2	pPD0265	pGGZ003	Ubi10::mTrq2:decoy:HSP18.2T::Kan
eGFP	pPD0266	pGGZ003	Ubi10::eGFP:decoy:HSP18.2T::Basta
mCirtine	pPD0267	pGGZ003	Ubi10:-mCit:decoy:HSP18.2T::Basta
mYPet	pPD0268	pGGZ003	Ubi10::mYPet:decoy:HSP18.2T::Basta
mRuby2	pPD0269	pGGZ003	Ubi10::mRuby2:decoy:HSP18.2T::Hyg
tagRFP-T	pPD0270	pGGZ003	Ubi10::tagRFP-T:decoy:HSP18.2T::Hyg
Venus	pPD0320	pGGZ003	Ubi10::Venus:decoy:HSP18.2T::Basta
mCherry	pPD0321	pGGZ003	Ubi10::Venus:decoy:HSP18.2T::Hyg
mNeonGreen	pPD0359	pGGZ003	Ubi10::mNeonGreen:decoy:HSP18.2T::Basta
mClover3	pPD0360	pGGZ003	Ubi10::mClover3:decoy:HSP18.2T::Basta
mRuby3	pPD0361	pGGZ003	Ubi10::mRuby3:decoy:HSP18.2T::Hyg

5.3 Primers used for cloning, sequencing and genotyping

Table 4.6 Primers used in this thesis

Description	Name	Sequence
CDS-Decoy with Stop codons like C-Decoy	oPD0052-fwd	gtgaagcttGGTCTCaGGCTgtggatcc
CDS-Decoy with Stop codons like C-Decoy	oPD0052-rev	GCGAgaattcGGTCTCaCTGAggtacca
cngc9-1 genotyping GK-802D06	oPD0192-LP	TGAAGCCGTGTCTGTACACAG
cngc9-1 genotyping GK-802D06	oPD0192-RP	CAGCAAGAGTTTGCGGATAAG
E-ind Promoter in pGGA_UBI10::XVE (pPD0161)	oPD0120-fwd	aacaGGTCTCtACCTgcaacaacgaatgttcatcatactc
E-ind Promoter in pGGA_UBI10::XVE (pPD0161)	oPD0120-rev	aacaGGTCTCaCTGATCTGGTTCGATGGCTGTTCTC
E-ind Promoter in pGGA_OlexTATA-35S (pPD0161)	oPD0121-fwd	aacaGGTCTCaTCAGCGATCGCaccaGGTACCAC
E-ind Promoter in pGGA_OlexTATA-35S (pPD0161)	oPD0121-rev	aacaGGTCTCaTGTTcagcgtgtcctctccaaatgaa
fer-5 genotyping SALK_029056C	oPD0196-LP	TGGTAGGATTCCGTTAAAATGC
fer-5 genotyping SALK_029056C	oPD0196-RP	CAGAGTATTTCAGACGGCAGC
Gef3 expression test after T-DNA insertion	oPD0232-fwd	TGGAGAGTAGACCAAGAGCAGA
Gef3 expression test after T-DNA insertion	oPD0232-rev	TCTCCATGTGTACATCGAAGCT
Gef3 expression test before T-DNA insertion	oPD0231-fwd	TGAAAACGACGATCATCAATCACC
Gef3 expression test before T-DNA insertion	oPD0231-rev	GGCTCTAACCTCAGATTCTGTCC
GEF3 ORF_PartA	oPD0191A-fwd	aacaGGTCTCaGGCTATGGAGAATTTATCGAATCCAGATGA
GEF3 ORF_PartA	oPD0191A-rev	aacaGGTCTCCACTACAGAAGCTGTTGGTTTCATCTATCTGGTCTGAAA ACCCTGAAGTGGTtTCTGAAC
GEF3 ORF_PartB	oPD0191B-fwd	aacaGGTCTCGTAGTGAAGCTTCTCCTTGTAACTG
GEF3 ORF_PartB	oPD0191B-rev	aacaGGTCTCaCTGATTATTCACTACCTCTCATGGTTTTGT
GEF3 Promoter	oPD0190-fwd	aacaGGTCTCtACCTctcgatcaacccttcacggt
GEF3 Promoter	oPD0190-rev	aacaGGTCTCaTGTTctttaaaatcttaaaacactccttaaaggtct
gef3-1 genotyping SALK_079879C	oPD0197-LP	TCGAATCCAGATGAAAACGAC
gef3-1 genotyping SALK_079879C	oPD0197-RP	TCCTGAATGATCCAGTCGAAG
GEF4 ORF	oPD0068-fwd	aacaGGTCTCtGGCTATGGAGAGTTCTTCGAATTCCGA
GEF4 ORF	oPD0068-rev	aacaGGTCTCtCTGACTAATCATCTCTGTTTCTCACTGTTCT
GEF4 Promoter	oPD0067-fwd	aacaGGTCTCtACCTctcaatgtgcataagctgctct
GEF4 Promoter	oPD0067-rev	aacaGGTCTCaTGTTcacgattgtgtataatgatcaatgttt
gef4-2 genotyping SALK_107520	oPD0181-LP	AACCTTCAGCAGGAACACATG
gef4-2 genotyping SALK_107521	oPD0181-RP	AGAGTTCTTCGAATTCCGACC
GEF10 ORF Part A	oPD0070A-fwd	aacaGGTCTCtGGCTATGTTCGATGGTCGGAACTCT
GEF10 ORF Part A	oPD0070A-rev	aacaGGTCTCCTGTCCCACCGCCTGACAT
GEF10 ORF Part B	oPD0070B-fwd	aacaGGTCTCGGACAGGGGAaACCTCTGCG
GEF10 ORF Part B	oPD0070B-rev	aacaGGTCTCTCGAAAAGCTCCCTCTTCTCT
GEF10 ORF Part C	oPD0070C-fwd	aacaGGTCTCTTTCGAAGTCCGAGCTGAaACCATTTTGG
GEF10 ORF Part C	oPD0070C-rev	aacaGGTCTCtCTGATCAGTGTCTGTCACTAGGGCT
GEF10 Promoter	oPD0069-fwd	aacaGGTCTCtACCTggattgtgacattgagatctaccg
GEF10 Promoter	oPD0069-rev	aacaGGTCTCaTGTTctttctaaaactaaaagatcttggcca
gef10-1 genotyping SALK_009456	oPD0110-LP	TTGACCGAAATAAGAAGTCCTC
gef10-1 genotyping SALK_009457	oPD0110-RP	TTTGAAACGATGTGGTGTTTG
GEF11 ORF	oPD0080-fwd	aacaGGTCTCtGGCTATGTTGGAAGGCAAAGCAATGG
GEF11 ORF	oPD0080-rev	aacaGGTCTCtCTGATCAGGAGTATCTTGCGGTTGG
GEF11 Promoter	oPD0079-fwd	aacaGGTCTCtACCTtttgattttgggttttgtttcgtcc
GEF11 Promoter	oPD0079-rev	aacaGGTCTCaTGTTctttctctatctctctctctctcaataac
gef11-1 genotyping SALK_126725C	oPD0168-LP	TCAGAGAGAGGTCAAAATTGAGG
gef11-1 genotyping SALK_126725C	oPD0168-RP	TACCTGCGAGATTGGTAATGG
GEF12 ORF Part A	oPD0140A-fwd	aacaGGTCTCtGGCTATGGTTCGTGCTTCGGAACA
GEF12 ORF Part A	oPD0140A-rev	aacaGGTCTCGATCCGGTGGCAGCCTCATCTAAACCaGTCTCGAC
GEF12 ORF Part B	oPD0140B-fwd	aacaGGTCTCCGGATCCCATGACGCTGAA
GEF12 ORF Part B	oPD0140B-rev	aacaGGTCTCTCTCGCTTCTCCAGACTTACTC
GEF12 ORF Part C	oPD0140C-fwd	aacaGGTCTCGCGAGAGGTCTTCGAAGAGCGAGCTGAaACCATTTTG
GEF12 ORF Part C	oPD0140C-rev	aacaGGTCTCtCTGATCAATGCCGTGCCGTTGG

GEF12 Promoter	oPD0139-fwd	aacaGGTCTCtACCTatctccttttctctgtttttttttttttattttttcttc
GEF12 Promoter	oPD0139-rev	aacaGGTCTCaTGTTtcctggtcccttgatggcaatagag
gef12-1 genotyping SALK_103614	oPD0175-LP	AGGAGTATCCTCTGCTCTCGC
gef12-1 genotyping SALK_103615	oPD0175-RP	ATGATTGATGCCTCGATTCTG
GEF14 ORF Part A	oPD0142A-fwd	aacaGGTCTCtGGCTATGATGCTGATGAGAAGAAGGTTG
GEF14 ORF Part A	oPD0142A-rev	aacaGGTCTCactataaagaaaaccccacctagtacat
GEF14 ORF Part B	oPD0142B-fwd	aacaGGTCTCtatagtcaaaatctgaacAgtctcttaatg
GEF14 ORF Part B	oPD0142B-rev	aacaGGTCTCTTAGCATCAAAATGTTGAGAtCTTCCAG
GEF14 ORF Part C	oPD0142C-fwd	aacaGGTCTCTGCTAAGGAGAAGAAGAAACAAGGC
GEF14 ORF Part C	oPD0142C-rev	aacaGGTCTCGGAGCTAGGGAAGCAACTCG
GEF14 ORF Part D	oPD0142D-fwd	aacaGGTCTCAGCTCCCGTGACCCTTATAGGACACCTGAaAGACCTC
GEF14 ORF Part D	oPD0142D-rev	aacaGGTCTCaCTGAAGGAGAAGTATCAGAAGGCACTTTAC
GEF14 Promoter	oPD0141-fwd	aacaGGTCTCtACCTGATGCATTGGTTGCTCACTTCA
GEF14 Promoter	oPD0141-rev	aacaGGTCTCaTGTTccttttcttctcttttgaattcttttgttga
gef14-2 genotyping SALK_046067	oPD0176-LP	TGGTAAGACACCGAAACTTGC
gef14-2 genotyping SALK_046068	oPD0176-RP	TGCTGATGAGAAGAAGGTTG
GFP as C-Tag with GAGAGA-Linker	oPD0002-fwd	aaaaGGTCTCaTCAGGAGCAGGGGCGGGTGCCatggtgagcaagggcgag
GFP as C-Tag	oPD0002-rev	aaaaGGTCTCaGCAGttacttgtacagctcgtcca
GFP as N-Tag	oPD0012-fwd	aaaaGGTCTCaAACAatggtgagcaagggcgagga
GFP as N-Tag with GAGAGA-Linker	oPD0012-rev	aaaaGGTCTCaAGCCCCCGCTCCTGCTCCcttgtacagctcgtccatgcc
HSP18.2 Terminator	oPD0064-fwd	aacaGGTCTCtCTGCatatgaagatgaagatgaaatatttgg
HSP18.2 Terminator	oPD0064-rev	aacaGGTCTCaTAGTcttatctttaatcatattccatagtcc
MRH3 Promoter+ORF Part A	oPD0078A-fwd	aacaGGTCTCtACCTagagatttccggccccatc
MRH3 Promoter+ORF Part A	oPD0078A-rev	aacaGGTCTCAGAGTGTCCCAATCATTGTCTTCT
MRH3 Promoter+ORF Part B	oPD0078B-fwd	aacaGGTCTCCACTCTTCTTGAGAGgGACCAGgtt
MRH3 Promoter+ORF Part B	oPD0078B-rev	aacaGGTCTCaCTGAGTCATAAAAACTATGCCTTTGTGGA
MRH3 ORF with oPD0078B-rev	oPD0132-fwd	aacaGGTCTCaGGCTATGAACAATAGAGGAAATAATGATGACCTAG
mCitrine A206K-Mutation with GFP-Primer	oPD0119A-rev	aacaGGTCTCgtcgccgatgggggtgttc
mCitrine A206K-Mutation with GFP-Primer	oPD0119B-fwd	aacaGGTCTCgcgacggccccgtgctgctgcccgacaaccactacctgagctaccagtccAAGctgagc
mClover3 from AddGene Vector with oPD0002-fwd	oPD0212-rev	aacaGGTCTCaGCAGttacttgtacagctcgtccatgccatgtgtaatcccGGCGGCGGTCACGAACTCC
mRuby2 as C-Tag with GAGAGA-Linker	oPD0050-fwd	aacaGGTCTCaTCAGGAGCAGGGGCGGGTGCCATGGTGTCTAAGGGCGAAGAG
mRuby2 as C-Tag	oPD0050-rev	aacaGGTCTCaGCAGTTACTTGTACAGCTCGTCCATCC
mRuby2 as N-Tag	oPD0051-fwd	aacaGGTCTCaAACAATGGTGTCTAAGGGCGAAGAG
mRuby2 as N-Tag with GAGAGA-Linker	oPD0051-rev	aacaGGTCTCaAGCCCCCGCTCCTGCTCCCTTGTACAGCTCGTCCATCCC
mYPet as C-Tag with GAGAGA-Linker	oPD0157-fwd	aaaaGGTCTCaTCAGGAGCAGGGGCGGGTGCCATGGCTGCAGCCAAGGGC
mYPet as C-Tag	oPD0157-rev	aaaaGGTCTCaGCAGTTATTTGTACAATTCATTCATACCCTCGG
mYPet as N-Tag	oPD0158-fwd	aaaaGGTCTCtAACAATGGCTGCAGCCAAGGGC
mYPet as N-Tag with GAGAGA-Linker	oPD0158-rev	aaaaGGTCTCtAGCCCCCGCTCCTGCTCCTTTGTACAATTCATTCATACCCTCGG
PCaP1 Promoter+ORF Part A	oPD0071A-fwd	aacaGGTCTCtACCTggtgacgtaacaagacttattttcc
PCaP1 Promoter+ORF Part A	oPD0071A-rev	aacaGGTCTCAGCCTGctcgttttaattttagtct
PCaP1 Promoter+ORF Part B	oPD0071B-fwd	aacaGGTCTCCAGGCTTTGGTGAGgGACCCTAAGG
PCaP1 Promoter+ORF Part B	oPD0071B-rev	aacaGGTCTCACAATCTCCTCTTTCTCACCACT
PCaP1 Promoter+ORF Part C	oPD0071C-fwd	aacaGGTCTCGATTGTTGAAGAGACAAAGAAAGGCGAaACCCCTGAA
PCaP1 Promoter+ORF Part C	oPD0071C-rev	aacaGGTCTCtCTGAAGGCTTTGGTGGTTCAGCC
PCaP1 ORF with pPD0071C-rev	oPD0128fwd	aacaGGTCTCaGGCTATGGGTTACTGGAATTCCAAGGT
PCaP2 Promoter+ORF Part A	oPD0040-fwd2	aacaGGTCTCtACCTcgacaagcagaagatggaagaa
PCaP2 Promoter+ORF Part A	oPD0061A-rev	aacaGGTCTCggctggttaaggaagtccgg
PCaP2 Promoter+ORF Part B	oPD0061B-fwd	aacaGGTCTCccagccaacagaatctgttctg
PCaP2 Promoter+ORF Part B	oPD0003-rev	aaaaGGTCTCtCTGAAGCCTTTTGTGGCGCAGCCG
PCaP2 ORF with oPD0003-rev	oPD0129-fwd	aacaGGTCTCaGGCTATGGGTTATTGGAAGTCGAAGGT
pGGA-cloning cassette with AD overhang	oPD0001D-rev	GCGAgaattcGGTCTCaCTGAggtaccac
pGGA-cloning cassette with AD overhang	oPD0001-fwd	AgtgaagcttGGTCTCaACCTccggat
PIP5K3 Promoter+ORF Part A	oPD0060A-fwd	aacaGGTCTCtACCTgccaatcttcttgtcatctacatcc
PIP5K3 Promoter+ORF Part A	oPD0060A-rev	aacaGGTCTCCAGCCGTATCACTCACCTCG

PIP5K3 Promoter+ORF Part B	oPD0060B-fwd	aacaGGTCTCCGGCTGCCGAGATTAGAATAGT
PIP5K3 Promoter+ORF Part B	oPD0060B-rev	aacaGGTCTCGATCCAAGTCTTTGAGTGTTGTcGTCTCGTCG
PIP5K3 Promoter+ORF Part C	oPD0060C-fwd	aacaGGTCTCTGGATCTCAAGTATGTGTTTCGACTCGAaACCTCATGG
PIP5K3 Promoter+ORF Part C	oPD0060C-rev	aacaGGTCTCCTCGTCACGCATGCCAGATTCACGGAAATGcAGACCAA TC
PIP5K3 Promoter+ORF Part D	oPD0060D-fwd	aacaGGTCTCGACGACATTTCCTTGGGCATC
PIP5K3 Promoter+ORF Part D	oPD0060D-rev	aacaGGTCTCtCTGATTTGTCTTCAATGAATATTTTGT
PIP5K3 ORF with oPD0060D-rev	oPD0127-fwd	aacaGGTCTCaGGCTATGCAAGAGACAGTGTTCCTCTT
pip5k3-3 genotyping	oPD0107-LP	TCAATTGCATCTTCTTCCCAC
pip5k3-3 genotyping	oPD0107-RP	TGATCCCAAGGATAAGCAATG
PRK7 Promoter+ORF Part A	oPD0072A-fwd	aacaGGTCTCtACCTatatcaattacgaaataaagggatcgc
PRK7 Promoter+ORF Part A	oPD0072A-rev	aacaGGTCTCTGGACCCGAGCGCTTGAA
PRK7 Promoter+ORF Part B	oPD0072B-fwd	aacaGGTCTCGGTCCATCCGCGGaCTCAAGAGTA
PRK7 Promoter+ORF Part B	oPD0072B-rev	aacaGGTCTCCGGATATAGCTCCTGATGTTGCT
PRK7 Promoter+ORF Part C	oPD0072C-fwd	aacaGGTCTCTATCCGTGGGAGGaCTCTCTCCAG
PRK7 Promoter+ORF Part C	oPD0072C-rev	aacaGGTCTCtCTGACATGAGTGAGAACTCCTCAGTCA
PRK7 ORF with oPD0072C-rev	oPD0134-fwd	aacaGGTCTCaGGCTATGACCCGTGATGACAAATTCC
RHD2 ORF Part A	oPD0087A-fwd	aacaGGTCTCaGGCTATGTCTAGAGTGAGTTTTGAAGTGT
RHD2 ORF Part A	oPD0087A-rev	aacaGGTCTCcacaccgctttattataatgaattaggt
RHD2 ORF Part B	oPD0087B-fwd	aacaGGTCTCggtgtgggagacGacaactaaaa
RHD2 ORF Part B	oPD0087B-rev	aacaGGTCTCCCCTCGTACTTCTTGTAGTCTTGTGC
RHD2 ORF Part C	oPD0087C-fwd	aacaGGTCTCACGAGGTGGTTCTACTAGTTGGTtTaGGGATTGG
RHD2 ORF Part C	oPD0087C-rev	aacaGGTCTCaCTGATTAGAAATTCTCTTTGTGGAAGGA
RHD2 Sequencing	oPD0148A-fwd	AGTTTTGATTCTCGGCTTAAG
RHD2 Sequencing	oPD0148B-fwd	TTGTCCCATTTGATGACAATC
RHD2 Sequencing	oPD0148C-rev	ctacatgtgatgtgcccata
rhd2-1 genotyping SALK_018814	oPD0169-LP	ATCCCCGCTCTTTGATTATTG
rhd2-1 genotyping SALK_018815	oPD0169-RP	GCGGATTTAGTCCGGTCTAAC
RHS16 Promoter+ORF Part A	oPD0091A-fwd	aacaGGTCTCtACCTatttgagcatagcgaaattcattgtttc
RHS16 Promoter+ORF Part A	oPD0091A-rev	aacaGGTCTCGGAGAGTACGGtGACCAAATACG
RHS16 Promoter+ORF Part B	oPD0091B-fwd	aacaGGTCTCCTCTCCAGTGTCTTGGAATACAACT
RHS16 Promoter+ORF Part B	oPD0091B-rev	aacaGGTCTCGATGATGATGAAGATCCTTTAGATTTTCCA
RHS16 Promoter+ORF Part C	oPD0091C-fwd	aacaGGTCTCATCATCATCATCATCCCAaGTCTCCAAAGAATTC
RHS16 Promoter+ORF Part C	oPD0091C-rev	aacaGGTCTCtggtaaagattaaaagtggtgatgtgt
RHS16 Promoter+ORF Part D	oPD0091D-fwd	aacaGGTCTCttaccattttggtcatgttAgtctcatcataaac
RHS16 Promoter+ORF Part D	oPD0091D-rev	aacaGGTCTCtCTGACCTTGCCATTGGGCCAAACG
RHS16 ORF with oPD0091D-rev	oPD0138-fwd	aacaGGTCTCaGGCTATGGGAGCTCACTCTGTTTTTCT
ROP2 Promoter	oPD0006-rev	aaaaGGTCTCtTGTTctctgccgcaagatcggaaa
ROP2 Promoter	oPD0038-fwd2	aacaGGTCTCtACCTgacaaataattataagaagctaccgtctg
ROP2 ORF/CDS	oPD0007B-fwd	aaaaGGTCTCaGGCTATGGCGTCAAGGTTTATAAAGTGTG
ROP2 ORF/CDS	oPD0007-rev	aaaaGGTCTCtCTGATCACAAGAACGCGCAACGGT
ROP2_CA_G14V with oPD0007-rev	oPD0092-fwd	aacaGGTCTCtGGCTATGGCGTCAAGGTTTATAAAGTGTGTGACCGTC GGAGATGtTGCCGTCGG
ROP2_DN_D120A Part A with oPD0007B-fwd	oPD0093A-rev	aacaGGTCTCTTGTCCCAACAAGGATAATGGGAA
ROP2_DN_D120A Part B with oPD0007-rev	oPD0093B-fwd	aacaGGTCTCGGACAAAACTCGcTCTTCGAGAT
ROP2_20-195 with oPD0007-rev	oPD0094-fwd	aacaGGTCTCtGGCTTGCATGCTCATTTCTTACACTAGC
ROP2_43-195 with oPD0007-rev	oPD0095-fwd	aacaGGTCTCtGGCTAGTGCTAATGTGGTTGTTGATGG
ROP2_80-195 with oPD0007-rev	oPD0096-fwd	aacaGGTCTCtGGCTTTCATTCTTGCTTTCTCTCTTATTAGCA
ROP2_122-195 with oPD0007-rev	oPD0097-fwd	aacaGGTCTCtGGCTCGAGATGACAAGCAATTCTTTATAGATC
ROP2_161-195 with oPD0007-rev	oPD0098-fwd	aacaGGTCTCtGGCTACACAGCAGAACGTGAAGGC
ROP2_1-160 with oPD0007B-fwd	oPD0099-rev	aacaGGTCTCtCTGAtcaCTTTGAACTACATTCAATGTAGACAGCA
ROP2 C8A Mutation	oPD0082M5-fwd	aacaGGTCTCaGGCTATGGCGTCAAGGTTTATAAAGgctGTGACCGTC
ROP2 C20A Mutation	oPD0082M20-fwd	aacaGGTCTCaGGCTATGGCGTCAAGGTTTATAAAGTGTGTGACCGTC GGAGATGGTGCCGTCGGAAAAACTgccATGCTCATTTC
ROP2 C8,20A Mutation	oPD0082M5,20-fwd	aacaGGTCTCaGGCTATGGCGTCAAGGTTTATAAAGgctGTGACCGTCG GAGATGGTGCCGTCGGAAAAACTgccATGCTCATTTC
ROP2 C157A Mutation with oPD0007B-fwd	oPD0083A-rev	aacaGGTCTCAGATCCAATCAGTTTCTTCAGTTCCT
ROP2 C157A Mutation with oPD0007-rev	oPD0083B-fwd	aacaGGTCTCGGATCTGCTGTCTACATTGAAgctAGTTCAAAG
ROP2 C192A Mutation	oPD0007M-rev	aaaaGGTCTCtCTGATCACAAGAACGCGGCACGGT

ROP2_K181,183-187,189A with oPD0007B-fwd	oPD0150-rev	aacaGGTCTCtCTGATCACAAGAATGCACATCGATTGGCGTTTGCGGC AGCCGCTGCTTGTGCTGGTGGCTGAAGCACCAC
rop2-1 genotyping SALK_055328C	oPD0104-LP	TCGAATTTGGGTGATTCTCAG
rop2-1 genotyping SALK_055328C	oPD0104-RP	TGTGGACTCGAAAGATTCACC
ROP4 ORF/CDS	oPD0009-fwd	aaaaGGTCTCaGGCTATGAGTGCTTCGAGGTTTAT
ROP4 ORF/CDS	oPD0009-rev	aaaaGGTCTCtCTGATCACAAGAACACGCAGCGGT
rop4-1 genotyping, Fu et al. (2005, Cell)	oPD0174-LP	TTGGTGTAGCAAATAGCTGGC
rop4-1 genotyping, Fu et al. (2005, Cell)	oPD0174-RP	ATGCAAGAATGAAGACATCGG
ROP6 ORF/CDS	oPD0011-fwd	aaaaGGTCTCaGGCTATGAGTGCTTCAAGGTTTAT
ROP6 ORF/CDS	oPD0011-rev	ttttGGTCTCtCTGATCAGAGTATAGAACAACCTT
SCN1 Promoter+ORF Part A	oPD0065A-fwd	aacaGGTCTCtACCTtgaagtatatgcatttttcgtAgtctcgg
SCN1 Promoter+ORF Part A	oPD0065A-rev	aacaGGTCTCtatggccaaaatcatttcccaaga
SCN1 Promoter+ORF Part B	oPD0065B-fwd	aacaGGTCTCgccatatttgggacccttgttag
SCN1 Promoter+ORF Part B	oPD0065B-rev	aacaGGTCTCTGGCATCACGTGGTTGTATG
SCN1 Promoter+ORF Part C	oPD0065C-fwd	aacaGGTCTCATGCCAGAAGAaACCACTCCT
SCN1 Promoter+ORF Part C	oPD0065C-rev	aacaGGTCTCtCTGAAAGCGCAGGCCATTCTTTAC
SCN1 ORF with pPD0065C-rev	oPD0130-fwd	aacaGGTCTCaGGCTATGTCTTTGGTATCTGGAGCCAG
TagRFP-T as N-Tag	oPD0154-fwd	aacaGGTCTCtAACAatggtgtctaagggcgaagag
TagRFP-T as N-Tag with GAGAGA-Linker	oPD0154-rev	aacaGGTCTCaAGCCCCCGCTCCTGCTCCagaattcgaagcttgagctcga
TMK1 Promoter+ORF Part A	oPD0088A-fwd	aacaGGTCTCtACCTccttgtagatcttgcagagagcc
TMK1 Promoter+ORF Part A	oPD0088A-rev	aacaGGTCTCCGTCTAGAGATTTTCTTCCCGTTATG
TMK1 Promoter+ORF Part B	oPD0088B-fwd	aacaGGTCTCTAGACGAATCGCAACCAGAAGAAAGCATTCACTTaGTC TCTTGG
TMK1 Promoter+ORF Part B	oPD0088B-rev	aacaGGTCTCCATGTCTGGcCTCTGGTAAGG
TMK1 Promoter+ORF Part C	oPD0088C-fwd	aacaGGTCTCGACATGGGACACGCAGTCAA
TMK1 Promoter+ORF Part C	oPD0088C-rev	aacaGGTCTCaCTGATCGTCCATCTACTGAAGTGAATGAC
TMK1 ORF with oPD0088C-rev	oPD0136-fwd	aacaGGTCTCaGGCTATGAAGAAAAGAAGAACCTTTCTTCTATTTTC
TMK3 Promoter+ORF Part A	oPD0089A-fwd	aacaGGTCTCtACCTctctatcgacttattttatcagtttcagtagg
TMK3 Promoter+ORF Part A	oPD0089A-rev	aacaGGTCTCGAATCATCGAGtCCGGTTTGAGA
TMK3 Promoter+ORF Part B	oPD0089B-fwd	aacaGGTCTCTGATTCGACTATGCAATCTCTCAAATC
TMK3 Promoter+ORF Part B	oPD0089B-rev	aacaGGTCTCTGGACGGTGAGTGAAGAAAGG
TMK3 Promoter+ORF Part C	oPD0089C-fwd	aacaGGTCTCCGTCCAATGGAAACCAACTGAaACCGACCC
TMK3 Promoter+ORF Part C	oPD0089C-rev	aacaGGTCTCtCTGAACGTCCATCCACAGAAGTGAAC
TMK3 ORF with oPD0089C-rev	oPD0137-fwd	aacaGGTCTCaGGCTATGTCAAATTCCCATTTGGGTACTC

Bibliography

Adams AE (1990) CDC42 and CDC43, two additional genes involved in budding and the establishment of cell polarity in the yeast Saccharomyces cerevisiae. The Journal of Cell Biology **111**: 131

Augustine RC, Vidali L, Kleinman KP, Bezanilla M (2008) Actin depolymerizing factor is essential for viability in plants, and its phosphoregulation is important for tip growth. The Plant Journal **54**: 863

Bajar BT, Wang ES, Lam AJ, Kim BB, Jacobs CL, Howe ES, Davidson MW, Lin MZ, Chu J (2016) Improving brightness and photostability of green and red fluorescent proteins for live cell imaging and FRET reporting. Scientific Reports **6**: 20889

Balcerowicz D, Schoenaers S, Vissenberg K (2015) Cell Fate Determination and the Switch from Diffuse Growth to Planar Polarity in Arabidopsis Root Epidermal Cells. Frontiers in Plant Science **6**: 1163

Balleza E, Kim JM, Cluzel P (2017) Systematic characterization of maturation time of fluorescent proteins in living cells. Nature Methods **15**: 47

Bascom CS, Hepler PK, Bezanilla M (2017) Interplay between Ions, the Cytoskeleton, and Cell Wall Properties during Tip Growth. Plant Physiology **176**: 28–40

Basu D, El-Assal SE-D, Le Jie, Mallery EL, Szymanski DB (2004) Interchangeable functions of Arabidopsis PIROGI and the human WAVE complex subunit SRA1 during leaf epidermal development. Development **131**: 4345–55

Bender A, Pringle JR (1989) Multicopy suppression of the cdc24 budding defect in yeast by CDC42 and three newly identified genes including the ras-related gene RSR1. Proceedings of the National Academy of Sciences **86**: 9976

Berken A, Thomas C, Wittinghofer A (2005) A new family of RhoGEFs activates the Rop molecular switch in plants. Nature **436**: 1176–80

Berken A, Wittinghofer A (2008) Structure and function of Rho-type molecular switches in plants. Plant Physiology and Biochemistry **46**: 380–93

Bi E, Park H-O (2012) Cell polarization and cytokinesis in budding yeast. Genetics **191**: 347–87

Bindels DS, Haarbosch L, van Weeren L, Postma M, Wiese KE, Mastop M, Aumonier S, Gotthard G, Royant A, Hink MA (2016) mScarlet: a bright monomeric red fluorescent protein for cellular imaging. Nature Methods **14**: 53

Birnbaum K, Shasha DE, Wang JY, Jung JW, Lambert GM, Galbraith DW, Benfey PN (2003) A gene expression map of the Arabidopsis root. Science **302**: 1956–1960

Bleckmann A, Alter S, Dresselhaus T (2014) The beginning of a seed: regulatory mechanisms of double fertilization. Frontiers in Plant Science **5**: 452

Blume B, Nürnberger T, Nass N, Scheel D (2000) Receptor-mediated increase in cytoplasmic free calcium required for activation of pathogen defense in parsley. The Plant Cell **12**: 1425–1440

Bonello TT, Perez-Vale KZ, Sumigray KD, Peifer M (2018) Rap1 acts via multiple mechanisms to position Canoe and adherens junctions and mediate apical-basal polarity establishment. Development. doi: 10.1242/dev.157941

Brady SM, Orlando DA, Lee J-Y, Wang JY, Koch J, Dinneny JR, Mace D, Ohler U, Benfey PN (2007) A high-resolution root spatiotemporal map reveals dominant expression patterns. Science **318**: 801–806

Brembu T, Winge P, Seem M, Bones AM (2004) NAPP and PIRP encode subunits of a putative wave regulatory protein complex involved in plant cell morphogenesis. The Plant Cell **16**: 2335–2349

Böhme K, Li Y, Charlot F, Grierson C, Marrocco K, Okada K, Laloue M, Nogué F (2004) The Arabidopsis COW1 gene encodes a phosphatidylinositol transfer protein essential for root hair tip growth. The Plant Journal **40**: 686–98

Cai Y, Hossain MJ, Heriche J-K, Politi AZ, Walther N, Koch B, Wachsmuth M, Nijmeijer B, Kueblbeck M, Kavur MM, et al (2017) An experimental and computational framework to build a dynamic protein atlas of human cell division. BioRxiv. doi: 10.1101/227751

Carol RJ, Takeda S, Linstead P, Durrant MC, Kakesova H, Derbyshire P, Drea S, Zarsky V, Dolan L (2005) A RhoGDP dissociation inhibitor spatially regulates growth in root hair cells. Nature **438**: 1013–6

Chalfie M, Tu Y, Euskirchen G, Ward WW, Prasher DC (1994) Green fluorescent protein as a marker for gene expression. Science **263**: 802–805

Chamberlain LH, Shipston MJ (2015) The physiology of protein S-acylation. Physiological Reviews **95**: 341–376

Chang F, Gu Y, Ma H, Yang Z (2012) AtPRK2 promotes ROP1 activation via RopGEFs in the control of polarized pollen tube growth. Molecular Plant **6**: 1187–1201

Chant J, Corrado K, Pringle JR, Herskowitz I (1991) Yeast BUD5, encoding a putative GDP-GTP exchange factor, is necessary for bud site selection and interacts with bud formation gene BEM1. Cell **65**: 1213–1224

Chiou J-G, Balasubramanian MK, Lew DJ (2017) Cell Polarity in Yeast. Annual Review of Cell and Developmental Biology **33**: 77–101

Cho W, Stahelin RV (2005) Membrane-protein interactions in cell signaling and membrane trafficking. Annual Review of Biophysics and Biomolecular Structure **34**: 119–151

Choi W-G, Hilleary R, Swanson SJ, Kim S-H, Gilroy S (2016) Rapid, Long-Distance Electrical and Calcium Signaling in Plants. Annual Review of Plant Biology **67**: 287

Choi W-G, Toyota M, Kim S-H, Hilleary R, Gilroy S (2014) Salt stress-induced Ca2+ waves are associated with rapid, long-distance root-to-shoot signaling in plants. **111**: 6497–6502

Clapham DE (2007) Calcium signaling. Cell **131**: 1047–1058

Clough SJ, Bent AF (1998) Floral dip: a simplified method for Agrobacterium-mediated transformation of Arabidopsis thaliana. The Plant Journal **16**: 735

Cole RA, Fowler JE (2006) Polarized growth: maintaining focus on the tip. Current Opinion in Plant Biology **9**: 579

Cormack BP, Valdivia RH, Falkow S (1996) FACS-optimized mutants of the green fluorescent protein (GFP). Gene **173**: 33

Craddock C, Lavagi I, Yang Z (2012) New insights into Rho signaling from plant ROP/Rac GTPases. Trends in Cell Biology **22**: 492

Cutler SR, Ehrhardt DW, Griffitts JS, Somerville CR (2000) Random GFP::cDNA fusions enable visualization of subcellular structures in cells of Arabidopsis at a high frequency. Proceedings of the National Academy of Sciences **97**: 3718

Cárdenas L, Lovy-Wheeler A, Kunkel JG, Hepler PK (2008) Pollen tube growth oscillations and intracellular calcium levels are reversibly modulated by actin polymerization. Plant Physiology **146**: 1611–1621

Dai N, Wang W, Patterson SE, Bleecker AB (2013) The TMK subfamily of receptor-like kinases in Arabidopsis display an essential role in growth and a reduced sensitivity to auxin. PLOS ONE **8**: e60990

Day RN, Davidson MW (2009) The fluorescent protein palette: tools for cellular imaging. Chemical Society Reviews **38**: 2887–2921

Denninger P, Bleckmann A, Lausser A, Vogler F, Ott T, Ehrhardt DW, Frommer WB, Sprunck S, Dresselhaus T, Grossmann G (2014) Male-female communication triggers calcium signatures during fertilization in Arabidopsis. Nature Communications **5**: 4645

Deslauriers SD, Larsen PB (2010) FERONIA is a key modulator of brassinosteroid and ethylene responsiveness in Arabidopsis hypocotyls. Molecular Plant **3**: 626–40

Di Mambro R, De Ruvo M, Pacifici E, Salvi E, Sozzani R, Benfey PN, Busch W, Novak O, Ljung K, Di Paola L, et al (2017) Auxin minimum triggers the developmental switch from cell division to cell differentiation in the Arabidopsis root. **114**: E7641–E7649

Digonnet C, Aldon D, Leduc N, Dumas C, Rougier M (1997) First evidence of a calcium transient in flowering plants at fertilization. Development **124**: 2867–2874

Djakovic S, Dyachok J, Burke M, Frank MJ, Smith LG (2006) BRICK1/HSPC300 functions with SCAR and the ARP2/3 complex to regulate epidermal cell shape in Arabidopsis. Development **133**: 1091–100

Do Heo W, Inoue T, Park WS, Kim ML, Park BO, Wandless TJ, Meyer T (2006) PI(3,4,5)P3 and PI(4,5)P2 lipids target proteins with polybasic clusters to the plasma membrane. Science **314**: 1458–1461

Dodd AN, Kudla J, Sanders D (2010) The language of calcium signaling. Annual Review of Plant Biology **61**: 593–620

Dong CH (2001) ADF Proteins Are Involved in the Control of Flowering and Regulate F-Actin Organization, Cell Expansion, and Organ Growth in Arabidopsis. The Plant Cell **13**: 1333

Dong J, MacAlister CA, Bergmann DC (2009) BASL controls asymmetric cell division in Arabidopsis. Cell **137**: 1320–1330

Donnelly SK, Bravo-Cordero JJ, Hodgson L (2014) Rho GTPase isoforms in cell motility: Don't fret, we have FRET. Cell Adhesion & Migration **8**: 526–534

Dovas A, Couchman JR (2005) RhoGDI: multiple functions in the regulation of Rho family GTPase activities. The Biochemical Journal **390**: 1–9

Dresselhaus T, Franklin-Tong N (2013) Male-female crosstalk during pollen germination, tube growth and guidance, and double fertilization. Molecular Plant **6**: 1018–36

Duan Q, Kita D, Li C, Cheung AY, Wu H-M (2010) FERONIA receptor-like kinase regulates RHO GTPase signaling of root hair development. Proceedings of the National Academy of Sciences **107**: 17821–6

Dupont G, Combettes L, Bird GS, Putney JW (2011) Calcium oscillations. Cold Spring Harbor Perspectives in Biology. doi: 10.1101/cshperspect.a004226

Edelstein A, Amodaj N, Hoover K, Vale R, Stuurman N (2010) Computer control of microscopes using μManager. Current Protocols in Molecular Biology **Chapter 14**: Unit14.20

Ehrhardt DW, Wais R, Long SR (1996) Calcium spiking in plant root hairs responding to Rhizobium nodulation signals. Cell **85**: 673–81

Escobar-Restrepo J-M, Huck N, Kessler S, Gagliardini V, Gheyselinck J, Yang W-C, Grossniklaus U (2007) The FERONIA receptor-like kinase mediates male-female interactions during pollen tube reception. Science **317**: 656–60

Etienne-Manneville S (2004) Cdc42 - the centre of polarity. Journal of Cell Science **117**: 1291–1300

Etienne-Manneville S, Etienne-Manneville R, Hall A (2002) Rho GTPases in cell biology. Nature **420**: 629–35

Feiguelman G, Fu Y, Yalovsky S (2017) ROP GTPases Structure-Function and Signaling Pathways. Plant Physiology **176**: 57–79

Feng W, Kita D, Peaucelle A, Cartwright HN, Doan V, Duan Q, Liu M-C, Maman J, Steinhorst L, Schmitz-Thom I, et al (2018) The FERONIA Receptor Kinase Maintains Cell-Wall Integrity during Salt Stress through Ca2+ Signaling. Current Biology **28**: 666

Fischer U, Ikeda Y, Ljung K, Serralbo O, Singh M, Heidstra R, Palme K, Scheres B, Grebe M (2006) Vectorial information for Arabidopsis planar polarity is mediated by combined AUX1, EIN2, and GNOM activity. Current Biology **16**: 2143–2149

Foreman J, Demidchik V, Bothwell JHF, Mylona P, Miedema H, Torres MA, Linstead P, Costa S, Brownlee C, Jones JDG, et al (2003) Reactive oxygen species produced by NADPH oxidase regulate plant cell growth. Nature **422**: 442–6

Frescatada-Rosa M, Stanislas T, Backues SK, Reichardt I, Men S, Boutté Y, Jürgens G, Moritz T, Bednarek SY, Grebe M (2014) High lipid order of Arabidopsis cell-plate membranes mediated by sterol and DYNAMIN-RELATED PROTEIN1A function. The Plant Journal **80**: 745–757

Frietsch S, Wang Y-F, Sladek C, Poulsen LR, Romanowsky SM, Schroeder JI, Harper JF (2007) A cyclic nucleotide-gated channel is essential for polarized tip growth of pollen. **104**: 14531–14536

Fu Y, Gu Y, Zheng Z, Wasteneys G, Yang Z (2005) Arabidopsis interdigitating cell growth requires two antagonistic pathways with opposing action on cell morphogenesis. Cell **120**: 687–700

Fu Y, Wu G, Yang Z (2001) Rop GTPase-dependent dynamics of tip-localized F-actin controls tip growth in pollen tubes. The Journal of Cell Biology **152**: 1019–32

Gilroy S, Swanson SJ (2017) Tip Growth. eLS 1

Goedhart J, Stetten von D, Noirclerc-Savoye M, Lelimousin M, Joosen L, Hink MA, van Weeren L, Royant A (2012) Structure-guided evolution of cyan fluorescent proteins towards a quantum yield of 93%. Nature Communications **3**: 751

Goedhart J, van Weeren L, Hink MA, Vischer NOE, Jalink K (2010) Bright cyan fluorescent protein variants identified by fluorescence lifetime screening. Nature Methods **7**: 137

Goley ED, Welch MD (2006) The ARP2/3 complex: an actin nucleator comes of age. Nature Reviews Molecular Cell Biology **7**: 713

Grebnev G, Ntefidou M, Kost B (2017) Secretion and Endocytosis in Pollen Tubes: Models of Tip Growth in the Spot Light. Frontiers in Plant Science **8**: 154

Grierson C, Nielsen E, Ketelaar T, Schiefelbein J (2014) Root hairs. The Arabidopsis Book **12**: e0172

Griesbeck O, Baird GS, Campbell RE, Zacharias DA, Tsien RY (2001) Reducing the environmental sensitivity of yellow fluorescent protein. Mechanism and applications. The Journal of Biological Chemistry **276**: 29188–94

Grossmann G, Guo W-J, Ehrhardt DW, Frommer WB, Sit RV, Quake SR, Meier M (2011) The RootChip: an integrated microfluidic chip for plant science. The Plant Cell **23**: 4234–40

Gu Y, Fu Y, Dowd P, Li S, Vernoud V, Gilroy S, Yang Z (2005) A Rho family GTPase controls actin dynamics and tip growth via two counteracting downstream pathways in pollen tubes. The Journal of Cell Biology **169**: 127–38

Gu Y, Li S, Lord EM, Yang Z (2006) Members of a novel class of Arabidopsis Rho guanine nucleotide exchange factors control Rho GTPase-dependent polar growth. The Plant Cell **18**: 366–381

Gu Y, Vernoud V, Fu Y, Yang Z (2003) ROP GTPase regulation of pollen tube growth through the dynamics of tip-localized F-actin. Journal of Experimental Botany **54**: 93-101

Guan Y, Guo J, Li H, Yang Z (2013) Signaling in pollen tube growth: crosstalk, feedback, and missing links. Molecular Plant **6**: 1053–64

Guo W (2015) The Exocyst at a Glance. Journal of Cell Science **128**: 2957–2964

Hamamura Y, Nishimaki M, Takeuchi H, Geitmann A, Kurihara D, Higashiyama T (2014) Live imaging of calcium spikes during double fertilization in Arabidopsis. Nature Communications **5**: 4722

Hamamura Y, Saito C, Awai C, Kurihara D, Miyawaki A, Nakagawa T, Kanaoka MM, Sasaki N, Nakano A, Berger F, et al (2011) Live-cell imaging reveals the dynamics of two sperm cells during double fertilization in Arabidopsis thaliana. Current Biology **21**: 497–502

Han J, Pluhackova K, Böckmann RA (2017) The Multifaceted Role of SNARE Proteins in Membrane Fusion. Frontiers in Physiology **8**: 5

Hancock JF, Magee Al, Childs JE, Marshall CJ (1989) All ras proteins are polyisoprenylated but only some are palmitoylated. Cell **57**: 1167

Harkins HA, Page N, Schenkman LR, De Virgilio C, Shaw S, Bussey H, Pringle JR (2001) Bud8p and Bud9p, Proteins That May Mark the Sites for Bipolar Budding in Yeast. Molecular Biology of the Cell **12**: 2497

Hartwell LH, Culotti J, Pringle JR, Reid BJ (1974) Genetic Control of the Cell Division Cycle in Yeast: A model to account for the order of cell cycle events is deduced from the phenotypes of yeast mutants. Science **183**: 46

Haruta M, Gray WM, Sussman MR (2015) Regulation of the plasma membrane proton pump (H(+)-ATPase) by phosphorylation. Current Opinion in Plant Biology **28**: 68–75

Haruta M, Sabat G, Stecker K, Minkoff BB, Sussman MR (2014) A peptide hormone and its receptor protein kinase regulate plant cell expansion. Science **343**: 408–411

Havelková L, Nanda G, Martinek J, Bellinvia E, Sikorová L, Šlajcherová K, Seifertová D, Fischer L, Fišerová J, Petrášek J, et al (2015) Arp2/3 complex subunit ARPC2 binds to microtubules. Plant Science **241**: 96–108

Hazak O, Bloch D, Poraty L, Sternberg H, Zhang J, Friml J, Yalovsky S (2010) A rho scaffold integrates the secretory system with feedback mechanisms in regulation of auxin distribution. PLOS Biology **8**: e1000282

Heilmann I (2016) Phosphoinositide signaling in plant development. Development **143**: 2044–2055

Heim N, Garaschuk O, Friedrich MW, Mank M, Milos RI, Kovalchuk Y, Konnerth A, Griesbeck O (2007) Improved calcium imaging in transgenic mice expressing a troponin C-based biosensor. Nature Methods **4**: 127–9

Heim R, Cubitt AB, Tsien RY (1995) Improved green fluorescence. Nature **373**: 663–664

Heim R, Prasher DC, Tsien RY (1994) Wavelength mutations and posttranslational autoxidation of green fluorescent protein. Proceedings of the National Academy of Sciences **91**: 12501

Hellens RP, Edwards EA, Leyland NR, Bean S (2000) pGreen: a versatile and flexible binary Ti vector for Agrobacterium-mediated plant transformation.

Helling D, Possart A, Cottier S, Klahre U, Kost B (2006) Pollen tube tip growth depends on plasma membrane polarization mediated by tobacco PLC3 activity and endocytic membrane recycling. The Plant Cell **18**: 3519–34

Hemsley PA, Kemp AC, Grierson CS (2005) The TIP GROWTH DEFECTIVE1 S-acyl transferase regulates plant cell growth in Arabidopsis. The Plant Cell **17**: 2554–63

Higashiyama T, Takeuchi H (2015) The mechanism and key molecules involved in pollen tube guidance. Annual Review of Plant Biology **66**: 393–413

Himschoot E, Beeckman T, Friml J, Vanneste S (2015) Calcium is an organizer of cell polarity in plants. Biochimica et Biophysica Acta **1853**: 2168

Hong D, Jeon BW, Kim SY, Hwang J-U, Lee Y (2015) The ROP2-RIC7 pathway negatively regulates light-induced stomatal opening by inhibiting exocyst subunit Exo70B1 in Arabidopsis. The New Phytologist **209**: 624

Huang G-Q, Li E, Ge F-R, Li S, Wang Q, Zhang C-Q, Zhang Y (2013) Arabidopsis RopGEF4 and RopGEF10 are important for FERONIA-mediated developmental but not environmental regulation of root hair growth. The New Phytologist **200**: 1089–101

Hwang J-U, Gu Y, Lee Y-J, Yang Z (2005) Oscillatory ROP GTPase activation leads the oscillatory polarized growth of pollen tubes. Molecular Biology of the Cell **16**: 5385–99

Hwang J-U, Jeon BW, Hong D, Lee Y (2011) Active ROP2 GTPase inhibits ABA- and CO2-induced stomatal closure. Plant, Cell & Environment **34**: 2172–82

Hwang J-U, Vernoud V, Szumlanski A, Nielsen E, Yang Z (2008) A tip-localized RhoGAP controls cell polarity by globally inhibiting Rho GTPase at the cell apex. Current Biology **18**: 1907–16

Hwang J-U, Wu G, Yan A, Lee Y-J, Grierson CS, Yang Z (2010) Pollen-tube tip growth requires a balance of lateral propagation and global inhibition of Rho-family GTPase activity. Journal of Cell Science **123**: 340–50

Hwang Y, Lee H, Lee Y-S, Cho H-T (2016) Cell wall-associated ROOT HAIR SPECIFIC 10, a proline-rich receptor-like kinase, is a negative modulator of Arabidopsis root hair growth. Journal of Experimental Botany **67**: 2007–2022

Icha J, Weber M, Waters JC, Norden C (2017) Phototoxicity in live fluorescence microscopy, and how to avoid it. BioEssays **39**: 1700003

Ichikawa M, Hirano T, Enami K, Fuselier T, Kato N, Kwon C, Voigt B, Schulze-Lefert P, Baluška F, Sato MH (2014) Syntaxin of plant proteins SYP123 and SYP132 mediate root hair tip growth in Arabidopsis thaliana. Plant & Cell Physiology **55**: 790–800

Iwano M, Igarashi M, Tarutani Y, Kaothien-Nakayama P, Nakayama H, Moriyama H, Yakabe R, Entani T, Shimosato-Asano H, Ueki M, et al (2014) A pollen coat-inducible autoinhibited Ca2+-ATPase expressed in stigmatic papilla cells is required for compatible pollination in the Brassicaceae. The Plant Cell **26**: 636–649

Iwano M, Ngo QA, Entani T, Shiba H, Nagai T, Miyawaki A, Isogai A, Grossniklaus U, Takayama S (2012) Cytoplasmic Ca2+ changes dynamically during the interaction of the pollen tube with synergid cells. Development **139**: 4202–9

Iwano M, Shiba H, Miwa T, Che F-S, Takayama S, Nagai T, Miyawaki A, Isogai A (2004) Ca2+ dynamics in a pollen grain and papilla cell during pollination of Arabidopsis. Plant Physiology **136**: 3562–71

Jarsch IK, Konrad SSA, Stratil TF, Urbanus SL, Szymanski W, Braun P, Braun KH, Ott T (2014) Plasma Membranes Are Subcompartmentalized into a Plethora of Coexisting and Diverse Microdomains in Arabidopsis and Nicotiana benthamiana. The Plant Cell **26**: 1698

Jeon BW, Hwang J-U, Hwang Y, Song W-Y, Fu Y, Gu Y, Bao F, Cho D, Kwak JM, Yang Z, et al (2008) The Arabidopsis small G protein ROP2 is activated by light in guard cells and inhibits light-induced stomatal opening. The Plant Cell **20**: 75–87

Johnson DI (1990) Molecular characterization of CDC42, a Saccharomyces cerevisiae gene involved in the development of cell polarity. The Journal of Cell Biology **111**: 143

Jones MA, Raymond MJ, Smirnoff N (2005) Analysis of the root-hair morphogenesis transcriptome reveals the molecular identity of six genes with roles in root-hair development in Arabidopsis. The Plant Journal **45**: 83

Jones MA, Shen J-J, Fu Y, Li H, Yang Z, Grierson CS (2002) The Arabidopsis Rop2 GTPase is a positive regulator of both root hair initiation and tip growth. The Plant Cell **14**: 763–76

Kaksonen M, Toret CP, Drubin DG (2005) A modular design for the clathrin- and actin-mediated endocytosis machinery. Cell **123**: 305–20

Kang E, Zheng M, Zhang Y, Yuan M, Yalovsky S, Zhu L, Fu Y (2017) The Microtubule-Associated Protein MAP18 Affects ROP2 GTPase Activity during Root Hair Growth. Plant Physiology **174**: 202–222

Kato M, Aoyama T, Maeshima M (2013) The Ca2+-binding protein PCaP2 located on the plasma membrane is involved in root hair development as a possible signal transducer. The Plant Journal **74**: 690–700

Kato M, Nagasaki-Takeuchi N, Ide Y, Maeshima M (2010) An Arabidopsis hydrophilic Ca2+-binding protein with a PEVK-rich domain, PCaP2, is associated with the plasma

membrane and interacts with calmodulin and phosphatidylinositol phosphates. Plant & Cell Physiology **51**: 366–79

Kaya H, Nakajima R, Iwano M, Kanaoka MM, Kimura S, Takeda S, Kawarazaki T, Senzaki E, Hamamura Y, Higashiyama T, et al (2014) Ca2+-Activated Reactive Oxygen Species Production by Arabidopsis RbohH and RbohJ Is Essential for Proper Pollen Tube Tip Growth. The Plant Cell **26**: 1069–80

Keinath NF, Waadt R, Brugman R, Schroeder JI, Grossmann G, Schumacher K, Krebs M (2015) Live Cell Imaging with R-GECO1 Sheds Light on flg22- and Chitin-Induced Transient [Ca2+]cyt Patterns in Arabidopsis. Molecular Plant **8**: 1188

Kimura S, Kaya H, Kawarazaki T, Hiraoka G, Senzaki E, Michikawa M, Kuchitsu K (2012) Protein phosphorylation is a prerequisite for the Ca2+-dependent activation of Arabidopsis NADPH oxidases and may function as a trigger for the positive feedback regulation of Ca2+ and reactive oxygen species. Biochimica et Biophysica Acta **1823**: 398–405

Knight MR, Campbell AK, Smith SM, Trewavas AJ (1991) Transgenic plant aequorin reports the effects of touch and cold-shock and elicitors on cytoplasmic calcium. Nature **352**: 524

Koncz C, Schell J (1986) The promoter of TL-DNA gene 5 controls the tissue-specific expression of chimaeric genes carried by a novel type of Agrobacterium binary vector. MGG Molecular & General Genetics **204**: 383

Kost B, Lemichez E, Spielhofer P, Hong Y, Tolias K, Carpenter C, Chua N-H (1999) Rac Homologues and Compartmentalized Phosphatidylinositol 4, 5-Bisphosphate Act in a Common Pathway to Regulate Polar Pollen Tube Growth. The Journal of Cell Biology **145**: 317

Kredel S, Oswald F, Nienhaus K, Deuschle K, Röcker C, Wolff M, Heilker R, Nienhaus GU, Wiedenmann J (2009) mRuby, a bright monomeric red fluorescent protein for labeling of subcellular structures. PLOS ONE **4**: e4391

Kremers G-J, Goedhart J, van Munster EB (2006) Cyan and Yellow Super Fluorescent Proteins with Improved Brightness, Protein Folding, and FRET Förster Radius†,‡. Biochemistry **45**: 6570

Kusano H, Testerink C, Vermeer JEM, Tsuge T, Shimada H, Oka A, Munnik T, Aoyama T (2008) The Arabidopsis Phosphatidylinositol Phosphate 5-Kinase PIP5K3 is a key regulator of root hair tip growth. The Plant Cell **20**: 367–80

Lam AJ, St-Pierre F, Gong Y, Marshall JD, Cranfill PJ, Baird MA, McKeown MR, Wiedenmann J, Davidson MW, Schnitzer MJ, et al (2012) Improving FRET dynamic range with bright green and red fluorescent proteins. Nature Methods **9**: 1005–1012

Lampropoulos A, Sutikovic Z, Wenzl C, Maegele I, Lohmann JU, Forner J (2013) GreenGate - a novel, versatile, and efficient cloning system for plant transgenesis. PLOS ONE **8**: e83043

Lavy M (2002) A Cell-Specific, Prenylation-Independent Mechanism Regulates Targeting of Type II RACs. The Plant Cell **14**: 2431

Lavy M, Bloch D, Hazak O, Gutman I, Poraty L, Sorek N, Sternberg H, Yalovsky S (2007) A Novel ROP/RAC effector links cell polarity, root-meristem maintenance, and vesicle trafficking. Current Biology **17**: 947–52

Lavy M, Yalovsky S (2006) Association of Arabidopsis type-II ROPs with the plasma membrane requires a conserved C-terminal sequence motif and a proximal polybasic domain. The Plant Journal **46**: 934

Leonard D, Hart MJ, Platko JV, Eva A, Henzel W, Evans T, Cerione RA (1992) The identification and characterization of a GDP-dissociation inhibitor (GDI) for the CDC42Hs protein. The Journal of Biological Chemistry **267**: 22860–22868

Leshem Y, Johnson C, Sundaresan V (2013) Pollen tube entry into the synergid cell of Arabidopsis is observed at a site distinct from the filiform apparatus. Plant Reproduction **26**: 93–99

Li H, Lin Y, Heath RM, Zhu MX, Yang Z (1999) Control of pollen tube tip growth by a Rop GTPase-dependent pathway that leads to tip-localized calcium influx. The Plant Cell **11**: 1731–1742

Li H, Wu G, Ware D, Davis KR, Yang Z (1998) Arabidopsis Rho-Related GTPases: Differential Gene Expression in Pollen and Polar Localization in Fission Yeast. **118**: 407

Li S, Gu Y, Yan A, Lord E, Yang Z-B (2008) RIP1 (ROP Interactive Partner 1)/ICR1 Marks Pollen Germination Sites and May Act in the ROP1 Pathway in the Control of Polarized Pollen Growth. Molecular Plant **1**: 1021

Liang P, Stratil TF, Popp C, Marín M, Folgmann J, Mysore KS, Wen J, Ott T (2018) Symbiotic root infections in Medicago truncatula require remorin-mediated receptor stabilization in membrane nanodomains. **115**: 5289–5294

Lin D, Nagawa S, Chen J, Cao L, Chen X, Xu T, Li H, Dhonukshe P, Yamamuro C, Friml J, et al (2012) A ROP GTPase-dependent auxin signaling pathway regulates the subcellular distribution of PIN2 in Arabidopsis roots. Current Biology **22**: 1319–25

Lin Y, Wang Y, Zhu JK, Yang Z (1996) Localization of a Rho GTPase Implies a Role in Tip Growth and Movement of the Generative Cell in Pollen Tubes. 'The Plant Cell **8**: 293-303

Lin Y, Yang Z (1997) Inhibition of Pollen Tube Elongation by Microinjected Anti-Rop1Ps Antibodies Suggests a Crucial Role for Rho-Type GTPases in the Control of Tip Growth. The Plant Cell **9**: 1647–1659

MEINHARDT H, GIERER A (1974) Applications of a theory of biological pattern formation based on lateral inhibition. Journal of Cell Science **15**: 321–346

Mangano S, Juárez SPD, Estevez JM (2016) ROS Regulation of Polar Growth in Plant Cells. Plant Physiology **171**: 1593–1605

Masucci JD, Schiefelbein JW (1994) The rhd6 Mutation of Arabidopsis thaliana Alters Root-Hair Initiation through an Auxin- and Ethylene-Associated Process. Plant Physiology **106**: 1335–1346

Mathur J (2005) The ARP2/3 complex: giving plant cells a leading edge. BioEssays **27**:377

Mathur J, Mathur N, Kernebeck B, Hülskamp M (2003) Mutations in actin-related proteins 2 and 3 affect cell shape development in Arabidopsis. The Plant Cell **15**: 1632–1645

Matz MV, Fradkov AF, Labas YA, Savitsky AP, Zaraisky AG, Markelov ML, Lukyanov SA (1999) Fluorescent proteins from nonbioluminescent Anthozoa species. Nature Biotechnology **17**: 969–973

McAinsh MR, Brownlee C, Hetherington AM (1990) Abscisic acid-induced elevation of guard cell cytosolic Ca2+ precedes stomatal closure. Nature **343**: 186

Mendrinna A, Persson S (2015) Root hair growth: it's a one way street. F1000Prime Rep **7**: 23

Merzlyak EM, Goedhart J, Shcherbo D, Bulina ME, Shcheglov AS, Fradkov AF, Gaintzeva A, Lukyanov KA, Lukyanov S, Chudakov DM (2007) Bright monomeric red fluorescent protein with an extended fluorescence lifetime. Nature Methods **4**: 555

Michard E, Lima PT, Borges F, Silva AC, Portes MT, Carvalho JE, Gilliham M, Liu L-H, Obermeyer G, Feijó JA (2011) Glutamate receptor-like genes form Ca2+ channels in pollen tubes and are regulated by pistil D-serine. Science **332**: 434–437

Molendijk AJ, Bischoff F, Rajendrakumar CS, Friml J, Braun M, Gilroy S, Palme K (2001) Arabidopsis thaliana Rop GTPases are localized to tips of root hairs and control polar growth. The EMBO Journal **20**: 2779–88

Monshausen GB, Bibikova TN, Messerli MA, Shi C, Gilroy S (2007) Oscillations in extracellular pH and reactive oxygen species modulate tip growth of Arabidopsis root hairs. Proceedings of the National Academy of Sciences **104**: 20996–1001

Monshausen GB, Bibikova TN, Weisenseel MH, Gilroy S (2009) Ca2+ regulates reactive oxygen species production and pH during mechanosensing in Arabidopsis roots. The Plant Cell **21**: 2341–56

Munnik T, Nielsen E (2011) Green light for polyphosphoinositide signals in plants. Current Opinion in Plant Biology **14**: 489

Mäser P, Thomine S, Schroeder JI, Ward JM, Hirschi K, Sze H, Talke IN, Amtmann A, Maathuis FJ, Sanders D, et al (2001) Phylogenetic relationships within cation transporter families of Arabidopsis. Plant Physiology **126**: 1646–1667

Müller A, Guan C, Gälweiler L, Tänzler P, Huijser P, Marchant A, Parry G, Bennett M, Wisman E, Palme K (1998) AtPIN2 defines a locus of Arabidopsis for root gravitropism control. The EMBO Journal **17**: 6903

Nagai T, Ibata K, Park ES, Kubota M, Mikoshiba K, Miyawaki A (2001) A variant of yellow fluorescent protein with fast and efficient maturation for cell-biological applications. Nature Biotechnology **20**: 87–90

Nakamura M, Verboon JM, Parkhurst SM (2017) Prepatterning by RhoGEFs governs Rho GTPase spatiotemporal dynamics during wound repair. The Journal of Cell Biology **216**: 3959–3969

Nakamura T, Kurokawa K, Kiyokawa E, Matsuda M (2006) Analysis of the Spatiotemporal Activation of Rho GTPases Using Raichu Probes. Methods in Enzymology 315

Ngo QA, Vogler H, Lituiev DS, Nestorova A, Grossniklaus U (2014) A calcium dialog mediated by the FERONIA signal transduction pathway controls plant sperm delivery. Developmental Cell **29**: 491–500

Nguyen AW, Daugherty PS (2005) Evolutionary optimization of fluorescent proteins for intracellular FRET. Nature Biotechnology **23**: 355–360

Oda Y, Fukuda H (2012) Initiation of cell wall pattern by a Rho- and microtubule-driven symmetry breaking. Science **337**: 1333–1336

Ott T (2017) Membrane nanodomains and microdomains in plant–microbe interactions. Current Opinion in Plant Biology **40**: 82

Palmgren MG (2001) PLANTPLASMAMEMBRANE H+-ATPases: Powerhouses for Nutrient Uptake. Annual Review of Plant Physiology and Plant Molecular Biology **52**: 817

Parekh AB, Putney JW (2005) Store-Operated Calcium Channels. Physiological Reviews **85**: 757

Park H-O, Bi E (2007) Central roles of small GTPases in the development of cell polarity in yeast and beyond. Microbiol Mol Biol Rev **71**: 48–96

Park H-O, Chant J, Herskowitz I (1993) BUD2 encodes a GTPase-activating protein for Bud1/Rsr1 necessary for proper bud-site selection in yeast. Nature **365**: 269

Park Y, Sutimantanapi D, Luo A, Cartwright H (2015) The SCAR/WAVE complex polarizes PAN receptors and promotes division asymmetry in maize. Nature Plants

Payne RJH, Grierson CS (2009) A theoretical model for ROP localisation by auxin in Arabidopsis root hair cells. PLOS ONE **4**: e8337

Peterson J (1994) Interactions between the bud emergence proteins Bem1p and Bem2p and Rho- type GTPases in yeast. The Journal of Cell Biology **127**: 1395

Petrášek J, Mravec J, Bouchard R, Blakeslee JJ, Abas M, Seifertová D, Wisniewska J, Tadele Z, Kubes M, Covanová M, et al (2006) PIN proteins perform a rate-limiting function in cellular auxin efflux. Science **312**: 914–918

Piston DW, Kremers G-J (2007) Fluorescent protein FRET: the good, the bad and the ugly. Trends in Biochemical Sciences **32**: 407–14

Platre MP, Noack LC, Doumane M, Bayle V, Simon MLA, Maneta-Peyret L, Fouillen L, Stanislas T, Armengot L, Pejchar P, et al (2018) A Combinatorial Lipid Code Shapes the Electrostatic Landscape of Plant Endomembranes. Developmental Cell **45**: 465

Poraty-Gavra L, Zimmermann P, Haigis S, Bednarek P, Hazak O, Stelmakh OR, Sadot E, Schulze-Lefert P, Gruissem W, Yalovsky S (2013) The Arabidopsis Rho of plants GTPase AtROP6 functions in developmental and pathogen response pathways. Plant Physiology **161**: 1172–1188

Potocký M, Pejchar P, Gutkowska M, Jiménez-Quesada MJ, Potocká A, de Alché JD, Kost B, Žárský V (2012) NADPH oxidase activity in pollen tubes is affected by calcium ions, signaling phospholipids and Rac/Rop GTPases. Journal of Plant Physiology **169**: 1654–63

Potocký M, Pleskot R, Pejchar P, Vitale N, Kost B, Zarsky V (2014) Live-cell imaging of phosphatidic acid dynamics in pollen tubes visualized by Spo20p-derived biosensor. The New Phytologist **203**: 483

Prasher DC, Eckenrode VK, Ward WW, Prendergast FG, Cormier MJ (1992) Primary structure of the Aequorea victoria green-fluorescent protein. Gene **111**: 229–233

Putney JW (1986) A model for receptor-regulated calcium entry. Cell Calcium **7**: 1

Qi Z, Stephens NR, Spalding EP (2006) Calcium entry mediated by GLR3.3, an Arabidopsis glutamate receptor with a broad agonist profile. Plant Physiology **142**: 963–971

Qin Y, Yang Z (2011) Rapid tip growth: insights from pollen tubes. Seminars in Cell & Developmental Biology **22**: 816–24

Raftopoulou M, Hall A (2004) Cell migration: Rho GTPases lead the way. Developmental Biology **265**: 23–32

Rapsomaniki MA, Kotsantis P, Symeonidou I-E, Giakoumakis N-N, Taraviras S, Lygerou Z (2012) easyFRAP: an interactive, easy-to-use tool for qualitative and quantitative analysis of FRAP data. Bioinformatics **28**: 1800–1801

Riquelme M (2013) Tip growth in filamentous fungi: a road trip to the apex. Annual Review of Microbiology **67**: 587–609

Roemer T, Madden K, Chang J, Snyder M (1996) Selection of axial growth sites in yeast requires Axl2p, a novel plasma membrane glycoprotein. Genes & Development **10**: 777

Rosero A, Oulehlová D, Stillerová L, Schiebertová P, Grunt M, Cvrčková F (2016) Arabidopsis FH1 Formin Affects Cotyledon Pavement Cell Shape by Modulating Cytoskeleton Dynamics. Plant & Cell Physiology pcv209

Rounds CM, Bezanilla M (2013) Growth mechanisms in tip-growing plant cells. Annual Review of Plant Biology **64**: 243–265

Russell SA, Bashaw GJ (2018) Axon guidance pathways and the control of gene expression. Developmental Dynamics **247**: 571–580

Schiefelbein JW, Shipley A, Rowse P (1992) Calcium influx at the tip of growing root-hair cells of Arabidopsis thaliana. Planta **187**: 455–9

Schiefelbein JW, Somerville C (1990) Genetic Control of Root Hair Development in Arabidopsis thaliana. The Plant Cell **2**: 235–243

Schindelin J, Arganda-Carreras I, Frise E, Kaynig V, Longair M, Pietzsch T, Preibisch S, Rueden C, Saalfeld S, Schmid B, et al (2012) Fiji: an open-source platform for biological-image analysis. Nature Methods **9**: 676–682

Schmidt A, Hall A (2002) Guanine nucleotide exchange factors for Rho GTPases: turning on the switch. Genes & Development **16**: 1587–1609

Schmidt A, Lv Z, Großhans J (2018) ELMO and Sponge specify subapical restriction of Canoe and formation of the subapical domain in early Drosophila embryos. Development. doi: 10.1242/dev.157909

Schmidt R, Kunkowska AB (2016) Role of Reactive Oxygen Species during Cell Expansion in Leaves. Plant Physiology **172**: 2098–2106

Shaner NC, Campbell RE, Steinbach PA, Giepmans BNG, Palmer AE, Tsien RY (2004) Improved monomeric red, orange and yellow fluorescent proteins derived from Discosoma sp. red fluorescent protein. Nature Biotechnology **22**: 1567–1572

Shaner NC, Lambert GG, Chammas A, Ni Y, Cranfill PJ, Baird MA, Sell BR, Allen JR, Day RN, Israelsson M, et al (2013) A bright monomeric green fluorescent protein derived from Branchiostoma lanceolatum. Nature Methods **10**: 407–409

Shaner NC, Lin MZ, McKeown MR, Steinbach PA, Hazelwood KL, Davidson MW, Tsien RY (2008) Improving the photostability of bright monomeric orange and red fluorescent proteins. Nature Methods **5**: 545

Shaner NC, Steinbach PA, Tsien RY (2005) A guide to choosing fluorescent proteins. Nature Methods **2**: 905–9

Shih H-W, DePew CL, Miller ND, Monshausen GB (2015) The Cyclic Nucleotide-Gated Channel CNGC14 Regulates Root Gravitropism in Arabidopsis thaliana. Current Biology **25**: 3119

Shimomura O, Johnson FH, Saiga Y (1962) Extraction, Purification and Properties of Aequorin, a Bioluminescent Protein from the Luminous Hydromedusan,Aequorea. Journal of Cellular and Comparative Physiology **59**: 223

Simon MLA, Platre MP, Assil S, van Wijk R, Chen WY, Chory J, Dreux M, Munnik T, Jaillais Y (2014) A multi-colour/multi-affinity marker set to visualize phosphoinositide dynamics in Arabidopsis. The Plant Journal **77**: 322–37

Skwarek LC, Boulianne GL (2009) Great Expectations for PIP: Phosphoinositides as Regulators of Signaling During Development and Disease. Developmental Cell **16**: 12

Smertenko AP, Jiang C-J, Simmons NJ, Weeds AG, Davies DR, Hussey PJ (1998) Ser6 in the maize actin-depolymerizing factor, ZmADF3, is phosphorylated by a calcium-stimulated protein kinase and is essential for the control of functional activity. The Plant Journal **14**: 187

Sorek N, Gutman O, Bar E, Abu-Abied M, Feng X, Running MP, Lewinsohn E, Ori N, Sadot E, Henis YI, et al (2011) Differential effects of prenylation and s-acylation on type I and II ROPS membrane interaction and function. Plant Physiology **155**: 706–20

Sorek N, Poraty L, Sternberg H, Bar E, Lewinsohn E, Yalovsky S (2007) Activation status-coupled transient S acylation determines membrane partitioning of a plant Rho-related GTPase. Molecular and Cellular Biology **27**: 2144–54 – RETRACTED

Sorek N, Poraty L, Sternberg H, Buriakovsky E, Bar E, Lewinsohn E, Yalovsky S (2017) Corrected and Republished from: Activation Status-Coupled Transient S-Acylation Determines Membrane Partitioning of a Plant Rho-Related GTPase. Molecular and Cellular Biology **37**: e00333–17

Sorek N, Segev O, Gutman O, Bar E, S, Richter S, Richter R, Poraty L, Hirsch JA, Henis YI, et al (2010) An S-acylation switch of conserved G domain cysteines is required for polarity signaling by ROP GTPases. Current Biology **20**: 914–20

Sormo CG, Leiros I, Brembu T, Winge P, Os V, Bones AM (2006) The crystal structure of Arabidopsis thaliana RAC7-ROP9: the first RAS superfamily GTPase from the plant kingdom. Phytochemistry **67**: 2332–2340

Stanislas T, Hüser A, Barbosa ICR, Kiefer CS, Brackmann K, Pietra S, Gustavsson A, Zourelidou M, Schwechheimer C, Grebe M (2015) Arabidopsis D6PK is a lipid domain-dependent mediator of root epidermal planar polarity. Nature Plants **1**: 15162

Stanley CE, Shrivastava J, Brugman R, Heinzelmann E, van Swaay D, Grossmann G (2017) Dual-flow-RootChip reveals local adaptations of roots towards environmental asymmetry at the physiological and genetic levels. The New Phytologist **217**: 1357–1369

Stegmann M, Monaghan J, Smakowska-Luzan E, Rovenich H, Lehner A, Holton N, Belkhadir Y, Zipfel C (2017) The receptor kinase FER is a RALF-regulated scaffold controlling plant immune signaling. Science **355**: 287

Steinhorst L, Kudla J (2012) Calcium - a central regulator of pollen germination and tube growth. Biochimica et Biophysica Acta **1833**: 1573–1581

Szymanski DB (2005) Breaking the WAVE complex: the point of Arabidopsis trichomes. Current Opinion in Plant Biology **8**: 103–112

Takeda S, Gapper C, Kaya H, Bell E, Kuchitsu K, Dolan L (2008) Local positive feedback regulation determines cell shape in root hair cells. Science **319**: 1241–4

Takeuchi H, Higashiyama T (2016) Tip-localized receptors control pollen tube growth and LURE sensing in Arabidopsis. Nature **531**: 245–248

Thole JM, Vermeer JEM, Zhang Y, Gadella TWJ Jr, Nielsen E (2008) Root hair defective4 encodes a phosphatidylinositol-4-phosphate phosphatase required for proper root hair development in Arabidopsis thaliana. The Plant Cell **20**: 381–95

Thomas C, Fricke I, Scrima A, Berken A, Wittinghofer A (2007) Structural evidence for a common intermediate in small G protein-GEF reactions. Molecular Cell **25**: 141–149

Tsien RY (1998) THE GREEN FLUORESCENT PROTEIN. Annual Review of Biochemistry **67**: 509

Turing AM (1952) The Chemical Basis of Morphogenesis. Philosophical Transactions of the Royal Society B **237**: 37

Ungermann C, Langosch D (2005) Functions of SNAREs in intracellular membrane fusion and lipid bilayer mixing. Journal of Cell Science **118**: 3819–3828

Vermeer JEM, Thole JM, Goedhart J, Nielsen E, Munnik T (2009) Imaging phosphatidylinositol 4-phosphate dynamics in living plant cells. The Plant Journal **57**:356

Vincent P, Chua M, Nogue F, Fairbrother A, Mekeel H, Xu Y, Allen N, Bibikova TN, Gilroy S, Bankaitis VA (2005) A Sec14p-nodulin domain phosphatidylinositol transfer protein polarizes membrane growth of Arabidopsis thaliana root hairs. The Journal of Cell Biology **168**: 801–12

Vogler F, Konrad SSA, Sprunck S (2015) Knockin' on pollen's door: live cell imaging of early polarization events in germinating Arabidopsis pollen. Frontiers in Plant Science **6**: 246

Wachsman G, Sparks EE, Benfey PN (2015) Genes and networks regulating root anatomy and architecture. The New Phytologist **208**: 26

Wang M, Casey PJ (2016) Protein prenylation: unique fats make their mark on biology. Nature Reviews Molecular Cell Biology **17**: 110

Wang P, Richardson C, Hawes C, Hussey PJ (2016) Arabidopsis NAP1 Regulates the Formation of Autophagosomes. Current Biology **26**: 2060

Wang S, Hazelrigg T (1994) Implications for bcd mRNA localization from spatial distribution of exu protein in Drosophila oogenesis. Nature **369**: 400

Wang X, Zhu L, Liu B, Wang C, Jin L, Zhao Q, Yuan M (2007) Arabidopsis MICROTUBULE-ASSOCIATED PROTEIN18 functions in directional cell growth by destabilizing cortical microtubules. The Plant Cell **19**: 877–89

Wang Y, Zhang W-Z, Song L-F, Zou J-J, Su Z, Wu W-H (2008) Transcriptome analyses show changes in gene expression to accompany pollen germination and tube growth in Arabidopsis. Plant Physiology **148**: 1201–1211

Wedlich-Soldner R, Altschuler S, Wu L, Li R (2003) Spontaneous cell polarization through actomyosin-based delivery of the Cdc42 GTPase. Science **299**: 1231–1235

Wedlich-Soldner R, Wai SC, Schmidt T, Li R (2004) Robust cell polarity is a dynamic state established by coupling transport and GTPase signaling. The Journal of Cell Biology **166**: 889–900

Whalley HJ, Knight MR (2012) Calcium signatures are decoded by plants to give specific gene responses. The New Phytologist **197**: 690

Wilkins KA, Matthus E, Swarbreck SM, Davies JM (2016) Calcium-Mediated Abiotic Stress Signaling in Roots. Frontiers in Plant Science **7**: 1296

Winge P, Brembu T, Bones AM (1997) Cloning and characterization of rac-like cDNAs from Arabidopsis thaliana. Plant Molecular Biology

Won S-K, Lee Y-J, Lee H-Y, Heo Y-K, Cho M, Cho H-T (2009) Cis-element- and transcriptome-based screening of root hair-specific genes and their functional characterization in Arabidopsis. Plant Physiology **150**: 1459–73

Wu G, Gu Y, Li S, Yang Z (2001) A genome-wide analysis of Arabidopsis Rop-interactive CRIB motif-containing proteins that act as Rop GTPase targets. The Plant Cell **13**: 2841–2856

Wu G, Li H, Yang Z (2000) Arabidopsis RopGAPs are a novel family of rho GTPase-activating proteins that require the Cdc42/Rac-interactive binding motif for rop-specific GTPase stimulation. Plant Physiology **124**: 1625–1636

Wu Y, Zhao S, Tian H, He Y, Xiong W, Guo L, Wu Y (2013) CPK3-phosphorylated RhoGDI1 is essential in the development of Arabidopsis seedlings and leaf epidermal cells. Journal of Experimental Botany **64**: 3327–38

Wudick MM, Portes MT, Michard E, Rosas-Santiago P, Lizzio MA, Nunes CO, Campos C, Damineli DSC, Carvalho JC, Lima PT, et al (2018) CORNICHON sorting and regulation of GLR channels underlie pollen tube Ca2+ homeostasis. Science **360**: 533-536

Xing S, Mehlhorn DG, Wallmeroth N, Asseck LY, Kar R, Voss A, Denninger P, Schmidt VAF, Schwarzländer M, Stierhof Y-D, et al (2017) Loss of GET pathway orthologs in Arabidopsis thaliana causes root hair growth defects and affects SNARE abundance. Proceedings of the National Academy of Sciences **114**: E1544

Xu T, Dai N, Chen J, Nagawa S, Cao M, Li H, Zhou Z, Chen X, de Rycke R, Rakusová H, et al (2014) Cell surface ABP1-TMK auxin-sensing complex activates ROP GTPase signaling. Science **343**: 1025–8

Xu T, Wen M, Nagawa S, Fu Y, Chen J-G, Wu M-J, Perrot-Rechenmann C, Friml J, Jones AM, Yang Z (2010) Cell surface- and rho GTPase-based auxin signaling controls cellular interdigitation in Arabidopsis. Cell **143**: 99–110

Yan A, Xu G, Yang Z-B (2009) Calcium participates in feedback regulation of the oscillating ROP1 Rho GTPase in pollen tubes. Proceedings of the National Academy of Sciences **106**: 22002–7

Yanagisawa M, Zhang C, Szymanski DB (2013) ARP2/3-dependent growth in the plant kingdom: SCARs for life. Frontiers in Plant Science **4**: 166

Yang TT, Cheng L, Kain SR (1996) Optimized Codon Usage and Chromophore Mutations Provide Enhanced Sensitivity with the Green Fluorescent Protein. Nucleic Acids Research **24**: 4592

Yi K, Guo C, Chen D, Zhao B, Ren H (2005) Cloning and functional characterization of a formin-like protein (AtFH8) from Arabidopsis. Plant Physiology **138**: 1071–1082

Yoo C-M, Quan L, Cannon AE, Wen J, Blancaflor EB (2011) AGD1, a class 1 ARF-GAP, acts in common signaling pathways with phosphoinositide metabolism and the actin cytoskeleton in controlling Arabidopsis root hair polarity. The Plant Journal **69**: 1064–1076

Yu Y, Song J, Tian X, Zhang H, Li L, Zhu H (2017) Arabidopsis PRK6 interacts specifically with AtRopGEF8/12 and induces depolarized growth of pollen tubes when overexpressed. Science China - Life Sciences **61**: 100–112

Zacharias DA, Violin JD, Newton AC, Tsien RY (2002) Partitioning of lipid-modified monomeric GFPs into membrane microdomains of live cells. Science **296**: 913–916

Zhang C, Mallery E, Reagan S, Boyko VP, Kotchoni SO, Szymanski DB (2013a) The endoplasmic reticulum is a reservoir for WAVE/SCAR regulatory complex signaling in the Arabidopsis leaf. Plant Physiology **162**: 689–706

Zhang S, Pan Y, Tian W, Dong M, Zhu H, Luan S, Li L (2017) Arabidopsis CNGC14 Mediates Calcium Influx Required for Tip Growth in Root Hairs. Molecular Plant **10**: 1004

Zhang Y, Immink R, Liu C-M, Emons AM, Ketelaar T (2013b) The Arabidopsis exocyst subunit SEC3A is essential for embryo development and accumulates in transient puncta at the plasma membrane. The New Phytologist **199**: 74–88

Zhang Y, McCormick S (2007) A distinct mechanism regulating a pollen-specific guanine nucleotide exchange factor for the small GTPase Rop in Arabidopsis thaliana. **104**: 18830–18835

Zhao Y, Araki S, Wu J, Teramoto T, Chang YF, Nakano M, Abdelfattah AS, Fujiwara M, Ishihara T, Nagai T, et al (2011) An Expanded Palette of Genetically Encoded Ca2+ Indicators. Science **333**: 1888

Zheng Y, Cerione R, Bender A (1994) Control of the yeast bud-site assembly GTPase Cdc42. Catalysis of guanine nucleotide exchange by Cdc24 and stimulation of GTPase activity by Bem3. The Journal of Biological Chemistry **269**: 2369–2372

Zheng ZL, Yang Z (2000) The Rop GTPase: an emerging signaling switch in plants. Plant Molecular Biology **44**: 1–9

Zhu L, Zhang Y, Kang E, Xu Q, Wang M, Rui Y, Liu B, Yuan M, Fu Y (2013) MAP18 regulates the direction of pollen tube growth in Arabidopsis by modulating F-actin organization. The Plant Cell **25**: 851–67

Zuo J, Niu Q-W, Chua N-H (2000) An estrogen receptor-based transactivator XVE mediates highly inducible gene expression in transgenic plants. The Plant Journal **24**: 265

Iweiler LG, Guan C, Iler AM, Wisman E, Mendgen K, Yephremov A, Palme K (1998) Regulation of Polar Auxin Transport by AtPIN1 in Arabidopsis Vascular Tissue. Science **282**: 2226

van Leeuwen W, Vermeer JEM, Munnik T (2007) Visualization of phosphatidylinositol 4,5-bisphosphate in the plasma membrane of suspension-cultured tobacco BY-2 cells and whole Arabidopsis seedlings. The Plant Journal **52**: 1014

Zhang Y, Kang E, Yuan M, Fu Y, Zhu L (2015) PCaP2 regulates nuclear positioning in growing Arabidopsis thaliana root hairs by modulating filamentous actin organization. Plant Cell Reports **34**: 1317–1330

Appendix

Abbreviations

All common abbreviations and units were used as generally acknowledged. Other used abbreviations were introduced in the text of this thesis and are listed below.

A. thaliana	*Arabidopsis thaliana*
A. tumefaciens	*Agrobacterium tumefaciens*
ABI1	ABL INTERACTOR 1
ACA	AUTOINHIBITED CALCIUM ATPase
ADF	ACTIN DEPOLYMERIZATION FACTORS
AGD1	ARF-GAP DOMAIN 1 (AGD1)
ARF	ADP RIBOSYLATION FACTOR
ARP	ACTIN REALATED PROTEIN
AXL	AXIAL BUDDING
BEM1	BUD EMERGENCE 1
BRK1	BRICK1
$[Ca^{2+}]_{cyto}$	Cytosolic calcium ion
CCCP	Carbonyl cyanide m-chlorophenyl hydrazine
CDC	CELL DIVISION CYCLE
cDNA	complementary DNA
CDS	coding sequence
CFP	Cyan Fluorescent Protein
CNGC	CYCLIC NUCLEOTIDE-GATED CHANNEL
Col-0	Columbia ecotype of *A. thaliana* (used as WT)
COW1	CAN OF WORMS1
CRIB	CDC42- AND RAC-INTERACTIVE BINDING)
DAG	diacylglycerol
dag	days after germination
dainf	days after infiltration
DMSO	Dimethylsulfoxid
E. coli	*Escherichia coli*
eGFP	Enhanced Green Fluorescent Protein
ER	endoplasmic reticulum
FER	FERONIA
FP	Fluorescent Protein
FRAP	fluorescence recovery after photobleaching
FRET	Fluorescent/Förster resonance energy transfer
FWHM	full width at half maximum
GAP	GTPase ACTIVTING PROTEINS
GDI	GDP/GTP DISSOCIATION INHIBITOR
gDNA	genomic DNA
GDP	guanosine diphosphate
GEF	GUANINE NUCLEOTIDE EXCHANGE FACTOR
Gent	Gentamycin
GET	GUIDED ENTRY OF TAIL-ANCHORD PROTEINS
GLR	GLUTAMATE-LIKE RECEPTORS
GTP	guanosine triphosphate
haind	hours after induction
Hyg	Hygromycin
ICR1	INTERACTOR OF CONSTITUTIVELY ACTIVE ROP 1
ind	β-estradiol inducible
IP3	inositol1,4,5-trisphosphate
Kan	Kanamycin
LUT	Look up table (displayed color mode for images)
mCit	monomeric Citrine
mClv	monomeric Clover3
mNG	monomeric NeonGreen
MRH3	MUTANT ROOT HAIR 3
mRNA	messenger RNA
MS-Medium	Mashuringe-Skoog-Medium
mYPet	monomeric YFP for energy transfer
N. benthamiana	*Nicotiana benthamiana*
NAP1	NCK-ASSOCIATED PROTEIN
NSF	N-ETHYLMALEIMIDE-SENSITIVE-FACTOR
P-ATPase	plasma membrane ATPases
PCAP	PLASMA MEMBRANE ASSOCIATED CALCIUM BINDING PROTEIN
PERK13	PROLINE-RICH EXTENSIN-LIKE RECEPTOR-LIKE KINASE 13

PGGT	PROTEIN GERANYLGERANLYTRANSFERASE
PI	propidium iodide
PIN	PIN-FORMED
PI4P	phosphatidylinositol-4-phosphate
PIP2	phosphatidylinositol 4,5-bisphosphate
PIP5K3	PHOSPHATIDYLINOSITOL-4-PHOSPHATE 5-KINASE 3
Pol-Ind	Polarity index (Signal Intensity$_{in}$ / Signal Intensity$_{out}$)
PRK	POLLEN RECEPTOR LIKE KINASE
PtdIns	phosphatidylinositols
QY	Quantum Yield
$_r$	resistance to the according antibiotic
RALF	RAPID ALKALINIZATION FACTOR
Ras	Rat sarcoma
RBOH	RESPIRATORY BURST OXIDASE HOMOLOG
REN1	ROP1 ENHANCER 1
RFP	Red Fluorescent Protein
R-GECO1	RED FLUORESCENT GENETICALLY ENCODED Ca^{2+} INDICATORS FOR OPTICAL IMAGING 1
RHD2	ROOT HAIR DEVECTIVE2
RHD4	ROOT HAIR DEVECTIVE 4
RHD6	ROOT HAIR DEVECTIVE 6
RHID	root hair initiation domain
Rho	Ras homologue
RHS	ROOT HAIR SPECIFIC
RIC	ROP-INTERACTIVE CRIB MOTIF-CONTAINING PROTEIN
Rif	Rifampicin
RLK	receptor-like kinase
ROP	RHO-TYPE GTPases OF PLANTS
ROS	reactive oxygen species
RSR1	RAS-RELATED GTPase 1
RT-PCR	reverse transcription PCR
SCAR	SUPRESSOR OF cAMP RECEPTOR
SCN1	SUPERCENTIPEDE 1
SD	standard deviation
SEC3A	EXOCYST COMPLEX COMPONENT SEC3A
SEM	standard error of mean
SNARE	SOLUBLE NSF ATTACHMENT RECEPTOR
SP	sperm cell
Spec	Spectinomycin
SRA1	SPECIFICALLY RAC1-ASSOCIATED PROTEIN 1
Strep	Streptomycin
SYP	SYNTAXIN OF PLANTS
Tet	Tetracycline
TIP1	TIP GROWTH DEFECTIVE 1
TMK	TRANSMEMBRANE KINASE
WAVE	Wiskott–Aldrich syndrome protein family Verprolin homologous
WT	wild type
YFP	Yellow Fluorescent Protein
ε	extinction coefficient

List of Figures

List of Tables

Plasmid maps

Supplemental Figure 1 Exemplary plasmid maps

pGGC000 represents entry vectors used for GreenGate cloning. All entry vectors only differ in the BsaI overhang sequence. pPD0161 is a filled entry vector based on pGGA000 and shows the module of the estradiol inducible promoter construct. pGGZ003 was used for all destination vector constructs. pPD0222 is a destination construct C-terminally tagged with mCit, under estradiol inducible promoter. pPD0042 is a destination vector N-terminally tagged with mTrq2 under native promoter